

MINISTRY OF EDUCATION AND SCIENCE OF UKRAINE

National Aviation University



**THEORY AND PRACTICE
OF UNMANNED AERIAL SYSTEMS OF THE
NATIONAL AVIATION UNIVERSITY**

*Under the general editorship of
by Prof. Maxim LUTSKY, Doctor of Technical Sciences*



KYIV
Publishing Lira-K
2023

UDC 623.746:629.014.9]:378.4(477.411)HAY](075.8)=111

*Recommended by the Academic Council of the National Aviation University
(protocol № 7 of 23 november 2022)*

Reviewers:

M. Kulyk – Doctor of Technical Sciences, Professor (National Aviation University);
Y. Ziatdinov – Doctor of Technical Sciences, Professor (Kyiv Professional College of Computer Technologies and Economics);
V. Kabaniachyi – Doctor of Technical Sciences, Professor (National Technical University of Ukraine «Igor Sikorsky Kyiv Polytechnic Institute»)

Authors:

M. Lutsky (foreword, Chapter 1, Chapter 6); M. Matiychyk (introduction, Chapters 1–6);
I. Kachalo (Chapter 1, Chapter 5); S. Shaptala (foreword, Chapter 2.6); O. Mykhatsky (Chapters 2);
N. Suvorova (Chapter 2); K. Trachuk (Chapter, 2, Chapter 5); O. Zhdanov (Chapter 2);
E. Udartsev (Chapter 2); Y. Romanenko (Chapter 5.4, Chapter 6.1); O. Mykhalchenko (Chapter 5);
O. Rybalchenko (Chapter 3, Chapter 4); D. Matiychyk (Chapter 3, Chapter 4); M. Fuzik
(Chapter 3, Chapter 5); V. Kharchenko (Chapter 4, Chapter 6.3); edited by M. Lutsky

Theory and Practice of Unmanned Aerial Systems of the National Aviation University:
monograph / M. Lutsky, M. Matiychyk, S. Shaptala, M. Fuzik [et al.]; under general ed. Dr. of
technical sciences, Prof. Maxim LUTSKY. Kyiv: Publishing Lira-K 2023. 256 p.
ISBN

*Under the general editorship of
by Prof. Maxim LUTSKY, Doctor of Technical Sciences*

Presents training and methodological materials on justification, development and use of
unmanned aircraft in civil aviation of Ukraine. The materials presented are the result of many
years of research in the field of creation and operation of unmanned systems.

For students of higher educational institutions studying in the specialty 272 «Aviation
transport» in accordance with educational programs, as well as for teachers of higher educational
institutions, specialists in the field of mechanics, automation, communication systems, air
navigation, feasibility study, organization of aviation work and others important areas of
technical and technological support for unmanned aircraft.

UDC 623.746-519: 378.4 (477-25) NAU (075.8)

© Lutsky M., Matiychyk M., Shaptala S.,
Fuzik M. [et al.], 2023

© Publishing Lira-K, 2023

ISBN

CONTENTS

LIST OF ABBREVIATIONS	5
FOREWORD	8
INTRODUCTION	11
CHAPTER 1. UNMANNED AERIAL SYSTEM AS PART OF THE AIR TRANSPORT INDUSTRY	12
1.1. Development of unmanned aviation as a component of the air transport industry.....	12
1.2. Formation of the unmanned aerial system concept as a component of civil aviation system	15
1.3. Typical types of aviation work and requirements for their performance.....	21
1.4. Global experience and trends in the application of unmanned aerial vehicles in civil aviation	27
1.5. Current status and operation of unmanned aerial vehicles in Ukraine	33
CHAPTER 2. RESEARCH OF FLIGHT TECHNICAL AND OTHER CHARACTERISTICS OF UAVs	41
2.1. Estimation of the main flight-technical characteristics of the unmanned plane M6-3T for carriage of small valuable cargoes	41
2.2. Influence of icing on aircraft performance of unmanned aerial vehicle M-10-2 «Oko»	57
2.3. Aerodynamic calculation of the accepted configuration of unmanned aerial vehicle M-56 «Module»	65
2.4. Kinematic and dynamic models of unmanned aerial vehicle movement (on the example of M-7-V5).....	79
2.5. Blowing results of the aerodynamic model of the unmanned aerial vehicle M-7-V5 «Nebesniy patrol»	85
2.6. Justification of propeller parameters for high-altitude flights of solar-powered aircraft	113
CHAPTER 3. UNMANNED AERIAL VEHICLES OF THE NATIONAL AVIATION UNIVERSITY FOR CARRYING SMALL LOADS	130
3.1. Unmanned four-engine PKM-14 «Saturnia» helicopter	130
3.2. Unmanned aerial vehicle M-6-3T «Zhayvir»	138
CHAPTER 4. UNMANNED AERIAL VEHICLES OF NATIONAL AVIATION UNIVERSITY AND THEIR COMPLEXES FOR REMOTE SURVEILLANCE, MONITORING, AND OTHER PURPOSES	148
4.1. Unmanned aerial vehicle complex «OVOD» M106.....	148
4.2. The unmanned aerial vehicle complex M-7-V5 «Nebesniy patrol»	162
4.3. Unmanned aircraft M-6 «Zhayvir» for technology of biological protection of agricultural crops.....	175
4.4. Unmanned aerial vehicle complex M-56 «Module».....	180
4.5. Planning self-guided mini-munition PMB-03.....	189

CHAPTER 5. FEASIBILITY STUDY OF UNMANNED AERIAL VEHICLES AND UNMANNED AERIAL SYSTEMS	193
5.1. Analysis of the components of the unmanned aerial system efficiency	193
5.2. Calculation of productivity and comparison of full consumption on performance of route flights using unmanned aerial vehicle M-7-V5 and superlight plane NARP-1	198
5.3. Method of calculating the cost of flight hours when performing aviation works using UAV M-7-V5	202
5.4. Methodology for calculating the cost per flight hour for unmanned aerial vehicle of different classes at the National Aviation University	208
CHAPTER 6. PROSPECTIVE PROJECTS OF UNMANNED AERIAL VEHICLE NATIONAL AVIATION UNIVERSITY	216
6.1. Rationale and design parameters of an optionally piloted cargo-passenger aircraft (project)	216
6.2. Double-engine multi-purpose convertible aircraft KM-3 «Kubok» (project).....	227
6.3. Stratospheric pseudosatellite PS-11 «Krokus»	233
Appendix. Developments of unmanned aerial vehicles of the Scientific and Production Center of Unmanned Aviation «Virage» of the National Aviation University in chronological order	248

LIST OF ABBREVIATIONS

AC – alternating current
ACHW – aviation chemical work
ACS – aircraft control system
ACW – aviation crane works
AEB – aircraft electrical batteries
AM – air management
APC – aircraft photcamera
APh – aerial photography
ASS – aviation specialized systems
ATC – Air Traffic Control
ATCA – Air Traffic Control Authority
ATM – Air Traffic Management
ATOL – automated take-off and landing
AW – aviation works
BLOS – beyond line of sight
CA – Civil Aviation
CG – center of gravity
CPD – combined piloting device
DAL – domestic airlines
DC – direct current
EB – electrical battery
EE – electro engines
EK – electric key
EW – electronic warfare
FAL – fuel and lubricants
FDR – flight data recorder
FTC – flight technical characteristics
GCS – ground control station
GNC – guidance, navigation and control
GPS – Global Positioning System
HAPS – high-altitude pseudo-satellite
HLC – High light compensation
HP – horizontal plumage

ICAO – International Civil Aviation Organization
IFR – Instrument Flight Rules
IR – infrared sensor
ISA – International Standard Atmosphere
LALE – Low Altitude Long Endurance
LOS – line of sight
LSMV – laser scanner of machine vision
MAC – mean aerodynamic chord
MALE – Medium Altitude Long Endurance
MC – meteorological conditions
MFR – mode of flight recorder
MT – maintenance
MTOW – maximum take-off weight
NAU – National Aviation University
NFO – number of flight operation
OPV – Optionally Piloted Vehicle
PC – personal computer
PP – power plant
PRC – portable remote-control
PS – pseudosatellites
PST – pitot static tube
PT – pitot tube
REE – radioelectronic equipment
RP – remote pilot
RPS – remote pilot station
SAAU – State Aviation Administration of Ukraine
SC – solar cells
SCC – special cargo container
SPCUA «Virage» – Scientific and Production Center of Unmanned Aviation «Virage»
SRTM – Shuttle Radar Topography Mission
SVFR – Special Visual Flight Rules
TLO – target load operator
TSSA – Transport System of Special-purpose Aviation
TTCH – tactical and technical characteristics
UA – unmanned aircraft

UAH – Ukrainian hryvnia
UAS – unmanned aerial systems
UAV – unmanned aerial vehicle
UAVC – unmanned aerial vehicle complex
UAVS – unmanned aerial vehicle system
UkSATSE – Ukrainian State Air Traffic Services Enterprise
USD – United States dollar
USSOCOM – United States Special Operations Command
VAT – value added tax
VFR – Visual Flight Rules
VLOS – visual line-of-sight
VP – vertical plumage
W – workstation
W1 – remote pilot`s workstation
W2 – operator and remote co-pilot`s workstation
WP – waypoint

FOREWORD



Today, modern aviation is experiencing perhaps the biggest revolutionary change in more than 100 years of development. The fact that we are talking about the deep penetration of unmanned systems into all spheres of life and, in particular, into air transport, is already obvious. It is known that some civil aviation aircraft can be in the air, perform take-offs and landings in automatic mode thanks to the equipment of modern avionics systems capable of fully controlling the aircraft, processing information from almost all sources and reacting very quickly to signals and accordingly to ensure the execution of the flight at all its stages.

A further indication of the reality of this transformation in aviation is the successful execution in 2021 of a fully autonomous, unmanned flight on the *Skyborg*, where the decision on board was made solely by artificial intelligence.

In fact, humanity is approaching a stage where transport operations, especially cargo transport, will be autonomous, bringing aviation to a new technical and technological level and significantly increasing its efficiency and competitiveness.

Transition aviation, the so-called optionally piloted aircraft and helicopters, is in its formative stages. Equipped with the appropriate automation, they can be operated either by a human or, in the absence of one on board, automatically execute an approved flight-plan.

The National Aviation University has also made a worthy contribution to the development of unmanned aviation over the past decades. Our scientists and graduate students have developed and implemented more than 30 very different designs for unmanned aerial vehicles with combustion engines and electrical power plants, right through to solar-powered drones. The overall dimensions of the structures ranged from 1,1 m to 14 m, and the take-off weight – from 1,5 to 300 kg.

With this educational and methodical work, we sum up certain results of the work of the scientific and pedagogical team of the National Aviation University and look with hope into the future of aviation in Ukraine, where the role of our specialists and their developments will only increase and thereby the prestige of our Alma Mater will rise.

Maxim LUTSKY, Rector of the National Aviation University



Dear friends, readers of our book!

Military aircraft that functioned without a human on board have been known since the 19th century. The earliest known type adapted for military tasks was the balloon, which is considered the first unmanned aerial vehicle (UAV). Balloons with mechanical drop timers were widely used in the 19th century by the Austrian army to bomb Venice. The facts of the use of tethered unmanned balloons to solve aerial photography tasks, which S. Langley was engaged in the USA, are known. Already at that time, it became clear that a small part of military tasks could be solved with the help of unmanned technologies.

Since the development of unmanned and manned aviation in general is closely linked, it can be said that the greater achievements in the use of aviation and UAVs in particular were made during the First World War. Between 1914 and 1918, for example, the British industry alone produced as many as 55,000 aircraft for a variety of purposes, namely fighters, bombers and scouts. At the same time in the US, one of the unmanned variants of the military aircraft was called the *«Hewitt-Sperry automatik Aeroplane»*.

In addition, the armed forces of the warring countries already had staffed units that launched tethered balloons and balloons with or without a man on board; in particular, the aviation of the young Ukrainian People's Republic (UPR), which was formed on the basis of imperial air detachments that were stationed on its territory, also used it. Between 1917 and 1921, the UPR's aircraft strength reached between 300 and 500. They were used for bombing, reconnaissance and aerial fire support. There were also aeronautical units which made extensive use of tethered aerostats, lifted without a man on board.

Before the Second World War, the outstanding Ukrainian scientist and designer S. Korolev, known at the time as the creator of the first guided cruise missiles and rocket gliders, worked fruitfully in the UAV field. They were not in serial production before the Second World War, but became the basis for the development of cruise missiles in the post-war period. Also during the war, under the leadership of S. Korolev, prototypes of guided ballistic missiles were developed, in particular the EKR and MKR projects. A total of six cruise missile projects with a launch weight of 22 kg to 230 kg and a range of up to 80 km were developed under his leadership between 1930 and 1940.

There is currently a steady trend towards the very rapid development of unmanned aviation both globally and in Ukraine. No one is surprised anymore by the unheard-of names «*Predator*», «*Bayraktar*», «*Sokil-300*» and the names of other ultramodern aircraft systems capable of carrying out complex flight missions without a man on board: reconnaissance, air strikes against moving and stationary targets and, ultimately, of performing functions unattainable by manned aircraft. Of course, we are dealing here with a new level of technological revolution, the prerequisites for which were laid much earlier.

Today, Ukrainian scientists and designers are maintaining a high level of development of competitive UAV of various classes and purposes.

The National Aviation University (NAU) has also made significant progress in this area. In particular, in 2015–2016, the M-10-2 «*Oko*» battlefield scout developed at NAU successfully passed decisive departmental tests, and under the name «*UA-beta*» entered controlled operation in the Armed Forces of Ukraine. In the period 2014–2022, the National Aviation University presented a wide range of samples of unmanned aerial vehicles: from «*copters*» to pseudo-satellites. The weight of some developed samples is up to 1,200 kg. The range of developments at the National Aviation University is quite broad, including state-of-the-art avionics, target payload, ground control stations, etc.

Undoubtedly, the presented book reveals details of this painstaking, long and hard work of scientists, designers, post-graduate students and students of the National Aviation University and demonstrates its significant potential in development of modern and advanced unmanned aerial vehicles and their components, which are so necessary for present and future of our Motherland – Ukraine.

Serhii Shaptala, Chief of the General Staff of the Armed Forces of Ukraine, Hero of Ukraine, Lieutenant General

INTRODUCTION

Since its inception, global civil aviation has always been at the forefront of scientific and technological progress. The formation of the first air carriers demonstrating unprecedented speed of transportation, the transition to large passenger aircraft with multiple piston engines, the replacement of these engines by gas turbines, the increase in cruising speed to supersonic, the continuous improvement in flight safety, etc. – all these milestones point to the urgent need for innovation in the aviation industry, which is ultimately the determining factor of its unshakable flagship position among other modes of transport.

In recent decades, a global trend towards automation of technological processes, including civil aviation processes, has clearly emerged in engineering and technology. Individual aircraft under human control can automatically perform all phases of flight, including takeoff, landing, avoidance of fixed obstacles, thunderstorms or other aircraft.

In addition, unmanned aircraft are gradually establishing themselves in the global aviation market in a qualitatively different way than traditional aviation. Although unmanned aerial vehicles (UAVs) are similar to manned aircraft in many ways, they do not require a human presence on board. However, the safety requirements for unmanned aerial vehicles in airspace are the same as for conventional manned aircraft.

Taking into account the above and realizing their leading role in the development of aviation technology, the staff of the National Aviation University over the past decade has made significant efforts to expand the scope of research in this area. The proposed publication is the result of many years of work of scientists and teaching staff of the university, which contains educational, methodological and scientific materials on mechanics, automation, communication systems, air navigation, feasibility studies, organization of aviation work and other important areas of technical and technological support for unmanned aircraft.

The book can be recommended to teachers, as well as to students and postgraduate students, doctoral candidates and a wide range of readers interested in the current state of technology in civil aviation, in particular unmanned aerial vehicles.

Chapter 1

UNMANNED AERIAL SYSTEM AS PART OF THE AIR TRANSPORT INDUSTRY

1.1. Development of unmanned aviation as a component of the air transport industry

Regulatory documents, in particular developed by International Civil Aviation Organization (ICAO), define air transportation and aviation works (AW) as a part of the implementation of the air transport industry functions. As for the ratio in volume, in general, transportation volumes take the lion's share. However, it is known that the volume of work performed by civil aviation also significantly affects both the development of the aviation industry and the efficiency of industries in which production involves the use of aviation. Therefore, the study of the formation of the market of aviation works is an urgent problem. In this context, the problem of forming the very structure of the aviation transport system is becoming important.

To establish the system-forming factors in the field of aviation works, it is important to first refer to the main regulatory document of civil aviation – the Air Code of the Ukraine. It provides definitions of air transportation and aerial work, particularly for Ukraine [1].

Thus, according to the Air Code, aviation works are flights during which an aircraft is used to provide specialized services (aviation chemical works, aerial photography, patrolling, etc.).

Accordingly, air transportation – is services for the carriage of passengers, cargo, and mail by air.

It is obvious that in the very definitions the foundation of system formation is laid, in which the common denominator is air transport. However, in order to further detail the terminology and content component, as well as to clarify the factors that determine the full range of aviation works, it is first necessary to establish elements and connections in a holistic air-transport system.

First of all, the Air Code divides aviation into state and civil. The transport function is performed by both parts, but state aviation is used in military, customs and border services, civil defence service, and law enforcement agencies. The costs are covered by the state budget. Accordingly, the commercial component is inherent only in civil aviation. The Air Code also

distinguishes in civil aviation «general aviation», i.e., not used for commercial regular air transportation and aviation work.

Regarding revenue generation, only the segment of airlines authorized to do so belongs to commercial aviation. It is embedded in the system of approvals/permits implemented by dividing the operating airlines into companies entitled to certain types of activities, i.e [2]:

A1 – passenger transportation;

A2 – freight transportation (including E11 – transportation of dangerous goods);

A3 – medical care;

A4 – aviation works.

Based on this, airlines using aircraft with permits for types A1 and A2 are not allowed to perform aviation works.

Thus, we can assume that at its core airlines with permits A3 and A4, taking into account all their relationships with each other and with the external environment, form a specialized system with the characteristics of «transport», which gives grounds for introducing the concept of «Transport System of Special-purpose Aviation» (TSSA). It is focused on the use of aircraft to provide specialized types of service, namely [3-4]:

- aviation chemical works;
- aerial survey flights;
- patrolling;
- sanitary service of the population;
- construction and installation works, etc.

Given the above facts, it can be concluded that the Transport System of Special-purpose Aviation is a component in the structure of the country's aviation transport system.

Based on the analysis, a structural scheme of the country's aviation transport system is developed, which is presented in Fig. 1.1. As can be seen, the Transport System of Special-purpose Aviation includes those airlines that provide services for various types of aviation works [5].

Without going into the details of certain types of aviation works, we should also pay attention to the formation of the structure of the modern aviation work market (Fig. 1.2). In fact, the specificity of the modern market is that it is already formed on the basis of orders from consumers of aviation works to operating companies with manned and unmanned aerial vehicles (UAV). The market known so far does not yet contain a component – companies with unmanned aerial vehicles [6].

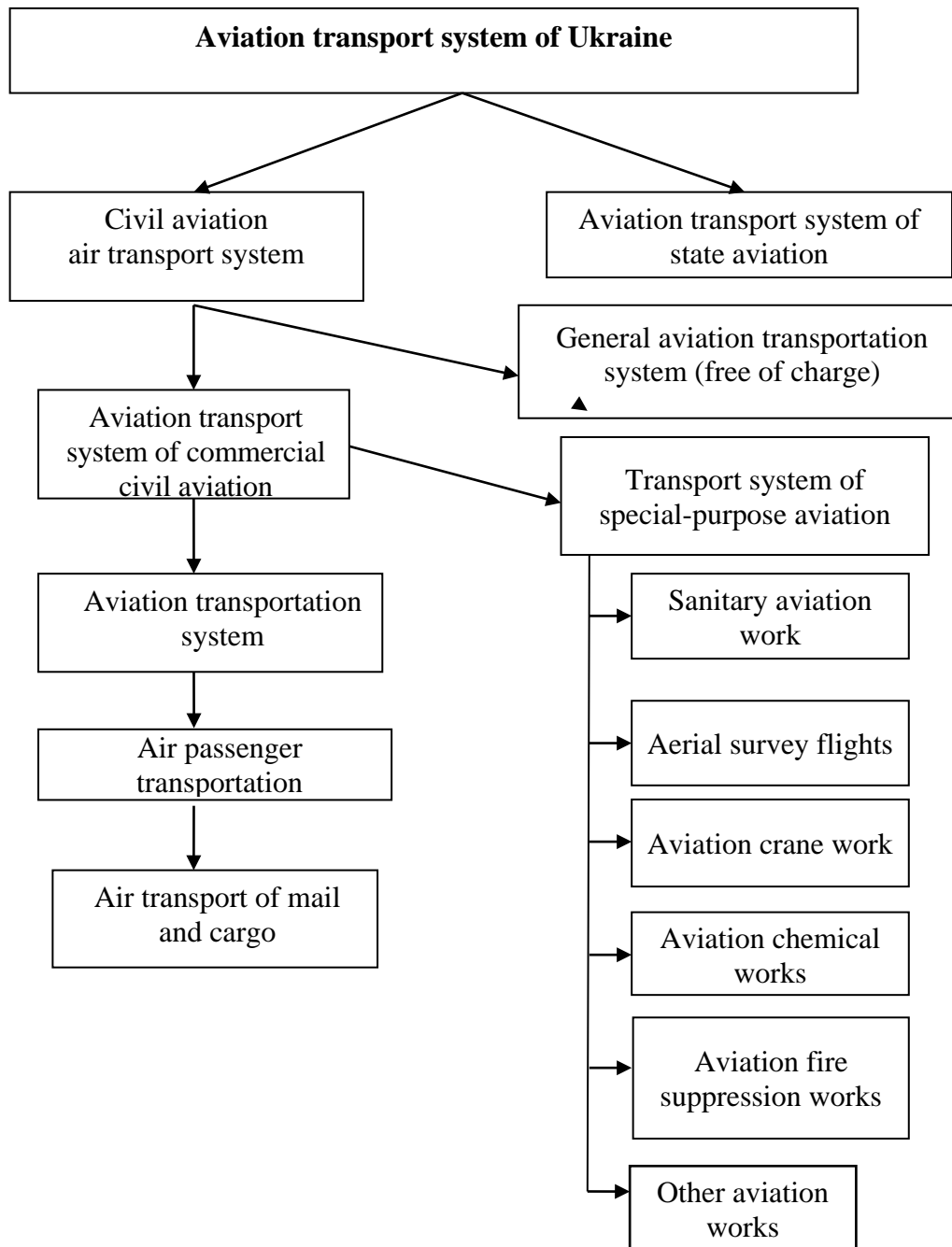


Fig. 1.1. The structural diagram of the aviation transport system of Ukraine

The fact that new «players» will appear in the market – operating airlines equipped with UAVs will contribute to a significant expansion of the aviation work market, as UAVs have certain specific properties that are a significant market resource. These include significant independence from the human factor, the ability to stay in the air without landing for a long time, low fuel consumption, and so on. For example, it is the company «Drone.ua» situated in Ukraine.

Therefore, in the near future, airlines using UAVs will constitute a significant share of the potential market for aviation work [7].

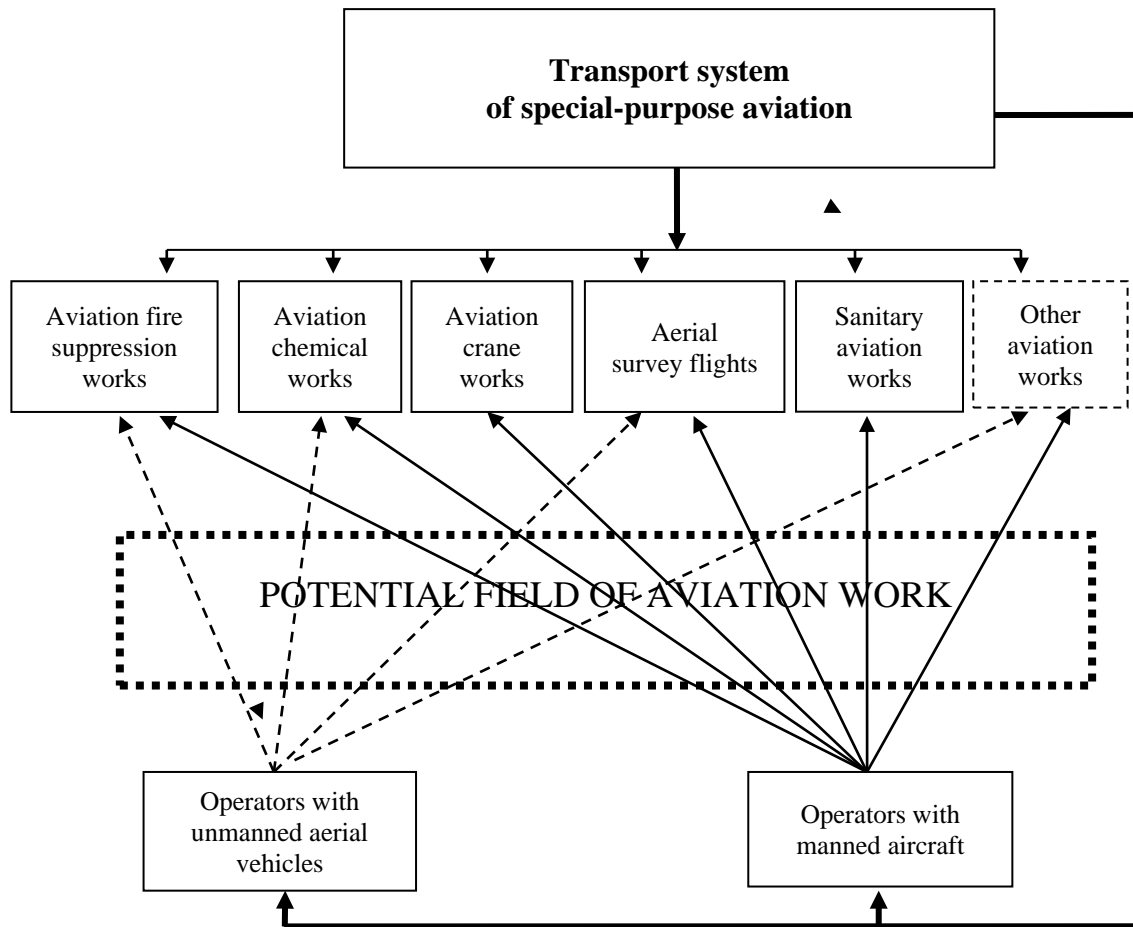


Fig. 1.2. Structure of the formation of the modern market of aviation works in Ukraine

1.2. Formation of the unmanned aerial system concept as a component of civil aviation system

The very issue of the commercial use of unmanned aerial vehicles in Civil Aviation (CA) is gradually becoming more topical given the global trends in the development of unmanned aviation in general. The development analysis of existing UAVs in the world over the past 20 years shows a steady trend to increase their size and weight, as well as altitude and endurance, and, ultimately, their number.

On the basis of the applications and scientific developments at the time of 2005–2007, one of the first UAV classifications was formed, based on the difference in take-off weight, speed, altitude, and the range of UAV flights (Table 1.1).

Table 1.1

Classification of UAVs by weight, flight altitude, endurance, and range

Acronym	Name of category	Weight, kg	Range, km	Flight altitude, m	Endurance, hours
TACTICAL UAVs					
micro	Micro	≤ 5	≤ 10	250	1
mini	Mini	$\leq 20/25/30/150$	≤ 10	150/250/300	≤ 2
CR	Close Range	25–150	10–30	3000	2–4
SR	Short Range	50–250	30–70	3000	3–6
MR	Medium Range	150–500	70–200	5000	6–10
MRE	Medium Range Endurance	500–1500	≥ 500	8000	10–18
LADP	Low Altitude Deep Penetration	250–2500	≥ 250	50–9000	0,5–1
LALE	Low Altitude Long Endurance	15–25	≥ 500	3000	≥ 24
MALE	Medium Altitude Long Endurance	1000–1500	≥ 500	5000–8000	24–28
STRATEGIC UAVs					
HALE	High Altitude Long Endurance	2500–5000	≥ 2000	20 000	24–48
Strato	Stratospheric	≥ 2500	≥ 2000	$\geq 20 000$	≥ 48
EXO	Exo-stratospheric	–	–	$\geq 30 500$	–
SPECIAL-TASK					
UCAV	Unmanned Combat Aerial Vehicles	≥ 1000	+/- 1500	12 000	2
LET	Lethal	–	300	4000	3–4
DEC	Decoys	150–500	0–500	50–5000	≤ 4

Besides, UAVs can be classified according to the following characteristics:

- by the method of creating lift: planes, helicopters, others;
- by the method of flight control: radio-controlled, automatic, combined;
- by the type of power plant: a reciprocating engine, a gas-turbine engine;
- electrical and others;

– by the method of transportation: light weight for manual transportation, heavy to transport by vehicles.

Undoubtedly, it is possible to apply other approaches in the selection of UAV classification criteria. However, it is well known that UAVs cannot perform their functions in isolation, apart from the so-called automatic. And even automatic UAVs at the time of activation require ground/basic service, which indicates the existence of a certain system which is called the – unmanned aerial systems (UAS). Conceptually, we can assume that the UAS consists of a UAV and a ground (aerial, overwater) control point and communication lines. In order for the UAV to be able to fly, the UAS must consist of the following elements:

- UAV itself;
- UAV control stations;
- software and systems for monitoring the condition of the UAV board;
- communication means (ground/air and air/ground) for air traffic control and the payload of a UAV;
- data processing terminals;
- landing system;
- launch systems and in-flight recovery systems;
- equipment for maintenance and controlling the state of the UAV and its systems;
- UAS storage and transportation systems.

Besides, the UAS should be serviced by qualified ground personnel.

Accordingly, in terms of systems analysis, the UAS – is an aircraft and related elements that are operated without a pilot on board.

The above facts indicate, first of all, only the functionality of the UAS – i.e. its ability to perform its direct function – of flying without a pilot on board. However, from the point of view of civil aviation, namely, from the point of view of the International Civil Aviation Organization, the UAS should become full air traffic participants.

Today there is a positive experience of UAS operation in some countries, in particular the «Altair» UAV in the United States [8].

As already established, the unmanned aerial systems consists of the aircraft itself, the ground control station and the corresponding communication lines. If the first two components are original and not related to the external environment, the communication lines, in addition to directly attaching a UAV to the ground station, act as an integrator of a UAV and a ground station to the environment, especially in air traffic management.

According to the policy adopted in the United States of America, UAS flights must be transparent and uninterrupted. This means that the UAS must meet the requirements for

navigation characteristics, taking into account the type of flight and the area of airspace in which the flight will be performed.

Article 8 of the «Convention on international civil aviation», signed in Chicago on December 7, 1944 and amended by the ICAO Assembly, states: «No unmanned aircraft shall fly unmanned over the territory of the contracting state except with the special permission of that state and in accordance with the terms of such agreement» [9].

The Global Conception of air traffic management has the following definition: «An unmanned aerial vehicle is an aircraft without a pilot as specified by article 8 of the «Convention...» that flies without an aircraft commander on board and is either completely remotely controlled from another location (from the ground, from another aircraft, from space), or is programmed and fully autonomous». This interpretation of the UAV was approved by the 35th session of the ICAO Assembly, regardless of whether UAVs are remotely piloted, fully autonomous or are some combination of such aircraft; all these kinds of UAVs are subject to the provisions [10].

The 11th Air Navigation Conference approved the global concept of Air Traffic Management (ATM) and has the following interpretation: «An unmanned aerial vehicle is an aircraft without a pilot according to article 8 of the «Convention on international civil aviation», which flies without an aircraft commander on board and or is completely remotely controlled from another location (from the ground, from another aircraft, from space), or is programmed and fully autonomous».

Pursuant to article 12 and Annex 2 of the «Convention...», the pilot-in-command shall be responsible for the performance of the aircraft's flight in accordance with the flight rules. This also applies to the authority to dispose the aircraft of which he is the commander. For the UAV, this is also true regardless of the fact that the commander is outside the aircraft.

Currently, the definition of the UAV according to the Air Code of Ukraine is as follows: an unmanned aircraft (UA) – is an aircraft designed to fly without a pilot on board, flight control and control of which is carried out by a special control station located outside the aircraft [11].

ICAO Circular № 329 provides the following key definitions for the UAS.

1. Unmanned aerial systems – is an aircraft and related elements that are operated without a pilot on board.
2. Unmanned aerial vehicle – is an aircraft that is designed to fly without a pilot on board.
3. Remote pilot – is a person who controls remotely piloted aircraft systems during flight.
4. Remote pilot's station – is a workstation from which a pilot controls the flight of an unmanned aircraft.
5. Remote crew member – is a crew member holding a «crew member» certificate who is responsible for the control of remotely piloted aircraft in flight [12].

The most important factor is the safe integration of the UAS into designated airspace and it will be their ability to operate and respond in the same way as aircraft with a pilot on board. Many components of this capability will be determined by technology – the ability of the aircraft to execute the control commands of an remote pilot and act as a link between the remote pilot and the Air Traffic Control Authority (ATCA), maintain the necessary performance (e.g. time and continuity of communication transactions) as well as the timely response of the aircraft to the ATCA's instructions.

In addition, ICAO's principal view on the UAS is that they will not carry passengers on board for a fee in the foreseeable future.

The UAS remote pilot and the pilot on board the aircraft have a similar ultimate responsibility for the safe flight of their aircraft and therefore must have the same level of knowledge in the field of air law, flight production and planning, flight loads, human factors, meteorology, navigation, operating procedures, flight principles, and radiotelephony. Pilots of both aircraft types must undergo flight training, demonstrate their skills, and gain some experience and relevant certificates. They must also be fluent in the language used in radiotelephony, meet the criteria for health fitness, although the latter may vary depending on the conditions of the UAS use.

The technical means used on unmanned aerial vehicles and aircraft with a pilot on board are constantly evolving; the role of automation is also growing accordingly, especially on transport aircraft. Automated systems are already able to actuate controls, maintain the course of an aircraft, regulate fuel consumption, transmit and receive data from various ground stations, detect conflict situations, and provide recommendations for resolving the risk of collision, create and maintain optimal decent profiles, and in some cases even perform take-off or landing procedures. Naturally, all these functions must be controlled by a remote pilot.

It follows that from the point of view of official civil aviation and the bodies that establish the aircraft's compliance with current standards in the industry, the UAS definition can be presented as follows: the UAS – is a set of configurable elements, which includes a remotely piloted aircraft, the associated station (stations) of the remote pilot, the necessary control and monitoring lines, as well as any other elements of the system that may be required at any time during the flight [13].

If we consider the current practice of UAV use and the requirements that are applied to it, it is necessary to clarify the very definition of the UAS for civil commercial aviation.

First of all, it is known that «civil aviation – is aviation used to meet the needs of the economy and citizens in air transportation and aviation works, as well as to perform flights for private purposes» [14]. Another provision that helps clarify the environment in which the UAS

should operate is that it will perform «aviation works – flights in which an aircraft is used to provide specialized services (aviation chemical works, aerial survey flights, patrolling, etc)».

The Air Code defines a UAV as «an aircraft designed to fly without a pilot on board controlled by a special control station located outside the aircraft».

According to the ICAO conception, UASs will operate in accordance with the ICAO standards for aircraft with a pilot on board and other special standards that reflect differences in operational and legal aspects, as well as flight safety aspects between piloted aircraft and unmanned aerial vehicles.

In order to ensure the UAS integration into the practice of using designated airspace and airfields, a pilot responsible for UAS flight is needed. Pilots may use appropriate equipment, such as the autopilot, to assist in the performance of their duties, but under no circumstances will the responsibility of the pilot be transferred to the technology in the near future.

In connection with the above facts, the final UAS definition that reflects the functionality and integration of UASs into the common airspace can be formulated as follows: unmanned aerial systems is a set of configured elements, which includes a UAV, a remote pilot station (RPS), necessary control and monitoring lines, as well as any other elements of the system that may be required at any time during the flight to ensure that the UAV is located in the designated airspace with an appropriate level of aviation safety. Based on the above, we can presumably determine the UAS composition.

Unmanned aerial vehicle:

1. UAV glider.
2. UAV power plants.
3. UAV control system including autopilot.
4. On-board UAV navigation system.
5. Air signal reception system.
6. On-board electrical system.
7. Other UAV vitally important system.
8. UAV target load.

UAV ground control station (GCS):

1. Workstation (W1) of the remote pilot (UAV commander).
2. Workstation (W2) of the payload operator (remote UAV co-pilot).
3. Payload control system.
4. Target data terminal on board an UAV.
5. GCS tracking antenna system.
6. GCS power supply system.

7. UAV storage and transportation system.

Communication lines:

1. UAS radio command line.
2. UAS radio telemetric line.
3. Line for receiving satellite positioning signals.
4. Satellite line.
5. Remote pilot's radio communication system with Air Traffic Control (ATC) authority.
6. Target image transmission/reception radio line (video-, photo).

Other configured UAS elements:

1. UAV automatic landing system.
2. System of UAV launch and recovery in flight.
3. UAV parachute descent system and other elements.

1.3. Typical types of aviation work and requirements for their performance

Execution of aviation works in the branches of economy is carried out by civil aviation enterprises under agreements with interested organizations.

Flights for aviation work performance, depending on their purpose, rules, and technology are divided into the following types:

- aviation chemical work;
- aerial survey flights;
- forest aviation work;
- construction and installation, loading and unloading works;
- transport and communication works;
- aviation works in Arctic, Antarctic, and on the islands of the high seas and oceans;
- from seagoing vessels and offshore drilling rigs;
- to provide medical care to the population and for sanitary measures;
- for experimental and research activities.

Today the following types of aviation works are performed in Ukraine:

- 1) aviation works in agriculture;
- 2) forestry maintenance (aviation works to control forest pests and diseases; flights for the purpose of aviation protection of forests from fires);
- 3) all aerial survey flights types;
- 4) flights for the purpose of providing medical care to the population;

5) inspection flights of high-voltage networks and communication networks, gas pipelines, oil pipelines, product lines, rivers, canals, and highways;

6) all types of helicopter flights, including areas selected from the air, except for flights for the transportation of passengers, luggage and cargo by scheduled helicopters;

7) all types of flights with equipment or devices specially installed on board an aircraft, with specialists of the customer on board;

8) sightseeing flights in the city area;

9) flights on aircraft in the salon version;

10) all types of flights on aircraft to serve the sectors of the economy with landings on sites prepared on contractual terms with customers, and sites selected from the air [15].

Out of the 40 airlines that perform aviation works in the national economy, 30 are involved in agriculture and forestry.

The organization and execution of flights for various types of aviation works are carried out in accordance with the Guidelines, UAV flight operation manuals, technology or instructions for the types of work.

At each CA enterprise, on the territory of which aviation works are performed, a general instruction on the organization, flight management, and their provision are developed taking into account the performance of the types of work. When performing works in the areas of other enterprises, flights are performed according to the instructions of the departments of these areas, and in their absence – according to the instructions developed by the head (commander) of the unit to which the crew is subordinated, agreed with the heads of departments (enterprises) on the territory of which flights are performed.

Flights for aviation works are performed according to the Visual Flight Rules of (VFR), Special Visual Flight Rules (SVFR), and Instrument Flight Rules (IFR) in the weather conditions specified for this type of work.

Before starting work, as well as in case of a delay of the aircraft at the destination for a time exceeding the validity of a weather forecast, the aircraft commander must update the forecast, determine the actual weather and decide on the flight. Flights without a weather forecast are prohibited.

During flights for the performance of aviation works, the aircraft commander is obliged to maintain radio communication with the air traffic controller in whose control zone the aircraft is, at least once an hour.

The altitudes occupied by aircraft performing aviation works in a given area must be free from other aircraft. An Air Traffic Control (ATC) is obliged to inform adjacent airports and crews about the air situation in the area of operation.

In the areas of works to be performed, the required number of working aerodromes (water areas) and landing sites must be prepared, their fitting with equipment is carried out on a contractual basis by representatives of economic organizations under aviation specialists' control. Flight instructions are drawn up for each aerodrome (landing area).

Landing sites (working airfields) are usually selected as a result of ground surveys. In some cases, their selection from the air is allowed.

Flights with the selection of landing sites from the air include:

- flights in the course of which aircraft land on unprepared areas, as well as operations performed by a helicopter in the hovering mode outside the aerodrome;
- flights on airplanes (except for ACW) with landings, on temporary airfields and landing sites prepared by the «customer», where there are no means of radio communication and no flight control is carried out;
- primary helicopter flights (throughout the day) to temporary heliports and landing sites prepared by the «customer», where there are no means of radio communication and no flight control.

When working in isolation from the base airline, a flight assignment is issued for the entire period of work. The aircraft commander at the request of the representative of the «customer» for production purposes has the right to change the flight route and landing site within the area of operation with a prior notification of an air traffic controller.

The aircraft commander is prohibited from following the instructions of the «customer's» representative, which contradict flight assignments and requirements such as flying regulations-86. When performing aviation works after landing at the intermediate airdrome, and during repeated flights, and at the base aerodrome, the commander of the aircraft is allowed to make decisions, informing about it an air traffic controller following the conditions below:

- preparation for the upcoming flight was carried out in full before the start of work (according to the report of the aircraft commander);
- on the route, there were no changes in the main and spare aerodromes (landing sites) that interfere with the flight;
- weather forecast ensures the fulfilment of the flight assignment or it was received by radio;
- aircraft parking time does not exceed 1 hour.

In this case, the responsibility for the validity of the decision to depart rests with the aircraft commander.

When performing a forced landing outside the aerodrome, the aircraft commander must inspect the intended landing site before approaching to assess its size, slopes and a surface

condition. The inspection must start from the altitude of at least 100 m above the obstacles and be performed with a descent in the selected landing direction to the altitude of at least 10 m.

Flights on aviation works are performed in strict accordance with the assignment and flight request issued by the «customer». The aircraft commander is prohibited from performing flights not related to production purposes.

Aerial survey flights

Aerial surveys include:

- air photography;
- exploring and survey;
- aerial shooting;
- aerovisual flights.

Before the start of aerial surveys, the «customer» and the commanders of the CA units agree on the areas of work and flight routes with the corresponding departments and bodies of the air management (AM). It is allowed two aircraft to fly over one section at the same time, if the distance between parallel routes is not less than 20 km. Aerial surveys performed by a group of aircraft are governed by instructions approved by the State Aviation Administration of Ukraine (SAAU). At the same time, aircraft commanders must inform each other of their location. Before starting work, the commander of the aircraft has to perform a test flying over the survey area at a safe altitude. When performing aerial filming flights at the actual altitude of less than 50 m, turns are performed with a roll angle of not more than 30°, and with exhaust devices – not more than 20°.

Flights to perform aerial surveys in the Arctic, Antarctic, open sea islands and oceans are carried out in accordance with the requirements of the flight regulations, the Instruction on the organization and conduct of flights in these regions and guidance on types of surveys.

Exploring and survey flights

Exploring and survey flights are performed in order to conduct various types of aerogeophysical surveys. These flights are performed at extremely low altitudes. When performing search and survey flights on aircraft equipped with exhaust devices, the minimum allowable flight altitudes are increased by the length of the released cable, unless there are other restrictions for this aircraft or camera equipment. The flights of helicopters with exhaust devices in the absence of an automatic instantaneous cable cutter are prohibited.

When flying in the mountains it is necessary to follow the slopes on the windward side and illuminated by the sun. It is forbidden to shoot at mountain tops on a downwind slope while dangling. Performing survey flights against the sun in the plains and hills at the true altitudes of less than 100 m, and in the mountains – at less than 200 m at a sun height above the horizon of less than 15° and a course angle of less than 30° are prohibited.

Flights in closed valleys and mountain gorges, the width of which at a given altitude is less than three turning radii at a roll angle of 20° for an aircraft of this type, are prohibited [16].

Aerial shooting flights

Aerial shooting flights are performed for the purpose of geological mapping, remote sensing of the Earth, as well as monitoring the state of the environment. Flights are performed at low, medium and high altitudes, with a constant altitude on the barometric altimeter. These flights are performed on routes in the specified areas. The length of the shooting routes, the flight altitude, the distance between the routes and other flight parameters are set by the «customer» [17].

Aerovisual flights

Aerovisual flights are performed with the «customer's» observer on board the aircraft for the purpose of the visual inspection of objects and the observation of the situation on the ground (patrolling power lines, communication lines, gas and oil pipelines, product pipelines, rivers, canals, highways; ice reconnaissance; the exploration of fish and animal stocks; wildlife inventory, etc.). Flights are performed at low, medium and high altitudes.

Aerovisual flights are performed:

a) during the day:

– in the plain and hilly area with the visibility of not less than 2000 m and the height of cloud base of not less than 150 m;

– in the mountainous area (up to 2000 m) – with the visibility of not less than 5000 m and the height of cloud base of not less than 400 m;

– in mountainous area (above 2000 m) – with the visibility of not less than 10 000 m the height of cloud base of not less than 600 m;

b) at night:

– in the flat and hilly area – with the visibility of not less than 4000 m and the height of cloud base of not less than 450 m.

Aerovisual flights at night in the mountainous area are prohibited. Descent for detailed observation of objects is allowed to perform up to a height of at least 10 m above the obstacles, and when inspecting high-voltage power lines – to a height of at least 20 m above the supports.

Ice reconnaissance is performed on aircraft with two or more engines at flight altitudes of at least 100 m. In order to clarify the ice situation, the aircraft may get down to 50 m above the obstacles. If it is impossible to transfer to the ship an ice map or other documents using the on-board phototelegraphic equipment, it is allowed to deliver it by a drop-message container. In this case, the flight altitude above the ship's masts must be at least 25 m.

Flights over a place of fish concentration or sea animals are allowed to be performed at an altitude of at least 100 m.

Forest aviation works

Flights in forest aviation works are performed for the purpose of:

- aviation protection of forests;
- survey and accounting of forests;
- service of forest industry organizations (logging, wood floating and other departments).

Aviation protection and forest inspection flights are performed according to VFR in the specified areas. Descending over ground fires is allowed at the edge of the fire to a height above the tops of trees not less than 200 m on planes and 100 m – on helicopters. Flights over fires as well as in smoky areas with visibility less than it is established for VFR are prohibited.

Message dropping at report reception points is carried out from a height above the obstacles not less than:

- in the plains and mountain valleys with a width of more than 1500 m – 50 m;
- in the mountains – 100 m.

In message dropping, it is forbidden to:

- perform approaches and U-turns up the slope;
- in case of a severe bumpiness to approach steep slopes, mountains at a distance of less than 300 m;
- perform evolutions over report reception points in order to attract attention at a height below the safe one.

Active fire extinguishing flights with the use of drainage devices, artificial precipitation, the use of parachutes, lowering equipment as well as dumping, and the delivery of explosives are carried out in accordance with the Forestry Aviation Manual.

Performing flights to serve organizations of the forest industry, logging, wood floating and other agencies is carried out in accordance with the Forestry Aviation Manual [18].

Air photography

Air photography flights are performed in order to photograph the area from an aircraft equipped with aerial photography equipment. Flights over air photography areas are performed at specified altitudes at a standard atmospheric pressure of 760 mm Hg. (1013,2 mbar). Flights from site to site, as well as changes in the height of photography are made with the permission of an air traffic controller. When performing air photography with the autopilot on, the aircraft commander has the right to transfer autopilot control to navigator-aerial photography ensuring constant control over the maintenance of the flight mode [19].

1.4. Global experience and trends in the application of unmanned aerial vehicles in civil aviation

Most UAVs today are considered to be full participants in modern military systems. The first mention of UAVs dates back to the 1920s, when in England the «DH» Company used a radio-controlled «Tiger Mot» biplane to train artillerymen. UAVs became widely known during World War II, such as the Hs239A (Germany) and «Baka» (Japan) cruise missiles, etc. In the 1930s, small drones appeared in America, which were used in radio control mode for various military purposes [20].

A deep military interest in UAVs was caused by a number of factors. First of all, the idea of transferring a person from the aircraft to the ground led to the taking out from the aircraft of equipment for human protection and service. As a result, its mass decreased; for example, if you convert a single light aircraft weighing of about 400 kg into an unmanned version, you can lighten it by 130...160 kg. This ultimately affects its value. Low-power engines are used in UAVs, it allows saving fuel costs dramatically.

Another source of the effectiveness of military UAVs is the reduction in the level of psychological tension for a person in extreme situations and the absence of flight personnel loss, which is perhaps the most important in the process of military operations. One of the main advantages of UAVs is that with the appropriate level of automation, they can perform a monotonous «rough» work for a long time, «without getting tired», which usually affects the quality of its implementation. In addition, UAVs can perform missions that are not possible for manned aircraft (e.g. indoor flights, in limited volumes atmosphere, etc.).

In addition, UAVs do not need concrete airfields. A dirt runway is sufficient, or a catapult launch can be used. In fact, most of these advantages are fully applicable to civilian UAVs as well.

Reports on civilian UAVs began to appear in the mid-1960s. The driving force behind this was the appearance on the market of portable remote-control (PRC) systems, which allowed operating large aircraft models with high reliability. Even then, the remote-control systems was characterized by low size (weight of the onboard part was 0,45...0,5 kg), proportional detection of deviations of the control levers and steering surfaces, sufficient range (within 2000 m), high reliability and moderate cost (in 1973, the European price for the six-channel remote-control systems «Varioprop-12» was 1670 German marks).

At the same time, studies started on the effectiveness of UAVs in remote monitoring of land and water surfaces, patrolling forests for early detection of fires, damage to power lines and pipelines, aerial work in the agricultural production, in fields and gardens.

Thus, in the 1970s, the Moscow aviation institute together with the Research institute of biological methods of plant protection (Kishinev) began to study the effectiveness of UAV application in the field of land surface mapping and biological protection of plants. The well-known researcher and designer V. Makeev made a conclusion about high efficiency of using UAV in mapping and aerial photography. At the same time, he noted that in plant protection the efficiency of UAV is high when they are used for processing small fields and fields that are difficult to access for «big aviation».

In 1983 in Moscow and Kursk an international seminar on the problems of unmanned aircraft application in the «Intercosmos» program was held. At the same time there were practical demonstrations of some works, including the UAV of the Warsaw institute of cartography Dr. A. Nowoselski.

The unmanned aircraft was equipped with a soft wing, a STG 71 single-cylinder piston engine with a displacement of 12 cm³, and a NAC MV 470 multispectral camera with four lenses. There was also a demonstration of the UAV «Sky Eyes» by «Developmentale Sciences Inc.» of California, R4E [21].

However, as the practice of modern production shows, there is no real «entry» of UAVs into civilian technological processes today, with the exception of such non-production sectors as scientific experiments, cinema, sports, entertainment industry, etc. Civilian UAVs are not yet technological machines. It can be assumed that their application is in the initial phase of the life cycle, characterized by a significant level of development, the UAVs themselves and their elements, on the one hand, and the lack of a basis for the use of UAVs in real technological processes, on the other. The resolution of this contradiction requires the solution of diverse tasks of conceptual, technical, technological, methodological, organizational and legally regulatory nature.

The analysis of the existing UAVs development in the world today reveals a strong trend to an increase in their size and weight, as well as the flight altitude and endurance. UAVs with a large mass can stay in the air longer, fly higher and continue to «see». The demand for UAVs of the «maxi» class is very high. They can change the situation in the global aircraft market. The most famous of them is «Global Hawk» (Fig. 1.3) climbing to the height of 20 km, it weighs 11,5 tons and has a cruising endurance of more than 24 hours. It is equipped with a turbojet.

Relatively recently, the concept of a «flying platform» was developed, according to which UAVs began to be constructed, providing the best conditions for placing a payload on them. By connecting the payload with on-board systems, you can get a full-fledged integrated complex, equipped with electronic equipment to the fullest extent (Fig. 1.4). It will be a qualitatively new type of aviation equipment – a stratospheric platform for carrying out tasks that are either beyond the power of low-, medium-altitude and unmanned aerial vehicles, or require unreasonably high costs when performed by the satellite fleet.



Fig. 1.3. UAV «Global Hawk» (Northrop Grumman, USA)



Fig. 1.4. Multipurpose UAV «Proteus» (USA)

In the civilian sphere, UAVs can also bring great benefits and savings. Their capabilities largely depend on the altitude. Today the limit is 20 km, and in the future, it is going to be up to 30 km. At this altitude, UAVs can compete with a satellite. Tracking everything that happens in an area of about a million square kilometres, it becomes a kind of an «aerodynamic satellite». UAVs can take over the functions of satellite constellations and perform them in real time throughout the region [22].

It is known that 24 satellites are needed to take photos and film movies from space or observe any object, but even then, information from them will come once an hour. The satellite is above the object of observation for only 15-20 minutes, and then goes out of its line of sight and returns to the same place, making a revolution around the Earth. The object during this time goes from a given point, because the Earth rotates, and again finds itself in it only after 24 hours.

Unlike the satellite, the UAV monitors the observation point constantly. After completing the task at an altitude of about 20 km for 24 hours, it returns to the base, and it is replaced by another one in the sky. Another UAV is in reserve. This is the main component of economic rationalization because an UAV is considerably cheaper than satellites. UAVs can also compete with satellites in the field of telecommunication networks and navigation systems. UAVs can be

used for continuous round-the-clock observation of the Earth's surface in a wide range of frequencies. Using them, you can create an information field of the country, covering the control and management of air and water transport, as UAVs are able to take over the functions of ground, air and satellite locators (common information from them gives a complete picture of what is happening in the sky, on water and land).

UAVs will help solve a range of scientific and applied problems related to geology, ecology, meteorology, zoology, agriculture, climate study, mineral exploration and more. They can monitor the migration of birds, mammals, fish, changes in meteorological conditions and ice conditions on rivers, the movement of ships, the movement of vehicles and people, do air photography and filming, radar and radiation reconnaissance, multispectral surface monitoring, penetrating to up to 100 meters, etc.

Nowadays, civilian UAVs can be used in the following areas:

1. Detection of small objects: airborne; surface; ground; search and rescue; assistance in emergencies.

2. Air traffic control: in hard-to-reach areas; in case of natural disasters and accidents; on temporary air routes when performing aviation works.

3. Maritime shipping control: search and detection of vessels; prevention of emergency situations in ports; control of sea borders; control of fishing rules.

4. Development of regional and interregional telecommunication networks: communication systems, including mobile ones; television and radio broadcasting; retransmission; navigation systems; advertising; TV; cinema.

5. Aerial surveys and control of the Earth's surface: air photography (cartography); inspection of compliance with contractual obligations («open sky» regime); control of hydro-, meteorological conditions; control of actively emitting objects; control of power lines, control over illegal migration; law enforcement activities (control of unauthorized riots); detection of forest fires; observation of the perimeter of objects; observation of industrial sites; control of railway tracks, control of power lines and other linear objects.

6. Environmental control: radiation control; gas chemical control; control of gas and oil pipelines; survey of seismic sensors; avalanche monitoring.

7. Application in agriculture and exploration; ACW execution; determination of soil characteristics; mineral exploration; subsurface (up to 100 m) sounding of the Earth.

8. Oceanology: ice reconnaissance; observation of sea waves; search for industrial fish concentration.

At present, the distribution of the world market demand for UAVs with high altitude and flight time can be represented as shown in Fig. 1.5.

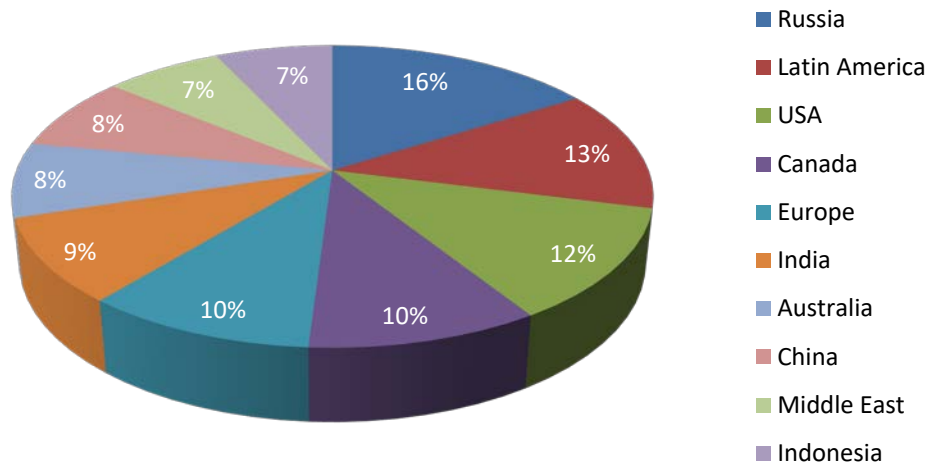


Fig. 1.5. Global market demand for UAVs with high altitude and flight time

In addition, global trends in UAV production and application show a rapid growth trend throughout 2005–2012. In particular, Fig. 1.6 shows that the absolute first place is held by military UAVs, which amounted to about 700 projects in 2009. The second position is held by double-purpose UAVs – 350 projects in 2012. The third position – is held by civilian UAVs, about 220 projects. In terms of the relatively small number of civilian developments and applications, there is a significant increase, which was about 350 % compared with 2006 (60 vs. 220 projects and applications) [23].

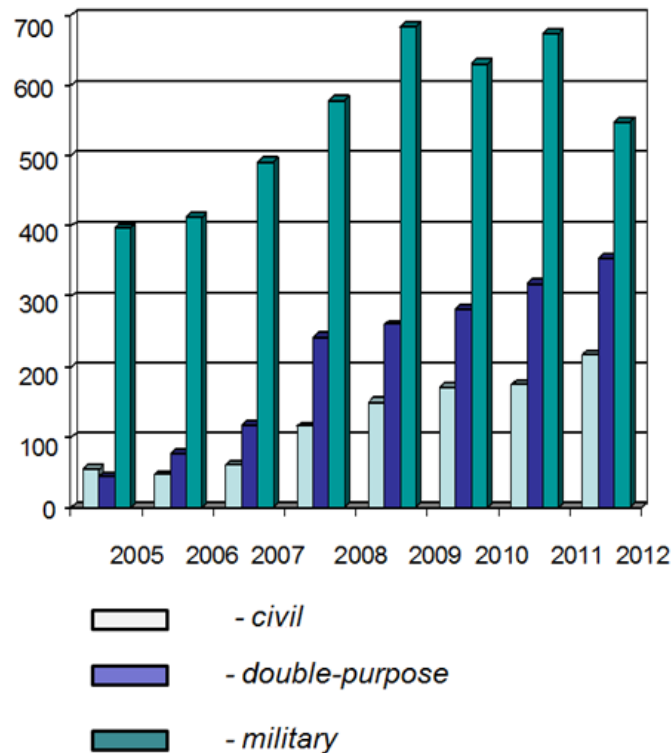


Fig. 1.6. Growth in UAV production and use worldwide (2005–2012)

In terms of the regional distribution of developments and applications worldwide, we can look at the distribution in European countries (Fig. 1.7). The diagram shows that the most developed countries – the Great Britain, Germany and France – lead the way. They account for 248 of the 336 projects, or around 73 %.

The remaining 27 % are assigned to countries with less developed economies or with economies in transition. In particular, as of 2012 Ukraine was represented by 18 projects, including the «Remez» UAV (Kharkiv), the M-7-V5 «Nebesniy patrol» UAV (Kyiv) and others.

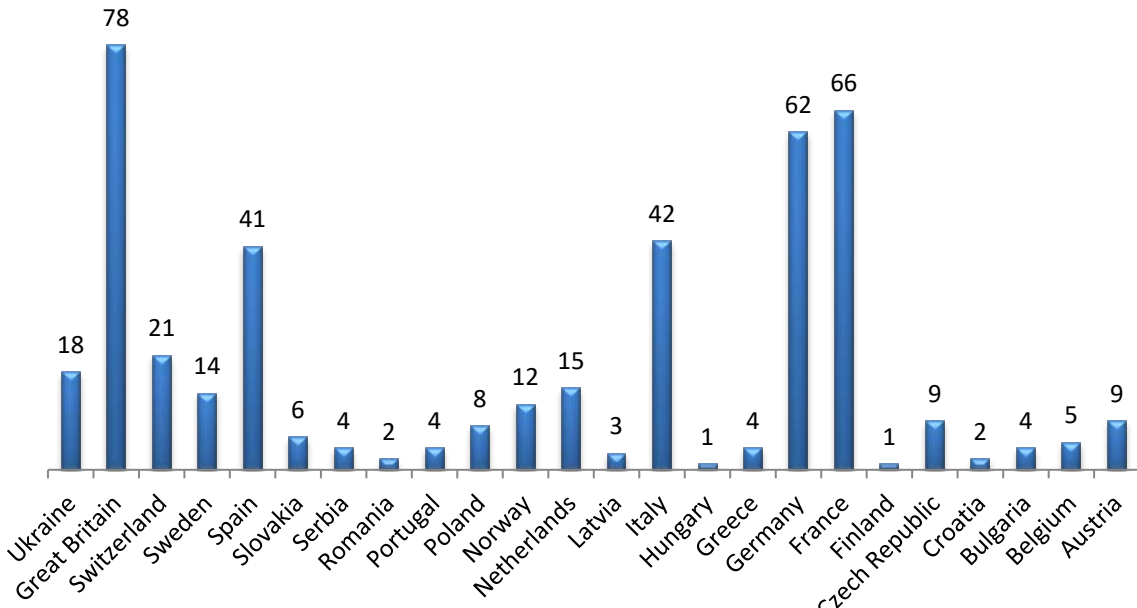


Fig. 1.7. Distribution of the number of UAV developments (335 units) in Europe (by developer country as of 2012)

According to statistics, during the period 2011–2020, the military UAV market is shared by the USA, China, Israel, Russian Federation, Latin American countries, Great Britain, Italy, and France. The ratio of global UAV market shares for the period 2011–2020 can be cited as follows:

- USA – 56 %;
- China – 12 %;
- Israel – 9 %;
- Russian Federation – 8 %;
- Latin American countries – 6 %;
- Great Britain – 3 %;
- Italy – 2 %;
- France – 2 %.

«Jane's» experts suggest that the USA will remain the most influential «player» in this market over the next 10 years, and its UASs will be the most technologically advanced.

1.5. Current status and operation of unmanned aerial vehicles in Ukraine

Procedure for the use of airspace by unmanned aerial vehicles.

According to the requirements of clause 4, section II of the Rules of Airspace Use, flights by unmanned aerial vehicles up to and including 20 kg shall be performed without applying for airspace use, without obtaining airspace use permits, without informing the Ukrainian Armed Forces Air Force and of the joint civil-military air traffic management system of Ukraine, of the State Border Guard Service of Ukraine, air traffic service authorities and departmental air traffic control authorities, subject to compliance with the following requirements [24]:

- 1) flights are operated without crossing the state border of Ukraine;
- 2) flights are performed outside the established prohibitions and restrictions on the use of airspace, except as specified in the Airspace Use Regulation;
- 3) flights shall not be performed closer than 5 km from the outer boundaries of airfield runways or closer than 3 km from the outer boundaries of a runway/helicopter pad, except as agreed upon with the airfield/runway/helicopter pad operator;
- 4) flights are carried out no closer than 500 m to manned aircraft;
- 5) flights are not carried out over:
 - crowds of people in open spaces and over densely built-up areas;
 - facilities (zones) defined by the Ministry of Defence of Ukraine, the Ministry of Infrastructure of Ukraine, the Ministry of Internal Affairs of Ukraine, the State Border Guard Service of Ukraine, the Security Service of Ukraine, the National Police of Ukraine, the National Guard of Ukraine, the State Fiscal Service of Ukraine, the Foreign Intelligence Service of Ukraine, the State Guard Department of Ukraine, other military formations and law enforcement structures established in accordance with the laws of Ukraine, and for which protection / state protection is provided (provided that the area around these facilities is marked with information signs prohibiting unmanned aerial vehicles flights and/or by making public the boundaries of such a prohibition), except when flights are authorized by the above-mentioned authorities;
- 6) flights are carried out visual line-of-sight (VLOS);
- 7) maximum flight altitude no higher than:
 - 120 m above ground (water) surface level outside CTR, AFIZ, ATCA, ATCZ, specially designated areas, other specially reserved airspace; 50 m above ground (water)

surface level within CTR, AFIZ, ATCA, ATCZ, specially designated areas, other specially reserved airspace, if no information on the actual status of the airspace structure is available at the time of flight;

– 50 m above static obstacles at a horizontal distance of not more than 100 m from such obstacles, as a deviation from the height limits stated above, at the request of the owner of such a facility;

8) the flight speed of the unmanned aerial vehicles is a maximum of 160 km/h.

In other cases, flights of unmanned aircraft up to and including 20 kg and all flights of unmanned aircraft over 20 kg shall, without exception, be performed within specially designated areas and routes in compliance with the requirements for applying for airspace use, obtaining permissions and conditions of airspace use, informing the Ukrainian Armed Forces Air Force command authority, Ukrainian State Border Guard Service authorities, and of the joint civil-military air traffic management system of Ukraine, air traffic service authorities and departmental air traffic control authorities.

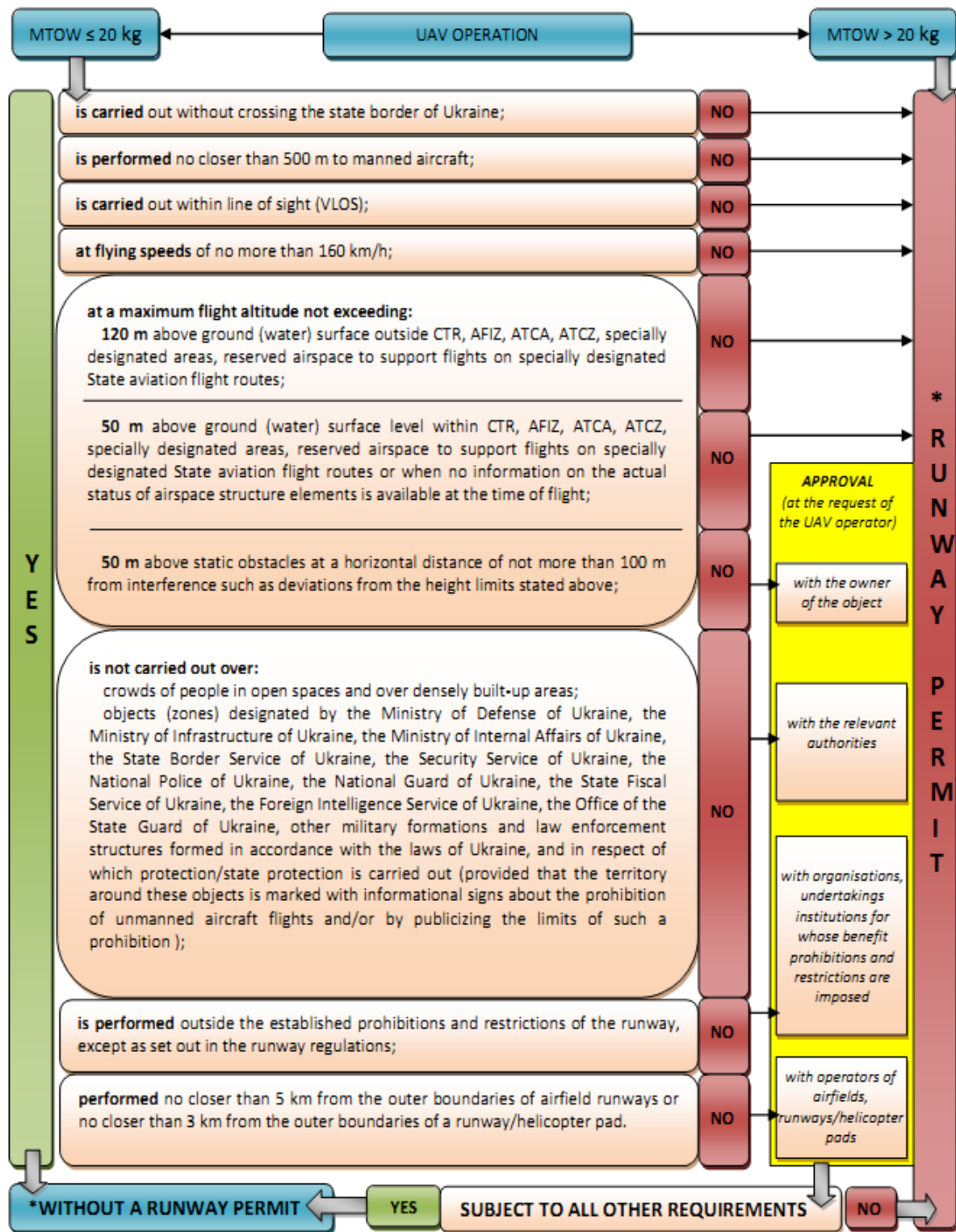
The procedure for obtaining permission to use airspace.

If it is necessary to apply for and obtain permission for the use of airspace as stipulated in the Aviation regulations of Ukraine «Rules of airspace use of Ukraine», operators of unmanned aerial vehicles should [25]:

- i. register in the Ukraerocenter database;
- ii. after confirmation of registration submit to Ukraerocenter a request for use of airspace in RUN format. Ukraerocenter processes airspace usage requests only from airspace users registered in its database;
- iii. add copies of permits/agreements to the airspace application (*if necessary*).

After submitting an application for the use of airspace, airspace users receive an e-mail informing them of the inclusion of the application in the airspace use plan, allowing airspace use, or prohibiting airspace use with the specified reason for the prohibition.

Where the Rules provide for an application for the use of airspace, airspace users may only fly unmanned aerial vehicles after obtaining permission to use airspace (i.e. when the application for the use of airspace is included in the airspace usage plan), to request and obtain airspace usage conditions, to inform Ukrainian Armed Forces Air Force command authority and, if necessary, the Ukrainian State Border Guard Service authorities. Corresponding schemes for permission and location in Ukraine of areas prohibited for UAV flights are presented in Fig. 1.8 and 1.9, respectively.



*The permissive procedure for runways involves applying for runways, obtaining runway permits, informing the Air Force of Ukraine and the Joint Civil-Military System authorities, the Ukrainian State Border Guard Service authorities, air traffic service authorities and departmental air traffic control authorities.

Fig. 1.8. Scheme of airspace clearance for unmanned aerial vehicles in Ukraine
(according to <https://avia.gov.ua/>)

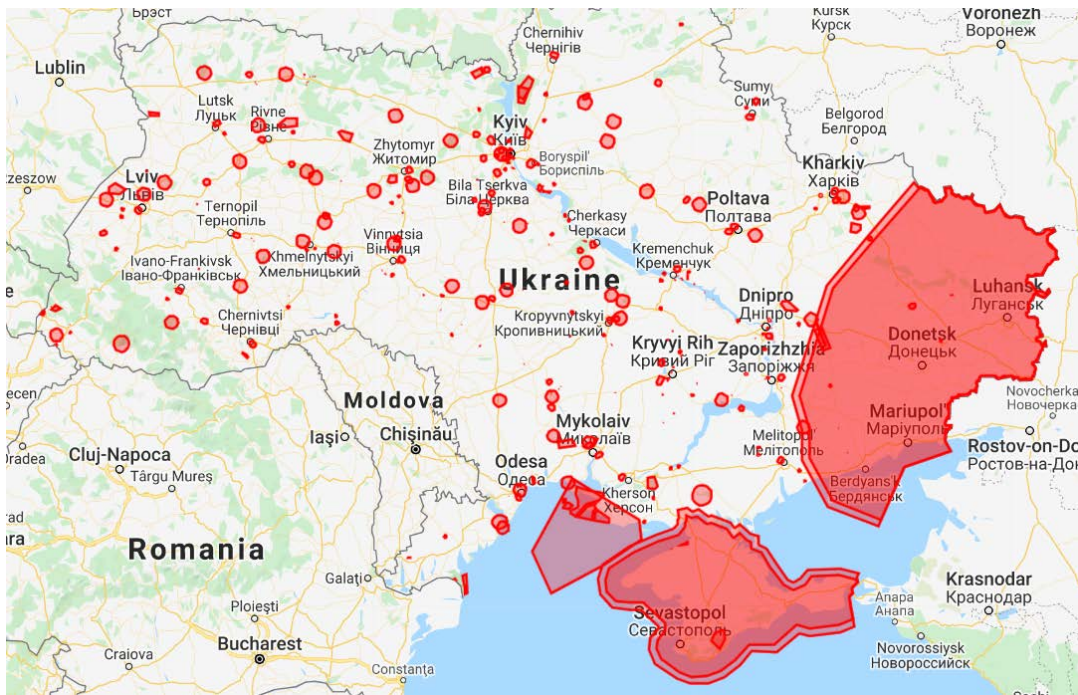


Fig. 1.9. Placement of UAV flight prohibited areas in Ukraine (based on <https://avia.gov.ua/>)

Airspace users flying unmanned aerial vehicle shall, on the basis of an application submitted and an airspace use permit obtained, arrange for operational telecommunication (in particular, mobile telecommunication) with:

- the chief air traffic controller (chief navigator) of the air traffic control centre (ATC) within whose area of responsibility unmanned aerial flights will take place;
- the command authority of the Air Force of the Armed Forces of Ukraine, within whose area of responsibility unmanned aerial vehicle flights will be carried out;
- air traffic authorities and air traffic control authorities in the case of flights within their areas of responsibility;
- with the State Border Guard Service of Ukraine – in case of flights within the zone with special regime of airspace use, established along the state border of Ukraine 25 km inland, for non-compliance with requirements of subparagraphs 1 – 8 of paragraph 4 of section II of the Rules or when the weight of an unmanned aerial vehicle exceeds 20 kg, for information on the activity of airspace use;
- at least one hour prior to the commencement of unmanned aircraft flights, by requesting permission and conditions for the use of the airspace to be determined of the air traffic control centre within which the unmanned aircraft are to fly, or by Ukrainian State Air Traffic Services Enterprise (UkSATSE) and provided to the user at least 30 minutes before the start of the flights;

–10 minutes prior to the scheduled commencement of flights, by informing the command authority of the Air Force of the Armed Forces of Ukraine and the air traffic control centre, within whose areas of responsibility unmanned aerial vehicle flights will be carried out, of the commencement of unmanned aerial vehicle flights, their cancellation or postponement of the start of flights;

–within 5 minutes of the actual time of the following events – the end of flights or a flight interruption of more than one hour;

–immediately – in the event of an emergency situation with an unmanned aircraft, an aviation event, a significant incident or incident, an emergency event (in particular, concerning the loss of control and monitoring line or transition of an unmanned aircraft into unguided flight), acts of unlawful interference with the control of an unmanned aircraft and cases with indications of violation of the airspace of Ukraine.

In order to perform flights within the temporary airspace restriction areas established in accordance with NOTAM, an unmanned aircraft operator shall additionally request, no later than one hour prior to the commencement of unmanned aircraft flights, permission to perform such flights from the authorities for whose benefit such restrictions are established, via Ukraerocenter.

If the activation of the temporarily reserved airspace zones (UKT-zones), restricted airspace zones (UKR-zones) and danger zones (UKD-zones) is planned for unmanned aircraft flights, an application to use the airspace of these zones shall be submitted by the entity/individual for whose benefit the zones are established.

Advice to remote pilots.

Remote pilots should be familiar with the relevant national regulations on safety, confidentiality, data protection, insurance, environmental protection and be mindful of the responsibility of carrying out each flight.

Before starting work, the remote pilot must [26]:

–be in a physical and mental condition that ensures the safe operation of unmanned aerial vehicles, and not suffer from any illness or injury that causes temporary or permanent disability and that may result in a sudden inability to control the unmanned aerial vehicle;

–be familiar with the UAV operator's manual;

–obtain updated information on the intended operation of the UAV, any restrictions on airspace use and flight conditions;

–familiarise themselves with the UAV flight area and check for conditions that may affect UAV flight, including the location of people, property, vehicles, roads, obstacles, airfields and other features to which the operation of the UAV may pose a threat;

–check that the weather conditions at the start of operation are compatible with the expected weather conditions over the entire period of operation as specified in the manufacturer's instructions;

–check lighting conditions and potential sources of electromagnetic energy that could cause undesirable effects, in particular electromagnetic interference or physical damage to UAV equipment;

–ensure that the UAV is airworthy for safe performance of the intended flight and that its mass, including payload and other restrictions, do not exceed the manufacturer's standards or limitations and comply with the manufacturer's instructions;

–make sure the geo-information data is up-to-date (if available);

–ensure that the UAV has sufficient propulsion power for its planned operation and for contingencies.

During the flight, the remote pilot must:

–ensure the safe operation of the UAV in relation to third parties on the ground and in the air by keeping the UAV at a safe distance from persons, animals, property, vehicles, airfields and airspace users;

–avoid manoeuvres that endanger the safe operation of the UAV and discontinue flight in case of danger to third parties;

–operate the UAV within the limitations set out in the manufacturer's instructions;

–conduct continuous close monitoring of the airspace around the UAV to track other aircraft to ensure flight safety;

–operate only one UAV at a time;

–comply with the prohibitions and restrictions on the use of airspace;

–not to use the UAV to drop any objects or transport dangerous goods, weapons, explosives and devices, other objects that can be used to commit an act of unlawful interference, except objects and substances used in agricultural, horticultural and forestry activities, and the transportation of these objects is not in conflict with the law;

–not to fly near or within areas where an aviation accident investigation or emergency response is in progress, unless authorised to do so.

List of references

1. The Air Code of Ukraine. Bulletin of the Verkhovna Rada of Ukraine. Approved 19.05.2011, № 25.
2. Ukrainian aviation industry results. Section «News». [Electronic resource]. Source access mode: www.avia.gov.ua – Screen title.
3. Matiychyk M. P., Yun G. M. Analysis of «small aviation» production processes by transport component: collected works of Kyiv University of Economics and Transport Technologies (KUETT). Ser. Economics and management. Issue. 11. 2008. P. 154–162.
4. Sarymsakov H. G. Agricultural aircraft. M.: Mashinostroenie, 1979. P. 43–64.
5. Derevyanko V. S. Application of aviation in sectors of the economy. Krasnodar: Sov. Kuban, 2002. P. 13–28.
6. Matiychyk M. P., Yun G. M., Mikhaylov G. M. Economic efficiency of plant protection with unmanned aerial vehicles: Proceedings of Kyiv University of Economics and Transport Technologies (KUETT). Ser. Economics and management. Vol. № 9. 2007. P. 175–181.
7. Vysotskaya I. I., Herasymenko I. M., Kachalo I. A. Development of Special Purpose Aviation as a component of Air Transport Industry. *Formation of market relations in Ukraine: collection of scientific works*. Vol. 3 (130) / Scient. ed. I. G. Mantsurov. K., 2012. P. 107 – 110.
8. Electronic resource: Past Projects: Altair UAV Technology Demonstrator. Source access mode: <https://www.nasa.gov/centers/dryden/history/pastprojects/Altair/index.html>.
9. Convention on International Civil Aviation. Doc ICAO 7300. Access to the source: <https://www.icao.int/publications/pages/doc7300.aspx>.
10. Global Air Traffic Management Operational Concept. Doc ICAO 9854. https://www.icao.int/Meetings/anconf12/Document%20Archive/9854_cons_en%5B1%5D.pdf.
11. The Air Code of Ukraine. Voice of Ukraine of 18.06.2011. № 110. Approved 19.05.2011; paragraphs: 1.2.2; 1.2.3; 1.2.14.
12. Eleventh Air Navigation Conference. Montreal. 22 September – 3 October 2003. Accessed from the source: [https://www.icao.int/Meetings/AMC/MA/Eleventh%20Air%20Navigation%20Conference%20\(ANConf11\)/anconf11_wp138_ru.pdf](https://www.icao.int/Meetings/AMC/MA/Eleventh%20Air%20Navigation%20Conference%20(ANConf11)/anconf11_wp138_ru.pdf).
13. Circular 328-AN/190 ICAO. Unmanned aerial systems: CIR328; ISBN 978-92-9231-780-5; 999 University Street, Montréal, Quebec, Canada H3C 5H7 © ICAO, 2011; 66.p. Source access mode: www.icao.int.
14. Kucheryaviy A. A. On-board information systems: course of lectures / ed. by V. A. Mishin, G. I. Klyuev. 2nd edition revised and supplemented. Ulyanovsk: Ulyanovsk State Technical University, 2004. 504 p.

15. On improving the classification of aviation works by type and purpose. MCA Order № 125. – M.: MCA, 1982. 3 p.
16. Flight Operations Manual for Civil Aviation of the USSR (FOM CA-85). Approved by Order № 77 of the USSR Minister of Civil Aviation dated 8 April 1985. 211 p.
17. Guidelines for navigating service in the civil aviation of the USSR (NGS CA-86). Approved by Minister of CA Bugaev B. P. on 10.07.1985. 315 p.
18. Electronic resource: www.avia.gov.ua // SAA of Ukraine. – Screen title.
19. Matiychyk M. P. Organization and technology of aerial survey works: lecture course. Kyiv: Publishing house of National Aviation University «NAU-Druk», 2009. 132 p.
20. Ganin S. M., Karpenko A. V. Unmanned Aerial Vehicles. St. Petersburg: Nevsky Bastion – Gangut, 1999. 160 p.
21. Matiychyk M. P., Bogolyubov V. M. Retrospects and modern problems of application of small-size radio-controlled aircraft. Kyiv. Scientific Notes of NaUKMA, 1999. Vol. 9. P. 371–377.
22. Marc Deli. Unmanned Aerial Vehicles. *Unmanned Aerial Vehicles and Targets*. IHS Jan'es. IHS Global Limited 2010. P 28–380.
23. RPAS. Remotelli piloted aircraft systems. The Global perspective. 2012/2013.10th Edition. June 2012 – Bluenburgh & CO. [Electronic resource]. Source access mode: www.uvs-info.com.
24. State Aviation Service of Ukraine. Unmanned Aerial Vehicle. [Electronic resource]. Source access mode: <https://avia.gov.ua/bezpilotni-povitryani-sudna-2/>.
25. State Aviation Service of Ukraine. Unmanned Aerial Vehicle. [Electronic resource]. Source access mode: <https://avia.gov.ua/poryadok-podannya-zayavok-na-vikoristannya-povitryanogo-prostoru/>.
26. State Aviation Service of Ukraine. Unmanned Aerial Vehicle. [Electronic resource]. Source access mode: <https://avia.gov.ua/zagalni-rekomendatsiyi-distantnijnim-pilotam-bps/>.

Chapter 2

RESEARCH OF FLIGHT TECHNICAL AND OTHER CHARACTERISTICS OF UAVs

2.1. Estimation of the main flight-technical characteristics of the unmanned plane M6-3T for carriage of small valuable cargoes

Unmanned aircraft (unmanned aircraft; abbreviated UAV M6-3T «Zhayvir» (in the following text UAV M6-3T) is designed to transport valuable cargo weighing up to 4 kg over a distance of 700 km in dedicated airspace at altitudes up to 1200 m and at a temperature of $-20\text{ }^{\circ}\text{C}$ to $+40\text{ }^{\circ}\text{C}$ (Fig. 2.1). The headwind limitations are up to -20 m/s and the side wind is -8 m/s .

The use of this UAV M6-3T for transportation is assumed within the framework of the existing infrastructure of civil aviation. The main control mode is automatic. Taxiing on the runway and taxiing into the parking lot is performed in «manual» mode by an remote pilot.



Fig. 2.1. View $\frac{3}{4}$ right on UAV M6-3T «Zhayvir»

Brief technical characteristics of the M6-3T. Unmanned aerial vehicle M6-3T «Zhayvir» (Fig. 2.2) is a single-engine free-carrying mid-plane with a V-tail. The power parts of the glider are made mainly of fiberglass and carbon fiber; the most loaded structural elements are made of aluminum alloys.

The fuselage is a semi-monocoque with a three-layer power cladding. Between the fuselage frames are located the main UAV systems. The top of the fuselage is covered by panels,

which contain electronic equipment, radio signal receivers and a rescue parachute. In turn, this equipment is covered with upper covers. The middle lid covers the compartment of a special cargo container. The front frame is power. The engine ignition unit is located on the opposite side of the front frame.

The landing gear is tricycle, it does not retract and is equipped with a front guide support. The wheels of the chassis rotate on ball bearings. To reduce the harmful aerodynamic drag wheel covers are provided. The main support is made of fiberglass. Spring front support material – D16T.

Single-spars wing design consisting of two removable planes. Spars wing spars made of fiberglass.

The sheath is rigid and made of two layers; outer layer of made fiberglass. The mechanization of the wing consists of two sections of a simple flaps. Elerons can also perform flaperone function (flaperone mode).

The V-shaped tail is described further. Stabilizer is performed with filler and rigid sheathing; outer layer of fiberglass. Rudder without spars and technologically executed similarly to the stabilizer.

The power plant includes a reciprocating single-cylinder engine MVVS-50 IRS with a three-bladed propeller constant pitch. Engine – gasoline, carburetor, two-stroke, air-cooled; it is fixed on the through the silent-blocks to the power frame. The engine compartment in the fuselage is separated by a antifire partition, i.e. a frame. Running an engine begins from a plug-in electric starter.

Fuel is located in the fuselage in two tanks totaling 8 liters, connected by fuel lines. The fuel system is equipped with a fuel filter. Filling of fuel tanks is carried out with the help of an external gear pump.

The power of the electric on-board system is carried out from full-time battery-operated batteries with a rated voltage of 14,2V, capacity of 4,8A×h, as well as from a regular electric generator, which is driven from the crankshaft of the engine. The wiring consists of signal and power lines connected to the combined cables.

The UAV M6-3T control is carried out in automatic, semi-automatic and manual modes. The main mode is automatic.

The onboard part of the control system UAV M6-3T consists of the necessary sensors, acquisition and processing units of information, flight controller, telemetric transceiver of the communication line and control, antenna device as well as servo drives of the steering, height control, flapperons, flaps, servo drive of the throttle of the engine power plant, servo drives for controlling the release and decoupling of the parachute. Permanent target load is the special cargo container for cargo up to 4 kg.

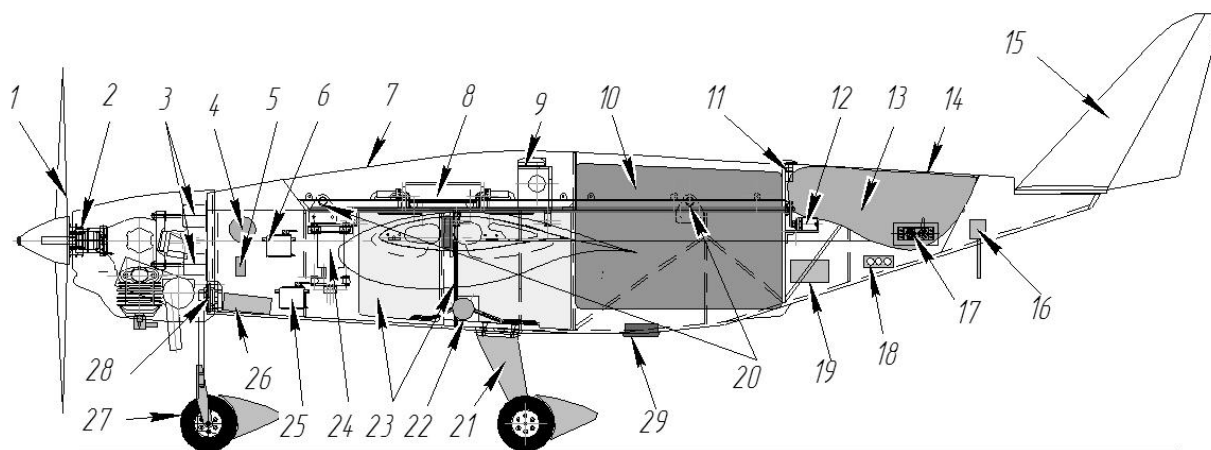


Fig. 2.2. The main functional elements and blocks of UAV M6-3T «Zhayvir»: 1 – air screw; 2 – electric generator; 3 – silent-block engine; 4 – fuel flow meter; 5 – onboard filling station; 6 – servo the drossel; 7 – front cover; 8 – the flight controller; 9 – signal receivers; 10 – special cargo container; 11 – servo opening the rear cover; 12 – servo separation of parachute; 13 – rescue parachute; 14 – back cover; 15 – V-tail; 16 – telemetry unit and telemetry modem antenna; 17 – servos of the V-tail; 18 – panel of switches, indicators and electrical connectors; 19 – accumulator; 20 – fastening hinges of the parachute launcher; 21 – the main supporting support; 22 – fuel filter; 23 – fuel tanks; 24 – onboard power supply unit; 25 – front wheel servo; 26 – the engine ignition unit; 27 – front guide support; 28 – the mechanism of rotation of the front support chassis; 29 – landing altimeter

In the course of performing test flights on a sample of transport UAV M6-3T revealed some deviations from the estimated values of FTC.

Accordingly, there was a need to establish the reasons for the deviations of the flight technical characteristics (FTC) and provide recommendations for their correction; estimation of deviations was carried out by calculation and experimental methods.

The calculation of individual FTC is based on certain modes, namely take-off, climb, cruise flight, coordinated turnovers on the route, loss of altitude and landing.

To calculate the FTC UAV, the following input data is applied:

- range of operating speeds: 20 – 45 m/s;
- average aerodynamic chord: 0,261 m.

In this flight, the UAV had an assigned cruising speed of 33 m/s. Accordingly, the numbers Re for the characteristic flight speeds of an airplane are:

$$Re_{vSI} = 70 \cdot V_{SI} \cdot b = 70 \cdot 20 \cdot 261 = 365\,400.$$

Respectively for speeds V_C and V_{NO} the number Re is equal to:

$$Re_{VC} = 70 \cdot V \cdot b = 70 \cdot 33 \cdot 261 = 602\,910;$$

$$Re_{VNO} = 70 \cdot V \cdot b = 70 \cdot 45 \cdot 261 = 822\,150,$$

where V_{SI} – minimum operating speed; V_C – estimated cruising speed; V_{NO} – maximum operating speed.

The *Wortmann FX61-184* profile is used in the wing of the aircraft [1]. The values of the aerodynamic quality K_{max} of the specified profile for these Re numbers are as follows: $K_{max.VSI} = 70$ and $K_{max.VNO} = 130$.

Assessment aerodynamic quality of profile. We calculate the values for the number Re_{VNO} . Accordingly, for this profile at $K_{max} = 130$, the lifting force coefficient is equal to $C_y = 1,6$ and the resistance coefficient: $C_x = 0,0123$. The plane the wings has an angle of fixing 0° , which, according to the structure of the plane, corresponds to the tangage pitch angle of 0° . For the angle of attack 0° , the coefficients (profile) are: $C_y = 0,7$ and $C_x = 0,009$.

Profile aerodynamic quality in mode: $C_y / C_x = 78$ (Fig. 2.3 a, b).

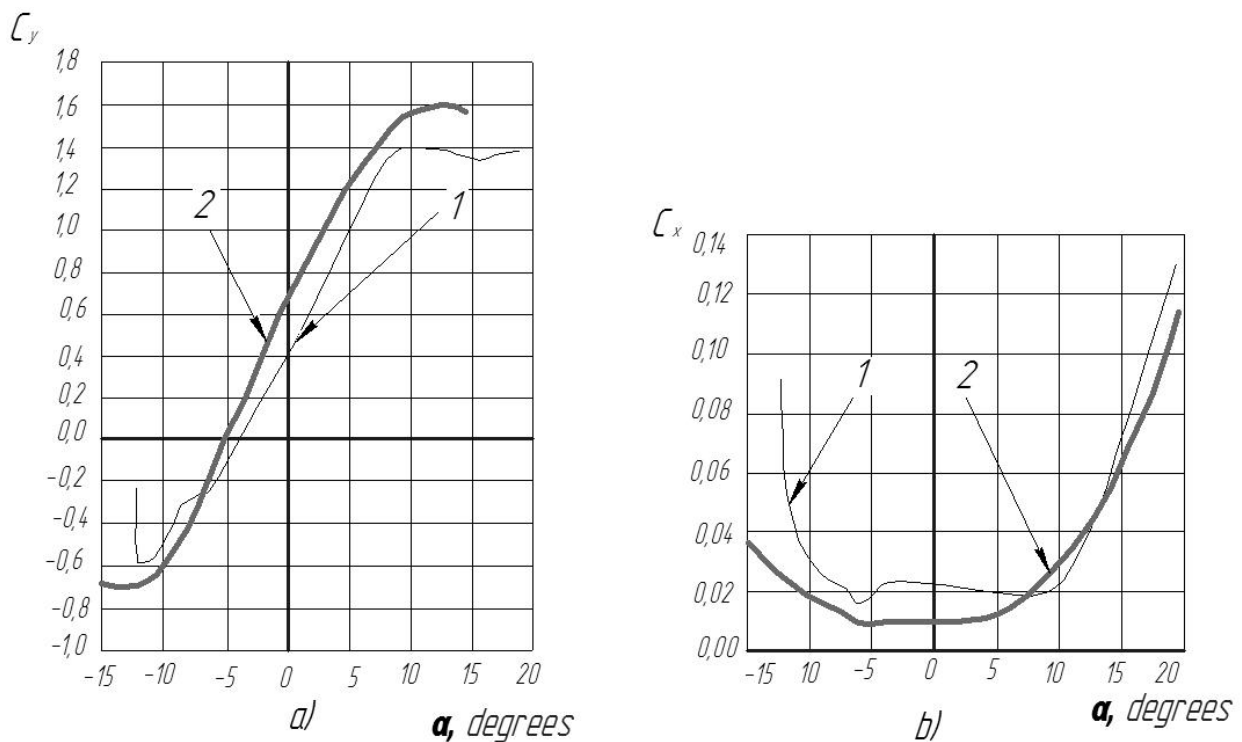


Fig. 2.3. Value of coefficients C_y (a) and C_x (b) of the *Wortmann FX61-184* for different Re numbers: line 1 – min. the value of the speed of the aircraft; line 2 – max. importance for the speed of the aircraft

All of the above values are for the wing of an infinite magnitude. In the Table 2.1 shows the main geometrical characteristics of the *Wortmann FX61-184* profile [2].

Basic geometric characteristics of profile *Wortmann FX61-184*

Parameter	\bar{c}	\bar{x}_c	\bar{f}	\bar{x}_f
Value	0,184	0,371	0,032	0,629

Notice: \bar{c} – relative profile thickness; \bar{x}_c – the relative coordinate of the position of the maximum thickness; \bar{f} – relative curvature of the profile; \bar{x}_f – the relative coordinate of the position of maximum curvature.

The aerodynamic layout of the aircraft is shown in Fig. 2.4.

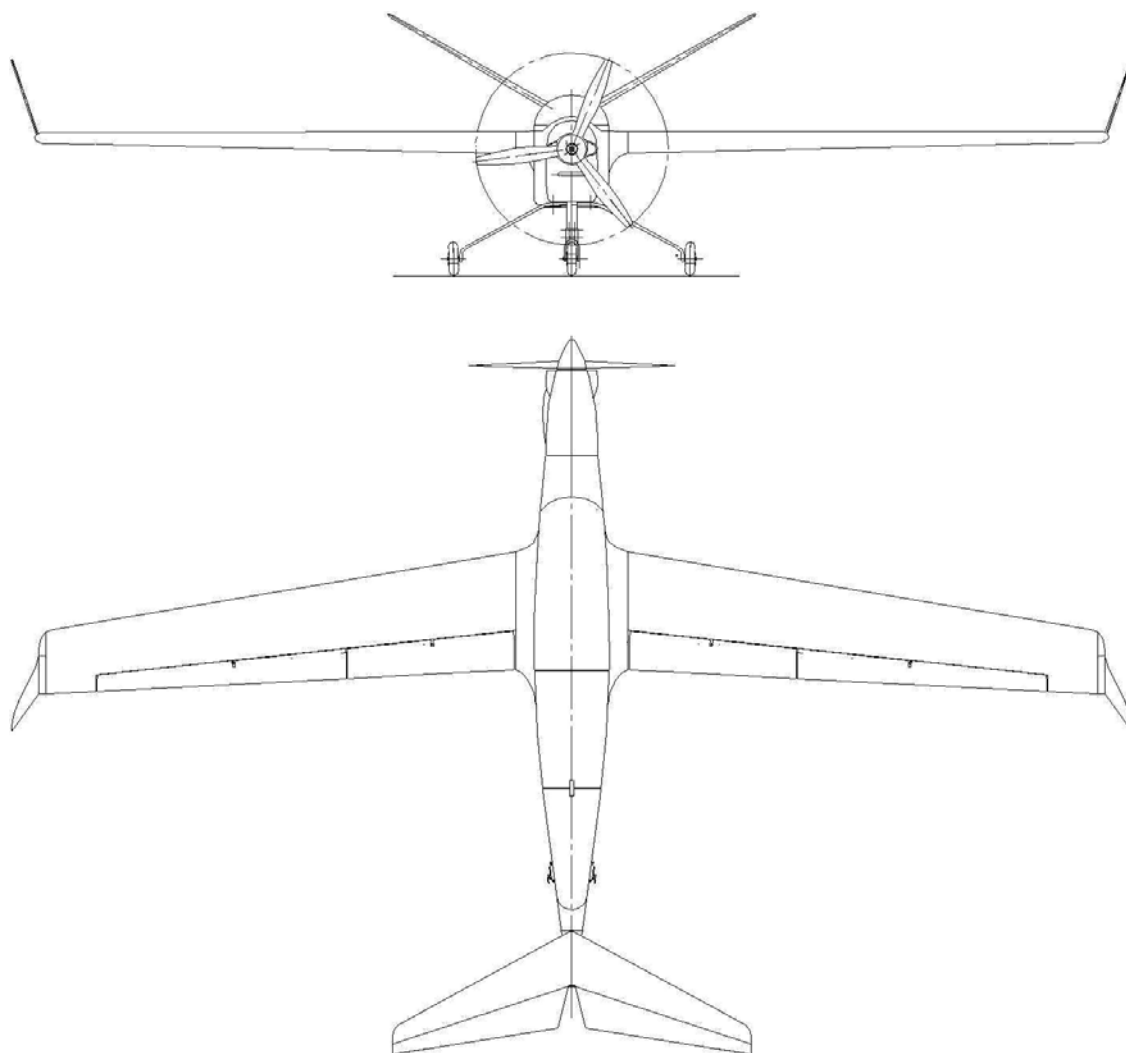


Fig. 2.4. Aerodynamic scheme of an unmanned transport aircraft M6-3T (projections)

As can be seen from Fig. 2.4, the wing of the aircraft is equipped with a simple flap and flaperons, as well as wings of *Whitcomb*, which are projected along the flow and turned outward with a vertical angle of 18°40'. The main data of the wings are given in Table 2.2.

Table 2.2

Basic geometric data of the wing of an unmanned transport aircraft M6-3T

Indicator	Unit	Value
Full Wing Area	m ²	0,706
Full Wing Span	m	3,0
Average aerodynamic chord of the wing	m	0,261
Elongation wing	un.	11,5
Ultimate chord	m	0,168
Root Chord (in the plane of symmetry M6-3T)	m	0,332
Wing narrowing	un.	1,976
Angle of wing installation	degrees	0°
Angle of transverse «V»	degrees	0,8°
Angle of arrows wing: along the front edge	degrees	9°30'
on the back edge	degrees	2°53'
along the line of focus	degrees	70°50'
Area of flaperons	m ²	0,08
Area of flaps	m ²	0,08

Assessment of the aerodynamic quality of the wing. According to Table 2.1 and 2.2 the aerodynamic quality of a specific UAV M6-3T wing is calculated, taking into account the corresponding harmful resistances [3, 4].

The coefficient of resistance of the wing was calculated by the formula:

$$C_{xa.w} = C_{xa.p} + \sum \Delta C_{xa}, \quad (2.1)$$

where $C_{xa.p}$ – coefficient of profile resistance; $\sum \Delta C_{xa}$ – the amount of harmful resistance.

The coefficient of profile resistance was determined from the formula:

$$C_{xa.p} = 0,925k_1C_f\eta_c\eta_M, \quad (2.2)$$

where k_1 – a coefficient that takes into account the presence/absence of a gondole (motogondole) on the wing; C_f – coefficient of friction of a flat plate; η_c – the coefficient taking into account the

transition from a flat plate to a wing profile; η_M – coefficient taking into account the effect of compression of air on the profile resistance.

To determine the coefficient C_f , it is assumed that for the *Wortmann FX61-184* laminarized profile the transition point of the laminar flow in the turbulent is approximately at the point of maximum thickness, that is:

$$\bar{x}_T \approx \bar{x}_c.$$

The coefficient C_f is determined from the formula:

$$C_f = C_{f1} \bar{x}_T + C_{fT}(1 - \bar{x}_T), \quad (2.3)$$

where C_{f1} – coefficient of friction under conditions of laminar flow; C_{fT} – coefficient of friction in conditions of turbulent flow.

The coefficient C_{f1} is determined from the formula [5]:

$$C_{f1} = 1,328\sqrt{Re_l}. \quad (2.4)$$

The number Re for the laminar flow is determined from the following relation:

$$Re_l = V_w MAC \bar{x}_T \nu, \quad (2.5)$$

where ν – kinematic coefficient of viscosity of air; MAC – mean aerodynamic chord.

The coefficient η_c was found depending on the maximum relative thickness of the profile from the graph shown in Fig. 2.5.

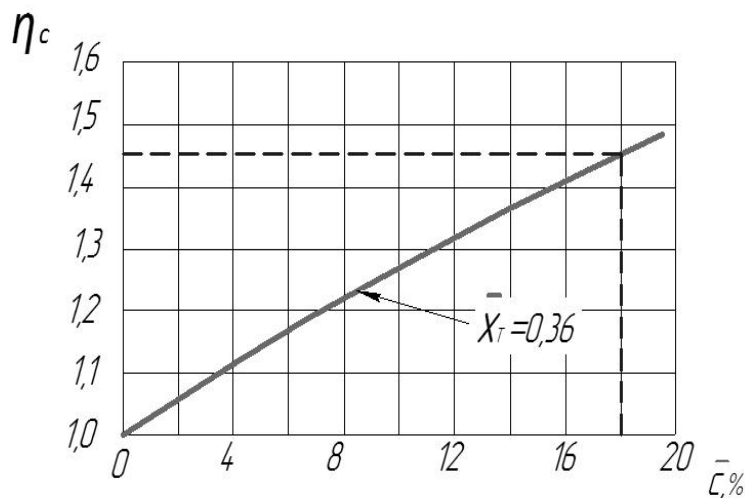


Fig. 2.5. Finding the value of the coefficient η_c .

The coefficient η_M is found from the graph in Fig. 2.6.

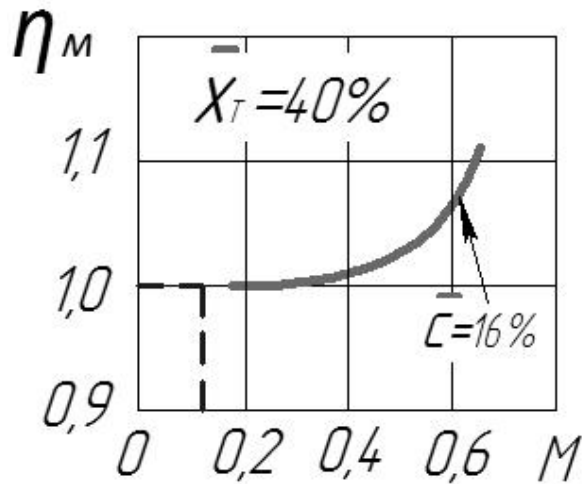


Fig. 2.6. Finding the value of the coefficient η_M

As a result of calculations by the formula (2.2), the coefficient of profile resistance has the following value: $C_{xa,p} = 0,008$. To calculate we accept the value of 0,0085 in connection with the fact that the coefficient of profile resistance, obtained from the graph (Fig. 2.3, b) reaches the value of 0,009.

Further calculated harmful supports that arise on the real wing. These include:

- harmful supports from crevices and flapperons;
- resistance from the air pressure receiver and its bracket (on the right wing);
- brackets for suspension brackets and flapperons;
- cracks between the halves of the wing and the rivulet;
- resistance from the protruding heads of the screws of the lids of the covers, hatches and so on;
- resistance from the levers and drives of the moving surfaces of the wing.

The calculations of $C_{xa,h}$ were carried out according to the method shown in the source [6]. Also, the inductive resistance that arises as a result of the flow of a stream from under the wing over its surface in the region of finiteness followed by the formation of a harmful vortex was taken into account. The coefficient of inductive resistance was calculated by the formula [7]:

$$C_{xi} = \frac{C_{y\alpha}^2}{\pi\lambda_{ef}}, \quad (2.6)$$

where C_y – lifting factor on the corner of the attack 0° ; λ_{ef} – effective wing elongation.

The effective elongation of the wing was determined from the formula:

$$\lambda_{ef} = \frac{\lambda}{1-\sigma}, \quad (2.7)$$

where σ – taking into account the geometry of the wing (lengthening λ , narrowing end angle of the arrowhead χ).

The value of σ is found from the formula:

$$\sigma = 0,02 \frac{\lambda}{\cos \chi} \left(3,1 + \frac{14}{\eta} + \frac{20}{\eta^2} + \frac{8}{\eta^3} \right). \quad (2.8)$$

However, the given inductive resistance estimation is incomplete, since it does not take into account the application of the winglete design – the small wing of the *Whitcomb* type, which is installed on the finite element and has a symmetrical thin profile (Fig. 2.4). According to the source, the use of the *Whitcomb* wings reduces the inductive resistance by 4–9 %, especially for take-off and lift modes [8]. For the cruise flight mode, the inductive resistance reduction was chosen to be 5 %, that is, the multiplication of the obtained value of $C_{x.i}$ on the coefficient of 0,95 was applied. Also, the interference resistance (influence) of the conjugation between the wing and the fuselage was taken into account. This resistance is characterized by the coefficient $C_{x.interfer}$.

Since the middle part of the *wings blow round* air propeller, was introduced the coefficient of resistance to blowing, which statistics were selected at the level: $C_{x.b.r.} = 0,0003$. The results of calculating the total C_x of the wing are given in Table 2.3.

Table 2.3

The results of calculations ΣC_x and aerodynamic quality of the wing M6-3T

Coefficient	The Wing M6-3T
$C_{xa.p}$	0,0085
$C_{x.i}$	0,0032
$C_{xa.h}$	0,00286
$C_{x.interfer}$	0,00004
$C_{x.b.r.}$	0,0003
$\Sigma \Delta C_x$	0,0149
K_{wng}	0,7/0, 0149 \approx 47

As can be seen from Table 2.3, the estimated aerodynamic quality of the wing of the transport M6-3T is within 47 units.

Assessment of the complete aerodynamic layout of the M6-3T aircraft. The resistance coefficient for the V-tail was adopted as follows:

$$C_{x.Vt.} = 0,01.$$

Assessment of airplane fuselage is summarized. Taking into account the features of the fuselage contours, namely the straight side walls, the lower surface of the tail beam and the flat bottom, the coefficient of resistance of the fuselage equals:

$$C_{x.fus.} = 0,017.$$

The obtained data from the resistance coefficients are summarized in the corresponding a note (Table 2.4).

Table 2.4.

Summary table of resistance coefficients

No	Part name	Number	Area/ midele, m ²	Σ area/ midele, m ²	C _{xa}	C _{xa} S _i
1	Wing	1	0,706	0,706	-	0,0149
2	Fuselage	1	1,0/0,052	1,0/0,052	-	0,017
3	Landing gear:					
	wheels	3	0,0021	0,0063	0,07	0,00045
	front support	1	0,003	0,003	1,5	0,01
	main support	1	0,0088	0,0088	1,1	0,004
4	V-tail	1	0,146	0,146	0,008	0,01
5	Separate details:					
	telemetric antenna	1	0,00085	0,00085	0,012	0,000012
	exhaust pipes of silencer	2	0,00061	0,00122	0,02	0,000018
	Total:			Σ S _{mid} = 0,32		Σ C _{xa} = 0,057

Thus, the aerodynamic quality of this specimen UAV M6-3T on the angle of attack $\alpha = 0^\circ$ from chassis that are not hidden reaches the value of:

$$K_{a0.ch} = C_y / \Sigma C_{xa} = 0,7/0,055 = 12,41.$$

For the configuration, when the chassis is hidden, the aerodynamic quality of the M6-3T will be equal to:

$$K_{a0.w-t a ch-s} = C_y / \Sigma C_{xa} = 0,7/0,042 = 18,5.$$

Determination of required thrust and characteristic flight speeds

The characteristic flight speeds were determined according to the requirements put forward in the source [9]. The calculated coefficient of resistance M6-3T is: $\Sigma C_{xa} = 0,055$ (on the corner of the angle attack 0°). The resistance strength at 33 m/s in cruising mode (for V_c speed) is equal to:

$$X_{V_c} = \frac{\rho V^2}{2} C_{xa} S_w = 1,225 \cdot \frac{33^2}{2} \cdot 0,055 \cdot 0,706 = 1334,025/2 \cdot 0,055 \cdot 0,706 = 2,6 \text{ kGf}$$

(kilogram of force).

Accordingly, the required traction at a speed of 33 m/s should be at least 2,6 kGf.

The required power $N_{H_{hf}}$ for a horizontal flight at a given speed and altitude is determined from the known formula:

$$N_{H_{hf}} = \frac{P_{F_{hf}} V}{75} = \frac{GV}{75K} = 17 \cdot \frac{33}{75} \cdot 12,41 = 0,61 \text{ hp.} \quad (2.9)$$

Finding characteristic speeds

Stalling speed was determined from the formula:

$$V_S = \sqrt{\frac{2G}{\rho C_{ya.max} \times S}}. \quad (2.10)$$

Under the condition $C_{ya.max} = 1,6$ and $G = 17 \text{ kg}$, the stalling speed will be equal to:

$$V_S = \sqrt{\frac{2G}{\rho C_{ya.max} S}} = 15,67 \text{ m/s}.$$

Lifting speed of the front support:

$$V_R \geq 1,1 V_S = 17,24 \text{ m/s}.$$

Take-off safety speed:

$$V_2 \geq 1,1 V_S \geq 17,3 \text{ m/s}.$$

Safe approach speed is:

$$V_{REF} \geq 1,3 V_S = 20,37 \text{ m/s}.$$

Safe climb speed:

$$V_{FTO} \geq 1,3 V_S \geq 20,37 \text{ m/s}.$$

Minimum steady flight speed in Take off:

$$V_{S1} = 1,3 V_S \approx 21 \text{ m/s}.$$

The design manoeuvring speed was determined by the formula [10]:

$$V_A = \sqrt{\frac{2mg}{C_y \rho S}} \cdot \sqrt{\frac{1}{\cos \gamma_\alpha}} = 25 \text{ m/s}, \quad (2.11)$$

where C_y – lifting factor in mode (0,7); ρ – air density over ISA; S – wing area; $\cos \gamma_\alpha$ – cosine of the permitted angle of the roll (30°).

Running distance is:

$$L_p = \frac{G}{2g} \frac{V_R^2}{(P_{md} - fG)}, \quad (2.12)$$

where $f = 0,05$ –rolling friction coefficient for solid soil / poor quality concrete runway; P_{md} – average thrust during the run-up, taken equal to the thrust at 0,7 breakaway speed.

The average thrust in the takeoff process was calculated by the formula:

$$P_{md} = \frac{N_0}{0,7V_R} = 6,62 \text{ kGf.} \quad (2.13)$$

Accordingly, the calculated take-off distance M6-3T is 45 m (according to formula 2.12)).

The experimental assessment of the flight technical characteristics of the unmanned aircraft M6-3T was made on the basis of telemetric test flight data that was carried out during 2017–2018 to confirm the airworthiness of the aircraft.

Analysis of experimental data was conducted to:

- assess the actual airplane thrust, including the characteristics of the power plant and the development of recommendations on the choice of runways and planning take-off modes;
- assess the aerodynamic quality of the aircraft and making recommendations for unmanned airplane flight operator at the stage of automatic landing;
- measure the actual dimensions of the touching area during automatic landing;
- estimate of the speed parameters of the M6-3T on different flight modes.

Fig. 2.7 shows the typical data of the UAV M6-3T at the run-up stage: the speed of rotation of the air propeller 1, longitudinal overload 2, air velocity 3, pitch of the air propeller 4 and distance from the runway surface 5. The rise of the front steering wheel *a* is carried out at speed of 20,2 m/s, separation *b* is performed at speed of 22,6 m/s.

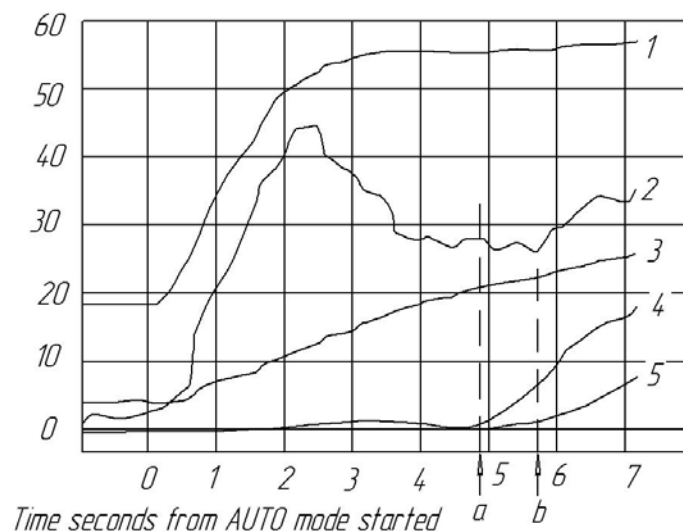


Fig. 2.7. Typical characteristics of the M6-3T during the run: 1 – speed of rotation of the air propeller (x100 rpm); 2 – longitudinal overload (/100); 3 – air speed, m/s; 4 – pitch, deg; 5 – height from the surface of he runway according to the laser altimeter, m

Fig. 2.8 shows the typical data of the M6-3T at the take-off stage, the safe take-off altitude is 40 m. Changing the barometric altitude at the start of the run (*a*) occurs due to the fusion of the fuselage. The maximum speed of rotation of the air propeller is 5930 rpm, vertical speed at the take-off stage reaches 6 m/s. Completion of take-off procedure (*b*) after reaching a height of 40 m is accompanied by lifting the ban on maneuvering the course, the distance from the start of the run is 230 m.

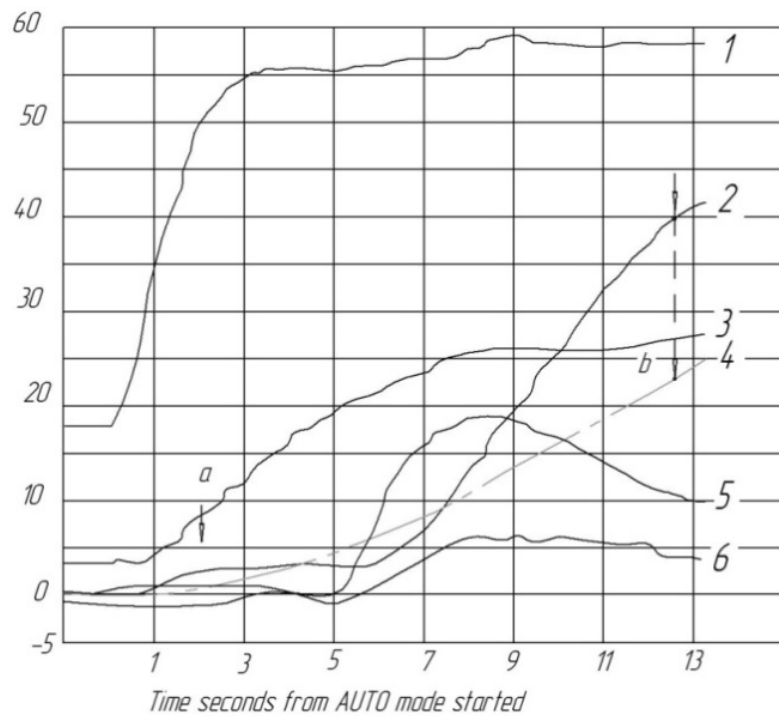


Fig. 2.8. Typical characteristics of the UAV M6-3T at the take-off stage: 1 – the speed of rotation of the air propeller (x100 rpm); 2 – height according to the barometer, m; 3 – air speed; 4 – distance from the onset of the run (x10 m); 5 – pitch, degrees; 6 – vertical speed, m/s; the altitude curve according to the laser altimeter is not indicated by the figure

The estimation of the actual traction was carried out on the basis of the following data: longitudinal overload at run-off, trajectory and air velocity at take-off, speed of rotation of the air propeller with known parameters (20"x12", profile RAF-6) [11]. The results of processing are summarized in Table 2.5. The mileage and the size of the take-off zone were determined on the basis of the road speed and according to the satellite navigation system. Integrating the measured values of the velocity, we obtain the actual distances of the run, shown in Table 2.6 together with the measured values of the take-off speed.

Table 2.5

Estimation of thrust of an unmanned aircraft M6-3T

Traction according to the longitudinal overload at the stage of run	6,8...8,1 kGf at the beginning of the run	5,2...5,7 kGf at the take-off Speed 19,5 m/s	no data	no data
Thrust at a given height, set by the angle of inclination of the trajectory	no data	no data	4,7 kGf at slope angle 10,2°	6,1 kGf at slope angle 14,7°
Estimated thrust according to the measured screw rotation speed	8,4 kGf at 5470 rpm at the beginning of the run	5,8 kGf at 5640 rpm at a speed of 19,5 m/s	4,9 kGf at 5900 rpm at a speed of 26 m/s	6,2 kGf at 6000 rpm at a speed of 24 m/s

Table 2.6

Actual parameters of unmanned aerial vehicle take-off

Flight number	1	2	3	4
Speed of the counter wind, m/s	4	6	5	2
Take-off distance, m	54	42	55	57
Safe take-off speed (air speed), m/s	20,4	20,8	21,1	22,6

Thus, summarizing the data from Table 2.5, for this UAV M6-3T with a take-off weight of 17 kg, it is possible to accept the average value of the propulsion of 0,35. Proceeding from this value, at a separation speed of 20 m/s, the calculated take-off distance will be 63 m. Based on runway statistics, recommended take-off zone is determined by the parameters in Fig. 2.9.

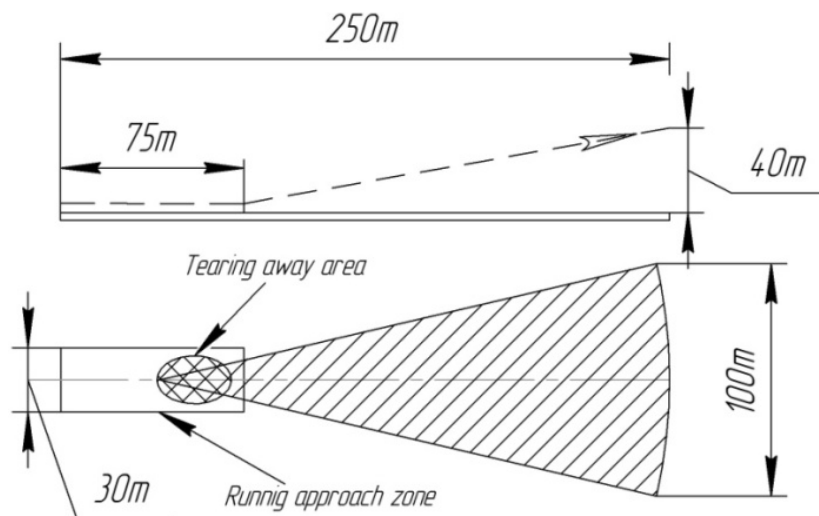


Fig. 2.9. Recommended take-off zone of the UAV M6-3T, taking into account the deviation of take-off direction caused by lateral wind

The actual aerodynamic quality of UAV M6-3T is evaluated in the following ways:

- at the rectilinear horizontal flight – by the ratio of the propeller thrust and mass UAV;
- at the landing approach with zero draft – by the ratio of horizontal and vertical velocities.

Fig. 2.10 shows the typical values of the UAV M6-3T parameters in the rectilinear flight at an air speed of 33 m/s, in which the average speed of the air propeller is 5460 rpm. Calculated values of the propeller thrust, according to various models range, from 1,3 to 1,6 kGf [12].

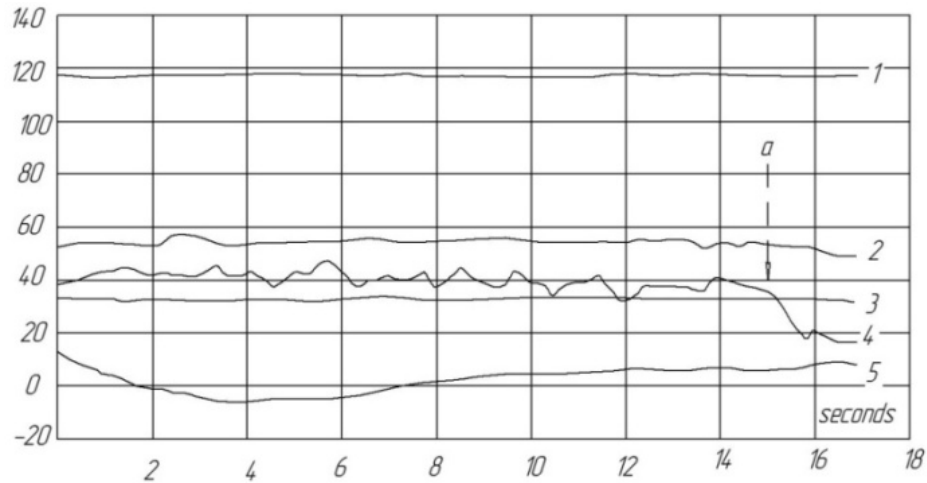


Fig. 2.10. Typical example of recording of horizontal flight data: 1 – height, m; 2 – speed of rotation of the air propeller, (rpm) · 100; 3 – air speed, m/s; 4 – throttle position of the engine in percents relative to the maximum; 5 – yaw (at time (a) was performed a command to reduce the flight speed)

Fig. 2.11 shows the typical values of the parameters of the UAV M6-3T in the mode of reduction in the thrust of the propeller near zero value (before touching the runway).

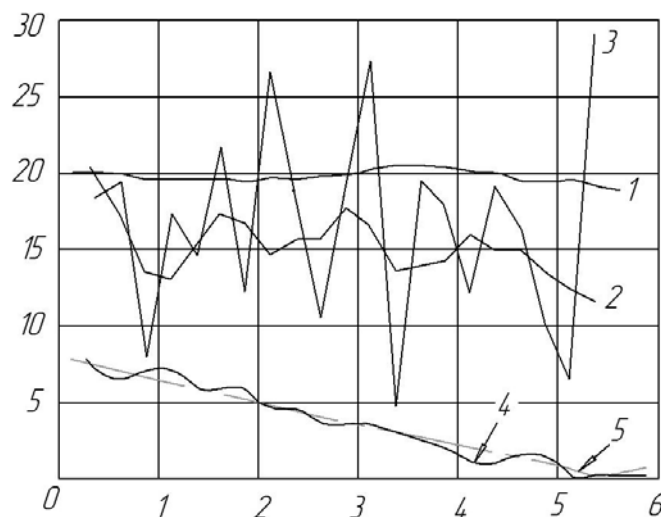


Fig. 2.11. A typical example of a flight data recording with the aircraft descending and the propeller thrust close to zero: 1 – air speed; 2 – vertical speed (x0,1 m/s) according to the optical altimeter; 3 – vertical speed according to barometer; 4 – height by barometric data; 5 – height according to the optical altimeter

Results of assessing the aerodynamic quality of UAV M6-3T by calculated and experimental methods in different flight modes are summarized in Table 2.7.

Table 2.7

Assessment of aerodynamic quality of UAV M6-3T

Flight Mode UAV M6-3T (17 kg)	Horizontal air speed, m/s	Vertical speed, m/s	Speed of rotation screws, rpm (average)	Estimated value of air propeller thrust	Aerodynamic quality, K
Rectilinear horizontal	33	0	5560	1,3...1,6 kGf	Between 10,6 and 13
Rectilinear horizontal	26	0	4920	1,35...1,6 kGf	Between 10,6 and 12,6
Rectilinear with decrease	33	3,0	5300	Thrust near zero	11,0
Rectilinear with decrease	26	2,3	4140	Thrust near zero	11,3
Rectilinear with decrease	20	1,56	3320	Thrust near zero	12,8

The basic scheduled and experimental flight technical characteristics of the UAV M6-3T for take-off/landing and cruise flight modes on the declared cruise speed of 33 m/s are given in Table 2.8.

Table 2.8

Results of the calculation and experimental estimates of individual flight technical characteristics (FTC) UAV M6-3T

Parameter/Name	Marking	Unit of measurement	Meanings received by calculation, R_{FTC}	Values are obtained by experiment, E_{FTC}
Aerodynamic quality	$K_{a0.ch}$	without unit	12,41	Between 10,6 and 13
Stalling speed	V_S	m/s	15,67	Does not exceed 15,9 m/s
Rotation speed	V_R	m/s	17,24	18,6...19 m/s
Safe take-off speed	V_2	m/s	17,24	Actually 20,8 m/s
Reference landing approach speed	V_{REF}	m/s	20,27	20 m/s
Safe climb speed	V_{FTO}	m/s	$\geq 20,37$	22,2 m/s
Stall speed or minimum steady flight speed	V_{S1}	m/s	21	21,3

End of table 2.8

Design maneuvering minimum speed	V_A	m/s	25	21,3*
Design cruising speed	V_C	m/s	33	33+/-1,2 m/s
Running distance	L_p	m	45	63
Average thrust during the run	P_{md}	kGf	6,62	6,0
Required thrust for speed 33 m/s	P_{VC}	kGf	2,6	1,3...1,6 kGf

*the minimum speed at which maneuvering is performed

2.2. Influence of icing on aircraft performance of unmanned aerial vehicle M-10-2 «Oko»

It is known that icing of aircraft lift surfaces has a negative influence on aircraft performance and can lead to an aviation accident. Deposits of ice on the earth are well considered in the works [13, 14]. Ice deposition on surfaces is assisted by coincidence of meteorological and other factors, among which the most import are dimensions and drops concentration, aircraft speed of flight, and air temperature [15, 16, 17].

Primary source analysis shows that attention is usually given to «regular» aircraft of general aviation [18]. However, information about UAVs is almost absent and icing influence is not considered.

Practical test flights of UAVs in winter period executed by specialists of Scientific and Production Center of Unmanned Aviation «Virage» (SPCUA «Virage») of National Aviation University shown, that ignorance of problem consideration can decrease the flight safety level up to preconditions of aviation accident.

As example we will take day flights of UAV M-10-2 «Oko» under next meteorological conditions (MC): air temperature: from 0 °C to minus 5 °C; speed of surface wind – up to 4 m/s; wind speed at altitude: up to 10 m/s; clouds bottom limit – 400 m [19].

Cruising speed of UAV on the route amounted 20 m/s; no precipitation. Before flight, during before flight tests there were no icing revealed. Aircraft launch performed in automatic mode without shortcomings. Planned and achieved flight altitude – 600 m; maximum distance – around 15,5 km. All ground and board systems operated in regular mode.

Above the mission area (15 km away from control station) UAV got into conditions, which led to icing. Ice formed at leading edge of capacity installed in UAV was 16 Ah; its charge at the launch moment was 95 % wing and tail unit, frontal surfaces of video antennas and on pitot static tube (PST). Icing fact was investigated after UAV landing. During flight recorded via telemetry that at the altitude 600 m UAV stall started. Autopilot managed to level off UAV without operator's assistance; however UAV lost altitude and descended at 400 m, but after leveling off returned to assigned altitude of flight and continued flight on planned route. After mission completed UAV returned to the launch position and performed parachute landing.

During study of consequences of glaciation UAV M-10-2 «Oko» icing scheme of ice deposits location on the surfaces was defined (Fig. 2.12).

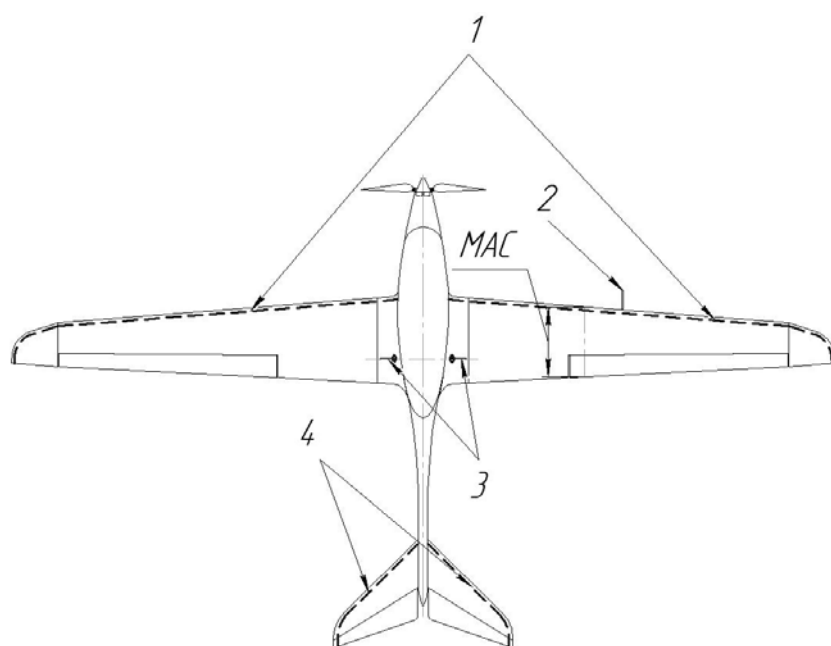


Fig. 2.12. Scheme of ice deposits location on the surfaces of unmanned aerial vehicle M-10-2 «Oko» (top view): 1 – on the wing leading edge; 2 – on the front part of the pitot static tube; 3 – on the front surfaces of the video antennas; 4 – on the leading edge of the tail unit; MAC – projections location of the MAC to the horizontal

The biggest ice formations observed on leading edge of the wing almost along all its length; ice formations also covered whole leading edge of winglets. Ice formations on wing were loose, without «gloss» signs. Formation binding is not strong, because during parachute landing part of them loosed of wing. Character and dimensions (mm) of wing leading edge icing are shown on Fig. 2.13 (formations on top view) and on Fig. 2.14 (formations on bottom view).

Tail unit surfaces covered with ice had character similar to wing formation: formation width from top view – 2 mm, bottom view 3,5 mm.

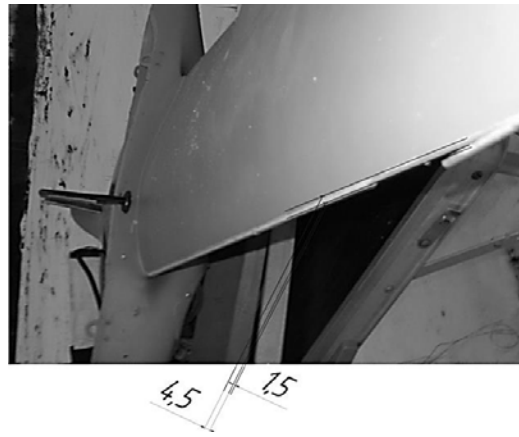


Fig. 2.13. Icing of the leading edge of the wing (top view)



Fig. 2.14. Icing of wing leading edge (bottom view)

Scheme of distortion of original wing profile *Wortmann FX61-184* was developed with ice deposits of specified dimensions (Fig. 2.15, *a*, *b*).

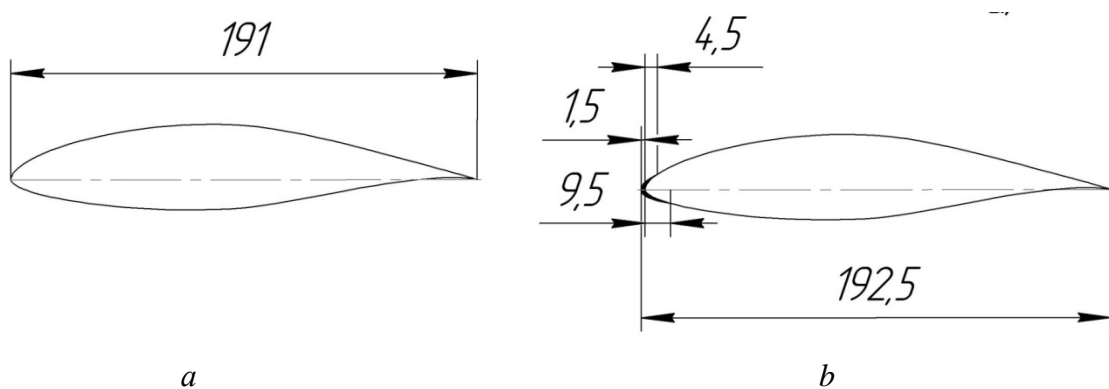


Fig. 2.15. Scheme of distortion and changes of geometrical dimensions of original wing profile *Wortmann FX61-184*: *a* – original profile contour along MAC; *b* – distorted profile contour along MAC

Specified that formation is related to icing type «pike-shape formation», which is characterized with opacity, dimness and looseness; ice contains a significant amount of small drops and ice crystals or their mix. Such type of ice is formed on relatively narrow section of profile [20, 21].

Icing of the PST inlet had gloss surface of grey color; formations closed measuring hole of dynamic pressure, and static pressure holes continued to be non-iced and passable. Formation binding with metal of PST is strong. Character and dimensions (mm) of PST icing is shown on Fig. 2.16.

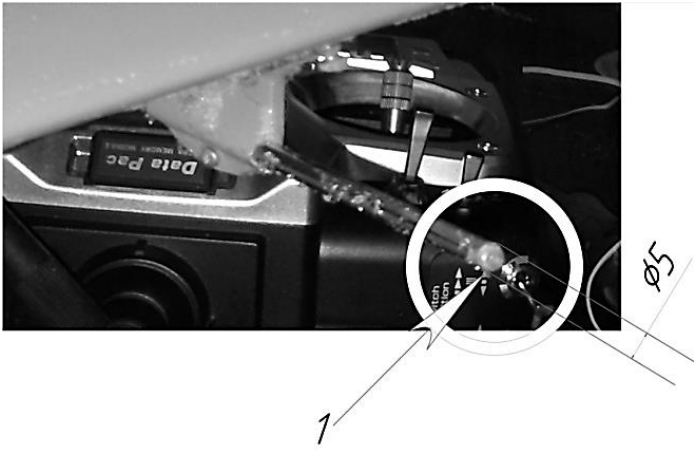


Fig. 2.16. Character and dimensions (mm) of PST icing: 1 – icing of tube cap (inlet) of PST

Antennas have been iced from the front side; formation surface has been solid on the top and gloss, and under the solid top there was a loose layer. Character and dimensions (mm) of video channel antennas icing is shown on Fig. 2.17.

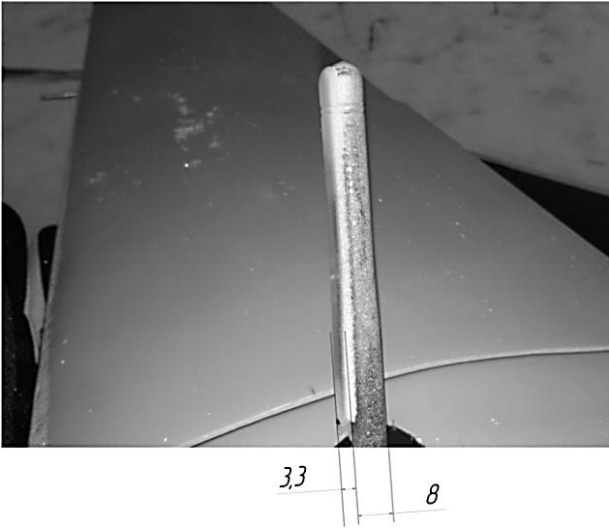


Fig. 2.17. Icing of the video channel antennas

Analysis of flight results in conditions of icing conducted using the design aircraft performance of the UAV and data obtained from mode of flight recorder (MFR). The hypothesis was that UAV in icing conditions successfully performs flight mission, but that achieved by significant excess of its energy consumption.

Input data for calculation:

Autopilot controlled cruising speed of flight of UAV – 20 m/s.

Maximum take-off weight (MTOW) – 5 kg (50N).

Wing area of UAV, S_w – 0,38 m².

Air density (for ISA) – 1,225 kg/m³.

$C_{y_{m.b.i}}$ – lift force coefficient for cruising mode before icing.

$C_{y_{m.a.i}}$ – lift force coefficient for cruising mode after icing.

Wing setting angle of UAV – +0,5 degrees.

The basis of calculation was estimation of increment of drag force as the result of icing.

It is known, that at the cruising mode of operation next condition must be fulfilled:

$$MTOW = Y. \quad (2.14)$$

During calculation known formulas were applied for lift and drag force estimation, also for lift force coefficient:

$$Y = \frac{\rho V^2}{2} C_y S_w. \quad (2.15)$$

$$X = \frac{\rho V^2}{2} C_x S_w. \quad (2.16)$$

Drag force coefficient was determined from next relation:

$$C_x = \frac{X}{\frac{\rho V^2}{2} S_w}. \quad (2.17)$$

The coefficient of lifting force was found from the ratio:

$$C_y = \frac{Y}{\frac{\rho V^2}{2} S_w}. \quad (2.18)$$

During results generation drag force before and after icing used a combined data array, taken from MFR and from UAV aerodynamic characteristics, obtained on design stage. Calculation algorithm was next.

1. Using data of MFR and input data: cruising speed, MTOW and air density defined in-flight value of $C_{y_{m.b.i}}$ (formula (2.18)).

$$C_{y_{m.b.i.calc}} = 50 / (1,225 \cdot 324 / 2) \cdot 0,38 = 50 / 198,45 \cdot 0,38 = 50 / 75,4 = 0,66. \quad (2.19)$$

From dependence $C_y f(\alpha)$ for UAV M-10-2 «Oko» (wing profile Wortmann FX61-184) was found respective values of angle of attack and drag force coefficient (Fig. 2.18).

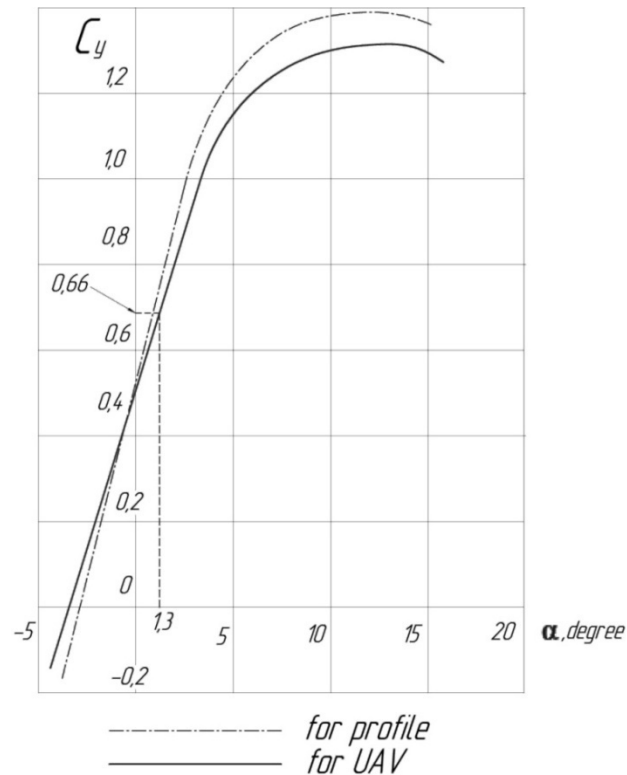


Fig. 2.18. Dependence of lift coefficient of UAV on an angle of attack

Upon respective value of angle of attack from polar curve defined coefficient $C_{x_{m.b.i}}$ for UAV.

Respectively calculated value of drag force before icing was (formula (2.16)):

$$X_{b.i} = \frac{\rho V^2}{2} C_x S_w = \frac{1,225 \cdot 20^2}{2} \cdot 0,06 \cdot 0,38 = 5,58 \text{ N.}$$

Calculation results are presented in Table 2.9.

Table 2.9

Results of drag force calculations before unmanned aircraft icing up

No	Parameter	Value
1	$C_{y_{m.b.i.calc}}$	0,66
2	Angle of attack α , degree	1,3°
3	$C_{x_{pc}}$ (from UAV polar curve)	0,06
4	The value of the resistance force X_{bi}	5,58N
5	Current aerodynamic quality, K	11 units

Similarly calculated drag force of UAV after icing. The difference was that current value of angle of attack at cruising mode we take from MFR through current value of pitch angle. Calculated value of drag force after icing equal:

$$X_{a.i} = \frac{\rho V^2}{2} C_x S_w = \frac{1,225 \cdot 20^2}{2} \cdot 0,095 \cdot 0,38 = 8,84 \text{ N.}$$

Calculation results of drag force after UAV icing are presented in Table 2.10.

Table 2.10

Calculation results of drag force after UAV icing

No	Parameter	Value
1	$C_{y_{m.b.i.calc}}$	0,74
2	Angle of attack α , degree	2,4°
3	C_{x_a} (polar curve of UAV)	0,095
4	The value of the resistance force X_{calc}	8,84N
5	Current aerodynamic quality, K	7,8 units

Upon the data from Table 2.9 and 2.10 it is apparent that before icing UAV had aerodynamic quality about 11 units. Wing surfaces, antennas etc. were not distorted by ice, so UAV performance was in design range. The aircraft was influenced by aerodynamic drag force 5,58 N at flight speed 20 m/s.

After icing UAV automatics independently taken into account deterioration of its aerodynamics from icing, to maintain cruising speed at level 20 m/s, that lead to setting new angle of attack, current wing angle of attack 2,4°, so as consequence, to increase of coefficient of aerodynamic drag C_{x_a} to value 0,095. Respectively drag force increased to value 8,84 N, that in comparison to drag force before icing is 40 % more. The result is correlated with the conclusions of the authors in the work [22].

For the actual proof of danger presence from icing of air frame surface of UAV were analyzed flight data, obtained from MFR at two segments during flight. First segment was taken during steady horizontal flight till the icing moment, second segment after icing.

Data comparison shows, that for maintaining given flight parameters autopilot had to increase thrust level on an average 10% (Fig. 2.19, *a*, *b*). Average value of current from battery increased respectively from 25,5A to 35A (Fig. 2.20, *a*, *b*).

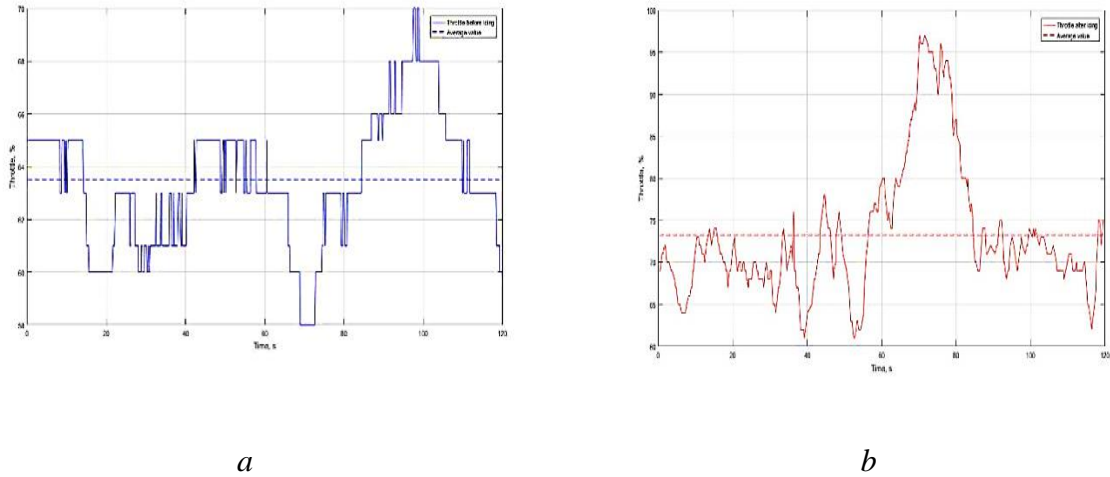


Fig. 2.19. Dependence of engine throttle level on time: *a* – before icing; *b* – after icing

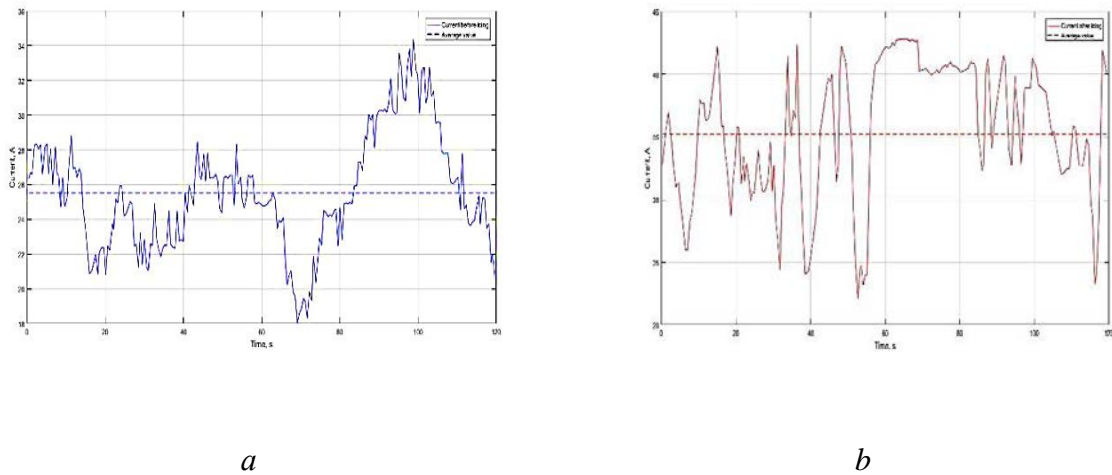
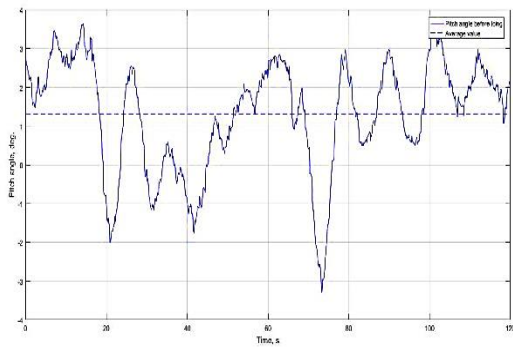
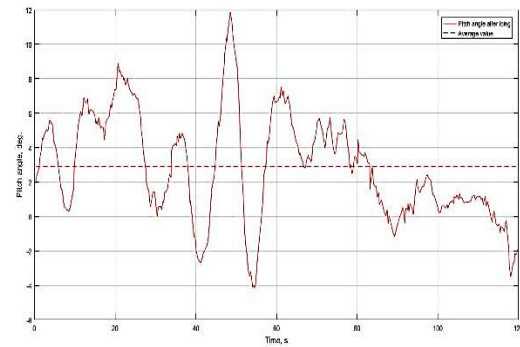


Fig. 2.20. Electrical energy consumption depending on time: *a* – before icing; *b* – after icing

The reason for these indices increase in general is increase of UAV control surface deflection to maintain given flight parameters. This can be clearly seen on Fig. 2.21, *a*, *b*, apparent, that average angle of positive pitch increased from 1,3° before icing to almost 3° after icing.



a



b

Fig 2.21. Dependence of the pitch angle level on time: *a* – before icing; *b* – after icing

Sharp increase of pitch has caused the wing to set a greater angle of attack, that has caused increase of C_x coefficient, aerodynamic quality of UAV has decreased, increased level of engine throttle and consequently greater electrical energy consumption.

2.3. Aerodynamic calculation of the accepted configuration of unmanned aerial vehicle M-56 «Module»

The accepted layout of unmanned aerial vehicle M-56 «Module» is an aircraft of the «flying wing» configuration (Fig. 2.22) with a pushing propeller and highly developed wing end edges – winglets designed to reduce induced drag.



Fig. 2.22. View ¾ left-side of UAV M-56 «Module»

In addition, along the stream the winglets are turned outward at an angle of about 3° to provide a small stabilizing course moment, because in this configuration there is no special tail unit [23].

Besides, the wing of this UAV has a significant, as for the subsonic aircraft, sweep, which is appropriate taking into account an additional increase in the course stabilizing moment. At the same time, the sweep allows locating the main controls – elevons – at a greater distance from the CG which will have a positive effect on the reduction of hinge forces during their rotation by servomechanisms.

The wing is made of airfoils that are scalable analogues of the Boeing-B-106-R airfoil section. The «R» index means that the airfoil has a so-called «S-likeness» and is intended for use on tailless aircraft configurations. The inboard wing panel has a mounting angle of $3^{\circ} 25''$. The end section has a mounting angle of $1^{\circ} 30''$; accordingly, the wing has a «twist», which enables to slightly increase the critical angles of attack and the course stability.

The main geometric characteristics of the wing and the entire UAV configuration are as follows:

- wingspan, m – 4,585;
- length, m – 1,71;
- height, m – 0,45 (without a propeller);
- height, m – 0,68 (with a propeller);
- height, m – 0,72 (on a temporary undercarriage);
- the area of the whole wing (with fuselage covering), m^2 – 1,38;
- the area of the wing covered with fuselage, m^2 – 0,134;
- wing aspect ratio, units – 14,32;
- wing taper ratio, units – 1,8;
- arrow-shaped angle of 1/4 chord – 21° ;
- leading-edge sweep angle – 22° ;
- trailing edge sweep angle – $17,3^{\circ}$;
- mean aerodynamic wing chord, m – 0,32;
- the area of elevons (two), m^2 – 0,098.

Selection of airfoil parameters for aerodynamic calculations. The used Boeing-B-106-R airfoil has the following geometric characteristics:

- \bar{c} – relative profile thickness – 0,131;
- \bar{X}_c – the relative coordinate of the position of the maximum thickness – 0,30;
- \bar{f} – relative curvature of the profile – 0,033;
- \bar{x}_f – the relative coordinate of the position of maximum curvature – 0,40.

For this Boeing-B-106-R wing airfoil, for the accepted Re number, the following values from the tables [24] are selected:

- the angle of attack α ;

- the lift force coefficient C_y and the corresponding aerodynamic drag coefficient C_x .

The selection results of C_y and C_x coefficients depending on the angles of attack α in the range from $-3,3^\circ$ to $+18,6^\circ$ are shown in Table 2.11.

Table 2.11

Values of C_y and C_x coefficients for Boeing-B-106-R airfoil ($Re - 3,2 \cdot 10^6$)

α , degrees	C_y	C_x
-3,3	-0,226	0,0099
-1,0	-0,006	0,0094
+0,8	0,082	0,0093
+3,0	0,386	0,010
+6,3	0,682	0,0118
+9,5	0,980	0,0158
+12,8	1,247	0,0242
+14,5	1,355	0,0335
+16,4	1,383	0,0704
+18,6	1,320	0,090

Calculation and construction of polar layout UAV M-56 «Module». To generate a drag polar, it is necessary to know the dependence of the coefficients of the lift force C_y and drag of the UAV at the angle of attack α . The drag coefficient of the UAV configuration is the sum of the coefficients of the section and induced drag [25]:

$$C_x = C_{x0} + C_{xi} = C_{x0} + AC_y^2, \quad (2.20)$$

where C_{x0} – is the drag coefficient at zero lifting force; $C_{xi} = AC_y^2$ – is the coefficient of induced drag that arises due to the creation of lift.

The drag coefficient of the UAV C_{x0} refers to the area of the wing S and is calculated by the formula:

$$C_{x0} = 1,1 \left(C_{x.wng} + C_{x.f} \cdot \frac{S_{mf}}{S} + \sum C_{xa} \cdot \frac{S_{ma}}{S} \right), \quad (2.21)$$

where $C_{x.wng}$, $C_{x.f}$, C_{xa} – are drag coefficients at $C_y = 0$ of the isolated wing, fuselage and additional parts; S_{mf} , S_{ma} – are a mid section of a fuselage and additional parts, m^2 .

Applying the corresponding M-56 configuration data to the formula (2.21) we obtain:

$$\begin{aligned} C_{x0} &= 1,1 \left(C_{x.wng} + C_{x.f} \cdot \frac{S_{mf}}{S} + \sum C_{xa} \cdot \frac{S_{ma}}{S} \right) = 1,1(0,00157 + \\ &+ (0,2 \cdot 0,046/1,38) + 0,0012 + 0,015) = 1,1(0,00157 + 0,0066 + 0,0012 + 0,015) = \\ &= 0,028 \text{ (we find 0,03)}. \end{aligned}$$

The aerodynamic wing drag coefficient when $C_y = 0$ is calculated by the formula:

$$C_{x.wng} = C_{xp} \left(1 - k_{a.b} \cdot \frac{S_{o.f}}{S} \right) + \sum \Delta C_x, \quad (2.22)$$

where C_{xp} – is the section coefficient; $k_{a.b}$ – is the coefficient of aerodynamic coupling of the wing and fuselage; $S_{o.f}$ – the wing area occupied by the fuselage, m^2 ; $\sum \Delta C_x$ – sum of the coefficients of additional drag to take into account the cleanliness of the wing surface, cracks in it, and superstructures.

After applying the corresponding values to the formula (2.22) the value of the coefficient of the aerodynamic drag of the wing at $C_y = 0$ was obtained:

$$\begin{aligned} C_{x.wng} &= C_{xp} \left(1 - k_{a.b} \cdot \frac{S_{o.f}}{S} \right) + \sum \Delta C_x = 0,0091(1 - 0,65 \cdot 0,134/1,38) + 0,001 = \\ &= 0,0091 \cdot 0,063 + 0,001 = 0,00157. \end{aligned}$$

The coefficients of the section drag of the wing were determined by the formula:

$$C_{xp.wng} = 1,85C_f\eta_c, \quad (2.23)$$

where C_f – flat plate drag coefficient; η_c – a factor that takes into account the transition from the flat plate to the selected wing profile.

After applying to the formula (2.23) the corresponding values for the wing and empennage, we received the following values of the coefficients of section resistance for individual configuration parts.

$$C_{xp} = 1,85C_f\eta_c = 1,85 \cdot 0,0035 \cdot 1,42 = 0,0091.$$

The value of the coefficient C_f depending on the Re number is shown on the graph Fig. 2.23.

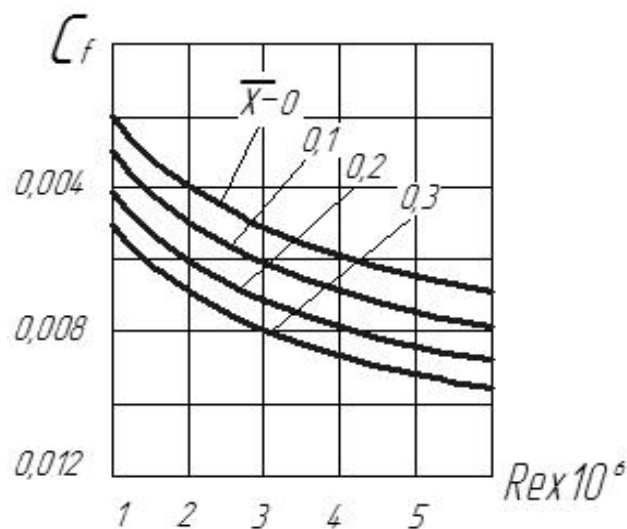


Fig. 2.23. Dependence of the C_f coefficient on the Re number for the wing

The maximum Re number for M-56 is taken from the calculation of $Re \approx 0,5 \cdot 10^6$; this value was specified by the formula:

$$Re = V_c MAC/\nu, \quad (2.24)$$

where V_c – flight speed, m/s; MAC – is the mean aerodynamic wing chord; ν – is the coefficient of kinematic air viscosity, $10^{-2} \cdot m^2/s$.

The specified value (in the second approximation) of the operational flight speed at an altitude of 0 m was taken as follows: $V_c = 24$ m/s; $Re = 0,53 \cdot 10^6$.

The C_f coefficient also depends on the position of the transition point \bar{x}_r of the laminar boundary layer to turbulent. Its position, in turn, is determined by a number of factors, the main of which are the shape of the airfoil and the cleanliness of its surface, as well as the uniformity of the oncoming flow.

It is known that for a fairly smooth surface of the wing, the coordinate of the \bar{x}_r point does not exceed the part of the airfoil chord located in front of its maximum relative thickness ratio. For most airfoils (except for laminarized ones) $\bar{x}_r < 0,15$. In the places of blowing the wing by a propeller $\bar{x}_r = 0$. For most wings that are blown by propellers, we can consider $\bar{x}_r = 0$.

The value of the η_c coefficient, which depends on the value of the airfoil thickness ratio \bar{c} and the position of the transition point \bar{x}_r is shown in Fig. 2.24.

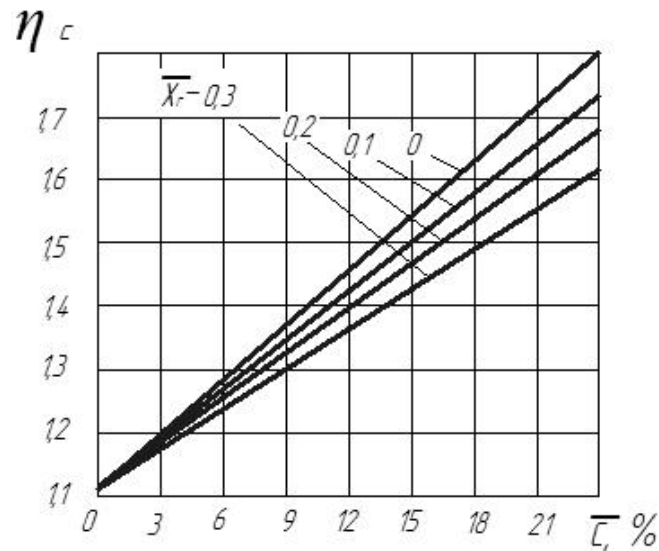


Fig. 2.24. Dependence of the η_c coefficient value on the value of the airfoil thickness ratio \bar{c} and the position of the transition point \bar{x}_r

The coefficient of aerodynamic coupling (interference) $K_{A,B}$ depending on the adopted UAV configuration and the shape of the cross section of the fuselage has the following values [26]:

- high-wing – 0,95;

- midwing – 0,65;
- low-wing with the cross section of the fuselage;
- round shape – 0,25;
- oval shape – 0,50;
- rectangular shape – 0,60.

Harmful wing resistance also depends on the surface roughness, especially its front part. If 20 % of the airfoil starting from the nose is free of protruding rivet heads then ΔC_x can be taken at the level of 0,0013. If the whole wing has protruding rivets, the value of the additional drag is approximately one-and-a-half times bigger and is 0,0020. The drag of openings between the wing and the elevons was not taken into account.

The coefficient of the fuselage drag without superstructures in the form of cabin lights, fillet fairings, etc. was found by the following formula:

$$C_{x\,p.f} = C_f \eta_\lambda S_{ox}/S_{m.f}, \quad (2.25)$$

where $C_{x\,p.f}$ – is the coefficient of section fuselage drag; $S_{m.f}$ – is the area of the fuselage midsection, m^2 ; η_λ – is the coefficient that takes into account the fuselage stretch; S_{ox} – fuselage area exposed to air, m^2 ; C_f – is the drag coefficient of a flat plate (for the fuselage of these dimensions).

The coefficients C_f and η_λ were obtained from the graphs in Fig. 2.25 and 2.26. Their values depend on the Re number and the fuselage stretch.

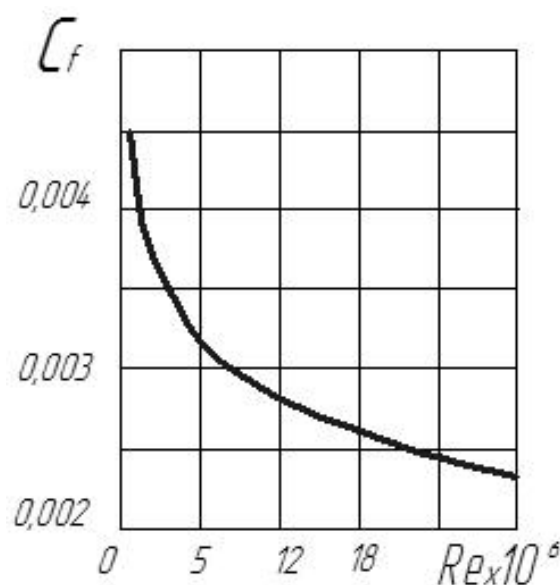


Fig. 2.25. Dependence of the C_f coefficient on the Re number for the fuselage

The value of the η_λ coefficient, which depends on the fuselage stretch is shown in Fig. 2.26.

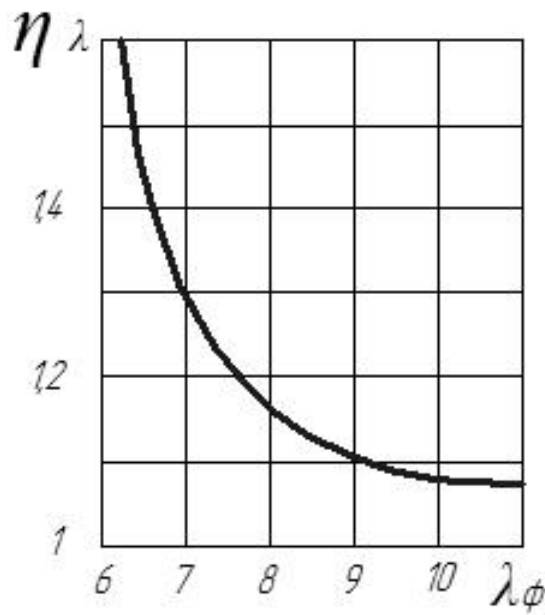


Fig. 2.26. Dependence of the η_λ coefficient value on the fuselage stretch

The fuselage stretch was determined by the formula:

$$\lambda_f = 0,88 l_f / \sqrt{S_{mf}}, \quad (2.26)$$

where l_f – is the fuselage length, m.

The Re number for the fuselage was calculated by the formula:

$$Re = V l_f / \nu. \quad (2.27)$$

The covered surface of the fuselage S_{ox} was determined using a three-dimensional model of the developed UAV M-56 configuration.

The coefficient of induced drag was determined from the following formula:

$$C_{xi} = \frac{1+\delta}{\pi \lambda_{ef}} \cdot C_y^2, \quad (2.28)$$

where δ – coefficient that takes into account the elongation and narrowing of the wing; λ_{ef} – effective elongation of the wing.

The value of the coefficient δ was determined from the graph shown in Fig. 2.27.

The calculated value of the C_{xi} coefficient for the configuration is equal to:

$$C_{xi} = (1 + 0,08/3,14 \cdot 19,3) \cdot 0,893 = (1,08/60,6) \cdot 0,893 = 0,0159.$$

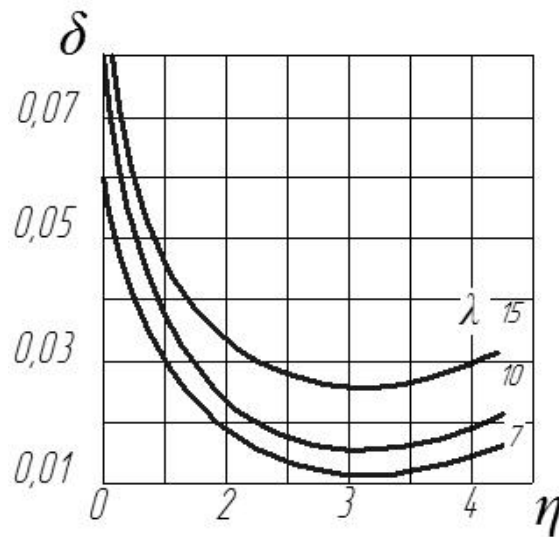


Fig. 2.27. Dependence of the coefficients δ and η on wing elongation λ

Effective wing elongation was calculated by the formula:

$$\lambda_{ef} = 0,9\lambda / \left(1 + \frac{S_{of}}{S_{wng}}\right), \quad (2.29)$$

where λ – wing elongation; S_{wng} – wing area occupied by the fuselage; S_{of} – is the area occupied by the fuselage.

To confirm the result of the induced drag calculations for the M-56 configuration it is used an alternative formula to identify this coefficient:

$$C_{xi} = A C_y^2. \quad (2.30)$$

Parameter A in formula (2.30) is called the coefficient of deviation of the polarity and is based on the relation:

$$A = \frac{(1+\delta)}{\pi\lambda_{ef}}. \quad (2.31)$$

Accordingly, the calculation of the values of A and C_{xi} are as follows:

$$A = 1 + 0,045/3,14 \cdot 8 = 0,0416;$$

$$C_{xi} = (1 + 0,045/3,14 \cdot 8) \cdot 0,81 = (1,045/25,12) \cdot 0,81 = 0,041 \cdot 0,81 = 0,0336.$$

For this UAV M-56 «Module» (flying wing configuration) we assume that the lift force is created by the wing only; Boeing-B-106-R wing airfoil data was used to calculate the lift coefficient.

The calculation of the lift force coefficient for M-56 «Module» is about the construction of a correspondence diagram $C_y = f(\alpha)$.

The maximum value of the coefficient of lifting force was determined by the formula:

$$C_{y,max} = C_{y,p,max}k_{\eta}(1 + \cos \chi)/2, \quad (2.32)$$

where $C_{y,p,max}$ – the maximum value of the coefficient of lifting force of the wing profile; χ – the angle of the arrow-shaped wing along the line of focus.

The calculated value of the maximum lift coefficient (according to formula 2.32) is equal to:

$$C_{y,max} = C_{y,p,max}k_{\eta}(1 + \cos \chi)/2 = 1,383 \cdot 0,94 (1 + 0,906)/2 = 1,30 \cdot 0,953 = 1,24.$$

The results of the calculations for the correspondence $C_y = f(\alpha)$ are presented in Fig. 2.28.

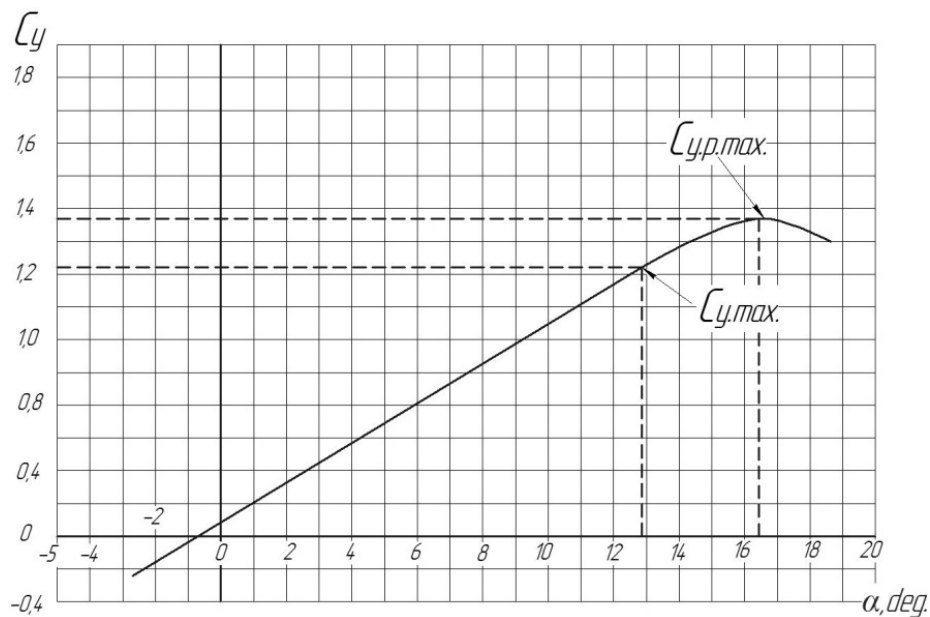


Fig. 2.28. The obtained correspondence $C_y = f(\alpha)$ for the complete UAV M-56 «Module» configuration

It is known that a polar is a curve that characterizes the dependence of the drag coefficient C_x and the lift force coefficient C_y on the angles of attack α [27].

To generate the UAV M-56 «Module» polar it is necessary to know the values of the coefficients C_x and C_y for the entire configuration by the angles of attack. To do this, it is

necessary to calculate the value of the configuration drag coefficient by the angle of attack to formula:

$$C_{x_a} = C_{x_o} + AC_y^2 + \Delta C_{x_p}, \quad (2.33)$$

where C_{x_o} – is the minimum configuration drag coefficient at zero lift force; ΔC_x – is the correction that takes into account an increase in the drag coefficient due to changes in the angle of attack; A – the coefficient polar deviation; $\bar{C}_{y_a} = C_{y,a}/C_{y,max}$ – is the relative increase in the lift coefficient due to changes in the angle of attack.

The following input data are required to build the polars of the entire layout of the M56 «Module» UAV:

$$C_{x_o} = 0,03 \text{ (calculated by formula (2.21));}$$

$$A = 1 + 0,035/3,14 \cdot 11,8 = 0,0278 \text{ (calculated by formula (2.31));}$$

$$C_{y,max} = 1,24 \text{ (calculated by formula (2.32)).}$$

Working formula (2.33) to obtain $C_x = f(\alpha)$ values:

$$C_{x_a} = C_{x_o} + AC_y^2 + \Delta C_{x_p}.$$

The results of calculating the drag coefficient C_{x_a} for M-56 configuration by the angle of attack:

$$C_{x-3,3} = 0,03 + (0,0278 \cdot 0,051) + 0,00 = 0,031;$$

$$C_{x-1} = 0,03 + (0,0278 \cdot 0,000036) + 0,00 = 0,03;$$

$$C_{x+0,8} = 0,03 + (0,0278 \cdot 0,007) + 0,00 = 0,0301;$$

$$C_{x+3} = 0,03 + (0,0278 \cdot 0,149) + 0,001 = 0,035;$$

$$C_{x+6,3} = 0,03 + (0,0278 \cdot 0,465) + 0,002 = 0,044;$$

$$C_{x+9,5} = 0,03 + (0,0278 \cdot 0,96) + 0,005 = 0,067;$$

$$C_{x+12,8} = 0,03 + (0,0278 \cdot 1,56) + 0,022 = 0,095;$$

$$C_{x+14,5} = 0,03 + (0,0278 \cdot 1,84) + 0,03 = 0,111;$$

$$C_{x+16,4} = 0,03 + (0,0278 \cdot 1,91) + 0,035 = 0,118;$$

$$C_{x+18,6} = 0,03 + (0,0278 \cdot 1,74) + 0,045 = 0,123.$$

The obtained $C_x = f(\alpha)$ calculation results and the input data are given in Table. 2.12.

Table 2.12

**Summarized aerodynamic coefficients for the generation of the M-56 «Module»
configuration polar ($Re \approx 0,3 \cdot 10^6$)**

Calculated value	Angles of attack of M-56 «Module» configuration									
	-3,3	-1,0	+0,8	+3,0	+6,3	+9,5	+12,8	+14,5	+16,4	+18,6
C_y	-0,226	-0,006	0,082	0,386	0,682	0,980	1,247	1,355	1,383	1,320
C_y^2	0,051	0,000036	0,007	0,149	0,465	0,96	1,56	1,84	1,91	1,74
$\bar{C}_{ya} = C_y$ $a/C_{y,max}$	0,182	0,005	0,066	0,311	0,55	0,79	1,005	1,09	1,115	1,006
ΔC_x	0,0	0,0	0,0	0,001	0,002	0,005	0,022	0,03	0,035	0,045
$C_{xa} = C_{xo} +$ $+AC_y^2 + \Delta C_{xp}$	0,031	0,03	0,0301	0,0351	0,044	0,067	0,095	0,111	0,118	0,123
K_1	-7,2	-1,5	2,8	11	15,2	14,6	13,1	12,2	11,7	10,6

The value of K_1 (aerodynamic quality of the aircraft in general) is obtained from the following ratio:

$$K_1 = C_y / C_{xa}, \quad (2.34)$$

where C_y – obtained from Table. 2.12 the current value of the lift coefficient for a given angle of attack; C_{xa} – is the current value of the drag coefficient of the configuration for a given angle of attack obtained from Table 2.12.

Fig. 2.29 shows the polar of the full UAV M-56 «Module» configuration: α_{ma} corresponds to the most appropriate angle of attack of the configuration.

The calculation of necessary power and thrust for the UAV M-56 «Module» was performed using the following formula, namely to calculate the required power:

- to find the required power (W):

$$N_{H0} = \frac{mV_0}{75K}, \quad (2.35)$$

where V_0 – is set operating speed, m/s; m – is take-off weight of the UAV, N; K – is the configuration quality (by the angle of attack).

The formula was used to find the stalling speed [28]:

$$V_s = \sqrt{\frac{2m}{\rho_0 S C_{ya}}}, \quad (2.36)$$

where ρ_0 – density at a altitude of 0 m, kg/m³; S – wing area, m²; C_{ya} – lift coefficient of (for a given angle of attack).

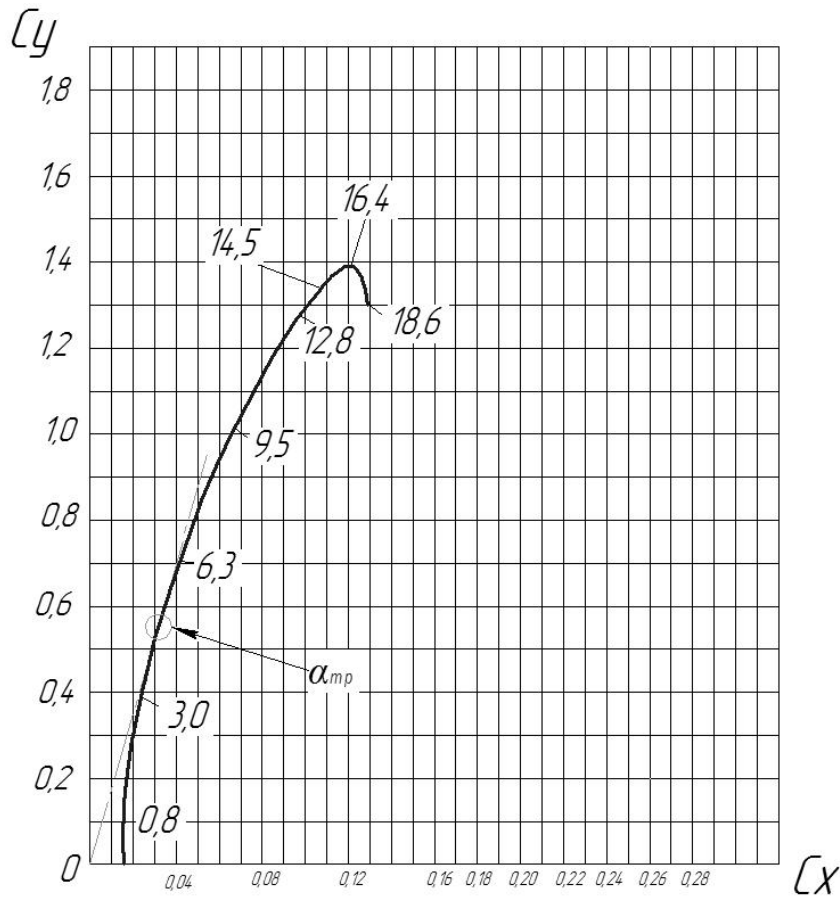


Fig. 2.29. The obtained polar of the full configuration of UAV M-56 «Module»

When changing the altitude, the following conversion formulas were used:

$$V_x = V_0 \sqrt{\Delta},$$

where $\Delta = \rho_{ah}/\rho_0$ –relative air density.

According to the power:

$$N_{np} = \frac{N_{H0}}{\sqrt{\Delta}}.$$

The required thrust (kGf) was calculated using the following formula:

$$P_u = \frac{m}{K}. \tag{2.37}$$

The results of the calculations were summarized in Table 2.13, 2.14 and 2.15.

Table 2.13

**The results of the calculation of the required speed, thrust and power for UAV M-56
«Module» configuration ($Re = 0,5 \cdot 10^6$, altitude 0 m; $m = 13$ kg)**

$H - 0$ m, $m - \text{const}$										
C_{ya}	-0,226	-0,006	0,082	0,386	0,682	0,980	1,247	1,355	1,383	1,32
K	-7,2	-1,5	2,8	11	15,2	14,6	13,1	12,2	11,7	10,6
V_s , m/s	-	-	40	19,3	14,8	12	11	10,5	10,4	10,3
N_H , kW	-	-	2,5	0,18	0,17	0,14	0,15	0,151	0,155	0,171
P_H , kGf	-	-	4,7	1,2	0,86	0,89	0,99	1,1	1,2	1,25
α , deg	-3,3	-1,0	+0,8	+3,0	+6,3	+9,5	+12,8	+14,5	+16,4	+18,6

Table 2.14

**The results of the calculation of the required speed and power for UAV M-56 «Module»
configuration ($Re = 0,5 \cdot 10^6$, $m = 13$ kg)**

$H - 1000$ m, Δ , $m - \text{const}$										
V_s , m/s	-	-	42	20,23	15,5	12,6	11,53	11	10,8	10,7
N_H , kW	-	-	2,62	0,152	0,178	0,147	0,157	0,158	0,163	0,18
$H - 2000$ m, Δ , $m - \text{const}$										
V_s , m/s	-	-	44,15	21,3	16	13,2	12,14	11,6	11,5	11,4
N_H , kW	-	-	2,75	0,16	0,187	0,154	0,166	0,167	0,162	0,16
α , deg	-3,3	-1,0	+0,8	+3,0	+6,3	+9,5	+12,8	+14,5	+16,4	+18,6

Table 2.15

**The results of the calculation of the required speed and power for UAV M-56 «Module»
configuration ($Re = 0,5 \cdot 10^6$, $m = 16$ kg)**

$H - 0$ m, Δ , $m - \text{const}$										
K	-	-	2,8	11	15,2	14,6	13,1	12,2	11,7	10,6
V_s , m/s	-	-	47	22	17,7	13,8	12,2	11,7	11,6	11,5
N_H , kW	-	-	0,76	0,43	0,25	0,21	0,198	0,205	0,22	0,235
α , deg	-3,3	-1,0	+0,8	+3,0	+6,3	+9,5	+12,8	+14,5	+16,4	+18,6

The obtained values of Δ and V_x at the transition to other heights were equal to:

- for a altitude of 1000 m:

$$\Delta = \rho_{ah}/\rho_0 = 1,1164/1,225 = 0,911;$$

$$V = V_0/\sqrt{\Delta} = V_S/0,954;$$

– for a altitude of 2000 m:

$$\Delta = \rho_{ah}/\rho_0 = 1,0065/1,225 = 0,821;$$

$$V = V_0/\sqrt{\Delta} = V_S/0,906.$$

Table 2.13 shows the results of calculations of aerodynamic quality K , stall speed V_S , the required power N_H and the required thrust P_H depending on the angle of attack α° (in the range from $-3,3^\circ$ to $+18,6^\circ$) for the full UAV M-56 «Module» configuration with the gross mass at takeoff of 13 kg for a altitude of 0 m.

Table 2.14 shows the results of calculations of the stall speed V_S and the required power N_H depending on the angle of attack α° (in the range from $-3,3^\circ$ to $+18,6^\circ$) for the full UAV M-56 «Module» configuration with the gross mass at takeoff of 13 kg for the altitude of 1000 m and 2000 m.

Table 2.15 shows the results of calculations of the stall speed V_S and the required power N_H depending on the angle of attack α° (in the range from $-3,3^\circ$ to $+18,6^\circ$) for the full UAV M-56 «Module» configuration with the gross mass at takeoff increased up to 16 kg for the altitude of 0 m. The graphical interpretation of the calculation results of K_{UAV} , the stall speed V_S and the required power N_H depending on the angle of attack α° of the full UAV M-56 «Module» configuration are presented in Fig. 2.30.

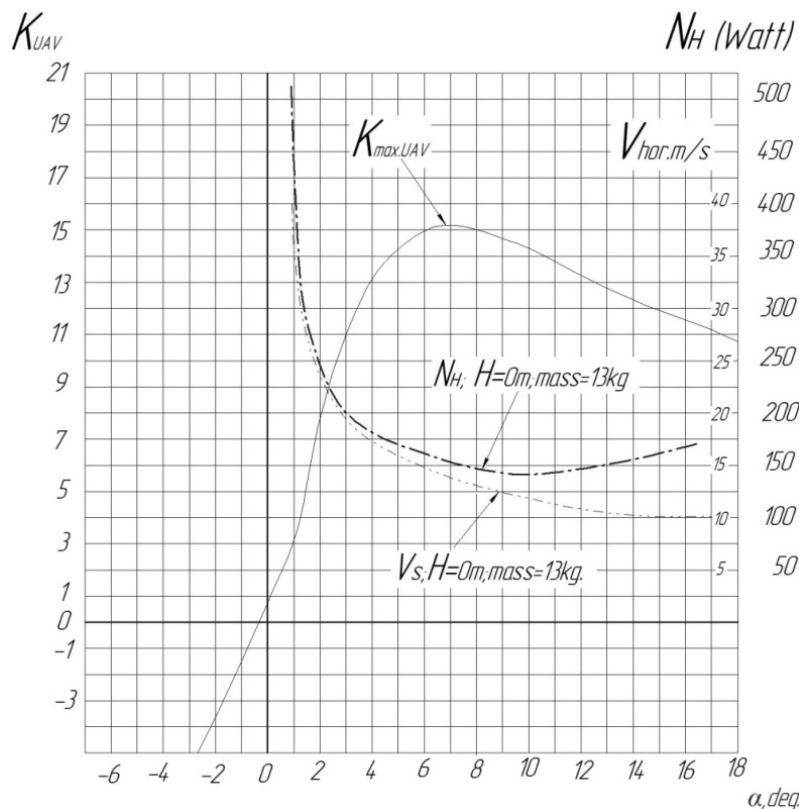


Fig 2.30. Dependence of aerodynamic quality K_{UAV} , stall speed V_S and required power N_H on the angle of attack for the M-56 «Module» configuration with Boeing-B-106-R airfoil ($Re = 0,5 \cdot 10^6$)

As can be seen from the graph, with respect to K , the maximum quality of the layout is achieved at the angle of attack near $\alpha \approx +7^\circ$. In this case, the required power N_H to ensure the flight speed $V_s \approx 14$ m/s (at an altitude of 0 m) is equal to 150 – 160 W. It should be noted that the stall speed V_s – minimum steady flight speed at which the UAV is still controlled.

2.4. Kinematic and dynamic models of unmanned aerial vehicle movement (on the example of M-7-V5)

In the process of developing the UAV motion model, 12 variables are used, given in Table. 2.16. Three of them, namely position variables and three speed variables, are related to the translational motion of the UAV.

Table 2.16

Variables used for the mathematical model

p_n	Northern inertial coordinate of the UAV position, measured in F^l along the \vec{i}^b axis
p_e	Eastern inertial coordinate of the UAV position, measured in F^l along the \vec{j}^b axis
p_d	The vertical coordinate of the UAV (axis to the center of the Earth) in the inertial system, measured in F^l along the \vec{k}^i axis
u	Velocity in a connected coordinate system, measured in F^b along the \vec{i}^b axis
v	Velocity in a connected coordinate system, measured in F^b along the \vec{j}^b axis
w	Velocity in a connected coordinate system, measured in F^b along the \vec{k}^i axis
ϕ	Roll angle given relative to F^{v2}
Θ	Pitch angle set relative to F^{v1}
ψ	Travel angle (yaw) given with respect to F^v
p	Roll velocity measured in F^b along the \vec{i}^b axis
q	Pitch speed measured in F^b along the \vec{j}^b axis
r	Yaw speed measured in F^b along the \vec{k}^b axis
$\det(J)$	The determinant of the matrix, where J – matrix
$\text{adj}(J)$	Attached matrix, where J – matrix

Angular positions also have three components; similarly, rotational motion is characterized by three variables of angular velocities [29].

UAV state variables (Fig. 2.31) are presented in the coordinate system: north – east and down UAV (p_n, p_e, p_d).

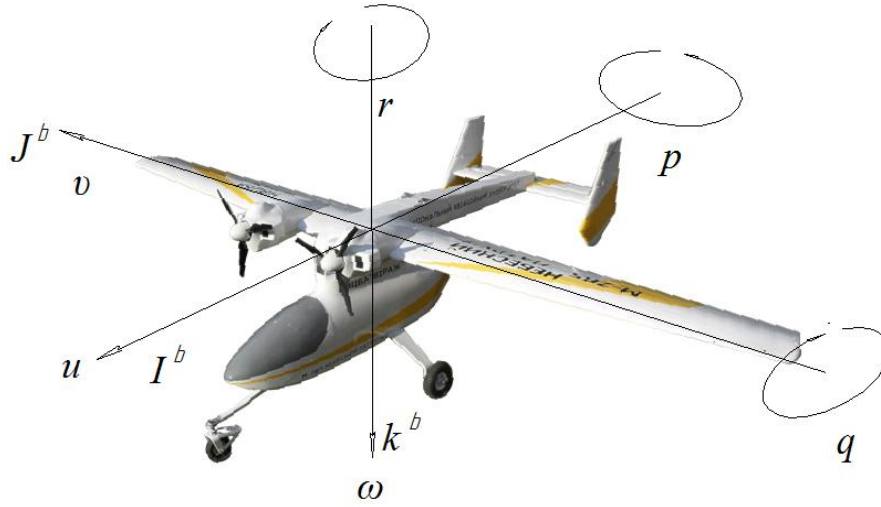


Fig. 2.31. Location on the UAV scheme of axes and corresponding position variables (translational and rotational movements)

Height is denoted as:

$$h = -p_d; \quad (2.38)$$

U, v, ω – linear velocities, which are determined relative to the connected coordinate system.

Similarly, the angular velocities p, q and r .

The angles φ, Θ and ψ , respectively, the angles of roll, pitch and yaw are Euler angles. Under certain circumstances, the angular velocities p, q and r are derived from the angles, namely, only for the case when $\varphi = \Theta = 0$. In this case $p = \dot{\varphi}; q = \dot{\Theta}$ та $r = \dot{\psi}$. In general, the velocities p, q and r are functions of time-derived angles of spatial position $\varphi, \dot{\Theta}$ and $\dot{\psi}$ and angles Φ and Θ .

Kinematics of motion. In this case, the mass of the UAV and the causes of movement are not taken into account. The linear velocities u, v, ω are projected on the axes I^b, J^b and k^b and correspond to the inertial velocity of the UAV. However, the position of the UAV is also determined in the inertial coordinate system. Accordingly, the relationship between inertial velocity and position in the coordinate system is described by a differential equation of the form:

$$\frac{d}{dt} \begin{pmatrix} p_n \\ p_e \\ p_d \end{pmatrix} = \mathcal{R}_b^v \begin{pmatrix} u \\ v \\ \omega \end{pmatrix} = (\mathcal{R}_b^v)^T \begin{pmatrix} u \\ v \\ \omega \end{pmatrix}. \quad (2.39)$$

The position of the UAV in the connected coordinate system is defined by the following expression:

$$\mathcal{R}_v^b(\varphi, \theta, \psi) = \mathcal{R}_{v_2}^b(\varphi) \mathcal{R}_{v_1}^{v_2}(\theta) \mathcal{R}_{v_1}^v(\psi). \quad (2.40)$$

Using the transformation of the UAV coordinate system into a connected coordinate system and provided that $c_\varphi \triangleq \cos \varphi$ and $s_\varphi \triangleq \sin \varphi$ we obtain the expression:

$$\begin{pmatrix} \dot{p}_n \\ \dot{p}_e \\ \dot{p}_d \end{pmatrix} = \begin{pmatrix} c_\theta & c_\psi & s_\phi s_\theta c_\psi - c_\phi s_\psi & c_\psi s_\theta c_\psi + s_\phi s_\psi \\ c_\theta s_\psi & s_\phi s_\theta c_\psi + c_\phi s_\psi & c_\psi s_\theta c_\psi - s_\phi s_\psi \\ -s_\theta & s_\phi c_\theta & c_\phi c_\theta \end{pmatrix} \begin{pmatrix} u \\ v \\ w \end{pmatrix}, \quad (2.41)$$

Dependence (2.41) shows the relationship between position derivatives and velocity without taking into account forces and accelerations.

Translational movement of the UAV. Substantiating the translational motion of the UAV, we assume that the velocity vector in the bound coordinate system is given in the form: $V_q^b = (u, v, w)^T$. This speed is considered to be the speed of the UAV relative to the Earth as expressed in a connected coordinate system.

The derivative of the velocity in the inertial coordinate system, which is written through the derivative in the connected coordinate system and the angular velocity, looks like this:

$$\frac{dV_q}{dt_i} = \frac{dV_q}{dt_b} + \omega_{b/i} V_q, \quad (2.42)$$

where $\omega_{b/i}$ – angular velocity of the UAV in the connected coordinate system.

Adding to equation (2.42) Newton's second law in differential form (for a body performing translational motion) leads to the following relationship:

$$m \left(\frac{dV_q}{dt_b} + \omega_{b/i} V_q \right) = f. \quad (2.43)$$

Correlation (2.43) combines the connected coordinate system with Newton's second law. *(In the ratio (2.43) the symbol «m» is given in a direct font and it means the mass of the UAV. Instead, the symbol «m» in italics further means the sum of the moments around the axes).*

For maneuvering UAV, the specified ratio takes the form:

$$m \left(\frac{dV_q^b}{dt_b} + \omega_{b/i}^b V_q^b \right) = f^b, \quad (2.44)$$

where $V_q^b = (u, v, w)^T$, and $\omega_{b/i}^b = (p, q, r)^T$; component f^b means the vector of application of the resulting external force through the following components:

$$f^b \triangleq (f_x, f_y, f_z)^T.$$

Due to the fact that the linear velocities u, v, ω are instantaneous projections V_q^b on the axis I^b, J^b and k^b , we can conclude that:

$$\frac{dV_q^b}{dt_b} = \begin{pmatrix} \dot{u} \\ \dot{v} \\ \dot{\omega} \end{pmatrix}. \quad (2.45)$$

By detailing the vector product (2.44) and regrouping the terms, we obtain the expression:

$$\begin{pmatrix} \dot{u} \\ \dot{v} \\ \dot{\omega} \end{pmatrix} = \begin{pmatrix} rv - gw \\ pw - ru \\ gu - pv \end{pmatrix} + \frac{1}{m} \begin{pmatrix} f_x \\ f_u \\ f_z \end{pmatrix}. \quad (2.46)$$

Rotating motion of UAV. The derivative of the torque of the UAV in the inertial system is equal to:

$$\frac{dh}{dt_i} = \frac{dh}{dt_b} + \omega_{b/i} \cdot h = m. \quad (2.47)$$

This is true when the torques are written around the center of mass and Newton's second law is true for rotation, namely:

$$\frac{dh}{dt_i} = m, \quad (2.48)$$

where h – is the internal torque, vector; m – is the total moment applied from the outside.

The relation (2.46) for the connected coordinate system (UAV) can be given as follows:

$$\frac{dh^b}{dt_b} + \omega_{b/i}^b h^b = m^b. \quad (2.49)$$

It is known from theoretical mechanics [30] that the torque for an absolutely rigid body is defined as the product of the inertia matrix J and the angular velocity vector

$$h^b \triangleq J \omega_{b/i}^b,$$

where J is given as the following expression:

$$\begin{aligned}
 J &= \begin{pmatrix} -\int (y^2 + z^2) d_m & -\int xy d_m & -\int xz d_m \\ -\int xy d_m & -\int (x^2 + z^2) d_m & -\int yz d_m \\ -\int xz d_m & -\int yz d_m & -\int (x^2 + z^2) d_m \end{pmatrix} \triangleq \\
 &\triangleq \begin{pmatrix} J_x & -J_{xy} & -J_{xz} \\ -J_{xy} & J_y & -J_{yz} \\ -J_{xz} & -J_{yz} & J_z \end{pmatrix}. \tag{2.50}
 \end{aligned}$$

The moments included in the diagonal of the matrix are called moments of inertia (J_x, J_y та J_z), and the off-diagonal elements are called centrifugal moments of inertia. Also moments of inertia counteract its rotation of a rigid body (UAV) around the corresponding axes.

Since the values in the matrix (2.50) are tied to the bound coordinate system (UAV) and are calculated relative to the axes I^b , J^b and k^b , for the observer from the UAV moment J is constant, ie:

$$\frac{dJ}{dt_b} = 0.$$

Taking the derivatives and substituting them in (2.49), we obtain:

$$J \frac{d\omega_{b/i}^b}{dt_b} + \omega_{b/i}^b \cdot (J \omega_{b/i}^b) = m^b. \tag{2.51}$$

The expression of the form $\frac{d\omega_{b/i}^b}{dt_b}$ in (2.51) shows the rate of change of angular velocity.

Since p, q, r are instantaneous projections $\omega_{b/i}^b$ on the I^b , J^b and k^b axes, we can say that

$$\dot{\omega}_{b/i}^b = \frac{d\omega_{b/i}^b}{dt_b} = \begin{pmatrix} \dot{p} \\ \dot{q} \\ \dot{r} \end{pmatrix}.$$

After regrouping (2.51) we get:

$$\dot{\omega}_{b/i}^b = J^{-1} [-\omega_{b/i}^b \cdot (J \cdot \omega_{b/i}^b) + m^b]. \tag{2.52}$$

Due to the symmetry of the majority of UAV relative to the plane formed by I^b and k^b (Fig. 2.31), the moments $J_{xy} = J_{yz} = 0$ which allows to present the right part of expression (2.50) in the form:

$$J = \begin{pmatrix} J_x & 0 & -J_{xz} \\ 0 & J_y & 0 \\ -J_{xz} & 0 & J_z \end{pmatrix}.$$

Accordingly, finding the torque \mathbf{J} is reduced to the following [31]:

$$J^{-1} = \frac{\text{adj}(J)}{\det(J)} = \frac{\begin{pmatrix} J_y J_z & 0 & J_y J_{xz} \\ 0 & J_x J_z - J_{xz}^2 & 0 \\ J_y J_{xz} & 0 & J_x J_y \end{pmatrix}}{J_y J_z J_x - J_{xz}^2 J_y} = \begin{pmatrix} \frac{J_z}{\Gamma} & 0 & \frac{J_{xz}}{\Gamma} \\ 0 & \frac{1}{J_y} & 0 \\ \frac{J_{xz}}{\Gamma} & 0 & \frac{J_x}{\Gamma} \end{pmatrix},$$

where $\Gamma \triangleq J_z J_x - J_{xz}^2$.

If the components of externally applied moments relative to the axes I^b , J^b and k^b are given in the form $\mathbf{m}^b \triangleq (l, m, n)^T$, then (2.52) can be rewritten as the following components:

$$\begin{aligned} \begin{pmatrix} \dot{p} \\ \dot{q} \\ \dot{r} \end{pmatrix} &= \begin{pmatrix} \frac{J_z}{\Gamma} & 0 & \frac{J_{xz}}{\Gamma} \\ 0 & \frac{1}{J_y} & 0 \\ \frac{J_{xz}}{\Gamma} & 0 & \frac{J_x}{\Gamma} \end{pmatrix} \left[\begin{pmatrix} 0 & r & -q \\ -r & 0 & p \\ q & -p & 0 \end{pmatrix} \begin{pmatrix} J_x & 0 & -J_{xz} \\ 0 & J_y & 0 \\ -J_{xz} & 0 & J_z \end{pmatrix} \begin{pmatrix} p \\ q \\ r \end{pmatrix} + \begin{pmatrix} l \\ m \\ n \end{pmatrix} \right] = \\ &= \begin{pmatrix} \frac{J_z}{\Gamma} & 0 & \frac{J_{xz}}{\Gamma} \\ 0 & \frac{1}{J_y} & 0 \\ \frac{J_{xz}}{\Gamma} & 0 & \frac{J_x}{\Gamma} \end{pmatrix} \left[\begin{pmatrix} J_{xz} p q + (J_y - J_z) q r \\ J_{xz} (r^2 - p^2) + (J_z - J_x) p r \\ (J_x - J_y) p q - J_{xz} q r \end{pmatrix} + \begin{pmatrix} l \\ m \\ n \end{pmatrix} \right] = \\ &= \begin{pmatrix} \Gamma_{1pq} - \Gamma_{2qr} + \Gamma_{3l} + \Gamma_{4n} \\ \Gamma_{5pr} - \Gamma_6 (p^2 - r^2) + \frac{1}{J} m \\ \Gamma_{7pq} - \Gamma_{1qr} + \Gamma_4 l + \Gamma_8 n \end{pmatrix}, \end{aligned} \quad (2.53)$$

where

$$\begin{aligned} \Gamma_1 &= \frac{J_{xz}(J_x - J_y + J_z)}{\Gamma}; \\ \Gamma_2 &= \frac{J_z(J_z - J_y) + J_{xz}^2}{\Gamma}; \\ \Gamma_3 &= \frac{J_z}{\Gamma}; \\ \Gamma_4 &= \frac{J_{xz}}{\Gamma}; \end{aligned} \quad (2.54)$$

$$\begin{aligned}\Gamma_5 &= \frac{J_z - J_x}{J_y}; \\ \Gamma_6 &= \frac{J_{xz}}{J_y}; \\ \Gamma_7 &= \frac{(J_x - J_y)J_x + J_{xz}^2}{\Gamma}; \\ \Gamma_8 &= \frac{J_x}{\Gamma}.\end{aligned}$$

The resulting mathematical model of kinematics and dynamics of UAV motion with six degrees of freedom and twelve variables of states is determined by equations (2.38), (2.39), (2.40) and (2.41) and can be definitively given as follows:

$$\begin{pmatrix} \dot{p}_n \\ \dot{p}_e \\ \dot{p}_d \end{pmatrix} = \begin{pmatrix} c_\theta c_\psi & s_\phi s_\theta c_\psi - c_\phi s_\psi & c_\psi s_\theta c_\psi + s_\phi s_\psi \\ c_\theta s_\psi & s_\phi s_\theta c_\psi + c_\phi s_\psi & c_\psi s_\theta c_\psi - s_\phi s_\psi \\ -s_\theta & s_\phi c_\theta & c_\phi c_\theta \end{pmatrix} \begin{pmatrix} u \\ v \\ w \end{pmatrix}; \quad (2.55)$$

$$\begin{pmatrix} \dot{u} \\ \dot{v} \\ \dot{w} \end{pmatrix} = \begin{pmatrix} rv - gw \\ pw - ru \\ gu - pv \end{pmatrix} + \frac{1}{m} \begin{pmatrix} f_x \\ f_u \\ f_z \end{pmatrix}; \quad (2.56)$$

$$\begin{pmatrix} \dot{\phi} \\ \dot{\theta} \\ \dot{\psi} \end{pmatrix} = \begin{pmatrix} 1 & \sin \phi \tan \theta & \cos \phi \tan \theta \\ 0 & \cos \phi & -\sin \phi \\ 0 & \frac{\sin \phi}{\cos \theta} & \frac{\cos \phi}{\cos \theta} \end{pmatrix} \begin{pmatrix} p \\ q \\ r \end{pmatrix}; \quad (2.57)$$

$$\begin{pmatrix} \dot{p} \\ \dot{q} \\ \dot{r} \end{pmatrix} = \begin{pmatrix} \Gamma_1 pq - \Gamma_2 qr \\ \Gamma_5 pr - \Gamma_6 (p^2 - r^2) \\ \Gamma_7 pq - \Gamma_1 qr \end{pmatrix} + \begin{pmatrix} \Gamma_3 l + \Gamma_4 n \\ \frac{1}{J_y} m \\ \Gamma_4 l + \Gamma_8 n \end{pmatrix}. \quad (2.58)$$

2.5. Blowing results of the aerodynamic model of the unmanned aerial vehicle M-7-V5 «Nebesniy patrol»

Aerodynamic characteristics of the aircraft model. During blowings in the wind tunnel TAD-2 NAU static aerodynamic characteristics of the aircraft model M-7-V5 «Nebesniy patrol» were studied.

The aim of the research was to determine the aerodynamic characteristics of the aircraft model at different positions of wing devices, different angles of deflection of elevators and the

rudder, flaperons, the angle of the horizontal stabilizer depending on the angle of attack and sliding.

Aerodynamic characteristics were determined in weight tests in the wind tunnel, the maximum speed of which reached 37 m/s. The TAD-2 wind tunnel is a direct-acting tube with a closed perforated test section in the Eiffel chamber. The degree of perforation of the test section walls – 9,5 %. The cross section of the test section is octagonal: 4 m wide, 2,5 m high and 9 m² in area. The measurement of aerodynamic loads on the model was performed on a 6-component electrotenometric scale. Data acquisition and processing were carried out by the corresponding measuring and computing complex [32].

The blown model of the aircraft is made at a scale of 1:3. Geometrical characteristics of the model and parameters of the model suspension carriage based on 6-KETV:

$l_x = 600$ mm – the longitudinal base of the suspension;

$l_z = 1000$ mm – transverse base of the suspension;

$\bar{x}_T = 140$ mm; $\bar{y}_T = 120$ mm – are the coordinates of the conditional center of mass.

Wing

$l = 2$ m – wing span;

$b_A = 0,194$ m – mean aerodynamic chord;

$S = 0,37$ m² – wing area;

$\bar{c} = 18$ % – airfoil thickness ratio;

$\psi = -0^\circ 4'$ the angle of transverse V-shaped wing along the line 1/4 chord;

$\lambda = -11,25$ – wing elongation;

$\eta = -1,63$ – wing narrowing;

$\chi_{1/4} = 4^\circ 19'$ – the sweep angle.

Flaps

type – single-slot, extending;

$l_F = 1,216$ m – flap span;

$b_F = 0,064$ m – chord of flaps;

$S_F = 0,08$ m² – the area of the flaps.

Flaperones

type – single-slotted;

$l_{F1} = 0,757$ m – flaperon span;

$b_{FI} = 0,084$ m – chord of flaperons;

$S_{FI} = 0,1714$ m² – area of flaperons.

Horizontal stabilizer

$S_{HS} = 0,115$ m² – the area of horizontal stabilizer;

$b_{AHS} = 0,16$ m – MAC of the horizontal stabilizer;

$l_{HS} = 0,72$ m² – the span of the horizontal stabilizer;

$\lambda_{HS} = 3,65$ – the aspect ratio of the horizontal stabilizer;

$\eta_{HS} = 1$ – the tail taper ratio of the horizontal stabilizer;

$\chi_{HS1/4} = 0$ – the sweep angle of the horizontal stabilizer;

$A_{HS} = 0,48$ – the area-moment ratio coefficient of the horizontal stabilizer;

$\bar{c}_{HS} = 10$ % – the airfoil thickness ratio of the horizontal stabilizer;

$b_{el} = 0,08$ m – the elevator chord;

$\delta_{el} = \begin{matrix} -31^\circ \\ +18^\circ \end{matrix}$ – the range of angles of deviation of the rudder.

Vertical stabilizer

$S_{VS} = 0,0468$ m² – the area of the vertical stabilizer;

$b_{AVS} = 0,18$ m – the MAC of the vertical stabilizer;

$\lambda_{VS} = 1,4$ – the aspect ratio of the vertical stabilizer;

$\eta_{VS} = 1$ – the tail taper ratio of the vertical stabilizer;

$\chi_{VS1/4} = 15^\circ$ – the sweep angle of the vertical stabilizer;

$A_{VS} = 0,186$ – the area-moment ratio coefficient of the vertical stabilizer;

$\bar{c}_{VS} = 10$ % – the airfoil thickness ratio of the vertical stabilizer.

Aircraft model configuration options. The options of the aircraft model configurations that were investigated in the experiment are shown in Table 17 when changing the angle of attack and in Table 18 when changing the angle of sideslip. The range of changes in the angles of attack covered both negative values and positive supercritical values $\alpha = -12^\circ \dots +22^\circ$, the range of changes in angle of sideslip was $\beta = -11^\circ \dots +22^\circ$.

Table 2.17

Options for studying the model of the aircraft by angle of attack

1	P1a	0	0	0	0	0	0	Notice
2	P19	0	0	0	0	0	0	Repeated
3	P43	0	0	0	0	0	0	Repeated
4	P7	0	8	0	0	0	0	

End of table 2.17

5	P8	0	18	0	0	0	0	
6	P9	0	23	0	0	0	0	
7	P6a	0	-11	0	0	0	0	
8	P22	0	-16	0	0	0	0	
9	P21	0	-21,5	0	0	0	0	
10	P20B	0	-26	0	0	0	0	
11	P23	0	-30	0	0	0	0	
12	P10	0	0	-11	0	0	0	
13	P11	0	0	-20	0	0	0	
14	P12	0	0	-25	0	0	0	
15	P24	10	0	0	0	0	0	
16	P25	20	0	0	0	0	0	
17	P29	25	0	0	0	0	0	
18	P26	30	0	0	0	0	0	
19	P27	35	0	0	0	0	0	
20	P28	40	0	0	0	0	0	
21	P13	0	0	0	10	0	0	
22	P14a	0	0	0	22	0	0	
23	P15	0	0	0	31	0	0	
24	P16	0	0	0	-7	0	0	
25	P17	0	0	0	-17	0	0	
26	P18	0	0	0	-26,5	0	0	
27	P44	0	0	0	0	0	-4,33	
28	P45	0	0	0	0	0	-2,17	
29	P46	0	without h.s.	without v.s.	0	0	0	
30	P38	0	-21	-20	0	0	0	
31	P35	30	0	0	25	25	0	
32	P34	30	-26	0	25	25	0	
33	P33	30	-30	0	25	25	0	
34	P36	30	-11	0	0	0	0	
35	P30	30	-16	0	0	0	0	
36	P31	30	-26	0	0	0	0	
37	P32	30	-30	0	0	0	0	
38	P37	30	-21	-20	0	0	0	
39	P47	0	0	0	0	0	0	holder β

In addition, additional blowing was performed to determine the effect of the Re number on the values of aerodynamic coefficients, the model was blown in the flight position to determine the true value of the angle of attack of the model at a zero position of the beam α -mechanism.

The setting angle of the wing relative to the fuselage centerline according to the measurements using the optical quadrant was $20'$. Based on the obtained results, corrections to the angles of attack in previous experiments were taken into account. Thus, on the dependence diagrams of the aerodynamic coefficients, the angle of attack corresponds to the true angle of attack on the chord of the wing.

Table 2.18

Options for research of the aircraft model by the angle of sideslip

Item number	Protocol number	δ_f°	δ_{el}°	δ_{rd}°	$\delta_{fl.r}^\circ$	$\delta_{fl.l}^\circ$	φ_{st}°	Notice
1	P48	0	0	0	0	0	0	
2	P49	0	0	-11	0	0	0	
3	P50a	0	0	19	0	0	0	
4	P51	0	0	0	31	0	0	
5	P52	0	0	0	-26,5	0	0	
6	P53B	0	18	0	0	0	0	
7	P54	0	-26	0	0	0	0	

Fig. 2.32 and 2.33 show photos of the aircraft model during the experiment in the test section during the research on the angle of attack α . Fig. 2.34 illustrates a model of the aircraft configuration without horizontal and vertical stabilizers. In Fig. 2.35 there is a model in the process of determining the effect of the longitudinal holder on the aerodynamic coefficients. Fig. 2.36 is a model on the weight suspension in the testing section during blowing at the angle of sideslip β .

During the processing of test results, forces from a suspension and a cross handle of a model during blowing at the angle of sideslip are considered. The results of the research are presented in the form of the dependence of aerodynamic coefficients on the angle of attack or sideslip for different configurations of the aircraft model, which differed in the deflection of the high lift devices or control surfaces at certain angles.

The results of the research do not take into account the effect of propeller blowing of the surface of the aircraft model on the aerodynamic coefficients.

The coefficients of aerodynamic forces c_x, c_y, c_z are presented in the projections on the axis OY_e, OX_e, OZ_e of the semi-connected coordinate system, to simplify the formula the coefficient indices «e» are omitted. The coefficients of aerodynamic moments m_x, m_y, m_z are given in the linked coordinate system.

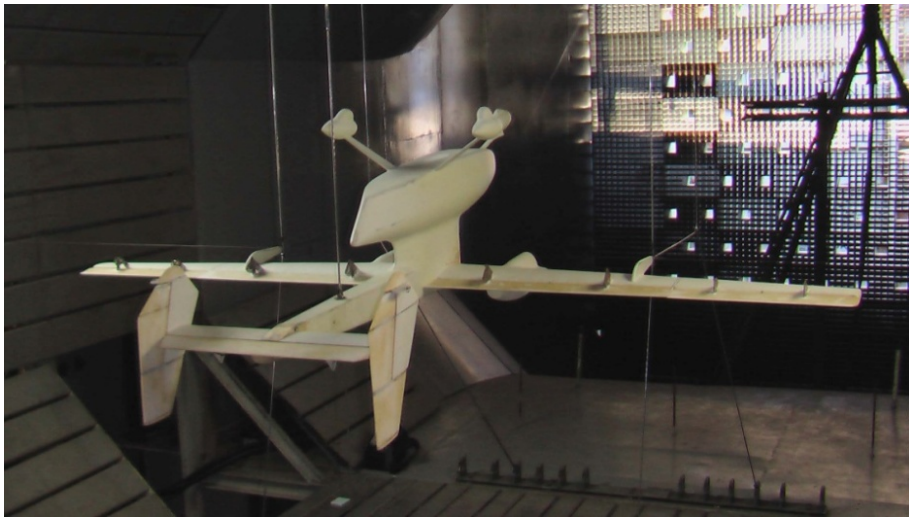


Fig. 2.32. Aircraft model in the test section of the wind tunnel during blowing at α

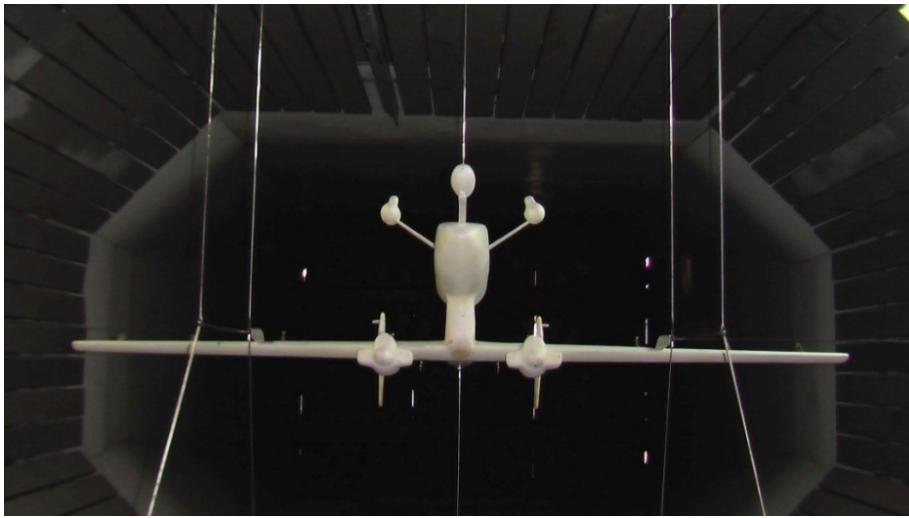


Fig. 2.33. Aircraft model in the test section of the wind tunnel in the tube position

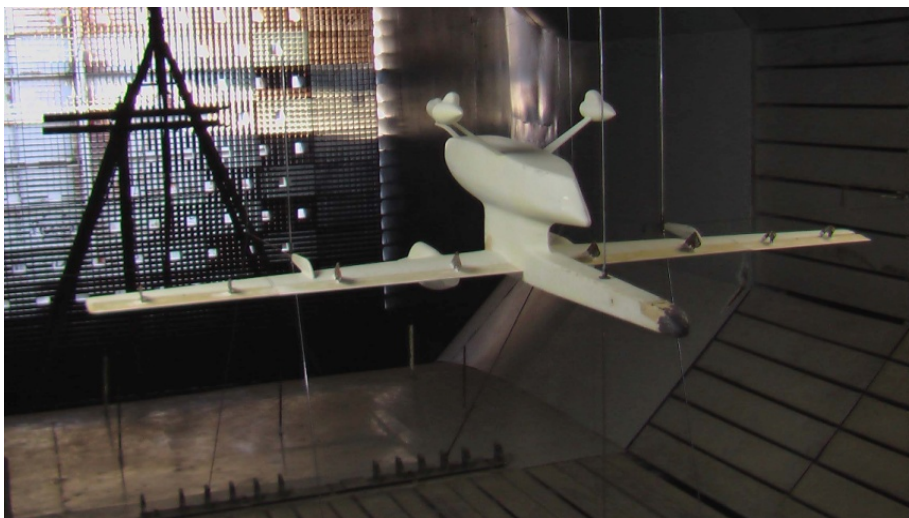


Fig. 2.34. Model of the aircraft configuration without stabilizers

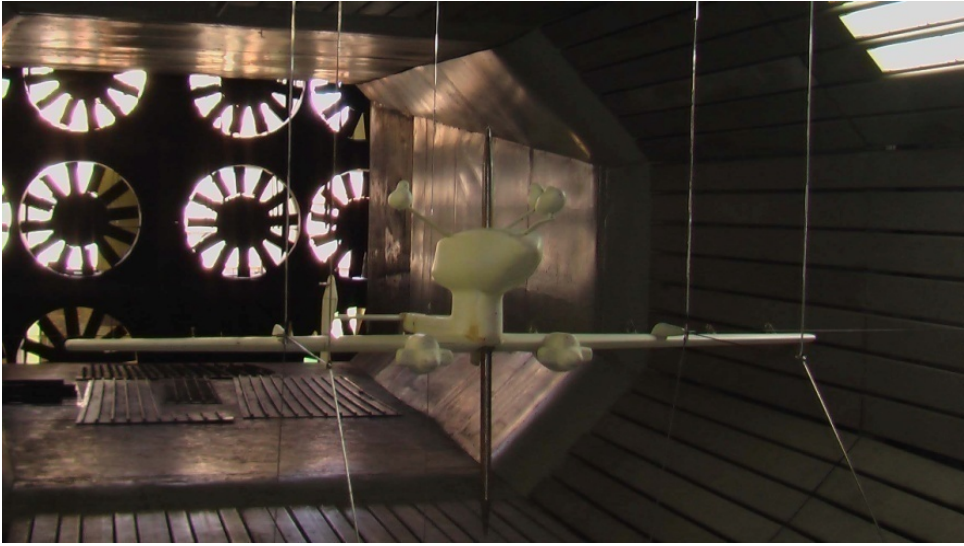


Fig. 2.35. Model of an aircraft with a longitudinal holder

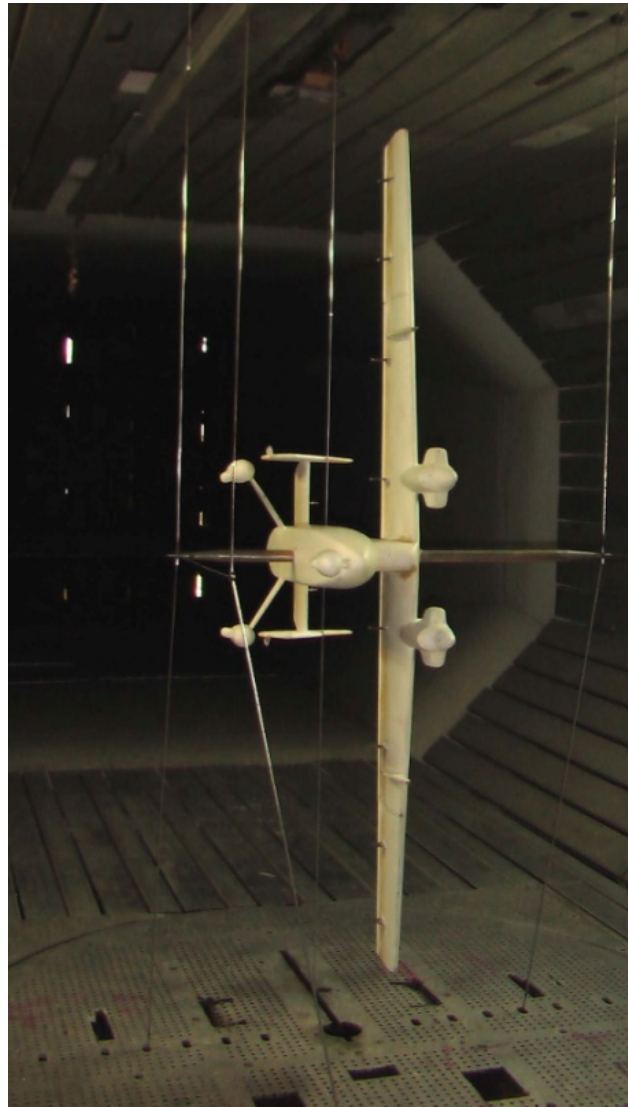


Fig. 2.36. Aircraft model in the test section of the wind tunnel during blowing at β

The model was in the initial or flight configuration, in which there was no deflection of high lift devices and control surfaces.

To control the repeatability of the blowing results throughout the experiment, the model was blown in the initial configuration. Fig. 2.37 shows the results of such blowing superimposed on one graph, which indicates the invariance of the characteristics of the model over time during the experiment. In addition, the graph shows the effect of the random component of the error in determining the aerodynamic coefficients. For the flight configuration, it can be noted that the value of the critical angle of attack is 16° , the linear area of correspondence $C_y = f(\alpha)$ reaches 8° . Judging by the behavior of the correspondence $m_z = f(\alpha)$ in the area of the critical angle of attack, the complete aerodynamic stall is already at $14^\circ \dots 15^\circ$, although it continues to increase slightly to 16° . The decrease in lift at critical angles of attack is smooth.

Fig. 2.38 illustrates the change in the aerodynamic quality of the aircraft model by the angle of attack, which shows that the maximum quality reaches a value of 12 in the flight configuration and takes place in the range of angles of attack $3^\circ \dots 8^\circ$. Fig. 2.39 shows the polarity of the aircraft model for the flight configuration.

From the graphs in Fig. 2.40 it is seen that the critical angles of attack decrease when the flaps deviate from $\alpha_{cr} = 16^\circ$ when the flaps are not deflected to $\alpha_{cr} = 12^\circ$ when the flaps are deflected by $\delta_{fl} = 10^\circ$ and to $\alpha_{cr} = 10,8^\circ$ when the flaps are deflected by $\delta_{fl} = 30^\circ$. Further flap deflection becomes ineffective, the lift force does not increase, and at $\delta_{fl} = 40^\circ$ significantly decreases, the critical angle of attack at $\delta_{fl} = 35^\circ$ was only $\alpha = 5,8^\circ$, and before this angle was reached, the range of correspondence $C_y = f(\alpha)$ was almost linear. But the behavior of the correspondence $C_y = f(\alpha)$ in the overcritical region of the angles of attack does not lead to a sharp and significant reduction in lift. The behavior of the correspondences $m_z = f(\alpha)$ is fully consistent with the behavior of the correspondences $C_y = f(\alpha)$ for the corresponding angles of deflection of the flaps. A gradual increase in the negative value of the derivative m_z^α at the angles of attack greater than 8° indicates a gradual stall progression on wing upper surface for the all angles of flap deflection up to 30° . The slight effect of flap deflection on the longitudinal moment for the selected position of the aircraft centre of gravity attracts attention. The influence of flap deflection on the aerodynamic quality of the aircraft model and the polar is shown in Fig. 2.41.

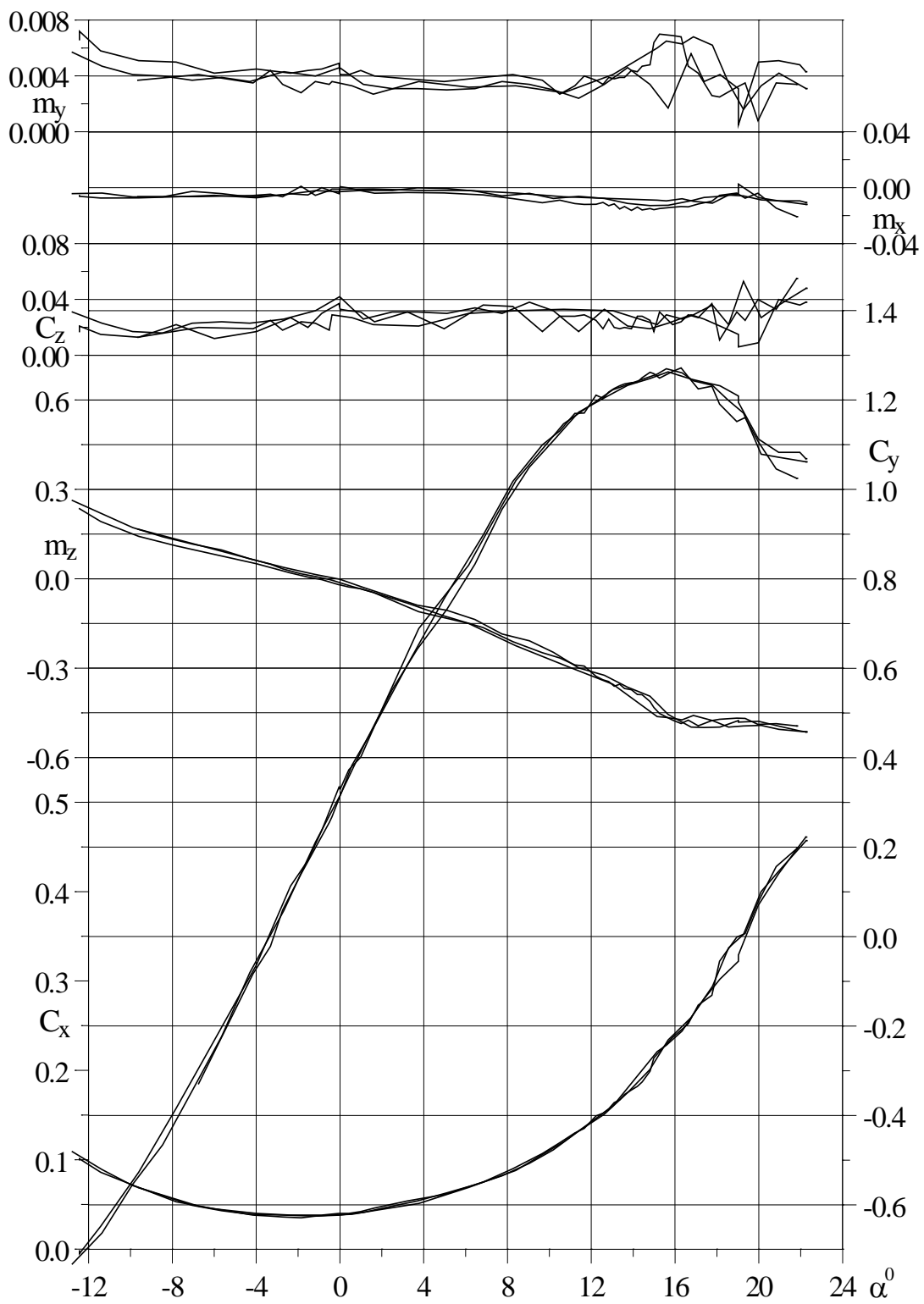


Fig. 2.37. Repeatability of the experiment results to determine the aerodynamic coefficients, protocols №№ P1a, P19, P43

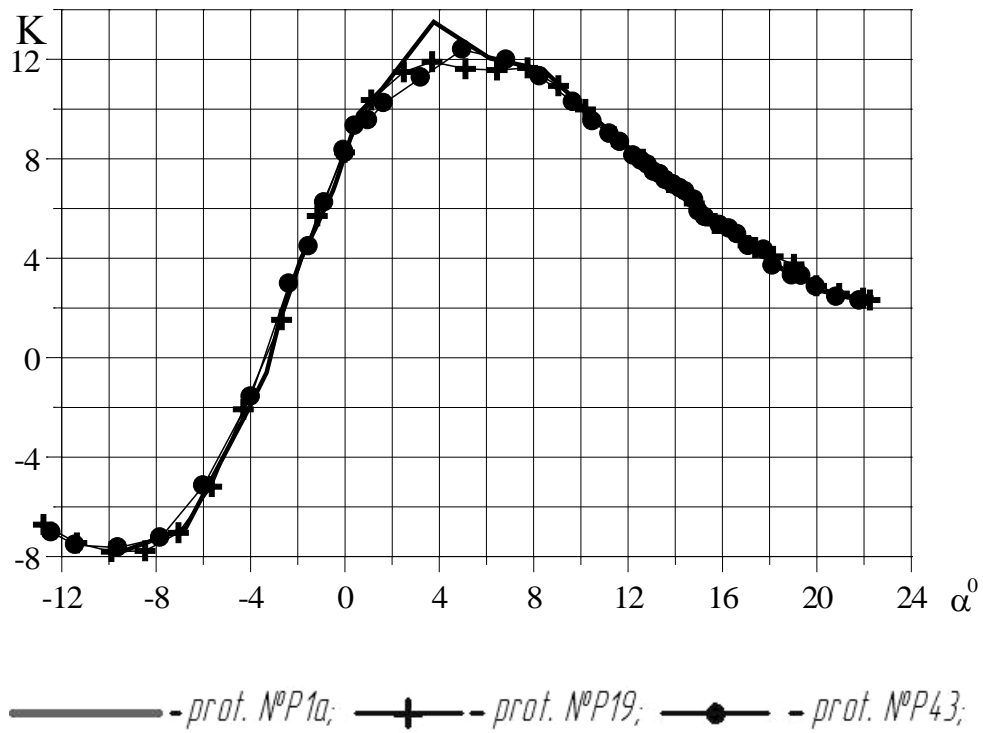


Fig. 2.38. Aerodynamic quality of the aircraft model in the flight configuration $\delta_f = 0$

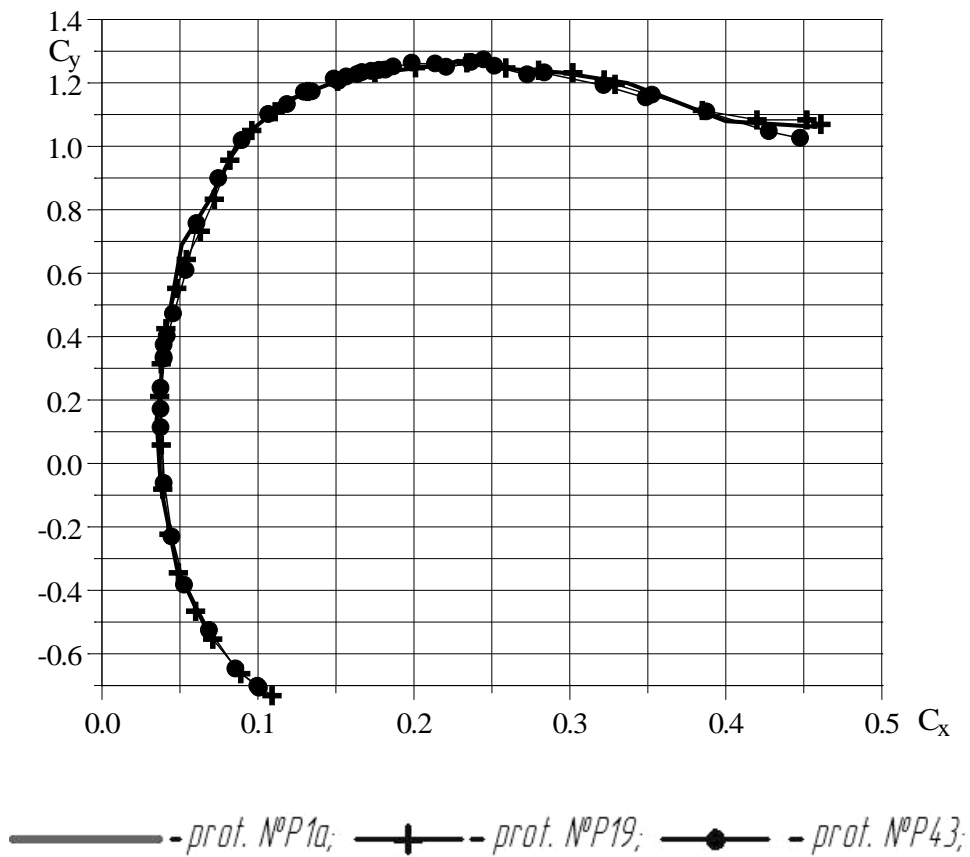


Fig. 2.39. Polar aircraft model in the flight configuration $\delta_f = 0$

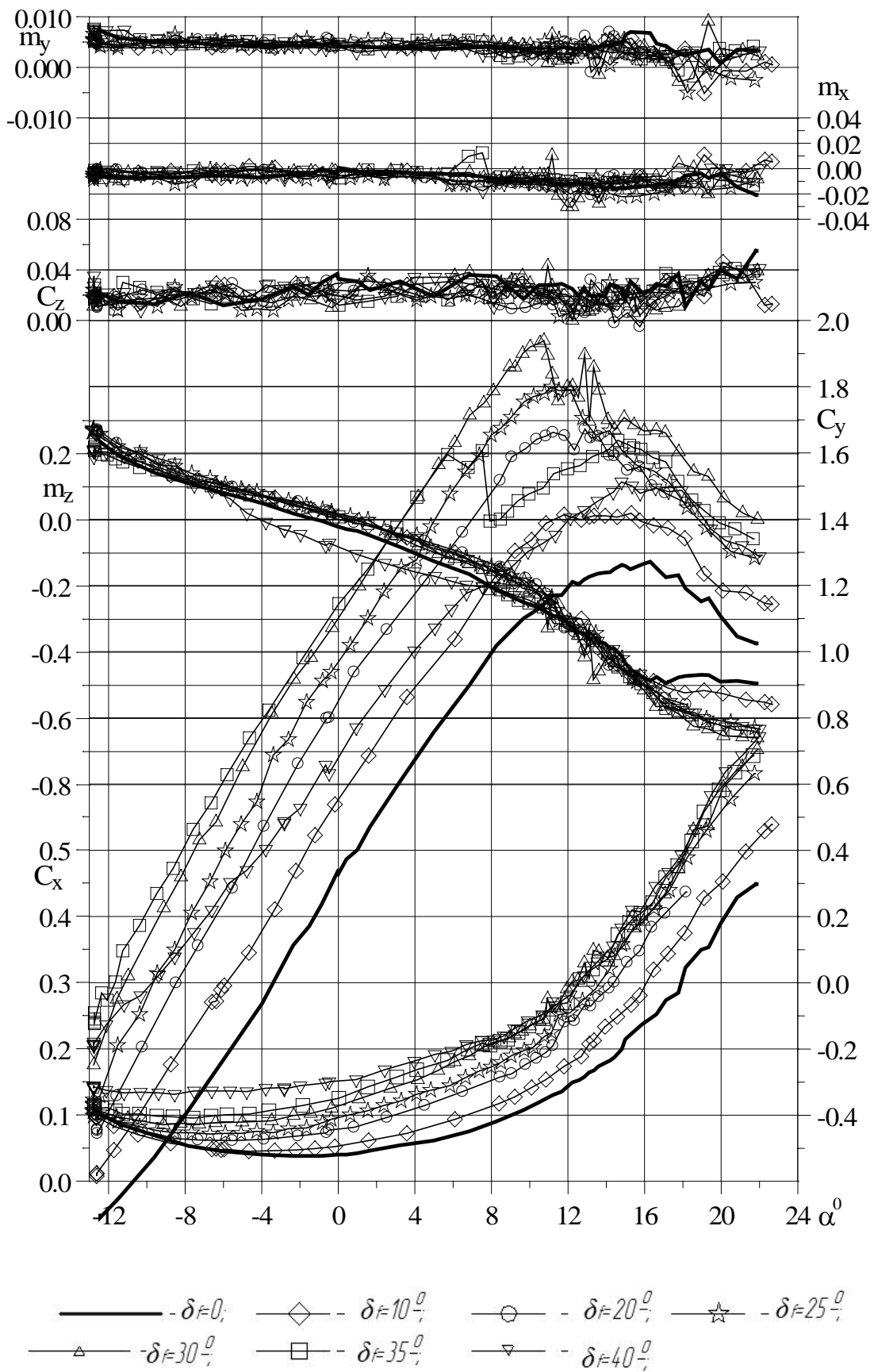


Fig. 2.40. The effect of flap deflection on the change of aerodynamic coefficients of the model by the angle of attack

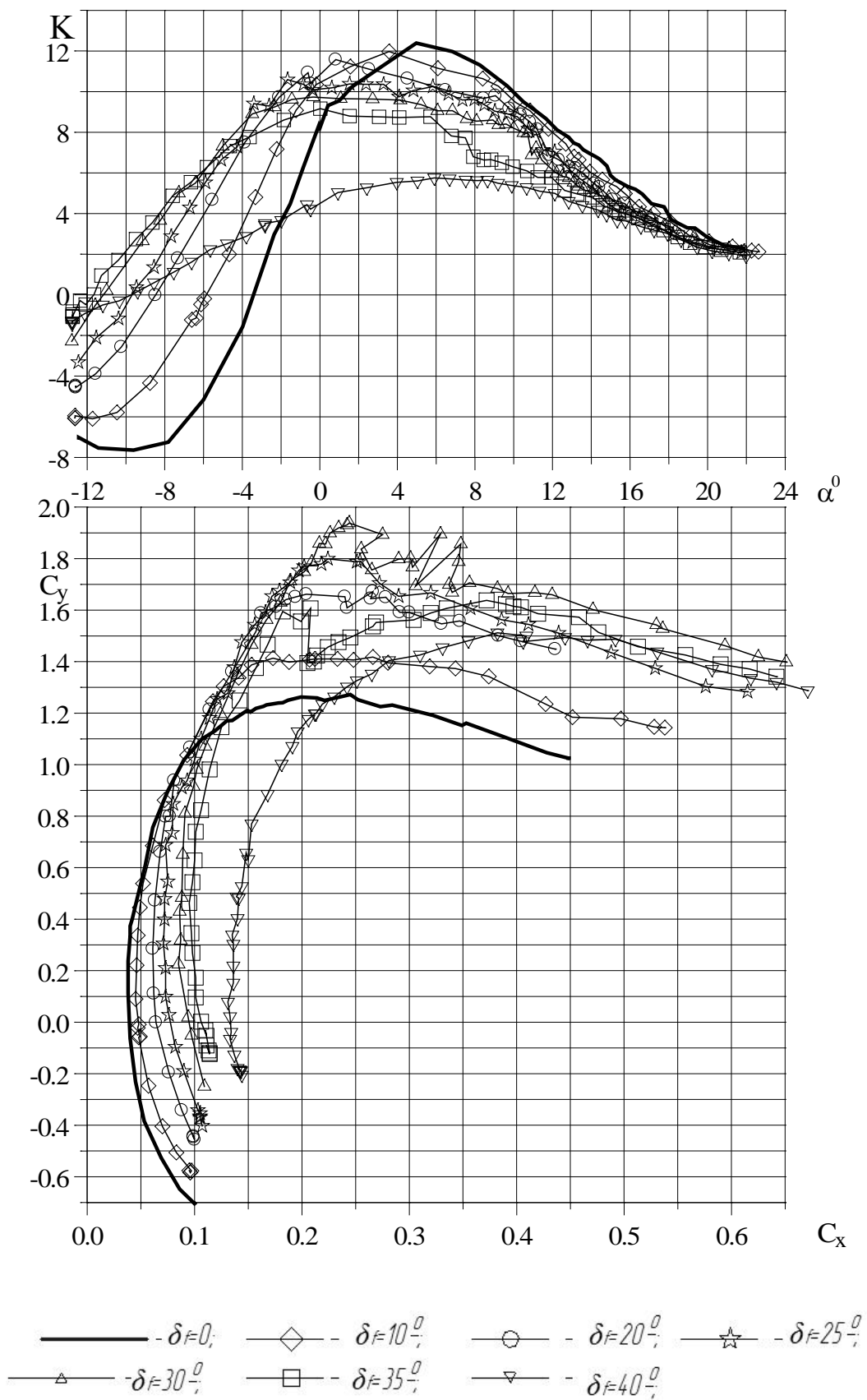


Fig. 2.41. The effect of flap deflection on the aerodynamic quality and the aircraft model polar

In Fig. 2.42 and 2.43, show the effect of height rudder deflection on aerodynamic characteristics with hidden flaps. The deflection of the elevators upwards leads to a significant reduction in lift in the entire range of the angles of attack, including a decrease in $C_{y \max}$ with the almost constant value of the critical angle of attack α_{cr} . The impact on the drag in a certain range of the angles of attack is small and significantly less than when elevators are deflected downwards in the same range of angles $\alpha = 0 \dots 15^\circ$.

When the elevators are deflected downwards the lift force and $C_{y \max}$ value increase with invariable α_{cr} . From the correspondences $m_z = f(\alpha)$ in Fig. 2.43, it can be concluded that the efficiency of the elevators m_z^δ remains constant up to almost -26° when it is deflected upwards in the range of the angles of attack $4^\circ \dots 12^\circ$ and decreases slightly outside this range, remaining constant when the elevator is deflected to $-21,5^\circ$. The efficiency of the elevator m_z^δ when it is deflected downwards remains the same as when it is deflected upwards to an angle of 8° , and then it decreases sharply (by ~ 15 times) and when deflection is more than 18° it is almost absent in the vicinity of the angle of attack of 8° . This phenomenon is a consequence of the horizontal stabilizer getting into the air shadow of the wing and fuselage. At the angles of attack of less than 6° there is an inverse reaction of the longitudinal moment to the deflection of the elevators of more than 18° . When the angle of attack has the large negative values of $-12^\circ \dots -11,5^\circ$, and the deflection of the elevators is $-21,5^\circ \dots -26^\circ$, the derivative m_z^α changes the sign indicating a stall on the lower surface of the horizontal stabilizer. At an angle of the elevator deviation to -31° , this phenomenon takes place when the angles of attack are less than -6° .

The deflection of the rudder in the flight configuration has almost no effect on the α_{kr} value and does not significantly reduce the $C_{y \max}$ value when it deflects by more than 11° , as shown in Fig. 2.44. There is also an increase in the drag coefficient and a small positive increase in the longitudinal moment coefficient. The efficiency of the rudder when creating a yaw moment remains constant up to a deflection angle of 20° , and then it slightly decreases.

Fig. 2.45 shows the effect of the simultaneous deflection of the elevators and rudder on the aerodynamic characteristics in comparison with the cases of their individual deflection in the flight configuration. Simultaneous deflection of the control surfaces has little effect on the efficiency of each of them separately.

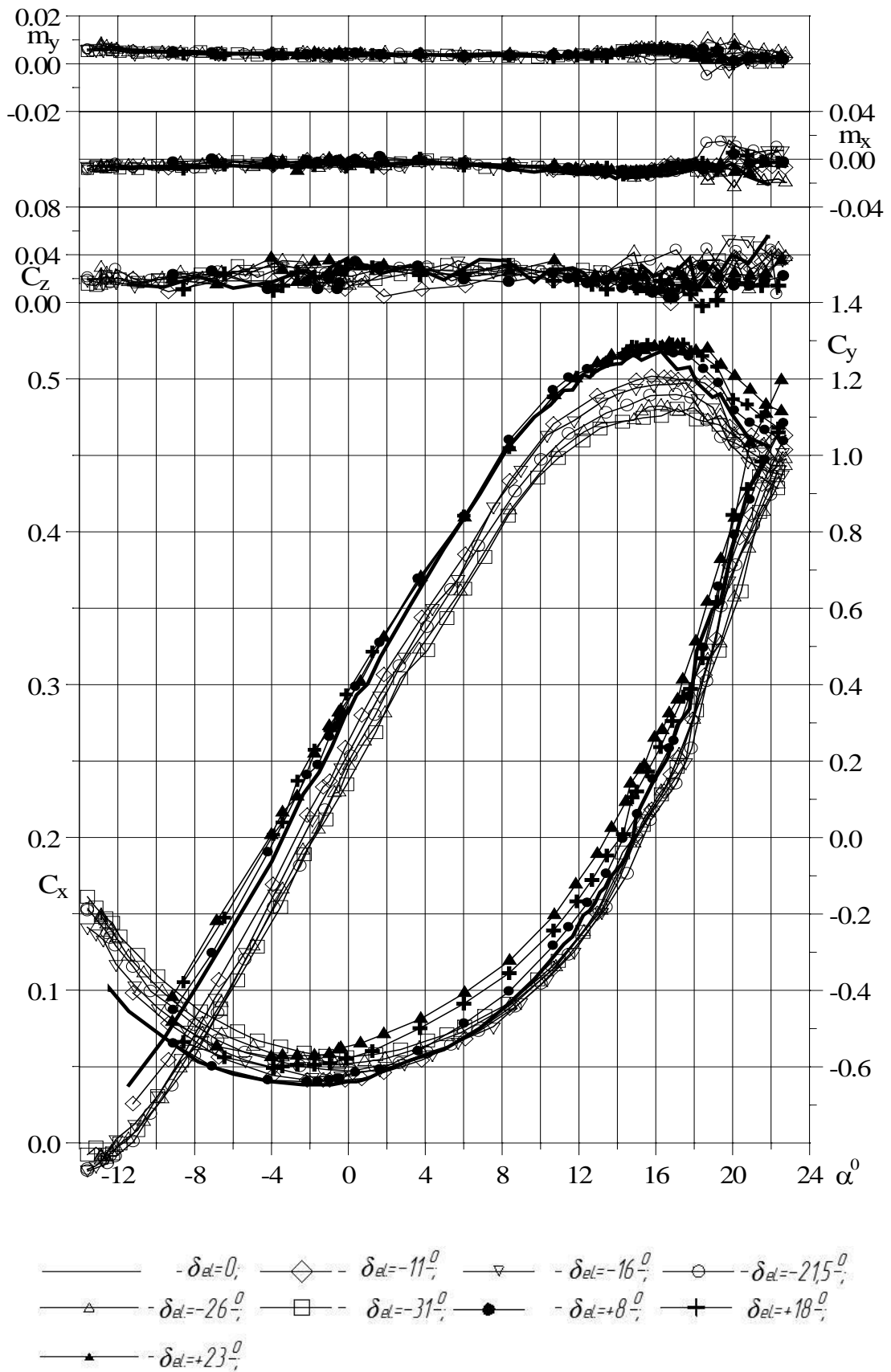


Fig. 2.42. Influence of the elevator deflection on the change of aerodynamic coefficients of the model by the angle of attack

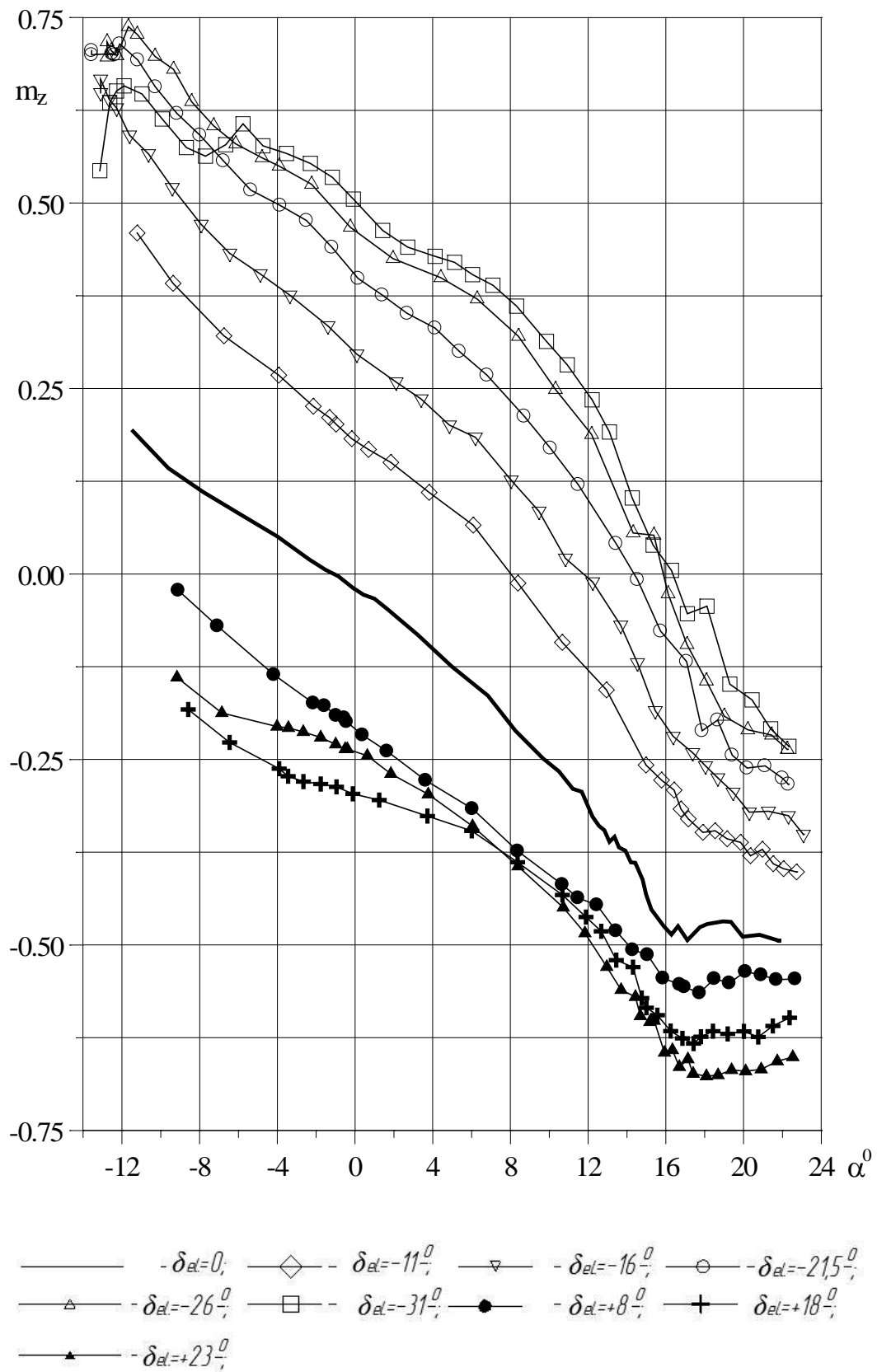


Fig. 2.43. Influence of the deflection of the elevators on the change in the longitudinal moment coefficient of the model by the angle of attack

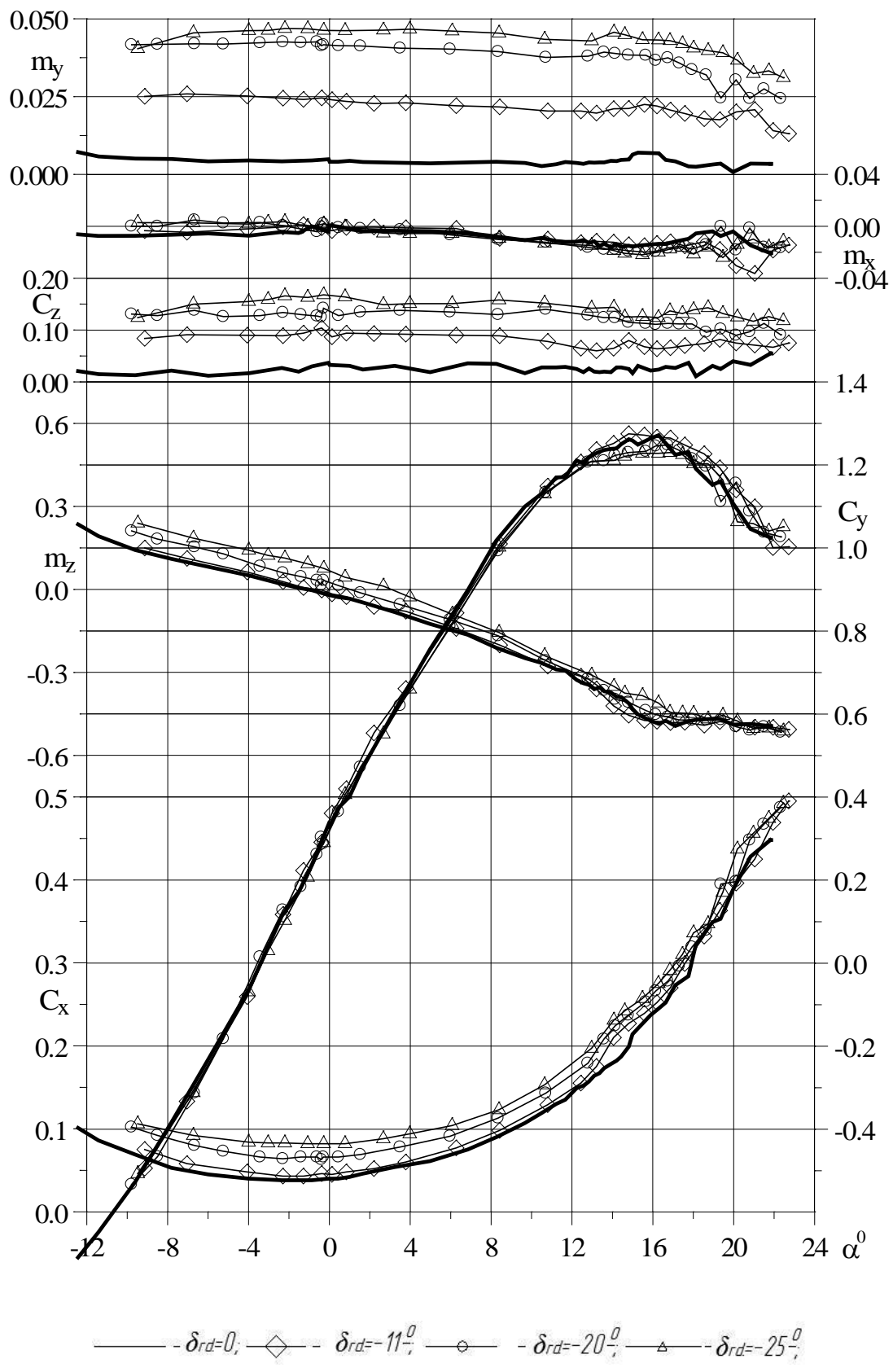


Fig. 2.44. Influence of the rudder deflection on the change of aerodynamic coefficients of the model by the angle of attack

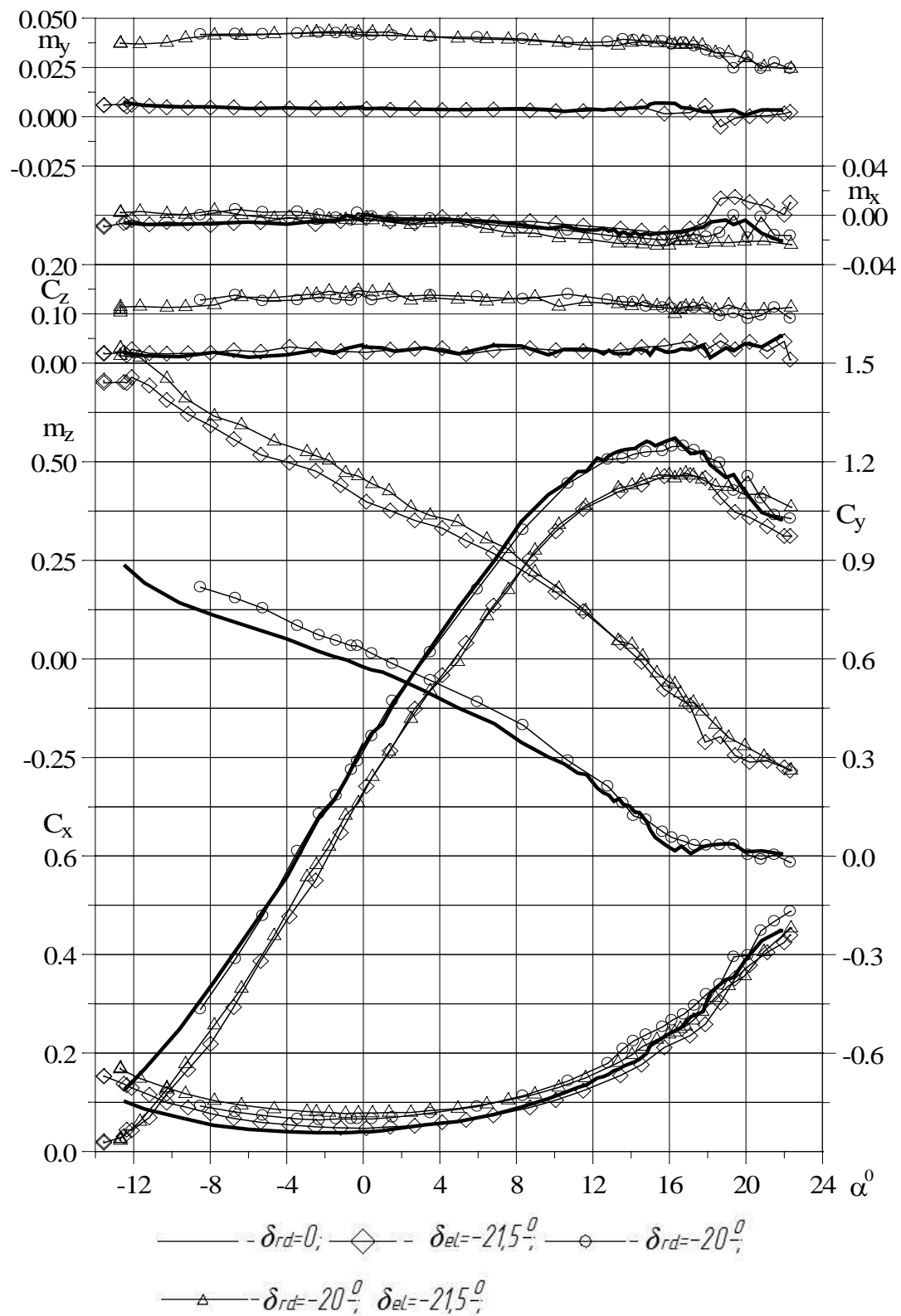


Fig. 2.45. Influence of the simultaneous deflection of the elevator and rudder on the change of aerodynamic coefficients of the model by the angle of attack for the flight configuration

The influence of the deflection of the right flaperon (aileron) on the aerodynamic characteristics of the aircraft model is shown on the graphs in Fig. 2.46. The deflection of the flaperon upwards leads to a decrease in lift by 0,1...0,15 and a small α_{cr} increase by $\sim 0,9^\circ$ when $\delta_{fl} = -26,5^\circ$.

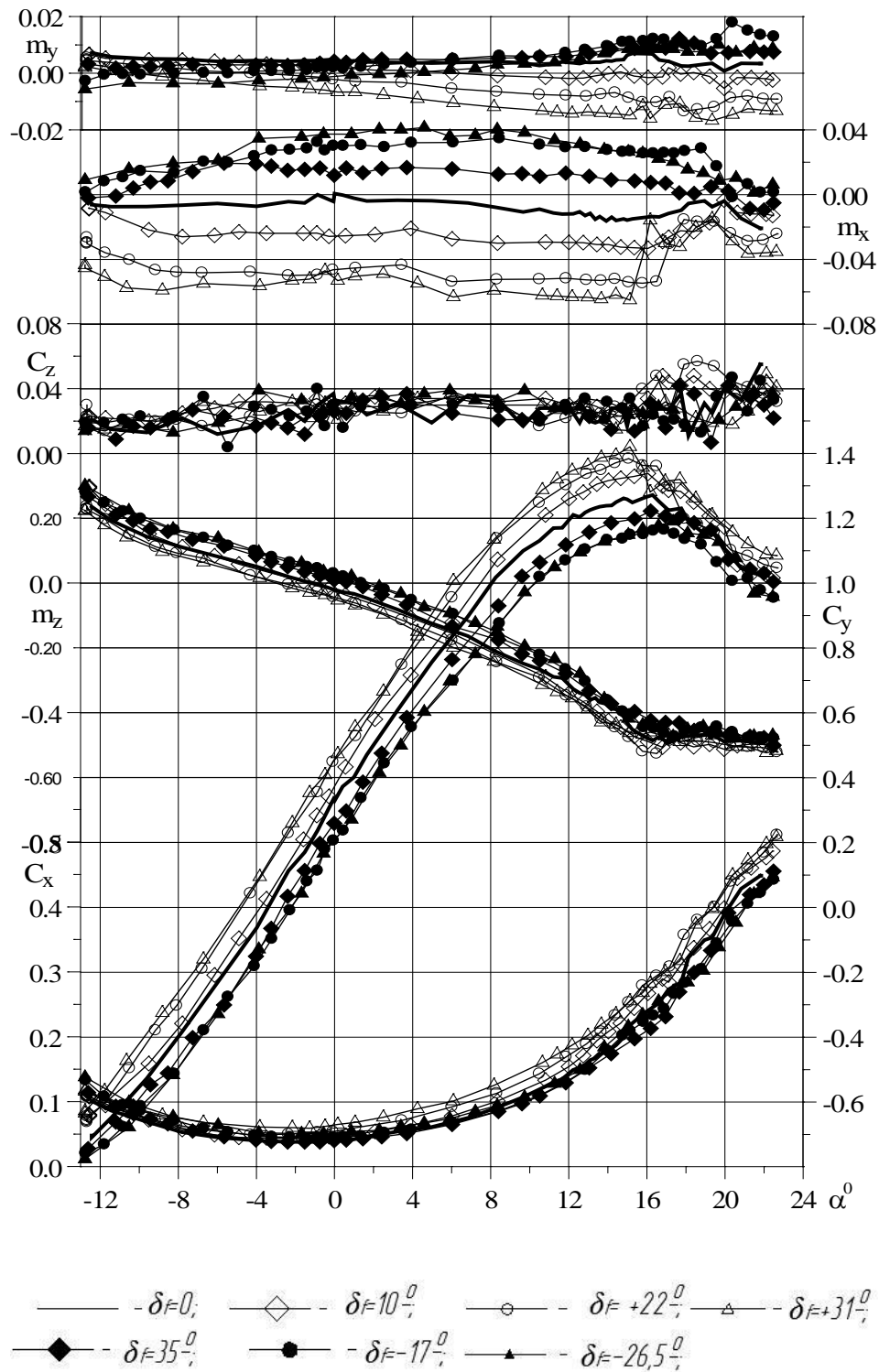


Fig. 2.46. Change in the aerodynamic coefficients of the model by the angle of attack when deflecting the right flaperon

Deviation of the flaperon downwards, on the contrary, slightly reduces α_{kr} and increases the lifting force approximately to the same extent as the deviation of the flaperone upwards.

The effectiveness of flaperone in creating the roll moment m_x is significantly reduced when it is deflected upwards by more than -17° , and when it is deflected downwards by more than $+22^\circ$.

The effectiveness of the flaperon when it is deflected downwards is maintained to the critical angle of attack, and then it decreases sharply due to the breakaway on the wing upper surface where the flaperon is mounted. When the flaperon is deflected upwards, its effectiveness decreases at the negative angles of attack of more than above $-4^\circ \dots -6^\circ$ due to the breakaway on the wing lower surface where the flaperon is mounted. The difference in the effectiveness of the flaperon in the deviation up and down can be compensated by the differential deviation of the right and left flaperons. The behavior of the coefficient of jerking moment at the angle of attack corresponds to the change in the coefficient of drag when the flaperon is rejected.

In the model configuration with the flaps deflected by 30° , the deviation of the elevators upwards leads to a decrease in lift and a decrease in the critical angle of attack by $1,3^\circ$ when $\delta_{el} = -31^\circ$, which illustrates on the graph in Fig. 2.47. The efficiency of the elevators begins to decrease at the angles of attack less than $-0,5^\circ$ when $\delta_{el} = -31^\circ$ due to the breakaway from the lower surface of the horizontal stabilizer at the large negative angles of attack, which occur due to a huge aerodynamics downwash by the deflected flap.

Within the elevator deflection to $-26,5^\circ$ the efficiency of the elevator is almost constant and is approximately the same as in the flight configuration in the range of the angles of attack from -2° to the critical angle of attack, except for the configuration with $\delta_{el} = -11^\circ$, where the elevator efficiency fell sharply at the angles of attack more of more than 9° .

The release of flaperons in the flap mode at 25° simultaneously with the release of flaps by 30° has led to an increase in $C_{y \max}$ of 0,2, the critical angle of attack can be considered as unchanged (Fig. 2.48). The effect of elevator deflection on aerodynamic characteristics remained the same as in the configuration with retracted flaperons when $\delta_f = 30^\circ$ (Fig. 2.47). The extension of flaperons added a negative increase to the longitudinal moment in the configuration with $\delta_f = 30^\circ$.

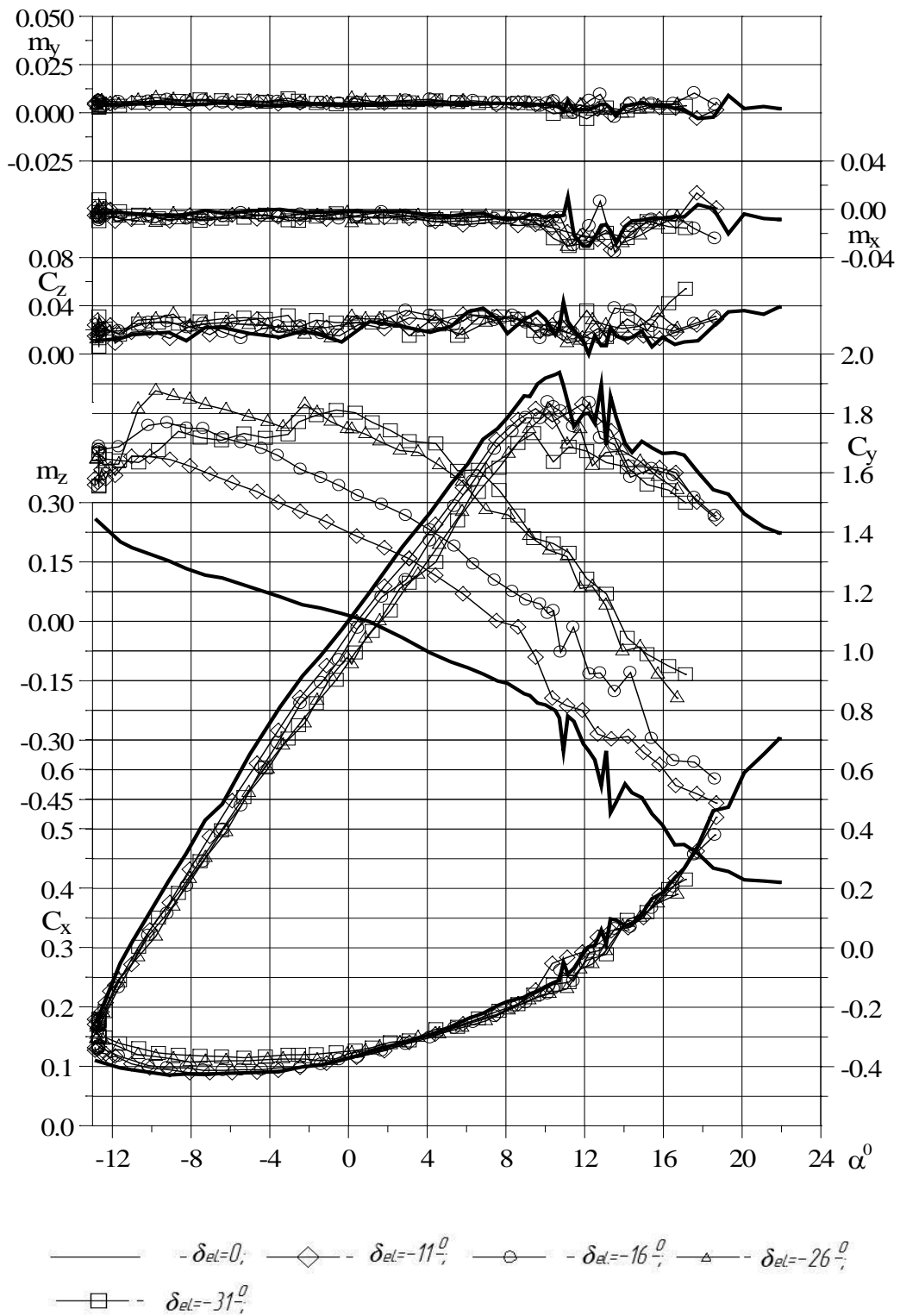


Fig. 2.47. The effect of deflection of the elevator on the change of the model aerodynamic coefficients in the configuration with $\delta_f = 30^\circ$

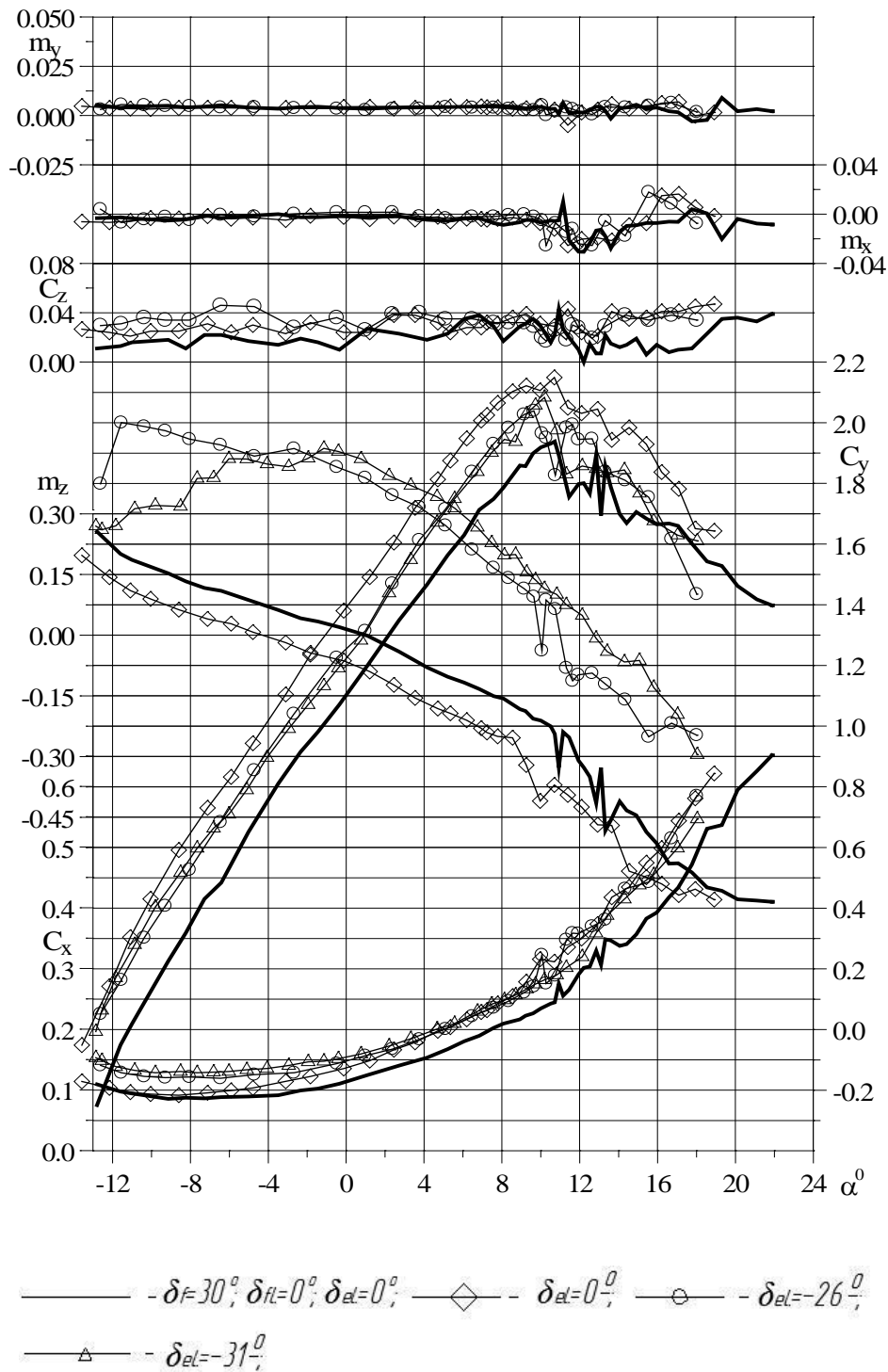


Fig. 2.48. Influence of elevator deflection on the change of model aerodynamic coefficients in the configuration with the extended flaps and flaperons by the angle of attack

Fig. 2.49 shows the effect of the simultaneous deviation of the elevators and the rudder in the configuration with $\delta_f = 30^\circ$ by the aerodynamic coefficients as a function of the angle of attack. The Simultaneous deflection of the control surfaces did not affect their efficiency. A smooth breakaway on the horizontal stabilizer with the elevator deflection of $-21,5^\circ$ starts at the negative

angles of attack of less than -5° . Returning to the previous graphs, it is worth noting that the beginning of the breakaway at $\delta_{el} = -26^\circ$ begins at the angle of attack of $\sim -2 \dots -2,5^\circ$, but its nature is somewhat different. The local breakaway occurs but does not develop until a certain negative angle is reached.

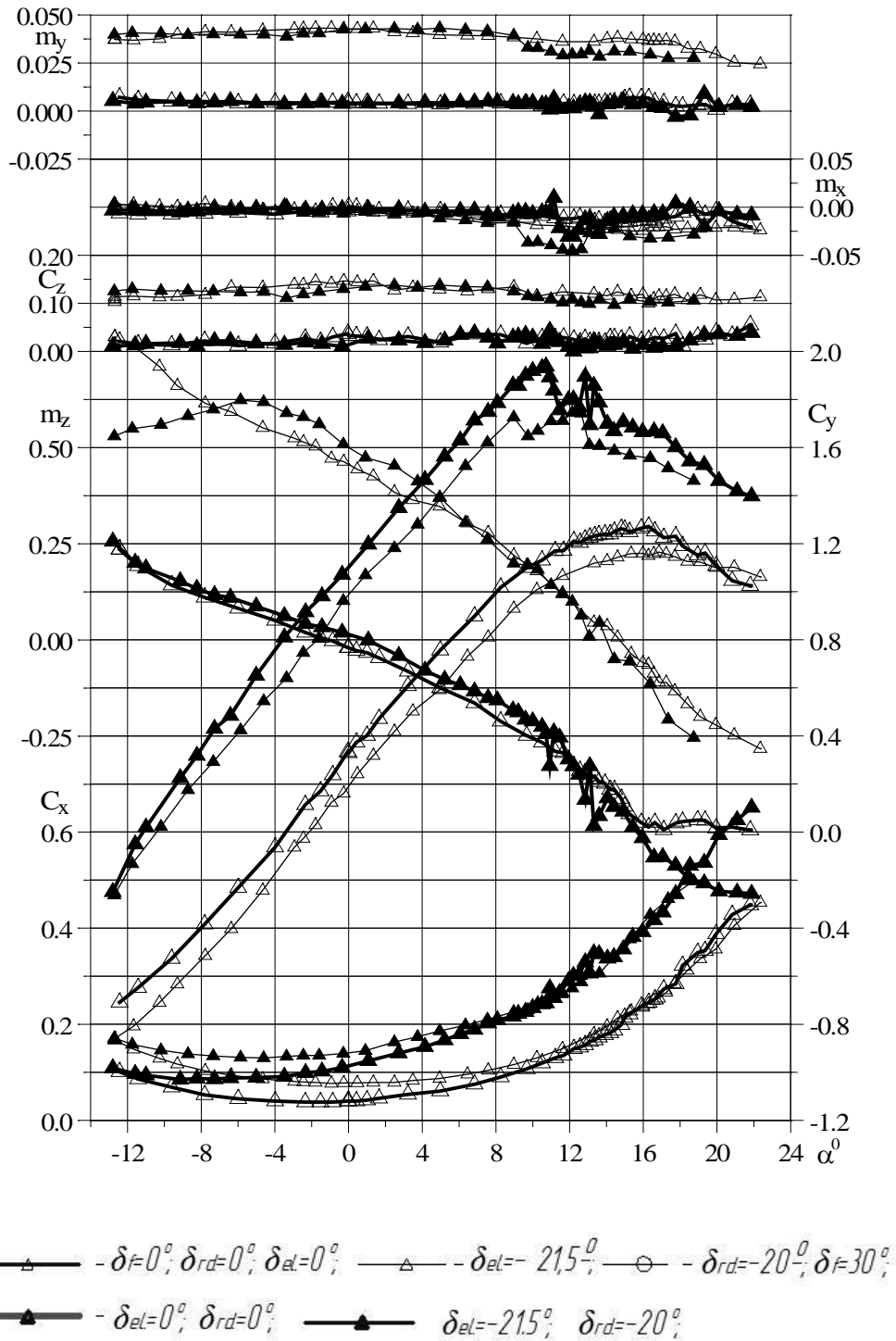


Fig. 2.49. The effect of simultaneous deviation of the elevator and rudder on the change of the model aerodynamic coefficients in the configuration with $\delta_f = 0$ and $\delta_f = 30^\circ$

Fig. 2.50 shows the aerodynamic characteristics of the aircraft model in the flight configuration at different tailplane angles and $\delta_{e1} = 0$. Stabilizer Pull-up Deflection slightly reduces the lift, leaving the critical angle of attack almost unchanged. The efficiency of the stabilizer deflection is $m_z^{\phi} = -0,0382\%$ when the deflection is $-2,17^{\circ}$ and $m_z^{\phi} = -0,0295\%$ with a further deflection up to $-4,33^{\circ}$ at the angle of attack $\alpha = 2^{\circ}$. The efficiency of the stabilizer slightly decreases when approaching the critical angle of attack.

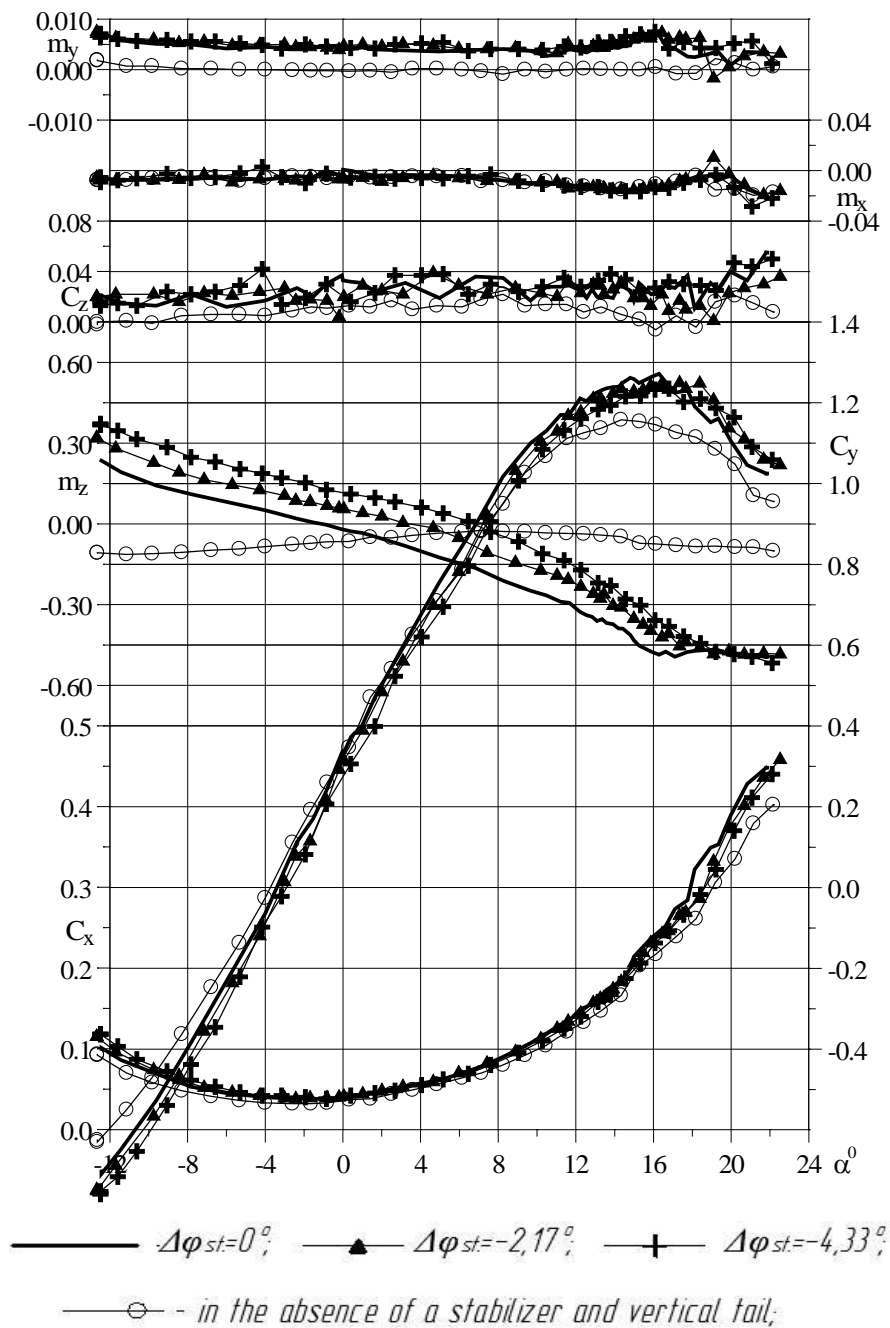


Fig. 2.50. The effect of the stabilizer on the change of model aerodynamic coefficients by the angle of attack

Fig. 2.50 also shows the aerodynamic characteristics of the aircraft model without the empennage. From the position of the correspondence $m_z = f(\alpha)$ diagram relative to the same dependence for the flight configuration, it can be concluded that when flying at an angle of attack $\approx 2^\circ$ the lifting force on the empennage is zero when $\delta_{el} = 0$ and the empennage resistance is minimal. From the comparison of graphs, one can also draw conclusions about the role played by the empennage in the asymmetry of the aircraft model.

Fig. 2.51 illustrates the effect of the transverse holder for blowing at the angle of sideslip on the aerodynamic characteristics of the aircraft model when blowing on the angle of attack. The obtained results are necessary for the definition of corrections to aerodynamic coefficients in blowing at a sliding angle. As you can see, the effect of the holder is manifested mainly in an increase in drag. Further purges at the sliding angle were carried out at the angle of attack of the model $0,33^\circ$. The results of the purge on the sliding angle, taking into account the corrections for the impact of the holder, plotted on the graph, indicate the accuracy of the amendments.

As can be seen from the graphs of changes in the aerodynamic characteristics of the aircraft model in Fig. 2.52, the influence of the angle of sideslip is manifested, in the occurrence of the transversal force C_z and yaw moment m_y aimed at the reduction in the angle of sideslip, which indicates the static directional stability of the model. The deflection of the elevators did not affect these characteristics. There is a somehow noticeable effect of sliding on the coefficient of roll moment in case of deflected rudder due to its blanketing by the vertical stabilizer. The longitudinal moment of the angle of sideslip is almost unchanged, and hence the efficiency of the elevator and the same can be said about the invariability of the lifting force, at least within the sliding angle of $\pm 10^\circ$.

The influence of the rudder deflection on the aerodynamic characteristics of the model depending on the angle of sideslip is shown in Fig. 2.53. It is noteworthy a reduction in the static directional stability m_y^β to a neutral one when the elevator is deflected to counteract sliding by 19° at the sliding angles greater than 8° . The reason for this is the peculiarities of the formation of flow on the vertical stabilizer and in between with the horizontal one.

These features are manifested in a noticeable increase in the longitudinal moment on the coupling and a small increase in the moment of roll on the windward side. And we still have a noticeable increase in frontal resistance due to the inhibition of flow in the gap between the keels with deflected rudders to prevent slipping. It is likely that the increase in pressure on the upper surface of the horizontal plumage leads to the appearance of the moment of calibration.

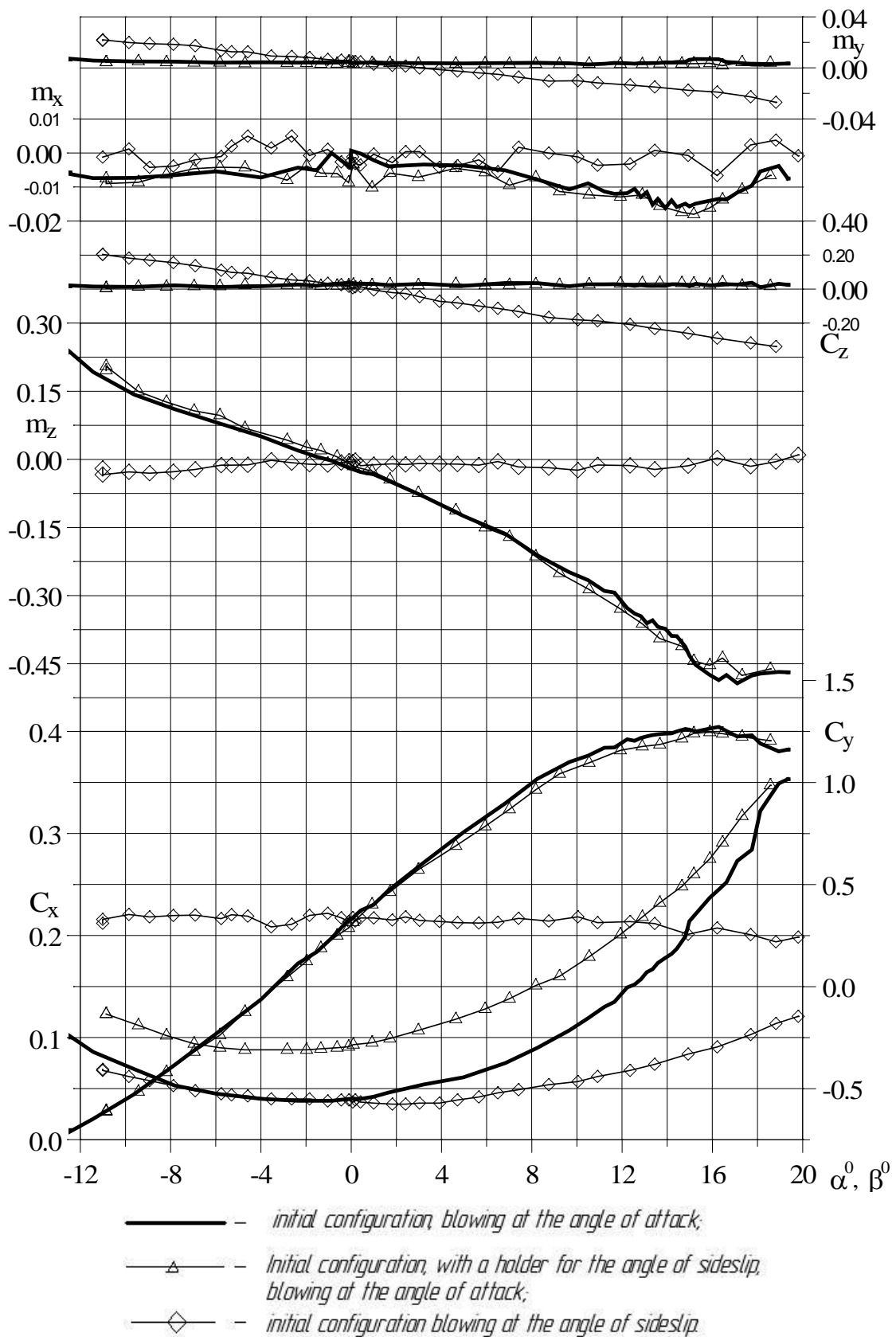


Fig. 2.51. Determination of the influence of the holder to analyze the model by the angle of sideslip on the aerodynamic coefficients

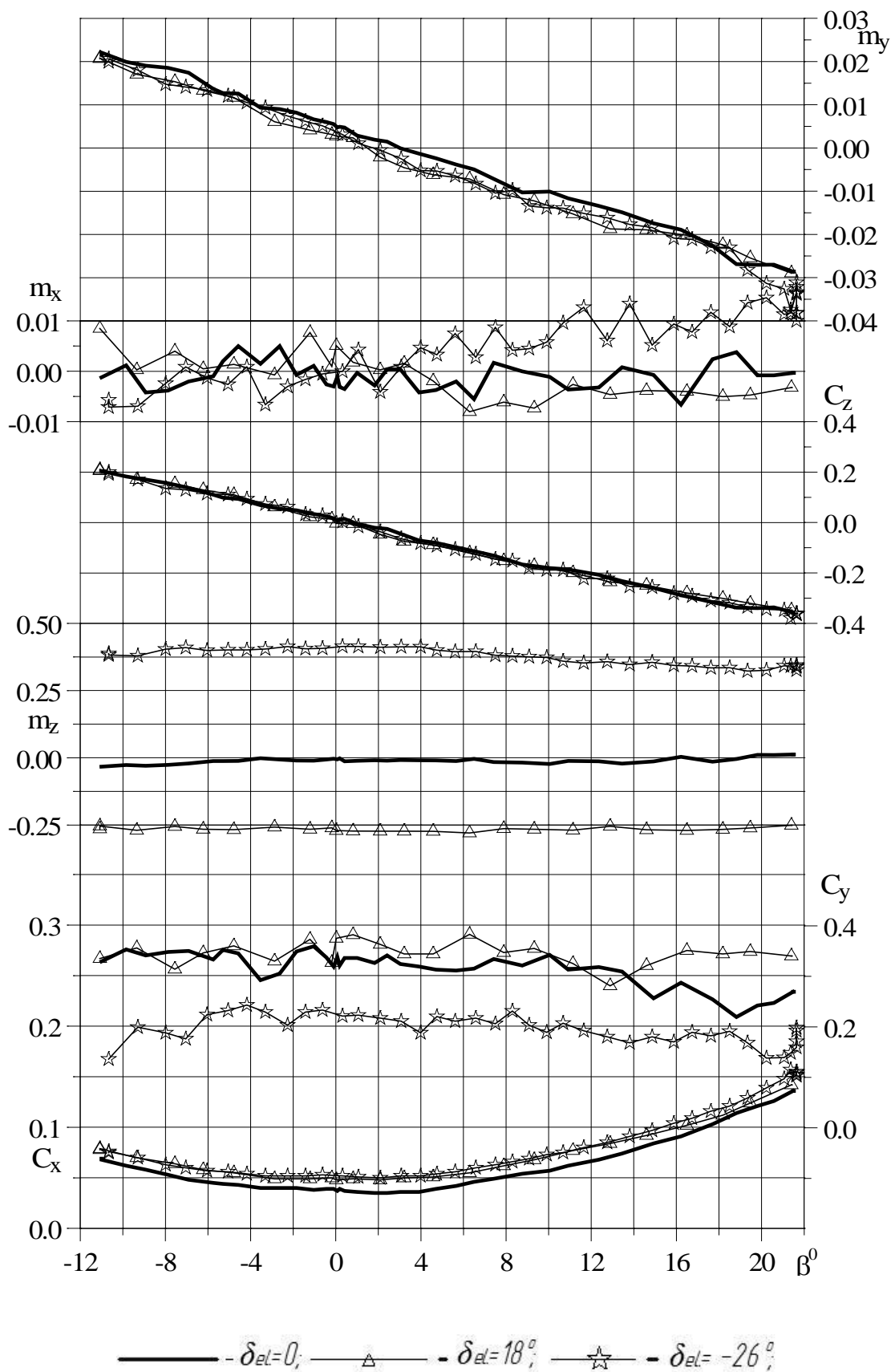


Fig. 2.52. Influence of elevator deflection on the change of model aerodynamic coefficients by the angle of sideslip

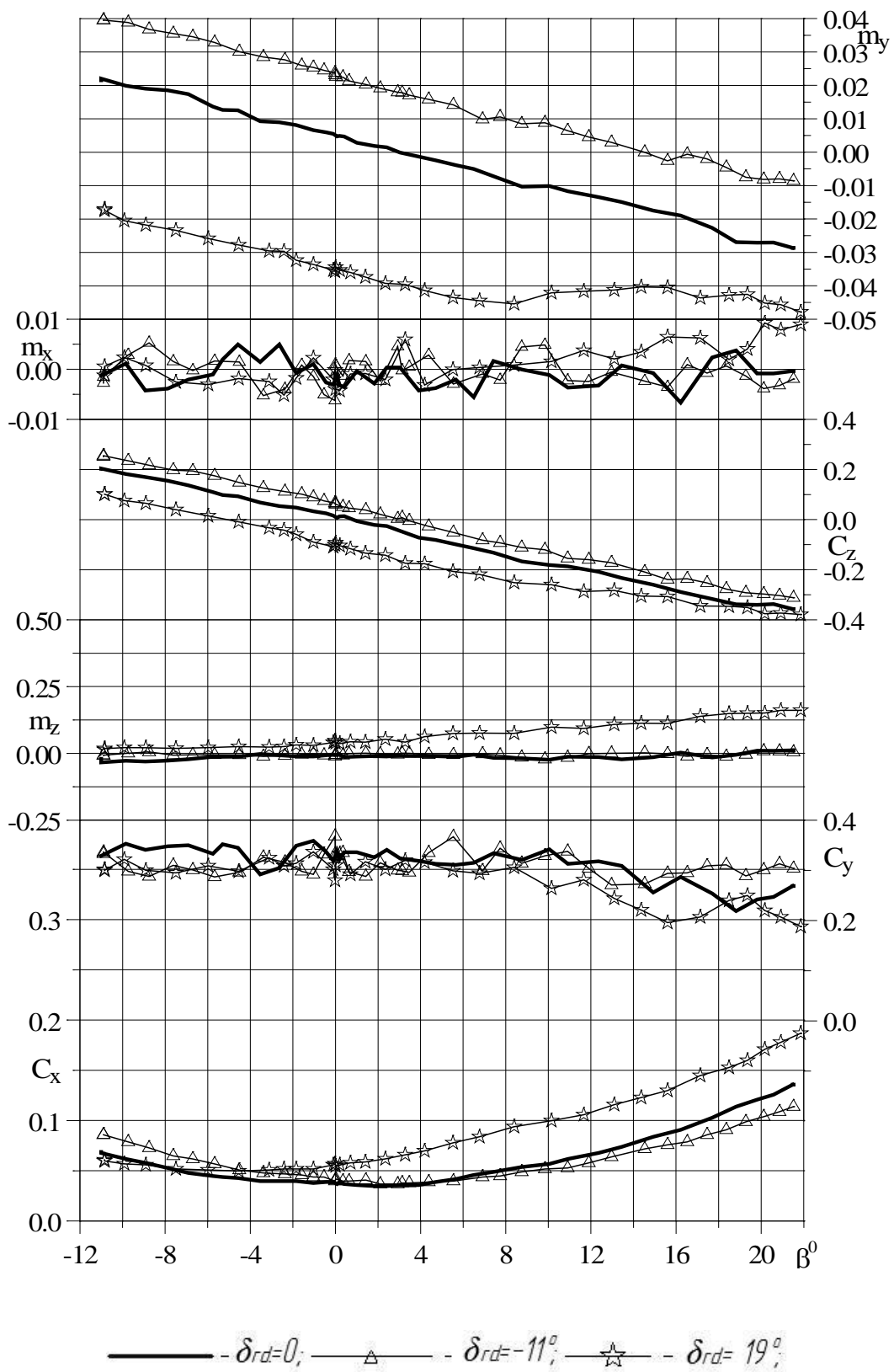


Fig. 2.53. The influence of the deflection of the rudder on the change of aerodynamic coefficients of the model by the angle of sideslip

Deviation of the flaperon (aileron) had almost no effect on static directional stability and roll control when changing the angle of sideslip. Graphs of the dependence of aerodynamic characteristics in Fig. 2.54 testify to this. The longitudinal effect of the deflected right flaperon will be compensated by the simultaneous deflection of the left flaperon.

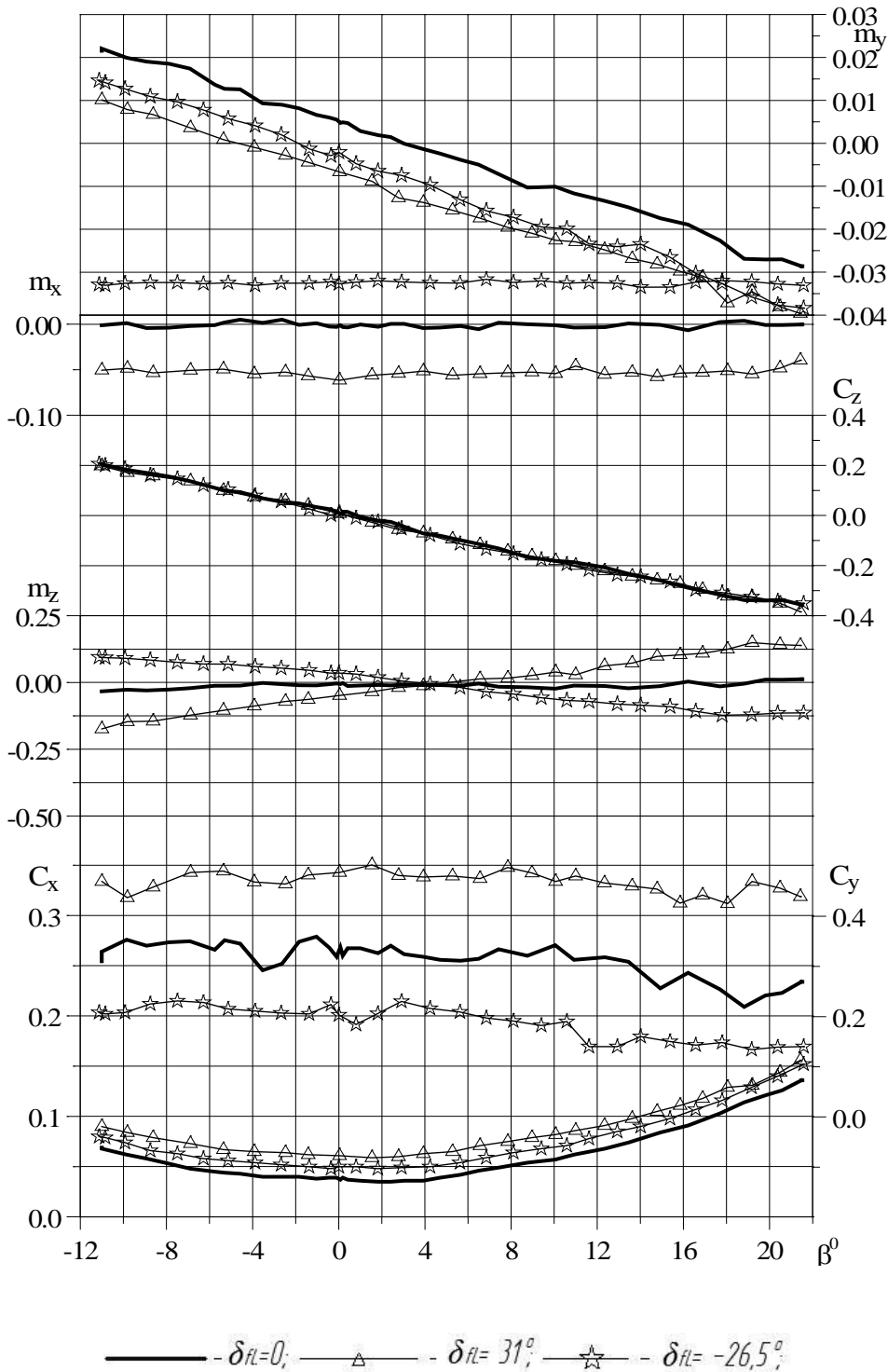


Fig. 2.54. The effect of deflection of the right flaperon on the change of aerodynamic coefficients of the model by the angle of sideslip

2.6. Justification of propeller parameters for high-altitude flights of solar-powered aircraft

The development refers to fixed-pitch propellers with folding blades, which should provide the necessary traction and speed to the aircraft on solar batteries in the altitude range from 0 m to 20 000 m.

To create thrust on aircraft with a solar-powered power plant, a constant-pitch propeller is used as a propeller, directly rotated by an electric motor. Examples are Solar Impulse (Switzerland), Pathfinder (USA), Solar Challenger (USA) and others [33, 35, 37].

In particular, the Solar Impulse aircraft with a launch weight of 2300 kg was equipped with four electric propulsion units (EPU) with a total power of about 54 kW and two-bladed constant-pitch propellers. The propellers had a diameter of 4 m and rotated at a speed of 525 rpm, which is a very atypical value for a conventional propeller. This circumstance is dictated by the fact that only about 11...12 % of direct solar radiation is converted into mechanical work. If we compare Solar Impulse with aircraft powered by internal combustion engines, then it has an ultra-low power-to-weight ratio (about 0,023 kW/kg versus ~ 0,15 kW/kg for An-2, for example), which dictates the use of atypical propellers for this type of power plant. Of the two components of the power plant – the engine and the propeller, modern three-phase electric motors with electronic regulators have an efficiency of 85...90 %, which is a very high indicator [36].

Accordingly, from the point of view of the efficiency of the power plant, the propeller remains problematic, which must meet a number of requirements, among which the most important are the highest thrust and the lowest drag losses at a given, specific flight speed. One of the shortcomings of Solar Impulse was its low altitude; the declared ceiling of the aircraft is only 8500 m, which, among other things, was limited to the use of a power plant with low-altitude propellers.

In the height range of 0 m...20 000 m, the parameters of the atmosphere change sharply, namely the temperature and density at height, that is, during high-altitude flights, there is a collision of changes in the speed of rotation of the propeller and its pitch. They are the only practical means of adapting the screw to changing atmospheric parameters; it is known that the density of air from a height of 0 m to a height of 20 000 m decreases by about 13 times.

To date, it has been established that it is not advisable to change the pitch of the propeller, since the overwhelming amount of time these aircraft must be at altitudes of 20 000 m or more [34]. Accordingly, it is not necessary to set a small pitch of the propeller, and the decrease in the efficiency of the propeller at low altitudes can be neglected.

From the beginning of the ascent from a height of 0 m, the propeller efficiency will increase with a drop in air density and a constant increase in flight speed. Thus, the stall speed of known aircraft, such as Zephyr 8, increases from about 7 m/s at a height of 0 m to 26 m/s at a height of 20 000 m.

At the same time, the temperature-dependent Reynolds number for a body of a certain size, for example, with a chord of 0,1 m (approximately corresponding to the chord of one of the sections of a solar-powered aircraft propeller) ranges from $0,15 \times 10^6$ to $1,0 \times 10^6$ and more; at the same time, the temperature changes from $+20^\circ \text{C}$ at an altitude of 0 m to $-56,5^\circ \text{C}$ at an altitude of 20 000 m.

The Mach number, which evaluates the presence of cavitation phenomena on the limbs of the blades with a rise to a height of 20 000 m, increases by 12...15 %, which indicates the need to limit the speed of rotation of the propeller.

The above evaluation criteria show how conflicting requirements are placed on a propeller for high-altitude flights of solar-powered aircraft. To a large extent, these requirements are taken into account in the propellers of the Aquila aircraft (USA) [38].

Its propulsion system consisted of four low-speed, electronically controlled, three-phase brushless electric motors equipped with non-folding fixed-pitch propellers.

The propeller of the Aquila aircraft has a hub with two large diameter blades attached to it, which in the front view have a strongly elongated elliptical shape; the connection of the blades with the hub makes it possible to move the blades to a different angle on the ground and thereby change the pitch of the propeller. The main disadvantages of these propellers of the Aquila aircraft are that they do not fold during the descent, which can lead to blade breakage, as well as insufficient consideration of the distribution of thrust along the radius of the blade, which leads to a decrease in thrust-to-weight ratio (kgf thrust/kg aircraft mass) and in accordance with the decrease in its overall efficiency.

The solution of the problem is based on the task of increasing the efficiency of a propeller for high-altitude flights of solar-powered aircraft by improving its design, as well as improving its geometric and aerodynamic characteristics.

The problem is solved by the fact that in the well-known propeller for high-altitude flights of solar-powered aircraft, consisting of a hub and blades having a highly elongated elliptical shape and combined with the hub by a terminal connection with the possibility of rearranging their installation angle on the ground, the following is improved:

- the hub is equipped with a mechanism for folding the blades along the flow;
- detachable connection of the blades for changing the angle of their installation is located in the movable cams;

- when viewed from the front, the blade is shaped differently from an elongated ellipse.

In addition, the developed propeller for high-altitude flights of solar-powered aircraft uses a concave-convex aerodynamic profile of the blade, and the wingtip of the blade is bent in the direction opposite to the flight direction.

The use of a hub equipped with a mechanism for turning the blades along the flow makes it possible to prevent propeller breakage during landing of aircraft with solar-powered power plants. At the same time, the rotation of the blades along the flow makes it possible to reduce harmful aerodynamic supports in the gliding mode, which is used during a long descent of a stratospheric aircraft from the maximum altitude reached.

The transfer of the detachable connection from the fixed part of the hub to the movable part made it possible to obtain in the folding propeller the function of changing its pitch by changing the angle of the blades.

The use of a concave-convex aerodynamic profile of the blade allows you to get maximum efficiency in cruising flight at maximum altitude and minimize the use of electrical energy from solar panels to power the power plant; thanks to this, it is possible to redirect part of the onboard electricity to recharge the batteries and power the payload of the aircraft for high-altitude solar-powered flights.

Bending the tip of the blade in the direction opposite to the flight, reduces the inductive drag of the blade, which leads to an increase in the efficiency of the propeller as a whole.

The proposed propeller for high-altitude flights of solar-powered aircraft uses the inertial-aerodynamic principle of keeping the blades in the working position: when the engine starts to rotate the propeller, the hinged blades turn to the working position. After the motor shaft stops, the centrifugal forces and the thrust force of the propeller cease to act. The forces of aerodynamic resistance of the stopped blade, significantly exceeding the moment of frictional resistance in the hinges of the hubs of the blades, return the blade to the folded position.

In Fig. 2.55 shows the design of the folding mechanism of the blades of the propeller for high-altitude flights in the projection from the side.

The hub *1* of the proposed propeller (Fig. 2.55) is attached to the engine *2* using screws *8*; the engine, in turn, is attached through the flange *3* to the supporting pylon *4*, which is attached to the aircraft. In the rotary cam *5*, a blade pin *6* is inserted and attached, which can rotate relative to the hub. The mechanism is partially protected by an aerodynamic fairing *7*.

In Fig. 2.56 shows the design of the mechanism for folding propeller blades for high-altitude flights in the front view.

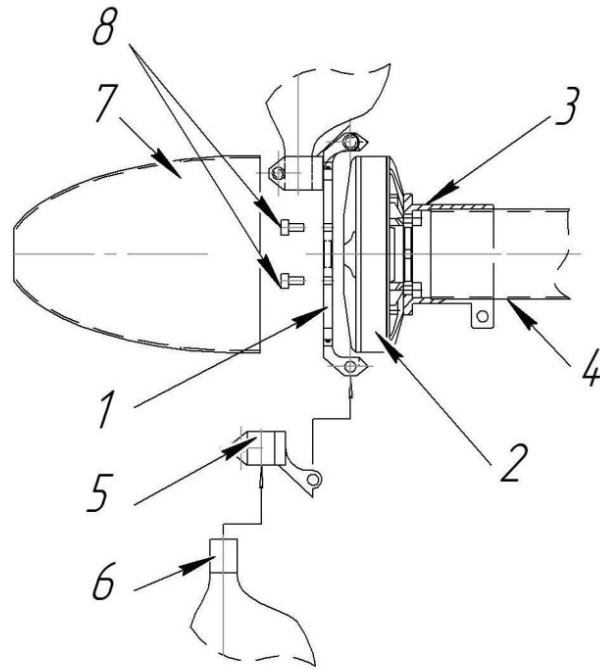


Fig. 2.55. The design of the folding mechanism of the blades of the propeller for high-altitude flights in the projection from the side

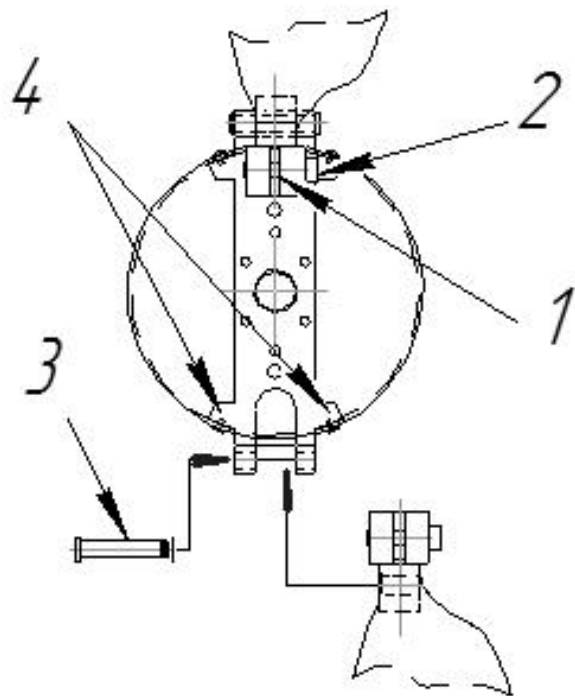


Fig. 2.56. The design of the mechanism for folding propeller blades for high-altitude flights in the front view

The blade of propeller is fixed in the cam by crimping in the terminal connection 1 (Fig. 2.56) with the help of screw 2. When this screw is released and the terminal connection is loosened, the blade can be turned to another installation angle. The rotation of the cam with the blade of propeller (from the working position to the folded position and vice versa) takes place on axis 3, which is equipped with a locking ring to prevent it from falling out. The fairing is fastened with the help of screws 4, which are screwed into the threaded protrusions, which are made together with the hub.

In Fig. 2.57 the scheme of turning the cam (the blade is conventionally not shown) into the working position is shown; pos. 1 marked cam-hub contact «spout» to ensure proper position and holding force. Stop 2 of the cam in the working position is raised vertically and released.

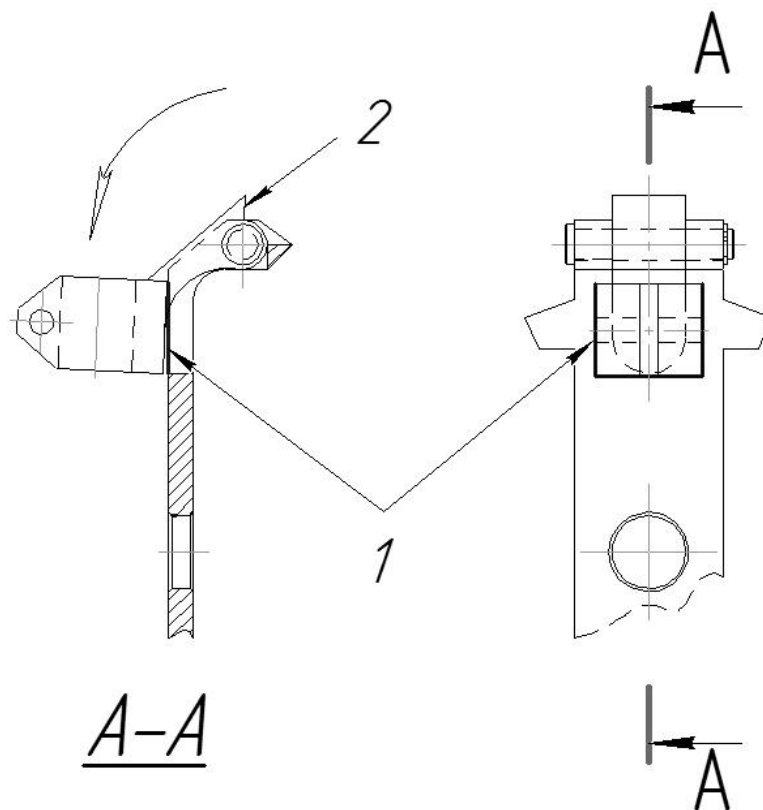


Fig. 2.57. Scheme of turning the cam to the working position

In Fig. 2.58 shows the scheme of turning the cam (the blade for propeller is conventionally not shown) to the non-working (the blade is folded) position. At the same time, the stop of the cam is pressed along the line of contact 2 to the jumper 1, which is located in the opening under the rotary cam of the hub itself. The return of the blades to the working position occurs as follows.

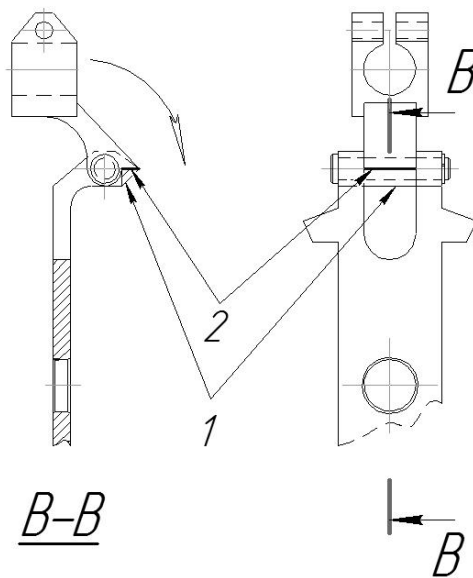


Fig. 2.58. The scheme of returning the cam of the blade for propeller to the non-working position

After the start of rotation of the screw (Fig. 2.59) with an angular velocity ω_{HV} each blade is affected by the resulting centrifugal force $F_{c,r}$, which is applied to the center of mass ($CG_{p,b}$) and depends on the mass of the blade and the current radius of rotation $R_{cg,a}$.

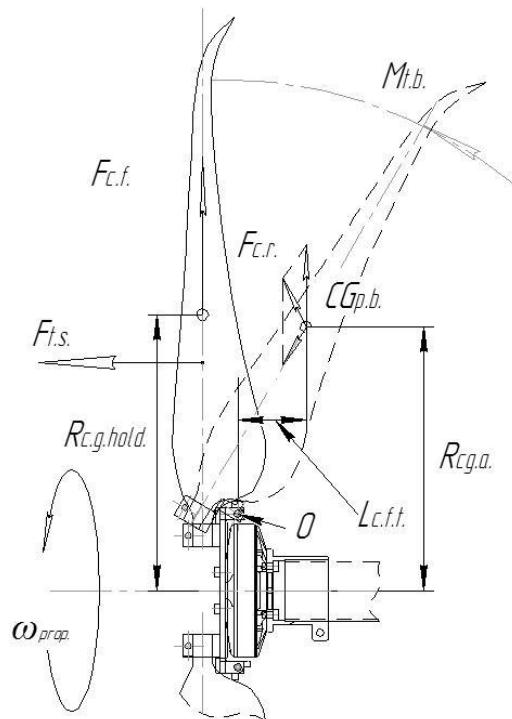


Fig. 2.59. Scheme of obtaining inertial and aerodynamic forces in the working, unfolded position of the blades

Torque on the propeller blade $M_{t,b}$ arises from the action of the inertial component $F_{c,r}$ on the shoulder $L_{c,f,t}$ and it is numerically equal:

$$M_{t,b} = F_{c,r} \cdot L_{c,f,t} \quad (2.59)$$

At the same time, the propeller blade rotates around the «O» point; because when the angle of rotation of the blade is about 90° , the shoulder $L_{c,f,t}$ becomes equal to $L_{c,f,t} = 0$, respectively, the moment $M_{t,b}$ is equal to:

$$M_{t,b} = F_{c,r} \cdot 0 = 0.$$

In the unfolded position of the blade at a radius $R_{cg,hold}$ the force $F_{c,f}$ develops, which by its nature is centrifugal in nature and depends on the speed of the screw.

At the same time, in a static position (when the aircraft is not moving), a thrust force $F_{t,c}$ develops on the blades of its propeller, which is aerodynamic in nature.

The simultaneous action of the force $F_{c,f}$ and forces $F_{t,c}$ traction screw, which change their values in proportion to the revolutions and are a means of holding the propeller blades in the unfolded (working) position in the parking lot with the engine running and in flight.

After stopping the engine in flight $F_{c,f}$ ceases to work, since the screw does not rotate and, accordingly, there is no component of ω_{prop} .

According to the nature of aerodynamic forces, an air flow rushes on to the blade, which turns it (Fig. 2.60) around the hinge (point «O») with the help of the force of aerodynamic resistance – $X_{b,p}$.

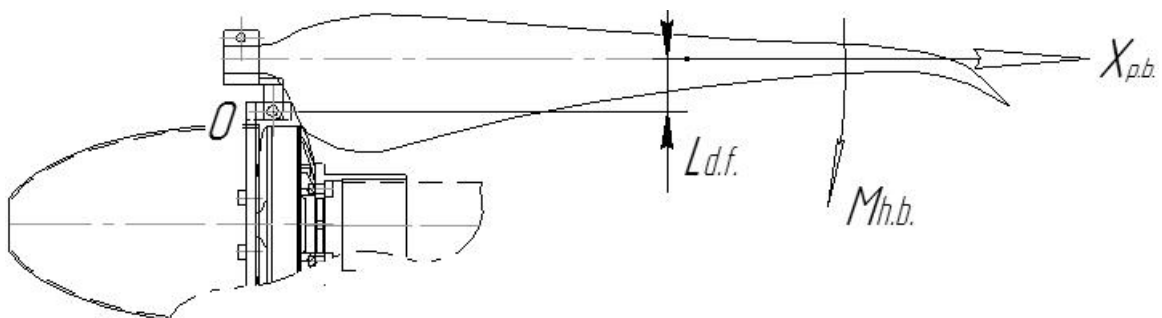


Fig. 2.60. The scheme for obtaining aerodynamic forces with the folded position of the propeller blades

In the «downstream» position, the force $X_{b,p}$ is applied along the blade (along the line of aerodynamic foci), and the point 0 is at a distance $L_{d,f}$. Correspondingly, the holding aerodynamic moment develops $M_{h,b}$:

$$M_{h,b} = X_{b,p} \cdot L_{d,f} \quad (2.60)$$

This holding aerodynamic moment will be present as long as the pseudo-satellite moves in the glide mode. In the «downstream» position, the propeller blade is held in the extreme position by the rear stop.

The image of the developed air propeller and the blade turning mechanism in the «blades half-folded along the flow» position is shown in Fig. 2.61.



Fig. 2.61. An image of the propeller and the turning mechanism of the propeller blades in the «blades half-folded along the flow» position

The aerodynamic justification of the proposed technical solution of the propeller is based, first of all, on the fact that the high rarefaction of the atmosphere at heights of about 20 000 m. requires a certain increase in the blade area, or an increase in the so-called overlap ratio (filling of the covered area) [39].

Secondly, the configuration of the blades should contain means of reducing the inductive resistance that occurs at the ends of the blades.

Thirdly, concave-convex profiles should be used for the blades, which have the maximum profile values of the lift coefficient at the minimum values of the aerodynamic resistance coefficient and small values of the linear speed of the blade elements.

The question of the suitability of a certain type of profile was solved by analyzing those propeller profiles that have proven themselves well, for example, in modern aircraft that are

driven by muscles [40]. By analyzing the main parameters, it was established that for R_e numbers close to $R_e = 1,0 \cdot 10^6$ and more, the MVA-301 profile has the best properties [41].

Fig. 2.62 shows the dependence of the aerodynamic quality K and the lift coefficient C_y on the angle of attack α for the MVA-301 profile.

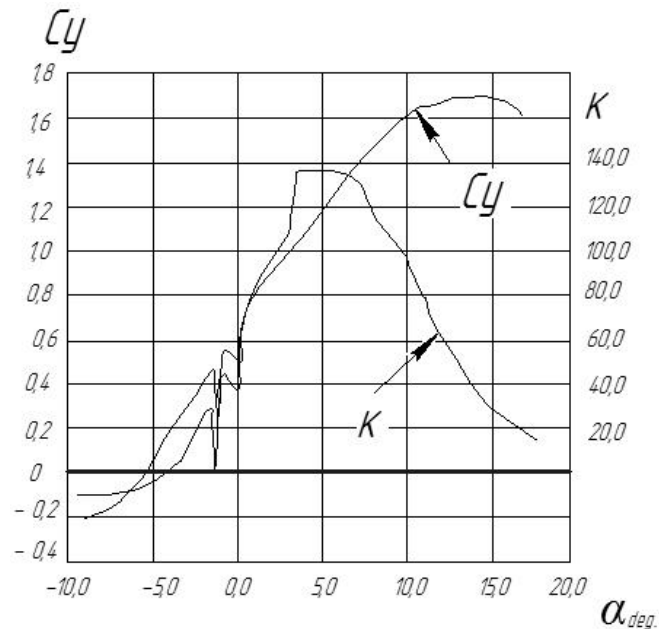


Fig. 2.62. Dependencies of the aerodynamic quality K and the lift coefficient C_y on the angle of attack α for the MVA-301 profile

To implement the point about the need to add additional area to increase the fill factor in Fig. 2.63 shows contour 1 of a traditional blade in the form of an ellipse, and contour 2 indicates the contour of the blade of the proposed utility model (ω indicates the direction of rotation of the propeller).

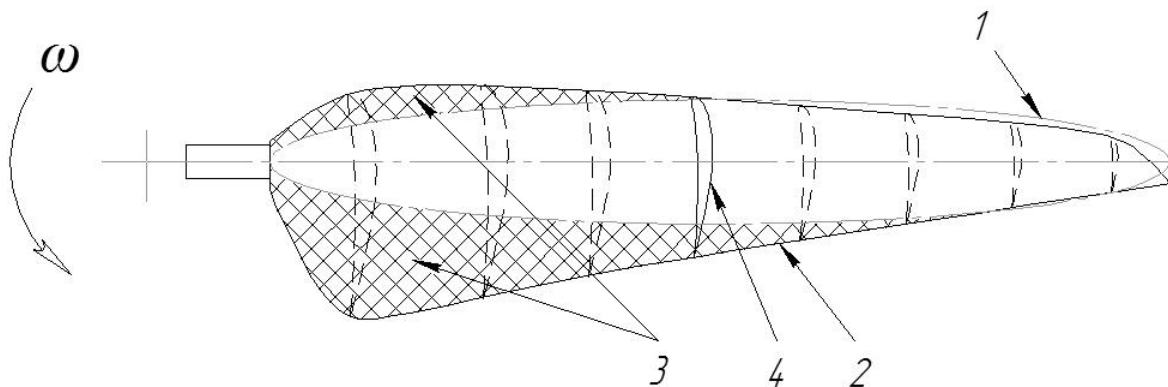


Fig. 2.63. Scheme of obtaining additional area to increase the filling factor of the area covered by the propeller

Shaded area 3 visualizes the attached area; the expansion of this area towards the tip of the blade allows you to additionally use the obtained resource of the area to increase the traction force and thereby increase the efficiency of the developed propeller. Position 4 indicates the contour of the aerodynamic profile proposed in the design of the MVA-301, which has a characteristic concave-convex shape; this profile is present along the entire radius of the propeller.

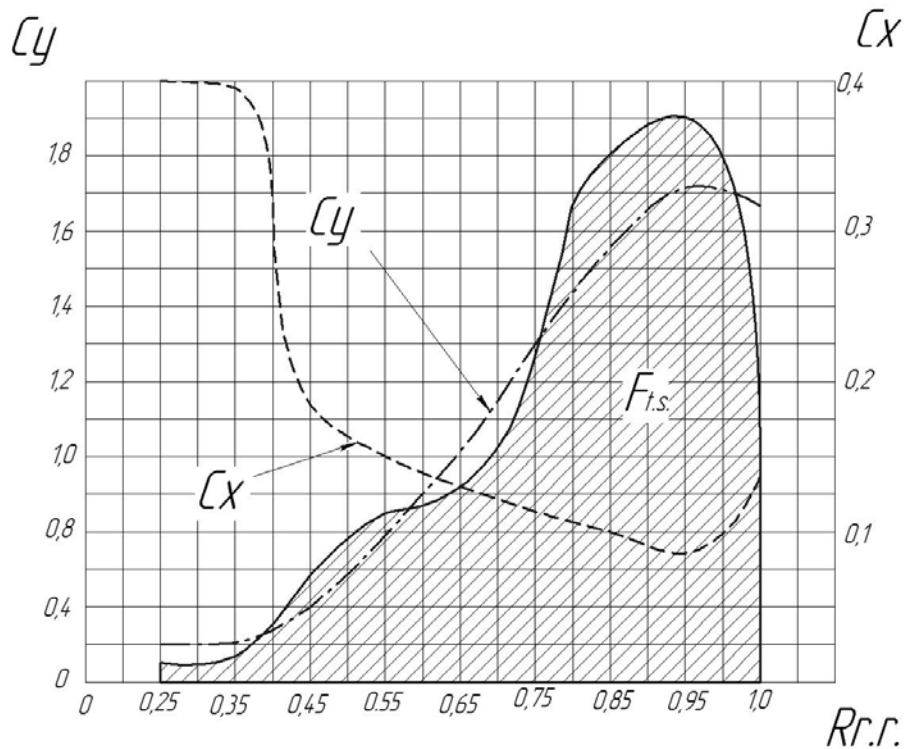


Fig. 2.64. Calculation results of the distribution of lift coefficient (C_y) and aerodynamic drag coefficient (C_x) values along the radius of the propeller blade

The value of the thrust force for one blade $F_{t,s}$ and its distribution along the relative radius $R_{r,r}$ obtained for a real sample of a useful model under the following conditions:

- radius, m – 0,375;
- pitch, m – 0,675; (at $R_{r,r} = 0,75$);
- number of revolutions, rpm – 890;
- height (according to ISA – international standard atmosphere), m – 100;
- air density, kg/m^3 – 1,213.

The absolute value of the calculated traction force $F_{t,s}$ (shaded area in Fig. 2.64) with the above parameters was 6,9 N for two blades or 3,45 N for each blade.

In Fig. 2.65. an image of a propeller blade for high-altitude solar-powered aircraft is presented; in order to reduce inductive resistance, the tip of the blade is bent in the direction opposite to the direction of flight.



Fig. 2.65. Image of the blade of the proposed technical solution of the propeller

Results of bench tests of a propeller for high-altitude flights of solar-powered aircraft

Dynamic bench tests of the propeller for high-altitude flights of solar-powered aircraft were carried out for the purpose of experimental evaluation of its efficiency. The research was carried out on a rotating stand with a tensometric head, which made it possible to directly measure the thrust $F_{t,s}$ of the propeller and the power P on the electric engine shaft using the following known ratios [42]:

$$F_{t,s} = \alpha \cdot \rho \cdot n^2 \cdot D^4,$$

$$P_{e,e} = \beta \cdot \rho \cdot n^3 \cdot D^5.$$

where D – propeller diameter; n – the number of revolutions of the propeller; ρ – air density; α – the traction coefficient; β – the power factor.

In addition, it was taken into account that the power on the engine shaft P is equal to the product of the speed of rotation of the propeller by the torque of the force on the shaft.

An aerodynamic brake of a known area installed perpendicular to the velocity vector was used as a brake for the stand (Fig. 2.66).

To obtain the final results, the angular frequency of rotation of the stand, the radius of rotation of the propeller axis, the torque from the propeller, its thrust force of the propeller, its rotation speed and the electrical power consumed by the engine were determined.

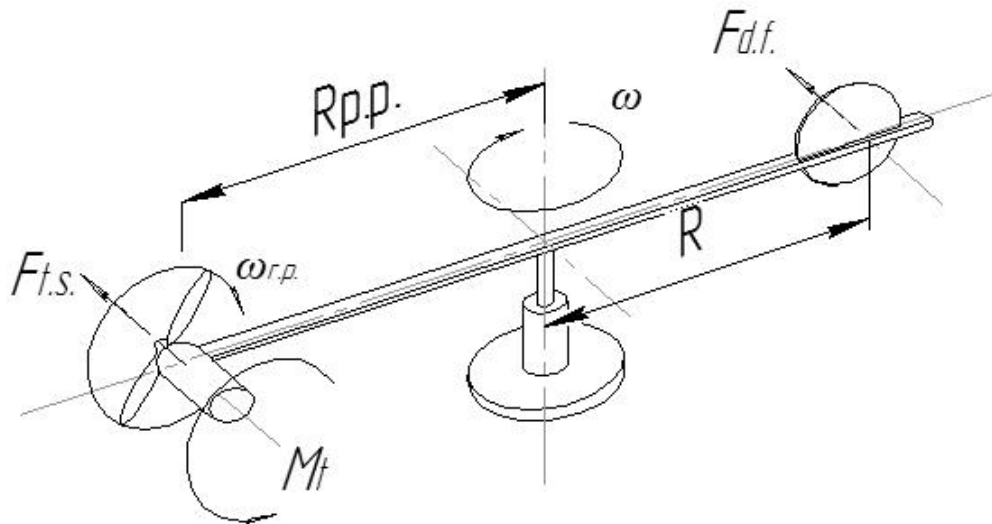


Fig. 2.66. The main parameters of the rotating stand:

angular frequency of rotation of the stand ω ; radius of rotation of the axis of the propeller $R_{p,p}$; propeller force torque M_t ; propeller thrust force $F_{t,s}$; propeller angular velocity $\omega_{r,p}$; radius of rotation of the air brake R ; resistance force of the aerodynamic brake $F_{d,f}$

The results of measurements on the stand became the basis for calculating the following values:

- air speed:

$$V_c = \omega \cdot R_{p,p}. \quad (2.61)$$

- power on the motor shaft:

$$P_e = M_t \cdot n_{prop} \cdot 2\pi. \quad (2.62)$$

- mechanical power to create propeller thrust:

$$P_s = F_{t,s} \cdot V_c. \quad (2.63)$$

The results of high-altitude propeller tests on a rotating stand are presented in Table 2.19.

For bench measurements, the air speed was limited by the radius of rotation of the crossbar of the bench and the corresponding maximum permissible centrifugal force. The thrust of the screw was limited by the rotation radius of the air brake.

Table 2.19

Results tests of high-altitude propeller

Measurement cycle number	Angular frequency of rotation of the stand ω	Consumed electrical power W	Propeller force torque M_t	Propeller thrust force $F_{t.s}$	Propeller speed rotation n_{prop}
1	2	3	4	5	6
Air speed: 6 m/s; $R_{p,p} = 5125$ mm					
1	1,168 Rad/s	78 W	0,64 Nm	1,86 N	14 rps
2	1,186 Rad/s	89 W	0,73 Nm	2,52 N	14,5 rps
In cycles 2 the air brake is adjusted to a larger radius					
Air speed: 7 m/s; $R_{p,p} = 5125$ mm					
3	1,360 Rad/s	99 W	0,78 Nm	2,16 N	15 rps
4	1,360 Rad/s	133 W	0,96 Nm	3,14 N	16,1 rps
5	1,380 Rad/s	140 W	1,015 Nm	3,24 N	16,9 rps
In cycles 3, 4, 5, the air brake is adjusted to a larger radius					
Air speed: 8 m/s; $R_{p,p} = 5125$ mm					
6	1,560 Rad/s	197 W	1,23 Nm	4,53 N	18,8 rps
7	1,570 Rad/s	202 W	1,28 Nm	4,75 N	19,1 rps
Air brake at the largest turning radius					

Results of measurement data processing from Table. 2.19 according to formulas (2.61), (2.62) and (2.63) are summarized in the Table. 2.20.

Table 2.20

Summary table based on measurement results

Measurement cycle number	Actual airspeed V_C	Propeller speed rotation n_{prop}	Propeller thrust force $F_{t.s}$	Consumed electrical power W	Power on the shaft P_s	Mechanical power from traction P
1	5,986 m/s	840 rpm	1,86 N	78 W	56 W	11,2 W
2	6,078 m/s	870 rpm	2,52 N	89 W	66 W	15,3 W
3	6,970 m/s	900 rpm	2,16 N	99 W	73 W	15,0 W
4	6,970 m/s	960 rpm	3,14 N	133 W	97 W	21,9 W
5	7,073 m/s	1010 rpm	3,24 N	140 W	107 W	22,9 W
6	7,995 m/s	1130 rpm	4,53 N	197 W	145 W	36,2 W
7	8,046 m/s	1140 rpm	4,75 N	202 W	153 W	38,2 W

According to the Table 2.20, traction coefficients α and power coefficients β were calculated (Table 2.21).

Table 2.21

Obtained values of propeller thrust and power coefficients

Measurement cycle number	1	2	3	4	5	6	7
Traction coefficient α	0,0244	0,0308	0,0247	0,0315	0,0294	0,0329	0,0338
The power factor β	0,0702	0,0745	0,0744	0,0815	0,0772	0,0747	0,0768

Based on the average value of the traction coefficient $\alpha_{av} = 0,03$ and the power coefficient $\beta_{av} = 0,075$, the thrust of the propeller was estimated at the maximum power of the solar power plant.

Provided that the electric power supplied to the engine regulator (P_{sup}) reached 300 W, the power on the engine shaft was:

$$P_{sup} = 300W \cdot 76\% \text{ (Regulator and motor efficiency)} = 228W.$$

At the same time, according to the average value of the power factor, the frequency of rotation of the propeller will reach:

$$n_{prop} = \sqrt[3]{\frac{P_{sup}}{\rho \cdot \beta_{av} \cdot D^5}} = \sqrt[3]{\frac{228}{1,225 \cdot 0,075 \cdot 0,745^5}} = 22,16 \text{ rps.}$$

Accordingly, the thrust force of the screw will be equal to:

$$F_{t,s} = \alpha_{av} \cdot \rho \cdot n_{prop}^2 \cdot D^4 = 0,03 \cdot 1,213 \cdot 22,16^2 \cdot 0,745^4 = 5,54N.$$

As a result of the development and research, improved technical solutions for a two-blade propeller have been obtained, which can be used to obtain appropriate thrust and speed in the altitude range from 0 to 20 000 m on an unmanned aerial vehicle with solar panels. The propeller has the ability to fold the blades to reduce the drag force of the aircraft during its descent to the ground: the folding of the blades also prevents the blades from breaking during landing.

The assessment carried out by calculation methods and experiment showed that the calculated thrust should be obtained at approximately 6,9 N at a height of 0 m and an air density of 1,225 kg/m³ and a temperature of +15°C.

It was experimentally established that the real thrust was 5,54 N, which is 19 % less than the calculated one. To a large extent, this can be explained by the fact that the experiment was carried out at an altitude of about 150–170 m above sea level, where the density is about 1,213 kg/m³, as well as by some errors in the measurement process.

In addition, the calculation methods of evaluation, in particular the method of discrete elements, do not fully take into account the real, continuous twist of the blades: the propeller is represented as a set of elements, for each of which the required values are calculated.

List of references

1. Kashafuddinov S. T., Lushin V. N. Atlas of Aerodynamic Characteristics of Wing Profiles. Novosibirsk: SibRIA, 1994. P. 69.
2. Internet resource. Access to the source: <http://airfoiltools.Com/airfoil/details?airfoil=fx61184-il>.
3. Internet resource. Access to the source: <http://airfoiltools.com/polar/details?polar=xf-fx61184-il-500000>.
4. Internet resource. Access to the source: <http://airfoiltools.com/polar/details?polar=xf-fx61184-il-200000>.
5. Gudmundsson S. General aviation aircraft Design: applied Methods and Procedures. Butterworth-Heinemann is an imprint of Elsevier. The Boulevard, Langford Lane, Kidlington, Oxford OX5 1GB, UK 225 Wyman Street, Waltham, MA 02451, USA. First edition 2014. P 680–683.
6. Badyagin A. A., Mukhamedov F. A. Design of light aircraft. M.: Mashinostroenie, 1978. P. 66–78.
7. Nikolaev L. F. Aerodynamics and dynamics of transport aircraft flight. M.: Transport, 1990. P. 80–82.
8. Scholz D. Definition and discussion of the intrinsic efficiency of winglets. *Aerospace Europe 6th CEAS Conference*. CEAS 2017 paper no. 926. Page 14.
9. STANAG 4671 (NATO Standard AEP-4671. Unmanned Aircraft Systems Airworthiness Requirements // Edition A VERSION 1 // February 2017). P.1–B-4.1–B5.
10. Udartsev E. P., Pereverzev A. M., Ishchenko S. A. Operational aerodynamics. Trajectory Tasks. Kyiv: KIUCA. 1998. P.105–109.
11. APC NASA Transonic Airfoil Analysis Computer Program. Online resource. Access to the source: <https://www.apcprop.com/technical-information/performance-data/>.
12. Teush V. L., Sidorov I. A. General course of propellers. M.: PCAI USSR, 1943. 280 p.
13. Storozhuk M. V. Ground icing of aircraft: measures to prevent aviation accidents. *Scientific Bulletin of MSTU CA*. 2015. № 219. P. 93–98.

14. Simonenkova R. V., Vinogradova L. M. Aircraft protection from ground icing. Proceedings of VNII aviation materials. *Aviation Industry*. № 8. 1982. Internet resource. Access to the source: <https://viam.ru/public/1982/mar>.
15. Mazin I. P. Physical bases of aircraft icing. Moscow: Gidrometeoizdat, 1957. 112 p.
16. Borovikov A. M. et al. Physics of clouds. *Leningrad: Gidrometizd*. 1961. 435 p.
17. Astapenko P. D., Baranov A. M., Shvarev I. M. Weather and aeroplane and helicopter flights. *Leningrad: Gidrometizd*. 1980. P. 186.
18. Electronic resource. Source access mode: <http://uav.nau.edu.ua/Mobile> unmanned complex M-10 "Oko 2"/.
19. Klemenkov G. P., Prikhodko Y. M. Modelling of aircraft icing processes in aeroclimate tubes. Proceedings of the Institute of Theoretical and Applied Mechanics. S. A. Khristianovich. *Thermophysics and Aeromechanics*. 2008. Vol. 15. № 4. P. 563–572.
20. Thomas P. Ratvasky. Billy P. Barnhart Bihrl. Sam Lee. Current Methods for Modeling and Simulating Icing Effects on Aircraft Performance, Stability and Control. *National Aeronautics and Space Administration Glenn Research Center Cleveland, Ohio 44135*. 2008. PP. 4–13.
21. Grzegorz Kowaleczko. Michał Wachłaczko. Aircraft dynamics during dynamics flight in icing conditions. *Journal of theoretical and applied mechanics* 50, 1, pp. 269–284, Warsaw 2012.
22. Xuan Zhang, Jingchun Min, Xiaomin Wu. Model for aircraft icing with consideration of property-variable rime ice. *International Journal of Heat and Mass Transfer June 2016*. Electronic resource. Access to the source: [//www.elsevier.com/locate/ijhmt](http://www.elsevier.com/locate/ijhmt).
23. Kapkowski J. Flying wings; translated from Polish by J. P. Terekhov. M.: DOSSAAF, 1988. P. 20–25.
24. Kravets A. S. Characteristics of aircraft profiles. M.: Voenizdat, 1939. P. 298–301.
25. Petrov K. P. Aerodynamics of aircraft elements. M.: Mashinostroenie, 1985. P. 51–62.
26. Chumak P. I., Krivokrysenko V. F. Calculation, design and construction of ultralight aircraft. M.: Patriot, 1991. P. 12–79.
27. Torenvik E. Designing subsonic aircraft; transl. from English M: Mashinostroenie, 1983. P. 586–589.
28. Gudmundsson S. General aviation aircraft design: applied methods and procedures. Elsevier Inc., Butterworth-Heinemann, 2014. XXI, 1034 p. – ISBN: 978-0-12-397308-5. P.997–1007.

29. Randal W. Beard and Timothy W. McLain. *Small Unmanned Aircraft: Theory and Practice*. 41 William Street Princeton, New Jersey 08540 United States. 2012.
30. Yablonsky A. A., Nikiforova V. M. *Course of theoretical mechanics. Part 1. Statics. Kinematics*. M.: Vyssh. shk., 1966. P. 328–337.
31. Gentmacher F. R. *The theory of matrices*. M.: Nauka, 1966. P. 87–90.
32. R. Fink. *USAF stability and control DATCOM*. Douglas Aircraft Company, Rev. 1998.
33. D. Mamontov. Round the world flight without a drop of fuel. *Journal «Popular Mechanics»*, № 3 (149) 2015. *Electronic resource*. Access to the source: <https://www.popmech.ru/technologies/56571-solar-impulse>
34. Nicholas J. Colella, Gordon S. Wenneker. *Pathfinder and the Development of Solar Rechargeable Aircraft*. University of California – Lawrence Livermore National Laboratory July. 1994. P.1–9. *Electronic resource*. Access to the source: <https://str.llnl.gov/content/pages/past-issues-pdfs/1994.07.pdf>
35. Internet resource: MacCready Solar Challenger. Access to the source: https://en.wikipedia.org/wiki/maccready_solar_challenger
36. Internet resource: Solar Impulse. Access to the source: https://en.wikipedia.org/wiki/Solar_Impulse
37. J. Morgado, M. Abdollahzadeh, M.A.R. Silvestre, J.C. Páscoa. High altitude propeller design and analysis. *Aerospace Science and Technology*. Volume 45, September 2015. Pages 398–407. Access to the source: <https://www.sciencedirect.com/science/article/abs/pii/S1270963815001881>
38. Internet resource: Facebook Aquila. Access to the source: https://en.wikipedia.org/wiki/Facebook_Aquila
39. Anthony Colozza. *High Altitude Propeller Design and Analysis Overview*. Federal Data Systems Cleveland, Ohio. 44135. March 1998. Access to the source: www.researchgate.net/publication/2517460_High_Altitude_Propeller_Design_and_AnalysisOverview
40. Chris Barrenger. *Tasmanian RC Human – Powered Aircraft Project*. Published by Samaria Concepts, RMB 1978, Benalla, Victoria, 3673. Access to the source: <https://catalogue.nla.gov.au/Record/2718162>
41. GOE 801 (MVA 301) AIRFOIL – Gottingen 801 (MVA 301) airfoil. Access to the source: <http://airfoiltools.com/airfoil/details?airfoil=goe801-il>
42. V. L. Alexandrov. *Air screws. Part 3. Aerodynamics of the propeller*. M.: Oborongis, 1951. 235 p.

Chapter 3

UNMANNED AERIAL VEHICLES OF THE NATIONAL AVIATION UNIVERSITY FOR CARRYING SMALL LOADS

3.1. Unmanned four-engine PKM-14 «Saturnia» helicopter

Unmanned aircraft PKM-14 «Saturnia» is intended for research flights for transportation of small loads on the distance of 3 km in the automatic mode [1].

Terms of PKM-14 «Saturnia» basing: airfields basing/without airfield basing.

Minimum composition of crew. Composition of ground crew is no less than 2 persons.

General flying limitations. Speed of steady wind – 7 m/s; maximum speed of local wind in gusts – no more than 10 m/s.

Unmanned aircraft PKM-14 «Saturnia» is classified:

- according to the aim – transportation;
- according to the scale of tasks – small radius of action;
- according to basing – ground basing;
- according to lifting capacity – aerodynamic four engine helicopter;
- according to frequency of use – reusable;
- according to the number of engines – four-engine;
- according to the type of engine in power plant – electric aviation engine with accumulator power supply;
- according to maximum takeoff weight – mini;
- according to maximum altitude – medium-altitude;
- according to maximum velocity – slow moving;
- according to maximum air time – short haul;
- according to the type of takeoff – vertical, automatic;
- according to the type of landing – vertical, automatic;
- according to flight control system – mixed;
- according to manoeuvrability – non-manoeuving.

UAV PKM-14 projections with main overall dimensions are shown on Fig. 3.1.

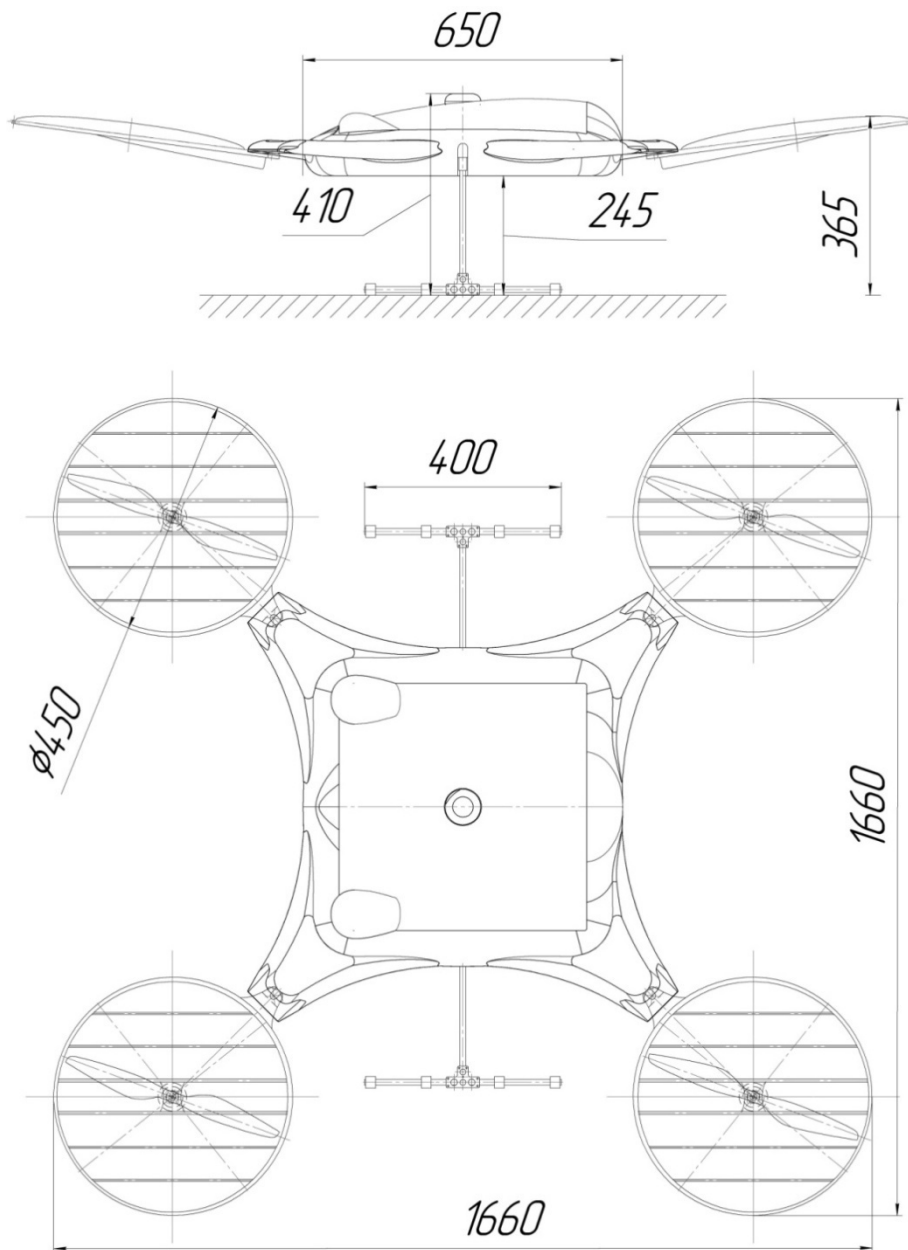


Fig. 3.1. UAV PKM-14 projections

Functional composition of UAV PKM-14. UAV PKM-14 is functionally composed of the following systems, equipment and devices.

Airframe

- central body (fuselage);
- four bodies of power plants with engine mounting frames;
- mechanism for fixing body in working and transport position;
- compartment of useful load with closing shutters;
- two chassis supports that are hidden.

Power plant

- four electric engines;
- four electronic engine regulators;
- four propellers.

Flight and navigational equipment

- system of navigational equipment;
- aircraft telemetry system.

Control system

- aircraft UAV controller/autopilot that includes flight data recorder (FDR) of modes.

Electro-technical equipment

- aircraft electrical batteries;
- power electric unit;
- aircraft electrical wiring.

Radio technical equipment

- devices of satellite navigation system.

Equipment of radio lines

- radio-line control devices (*air/ground – radio control; ground/air – telemetry*);
- radio-line video connection devices (*air/ground/air – target video signal*).

UAV additional payload

- day video camera.

Functional structure of ground control station (GCS). Unmanned aerial vehicle ground control station includes the following systems, equipment and devices.

Remote command pilot`s workstation (W)

- UAV control post;
- remote command pilot`s data monitor;
- personal computer (PC);
- devices of ground telemetry and radio command system;
- ground telemetry;
- tools to obtain and display video information.

UAV flight support systems

- power supply system for GCS*;
- system of meteorological support*;

- system of objective control (*data flight recorder*);
- control and inspection equipment:
- a kit of control, measuring and special equipment for before and after flight MT*;
- UAV flight-simulator*;
- tools for UAV storage and transportation;
- assembly kit комплект*;
- spare parts, instrument and accessories*;
- a kit of tools*;
- set of operational documentation.

**it is not contained in basic kit.*

A brief technical specification of UAV PKM-14 «Saturnia». Unmanned aircraft PKM-14 «Saturnia» (Fig. 3.2) is a multi propeller helicopter (*borrowed from english – polycopter*) with four electric power plants. UAV PKM-14 «Saturnia» has been designed for basing without airfield and intended for imitation of loads transportation with dimensions no more than 500 mm × 500 mm × 50 mm and weight no more than 2 kg [2].



Fig. 3.2. ¾ right side top view of UAV PKM-14 «Saturnia» (in comparison with people's size)

Glider is made mostly from of fiberglass and carbon fiber, some loaded elements of the construction are made of aluminium alloy.

Fuselage (main body) is a composite product pasted from of fiberglass and carbon fiber with corresponding niches, cavities, hatches and four «L»-shaped brackets for mounting the power plant.

The upper part of the fuselage is covered by fairing-cowling, under which the compartment of aircraft electronic equipment, aircraft EBs, navigational equipment and engine controllers are located. There are two moulded drop-like projections for GPS receivers in the front part of the fairing – cowling. The fairing is fixed by screws along the perimeter of the opening. The central part of the fairing has easy removable hatch for EB assembly/disassembly. In the center of the hatch there is an opening for rotating head of laser scanner of machine vision.

In the lower part of the fuselage there is a deepening (box) 510 mm × 510 mm × 55 mm for payload. The box is closed by two bushings operated by servos. Bushings partially shelter load from atmospheric precipitation and mechanically keep the load in the box during flight. On the right and left side of the fuselage near the bottom there are chassis hiding mechanisms which in basic configuration of UAV automatically lower/retract it away during flight. In «semi-automatic» mode landing gear can be lowed/retracted from ground control station. From the front of the fuselage (closer to the bottom) there is an electric on/off switch on the UAV board as well as a laser altimeter sensor.

In the rear part of the fuselage there is telemetric antenna in the range of 0,915 GHz, protruding to 20 mm from the cladding.

The electrical wiring from the engines runs along the spokes of the power plant housings and along their perimeter. With the aim to increase the reliability of the electrical wiring of the power plant housing is connected to the corresponding wiring of the fuselage by soldering.

Landing gear – has springs and two T-shaped supports, which are made of aluminum pipe. Gear clearance – 210 mm that allows unhindered opening of load box bushing and unloading under its own weight. With the aim of reducing impact load at the moment of touching ground by UAV the springs are equipped by couplings from microporous rubber.

Chassis retraction is performed by individual servos for each support; the angle of rotation from position «released» to position «hidden» – 90°.

Power plant (PP) has three-phase electric direct current (DC) motors with electronic regulators and two-blade fixed-pitch propellers. Motors are fixed on engine mounting by screws M4. Air screws are fixed directly on motor shaft by screws M3. Engines are cooled by air passing through openings in their shells. UAV PKM-14 main functional parts and blocks are presented on Fig. 3.3.

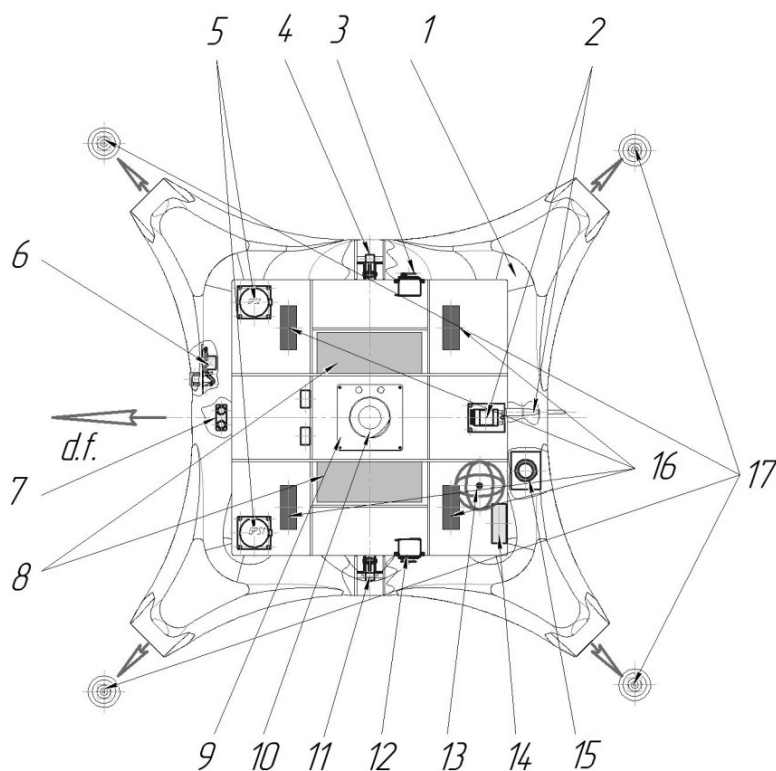


Fig. 3.3. UAV PKM-14 main functional parts and blocks:

1 – fuselage; 2 – telemetry block 0,9 GHz (TB-0,915) with antenna; 3 – servo for opening/closing of right bushing in load box; 4 – servo for lowering/retracting of right chassis support; 5 – dubbed navigation block (NB PKM-14); 6 – electric key of switching on/switching off the board (EK PKM-14); 7 – landing laser altimeter (LLA PKM-14); 8 – aircraft electrical batteries (AEB PKM-14); 9 – rack of aircraft controller, power supplies and RS-receiver; 10 – laser scanner of machine vision (LSMV PKM-14); 11 – servo for lowering/retracting of left chassis support; 12 – servo for opening/closing of left bushing in load box; 13 – antenna of video channel (AOV-1, 2); 14 – block of video image transmission (BOV-1,2); 15 – day video camera (CAM PKM-14); 16 – electro engine regulators of PP; 17 – electric engines of power plants (EE PKM-14)

Electric system. Electrical power supply of aircraft system UAV is provided by normal lithium polymeric battery with six elements with the capacity of 16A · h. Due to the peculiarities of the layout, the onboard battery (battery) is divided into two equal parts of three elements. Wiring consists of signal and power lines joined in combined cables. Some consumers are supplied by relative voltage from aircraft power block.

Cargo compartment. Cargo compartment (Fig. 3.4, a, b) is at the bottom of fuselage and closed in flight by bushings, which are located along flight direction. In «open» position cargo falls out from the compartment under its own weight. After unloading the compartment bushings close automatically and are kept closed by locks. Maximum cargo weight for transportation – 2 kg; cargo dimensions – 500 mm × 500 mm × 50 mm [3].



a



b

Fig. 3.4. UAV PKM-14 «Saturnia» load compartment view: *a* – bushings of the compartment are in «open» position and load has been dropped; *b* – bushings of the compartment are in «open» position and load is dropped, helicopter is returning to the station

Additional payload – day video camera used for either preliminary visual inspection of the place of future landing or with the aim of video recording of all stages in UAV flight. Communication line – analog, working frequency – 1,2 Ghz.

UAV control is conducted in automatic and semiautomatic mode. Basic mode is automatic. Onboard part of the UAV control system consists of necessary sensors, data receiving and handling blocks, autopilot, receiving and transmitting unit of communication and control lines, antenna devices, electronic regulators of differential control of electric engines, as well as servo drives to control the release/concealment of the chassis and the opening/closing of the flaps of the box with the load.

Technical characteristics of UAV PKM-14

Geometrical characteristics:

- dimension on edges of cases of PP, m × m – 1,66 × 1,66;
- dimension on centers PP, m × m – 1,18 × 1,18;
- maximum height (chassis released), m – 0,42.

UAV main weight characteristics:

- maximum take-off weight, kg – 10;
- maxim weight of payload, kg – up to 2;
- weight of empty AC (without EB), kg – 5,5;
- maximum weight of power battery, kg – 2,5.

Main characteristics of PP UAV:

- type of engine – electric three phase direct current motors, air-cooled Foxtech X5010; KV 288;
- speed controller – Hobbi-Wing Skywalker 40A;
- type of propeller/diameter, mm – two blade fixed pitch propeller – 18/6,1;
- weight of one engine, kg – 0,213;
- number of engines, un – 4;
- engine capacity kW – $4 \times 1,8$.

UAV main flight characteristics:

- maximum horizontal velocity, km/h – 30;
- cruising velocity, km/h – 25;
- service ceiling, m – up to 500.

Main operational characteristics:

- flight time, min – up to 30;
- operational range with «on-line» communication, km – up to 3;
- time of moving into operating position, min – 30.

Technical description of UAV PKM-14 «Saturnia» control system

1. UAV PKM-14 control system is automatic and provides its flight according to the plan drawn up in advance with waypoints (WP) beyond optical visibility. Flight plan can be replanned or updated remotely. Control system allows operation of UAV according to instrument flight rules (IFR) and is restricted according to visual flight rules (VFR) in automatic and semi-automatic mode.

2. Flight plan is performed by aircraft autopilot in automatic mode. In semi-automatic mode waypoint (WP) is reached by remote pilot (RP). In this case aircraft stabilizers maintain stabilize mode for UAV main functions and its velocity. Semi-automatic piloting of UAV can be applied in the extreme cases with help of method «see UAV from aside» within optical visibility.

3. UAV control system includes unmanned aerial vehicle ground control station (GCS) and aircraft control system (ACS), necessary on-air control and communication lines. Radio command line 2,4 Ghz and telemetric radio line 0,915 Ghz are used in this model of UAV.

4. Unmanned aerial vehicle ground control station (GCS) consists of remote pilot's workstation (W), remote control, remote devices of displaying data on screens and transmission on the air. The image of combined piloting device (CPD) and telemetric data necessary for piloting UAV as well as virtual image of the location (map) from ground video archive are displayed on remote pilot's screen.

5. Aircraft part of UAV control system provides receiving control signals, execution of commands by all its necessary parts, automatic stabilization of its position and support of flight navigational parameters, flight planning considering waypoints and flight plan adhering, replanning of flight plan, automatic/semi-automatic execution of flight plan, autopilot turning on/turning off as well as manual/automatic turning on the system of «self return to UAV base».

6. Aircraft part of UAV control system consists of necessary sensors, blocks of data receiving and handling, receiving and transmitting unit of communication and control lines, antenna devices and servos for lowering/retracting landing-gear and opening/closing load box bushings.

7. Power supply of UAV aircraft control system is carried out from aircraft electrical batteries.

8. Power supply of UAV ground control station (GCS) is carried out from ground electrical battery.

3.2. Unmanned aerial vehicle M-6-3T «Zhayvir»

Intended use: UAV M-6-3T «Zhayvir» is intended for transportation of loads weighing up to 4 kg in automatic mode over a distance up to 800 km. UAV M-6-3T «Zhayvir» is intended for airdrome basing (Fig. 3.5).



Fig. 3.5. Left view of the UAV M-6-3T «Zhayvir»

Brief technical specification of UAV M-6-3T. Unmanned aerial vehicle M-6-3T «Zhayvir» – one-engine free flight mid-wing aircraft with V-like tail surfaces. The glider is made mainly of fiberglass, carbon fiber compound and wood; the most loaded elements of the construction are made from aluminum alloy [6].

Fuselage is a semi-monocoque construction with three-layer composite panel with removable inoperative upper fairing-cowling. There are main systems of UAV between bulkheads of fuselage. The top of fuselage is covered by structural panel with radio electronic equipment, signal receiver and rescue parachute. In its turn this equipment is covered by upper fairing. Middle fairing covers compartment of special cargo container (SCC). At the moment of releasing parachute relative airflow throws lower fairing and pulls out parachute. Front frame – load-carrying and has engine silent-blocks. There is block of engine ignition on the back of front frame.

Landing gear. The three-support landing gear with a forward controlled support. The wheels of landing gear revolve on ball bearings. Wheel fairings are expected to reduce harmful aerodynamic drag. Spring of main support is made from glass-roving, spring of front support – of D16T material.

Wing is single-spar structure, consists of two removable planes. Spar caps are made of glass-roving. Wing has two-layer rigid skin; outer layer is made from fiberglass cloth. Lift devices have two sections of conventional flaps. Flaperons have axial aerodynamic compensation.

The V-shaped tail. The stabilizer is single-spar with filler and a rigid skin; outer layer is made from fiberglass cloth. Rudders without spars and produced with the help of the same process technology as stabilizer.

Parachute has 12 cords with an axial cord and rubber buffer on the harness. Deployment of parachute is performed by upper fairing which is thrown by relative airflow. In order to avoid pulling over UAV by parachute on the ground after landing, harness with parachute is unhooked from UAV automatically.

Power plant includes one-cylinder petrol engine MVVS-50 IRS with wood three-blade propeller of fixed pitch. The engine – gasoline, carbureted, two-stroke, air-cooled. The engine is fixed on engine mounting to main frame over four silent-blocks. The engine is started from attached electric starter. Fuel is contained in two fuselage tanks of full capacity 8 l, connected by fuel lines. Engine fuel system is equipped by streamline fuel filter. Tank filling is carried out with the help of outboard cogwheel electric pump.

Electric system. Power supply of aircraft electric system is provided by aircraft electrical batteries with rated voltage of 8 – 12V, capacity 2,5A · h and by regular generator driven by engine crankshaft. Electric wiring consists of signal and power lines joined in combined cables.

UAV control is carried out in automatic, semi-automatic and manual mode. The main mode is automatic. Aircraft UAV control system consists of necessary sensors, data receiving and handling blocks, autopilot, receiving and transmitting unit of communication and control lines, antenna devices, as well as servos of rudder, elevator, flaps, servo of power plant engine throttle, servos of releasing and unhooking parachute.

Payload being carried (Fig. 3.6) – is a special cargo container for cargo up to 4 kg.



Fig. 3.6. Special cargo container for cargo of UAV M-6-3T «Zhayvir»

Operational and functional characteristics of UAV M-6-3T «Zhayvir»

UAV main weight characteristics:

- maximum takeoff weight, kg – 22;
- maximum weight of payload, kg – 4;
- weight of empty AC, kg – 13;
- maximum load capacity of wing area, kg/m^2 – 31;
- minimum load capacity of wing area, kg/m^2 – 24.

Main characteristics of PP UAV:

- type of engine – MVVS-50 IRS, gasoline, carbureted, two-stroke, single-cylinder, air-cooled;
- type of propeller /diameter/pitch, mm – three-blade propeller of fixed pitch /520/250;
- PP weight, kg – 1,6 (together with ignition system);
- number of engines, un. – 1;

- number of revolutions, r/min – 2000 – 7500;
- engine capacity, h.p. – 5.

UAV main flight characteristics:

- maximum horizontal velocity, km/h – 160;
- maximum nosedive velocity, km/h – 200;
- cruise velocity, km/h – 110 – 120;
- lift-off speed, km/h – 67;
- reference speed, km/h – 70;
- stall speed, km/h – 51;
- maximum rate of climb, m/s – 14;
- operating ceiling, m – up to 4000.

Main operational characteristics:

- fuel capacity, l – 8;
- fuel reserve, l – 0,3;
- fuel specification – gasoline-synthetic oil mixture (30:1);
- flight duration, h – 6*;
- operating range with «on-line» connection, km – up to 600;
- operating range (according to fuel capacity at cruise velocity), km – 700*;
- time of placing to operative position, min – 30;
- launch/landing approach – aircraft type.

* calculation are made with fuel capacity 8 l.

In Table 3.1 input values for calculation of UAV flight velocities are presented. The results of calculation of datum velocities for UAV M-6-3T «Zhayvir» with lift-off weight 12 kg are shown in Table 3.2.

Table 3.1

Input values for calculation of UAV flight velocities

UAV lift-off weight UAV (assigned)	M_0	kg	12	H	98
Flight conditions					
Normal operating velocity (assigned)	V_{\max}	km/h	110	m/s	30,6
Flight altitude (assigned)	H	m	200		
Maximum operating overload of maneuver	$n_{\text{om. max(a)}}$		+4; – 2		
Air density at assigned altitude ($t = 15 \text{ }^\circ\text{C}$)	ρ	kg/m ³	1,2052		

Table 3.2

The results of calculation of datum velocities for UAV M-6-3T «Zhayvir»

Name of datum velocities	Datum velocities					
	Unit of measurement	Values	Unit of measurement	Values	Symbol (AR-23)	Method of matching
Stalling speed	m/s	14,78	km/h	53,2	V_s	Calculation
Minimum steady flight speed in landing	m/s	14,16	km/h	51	V_{s0}	Calculation
Minimum steady flight speed in take-off	m/s	14,78	km/h	53,2	V_{s1}	Calculation
Safe take-off speed	m/s	16,26	km/h	58,5	V_2	Flight tests
Rotation speed	m/s	16,26	km/h	58,5	V_R	Flight tests
Reference landing approach speed	m/s	19,21	km/h	69,2	V_{REF}	Flight tests
Design cruising speed	m/s	29,23	km/h	105	V_C	Calculation
Design manoeuvring speed	m/s	29,56	km/h	106	V_A	Calculation

In Fig. 3.7 shows the dependence of aerodynamic quality, stalling speed and required power UAV on the angle of attack.

Brief technical description of UAV M-6-3T control system. Control system of UAV M-6-3T «Zhayvir» is automatic and provides its flight according to preliminary specified flight plan with waypoints beyond optical visibility. Flight plan can be replanned or updated remotely. Control system allows operation of UAV according to instrument flight rules (IFR) and is restricted according to visual flight rules (VFR) in automatic, semi-automatic and manual modes.

Flight plan is performed by aircraft autopilot in automatic mode. In semi-automatic mode waypoint (WP) target values are reached by manual control of remote pilot. In this case aircraft stabilizers maintain stabilize mode for UAV main functions and its velocity. Semi-automatic piloting of UAV or manual control (without stabilization) can be applied in the extreme cases with the help of method «see the plane from the side» within optical visibility.

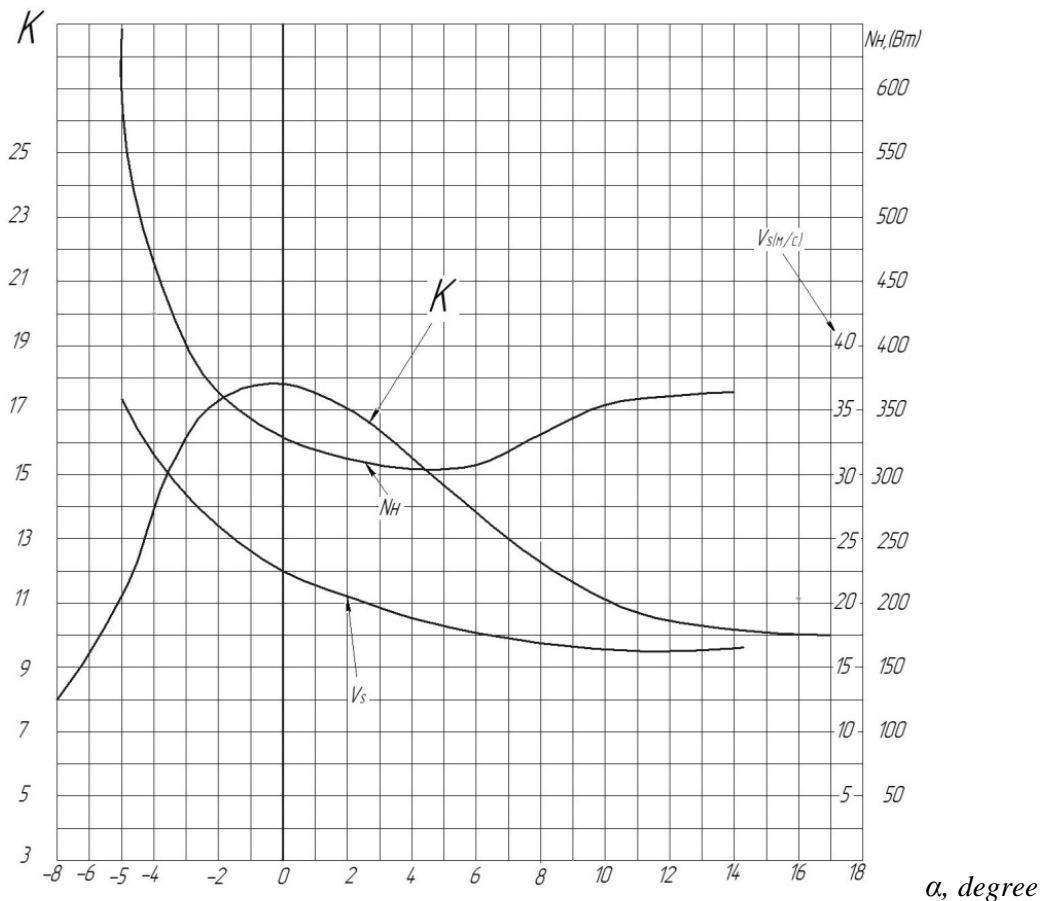


Fig. 3.7. Dependence of aerodynamic quality, stalling speed and required power UAV M-6-3T from the angle of attack

UAV control system includes ground control station (GCS) and aircraft control system (ACS), necessary on-air control and communication lines. Radio command and telemetric radio line 0,915 Ghz is used in this model of UAV.

Unmanned aerial vehicle ground control station (GCS) consists of first and second remote pilots' workstation (W), remote controls, remote devices of displaying data on screens and transmission on the air. The image of combined piloting device (CPD) and telemetric data necessary for piloting UAV as well as virtual image of the location (map) from ground video archive or real image of location taken by UAV are displayed on remote pilot's screen.

Aircraft part of UAV control system provides receiving control signals, execution of commands by all its necessary parts, automatic stabilization of its position and support of flight navigational parameters, flight planning considering waypoints and flight plan adhering, replanning of flight plan, automatic/semi-automatic execution of flight plan, autopilot turning on/turning off as well as manual/automatic turning on the system of «self return to UAV base» deployment of parachute.

Aircraft part of UAV control system consists of necessary sensors, blocks of data receiving and handling, receiving and transmitting unit of communication and control lines,

antenna devices and servos for rudder/elevator, flaperons, flaps, servo of power plant engine throttle, servos of releasing and unhooking parachute.

Power supply of UAV aircraft control system is carried out from aircraft regular electrical batteries and two aircraft generator driven by engine crankshaft.

Power supply of UAV ground control station (GCS) is carried out from outboard generator by devices of no-break power supply or from outboard power network 380/220V.

Functional composition of UAVS M-6-3T. Unmanned aerial vehicle system (UAVS) M-6-3T functionally consists of the following systems, equipment, devices [5].

Glider and power plant UAV

Glider:

- right half-wing;
- left half-wing;
- fuselage in the kit;
- V-like empennage;
- engine mount frame;
- main landing gear;
- front steering landing gear.

Power plant:

- engine;
- intake system;
- exhaust system;
- fuel system;
- engine cooling system;
- propeller.

Recovery parachute system

*System of warming air in fuselage**

UAV aviation equipment

Piloting navigation equipment:

- system of navigation equipment;
- sensor of air signal;
- aircraft system of telemetry.

Control system:

- servos of control system;
- mechanical wiring of control system;
- UAV autopilot.

Unmanned aircraft automatic landing system

Electro-technical equipment

Power supply system:

- aircraft electric batteries;
- power electro-block;
- aircraft electro-generator;
- aircraft electric wiring.

Aircraft system of objective control:

- flight recorder;
- accumulator of flight condition objective data.

UAV avionics

Radio-technical equipment:

- devices of satellite communication and navigation system.

Radio-line equipment:

- devices of radio-link control (*air/ground – radio control; ground/air – telemetry*).

UAV cargo compartment

- special cargo container (SCC);
- cargo container ballasts.

Functional composition of ground control station

The ground control station (GCS) consists of such systems, equipment and devices.

Remote pilot's workstation – pilot-in-command (W1)

UAV control system:

- UAV control position №1;
- data displaying screen of remote pilot;
- personal computer;
- devices of ground radio-control system.

Devices of ground navigation system:

- ground telemetry.

Radio-communication system of distant pilot:

- devices of command radio-link;

- devices of radio-communication system.

System of distant pilot's video communication:

- devices of data receiving and displaying.

Devices of control and monitoring of the UAV parachute descent system

Remote co-pilot's workstation (W2)

UAV control system:

- UAV control position №2;
- data displaying screen of remote pilot;
- personal computer;
- devices of ground radio-control system.

Antenna tracking system GCS:

- mechanism of azimuthal rotation of antenna;
- telemetric antenna;
- video system antenna.

UAV flight support system:

- GCS power supply system;
- GCS air conditioning and ventilating system;
- meteorological support system;
- fire extinguishing system;
- topographic (cartographic) support system and additional radio-navigation;
- system of objective control (data flight recorder).

Lighting facilities of UAV takeoff and landing:

- aircraft air navigation lights;
- ground landing lights.

Verification equipment:

- a kit of control, measuring and special equipment for before- and after flight MT.

Equipment for UAV storage and transportation.

Mounting kit.

Spare parts, tools and accessories.

Technological equipment.

A kit of tools.

Set of operational documentation.

List of references

1. Unmanned helicopter for cargo delivery. M. P. Matiychyk, O. S. Rybalchenko, D. M. Matiychyk, V. O. Dvigon, M. I. Fuzik Ukraine's patent for a useful model. №113343. Published on 10.01.2019. Bulletin № 1.
2. Unmanned multi-engine helicopter for small cargo transportation. M. P. Matiychyk, O. S. Rybalchenko, D. M. Matiychyk, V. O. Dvigon, M. I. Fuzik, Y. Litvin Ukraine's patent for a useful model. №119261. Published: 25.09.2017. Bulletin № 18.
3. Flight tests of the PKM-14 «Saturnia» unmanned cargo helicopter have been completed at NAU. Source access mode: <http://uav.nau.edu.ua/Saturnia%2026.02.18-UA.html>.
4. Unmanned aerial vehicle for small cargo transportation. M. P. Matiychyk, V. O. Dvigon, D. M. Matiychyk, O. S. Rybalchenko Ukraine's patent for a useful model. №130978. Published on 10.01.2019. Bulletin №1.
5. «Nova poshta» has revealed the drone it will use to deliver goods. Internet resource. Intermarium – Intermarium news. Source access mode: <https://intermarium.news/kompaniya-nova-poshta-pokazala-bezpilotnyk-yakym-dostavlyatyme-tovary/>.
6. Matiychyk M. P. Unmanned aerial vehicle for transporting postal items. Ukraine's patent for a useful model. №119235. Published: 11.09.2017. Bulletin №17.

Chapter 4

UNMANNED AERIAL VEHICLES OF NATIONAL AVIATION UNIVERSITY AND THEIR COMPLEXES FOR REMOTE SURVEILLANCE, MONITORING, AND OTHER PURPOSES

4.1. Unmanned aerial vehicle complex «OVOD» M106

The multi-use «OVOD» M106 unmanned aerial vehicle complex (UAVC) meets the requirements of DSTU V7371:2013 and is designed for day and night aerial reconnaissance with the transmission and recording of video or infrared sensor (IR) images in the «on-line» mode. Also, «OVOD» M106 can perform aerial photography in different spectrum ranges.

The ground control station (GCS) is intended for control and monitoring of unmanned aircraft «OVOD» M106 on the ground and when flying in the allocated airspace. UAV and its GCS are operated by a remote crew of not less than three people. The unmanned aerial vehicle «OVOD» M106 and its ground control station are housed in two containers. Unmanned aerial vehicle complex «OVOD» M106 is designed for airfield-free basing.

The main advantages of the complex are its ability to base without an airfield, and high aerodynamic characteristics allow the «OVOD» M106 to be operated in almost any conditions of location in the temperature range from -22°C to $+40^{\circ}\text{C}$. Thanks to the design features and small size, the UAV «OVOD» M106 has a small optical, acoustic and radar sensitivity. A significant load per unit area of the wing allows keeping the top operational value of the wind component up to 23 m/s.

Intellectual property protection status. Patent of Ukraine for the utility models: №132969 (2019), №133753 (2019), №140038 (2020).

The unmanned aerial vehicle complex «OVOD» M106 consists of the following parts:

- unmanned aircraft in a set (2–3 depending on the configuration);
- ground control station (GSC) of the «OVOD» M106 complex;
- KP-5 launcher (catapult);
- spare sets of power batteries (airborne/ground);
- charger for airborne and ground batteries;
- tools for UAV storage and transportation;
- spare parts, instrument and accessories;
- a kit of tools;
- a set of operational documentation.

A brief technical specification of UAV «OVOD» M106

The «OVOD» M106 unmanned aerial vehicle (Fig. 4.1) – is a single-engine free-floating midplane with V-shaped tail fins. The glider is made of fiberglass and carbon fiber reinforced plastic; some structural elements are made of aluminum alloys.



Fig. 4.1. General view of UAV «OVOD» M106 on the launcher KP-5

The fuselage is a semi-monocoque structure with a fiberglass multilayer power skin with a removable upper fairing. Gluing takes place in negative matrices with subsequent hardening of blanks. Between the fuselage frames are the main systems of the UAV. Under the front fairing is a power battery with a logement. Under the battery there is a biaxial target load gyrostabilizer, which is covered by a transparent fairing from below the fuselage (Fig. 4.2).

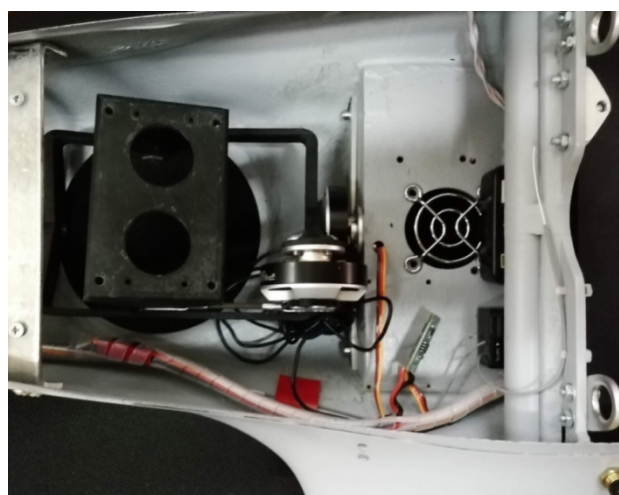


Fig. 4.2. Biaxial gyrostabilizer of the target load UAV «OVOD» M106
(top view; power battery logement removed)

The general layout of the equipment and systems of the «OVOD» M106 UAV is shown in Fig. 4.3.

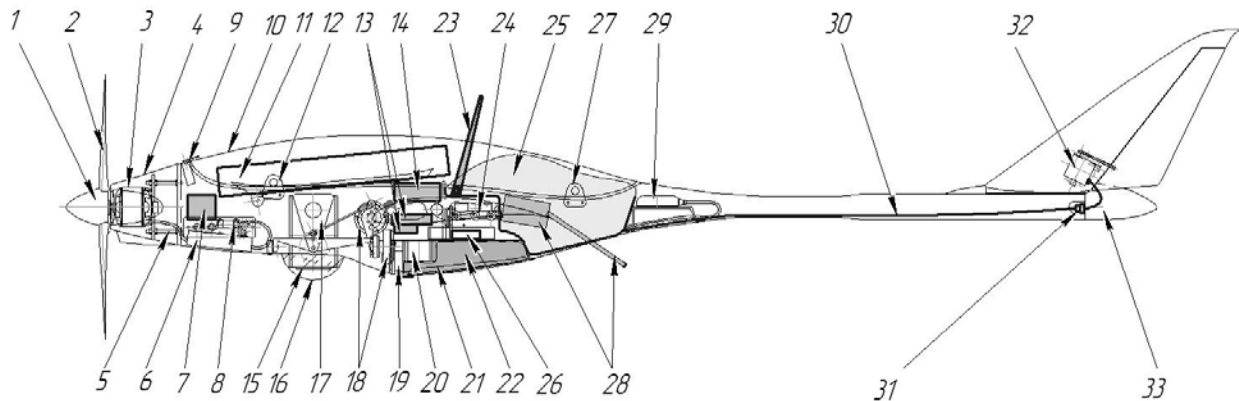


Fig. 4.3. Location of equipment and systems of UAV «OVOD» M106: 1 – propeller fairing; 2 – propeller; 3 – electric engine of the power plant; 4 – removable engine hood; 5 – engine mount; 6 – electronic engine speed controller; 7 – camera and thermal imager video signal converter; 8 – autopilot power supply; 9 – servo for dropping the upper fairing-cowling; 10 – upper fairing-cowling; 11 – UAV power battery; 12 – front bypass parachute sling bracket; 13 – power supply units of target load cameras; 14 – telemetry power supply unit; 15 – day camera target load; 16 – clear camera lens fairing; 17 – moving (pitch) gyro stabilizer frame; 18 – gyrostabilizer electro engine; 19 – servo for opening the hatch of the shock-absorbing cushion; 20 – compressor inflating the shock-absorbing cushion; 21 – shock absorber cushion shaft cover; 22 – shock-absorbing cushion (when folded); 23 – airborne video antenna; 24 – on-board video modem; 25 – parachute (folded down); 26 – parachute unhooking servo; 27 – the rear bypass bracket of the parachute sling; 28 – telemetry modem and its antenna; 29 – navigation unit (magnetometer + GPS receiver); 30 – tail wiring harness; 31 – connector of the tail wiring harness; 32 – servo of the steering surfaces of the empennage; 33 – removable fuselage tail fairing

The autopilot panel is located in the middle part of the fuselage. Under the fairing-cowling is the descent parachute with the unhooking mechanism. Opening of the fairing-cowling for parachute release is done by servo drive; during parachute release the fairing is dropped by the spring and the incoming air stream extracts the descent parachute. Communication modems are located in the middle part of the fuselage. The antennas of the modems are outside the fuselage. The electric propulsion motor is attached to the engine.

Under the bottom of the fuselage is a hatch that closes the folded pneumatic cushion. The cushion is filled by an axial compressor with an electric engine. For the installation of the cushion and compressor there is a tray in the fuselage.

The wing of UAV «OVOD» M106 is fundamentally new, a ogival wing, and differs as follows (Fig. 4.4):

- the shape of the wing profile and its thickness are selected for the Re number, which corresponds to the speed for the economic mode; each wing cantilever is united with a wingtip that is bent up and back and is given a united ogival form in plan view, and when viewed from the front the chordal plane of each wing is transformed into a set of at least three surfaces, the middle of which is a plane and the V-like the empennage are equipped with wingtips bent back;
- the middle surface of the chords of each wing, which is a plane, is used to locate the transverse control body in it.

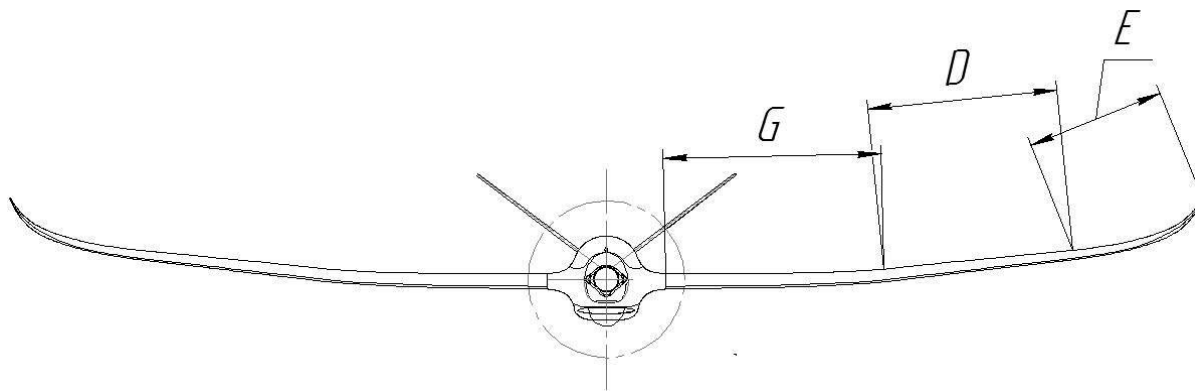


Fig. 4.4. Front view on the wing of the M106 UAV «OVOD»:

G – ogival surface of the center wing; D – the plane of the middle airfoil chord, equipped with transverse control bodies; E – is an ogival surface of the limb with an attached winglet

Wing single-spar design, consists of two removable planes; their connection with the fuselage is provided by a tubular bolt, and the consoles are held by automatic locks. The wings of the spar caps are made of glass-roving. The casing is rigid in the form of three-layer panels glued to the profiles.

The application of the wing with ogival contours makes it possible to obtain the aerodynamic quality of the layout in the range of 20–22 units in the economic mode of flight of the UAV.

The V-shaped tail, single-spar with a rigid three-layer skin. The rudder is sparless and technologically similar to the stationary part of the plumage. The connection of the tailplane to the tail boom is made with an M3 threaded screw. The tail boom is covered by a removable cowling, under which is the servo connector with the tail wiring harness.

The power plant (PP) includes a three-phase electric motor of constant excitation with an electronic regulator and a two-bladed propeller of constant pitch. The engine is installed on a transition mount, with the help of which you can change the direction of the PP thrust vector. The engine is cooled by air passing through the inlets in the fuselage hood.

Electric system. Power supply of aircraft electric system of the UAV is powered by a regular power lithium-polymer battery with four cells. Electric wiring consists of signal and power lines joined in combined cables. Individual consumers are provided with appropriate voltages from on-board power supply units.

UAV control is carried out in automatic and semi-automatic mode. The main mode is automatic. The control signals are transmitted via a digital secure radio line. In case of an emergency, it is possible to switch to the «manual» mode.

Regular target load – gyro-stabilized video camera/IR-camera controlled by control system channels.

Video camera digital SONY FCB-EV7500 (Fig. 4.5), matrix approximately 3 Mp; optical magnification is 30x.



Fig. 4.5. Day video camera SONY FCB-EV7500 in a transitional case

MT 640 «Microthermo» thermal imager, resolution of about 640×480, uncooled microbolometer. Canon Power Shot SX100 IS camera (optional) or similar.

The KP-5 launcher is collapsible and is intended for an organized non-aerodrome automatic launch of the UAV at a wind speed of up to 20 m/s (Fig. 4.6 and 4.7). The launcher consists of a launch frame with a rubber shock absorber and a moving carriage. Tensioning the shock absorber – manually. The weight of the launcher is up to 5 kg. When folded, *KP-5* has the following dimensions: 200 mm × 350 mm × 1200 mm.



Fig. 4.6. General appearance and dimensions of the KP-5 launcher in working condition

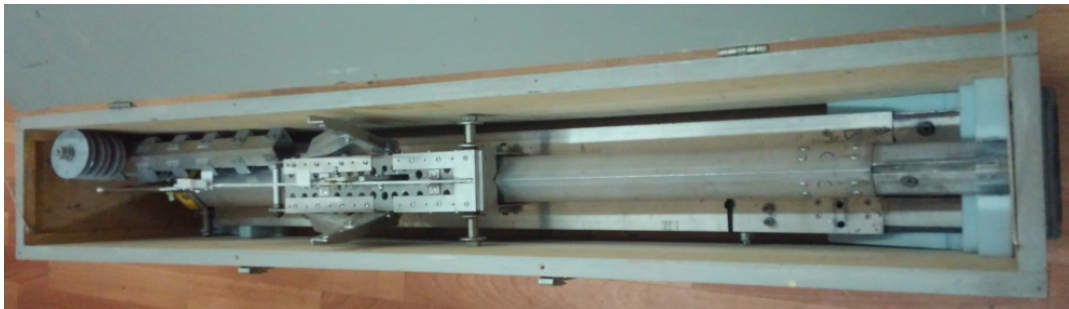


Fig. 4.7. General appearance and dimensions of the KP-5 launcher in the folded state (container for KP-5 size $200 \times 350 \times 1200$; weight together with KP-5 is about 18 kg)

The general appearance of the «OVOD» M106 UAV in the transport container is shown in Fig. 4.8.



Fig. 4.8. General appearance and dimensions of the transport container for UAV «OVOD» M106 (container size $380 \text{ mm} \times 800 \text{ mm} \times 1400 \text{ mm}$; weight – 35 kg)

Table 4.1 shows abbreviations of some blocks of aviation equipment of the «OVOD» M106 and their purpose.

Purpose of some blocks of aviation equipment UAV «OVOD» M106

№	Block name	Abbreviated designation	Purpose of the block
1	On-board automation unit	BA-2,6	Automatic UAV control (flight controller)
2	Radio control receiver unit	BPR-2,4	Manual radio control UAV (on-board radio control receiver)
3	Autopilot power supply	BGA	Preflight/postflight activation/deactivation of autopilot of UAV in order to provide them with voltages with the necessary characteristics
4	Servo power supply unit	BGS	Power supply to the servo drives of the control system
5	Telemetry power supply	BGT	Powering the on-board UAV telemetry system
6	Day camera power supply of the target load	BGK	Providing power to the onboard day chamber of the target load
7	Day camera power supply of the target load	BGT	Power supply of the on-board thermal imager
8	Camera and thermal imager video signal converter	KVS	Converting analog signals from cameras to TCPIP protocol signal
9	Onboard telemetry unit	BT-0,915	Providing two-way communication to transmit onboard telemetry information from the UAV to the GCS and control commands from the GCS to the UAV
10	On-board telemetry antennas	AT-0,915	Two antennas for transmission/reception on the air/from the air of the signal from the block/to the telemetry communication block BT-0,915
11	On-board video transmission unit	BPV-2,4	Provision of two-way communication for the transmission of video images of the UAV to the GCS
12	On-board video signal antennas	APV-2,4	Two antennas for transmitting video signals to the air from the BPV 2,4 unit
13	Parachute storage system on board	SZP-106	Storing the parachute in the folded condition on the UAV and its release at the command of the BA 2,6 unit
14	Target load control unit	BCV	Current control of orientation and other functions of the video camera (IR camera) UAV
15	Electronic speed controller	ERD-M106	Motor speed control in all modes of operation
16	On-board navigation unit	NB	Providing the onboard autopilot with data from the GNS system and magnetometer
17	Air pressure receiver	PPT	Providing the onboard autopilot with data about the airspeed of the aircraft
18	Landing cushion compressor	KPP	Ensuring the inflation of the landing cushion

Technical characteristics of UAV «OVOD» M106 and UAC on its basis

Geometrical characteristics:

- wing span, m – 2,513;
- length, m – 1,434 (with propeller fairing);
- altitude, m – 0,349 (without a propeller); 0,298 (without telemetry antenna);
- altitude, m – 0,419 (with a propeller); 0,368 (without telemetry antenna);
- the area of the whole wing (with fuselage covering), m^2 – 0,45;
- wing aspect ratio, units – 13,8;
- wing taper ratio, η – 1,98;
- arrow-shaped angle of $\frac{1}{4}$ chord – $3,5^\circ$;
- mean aerodynamic wing chord, m – 0,191;
- the area of differential ailerons (two), m^2 – 0,038;
- the area of V-tail (horizontally), m^2 – 0,074;
- the area of the fixed part of of V-tail, m^2 – 0,062;
- area of the moving part of V-tail, m^2 – 0,0266;
- horizontal arm, m – 0,7;
- the span of horizontal tail, m – 0,542.

UAV main weight characteristics:

- maximum take-off weight, kg – 4,95;
- maximum weight of payload, kg – 0,8;
- weight of empty aircraft (without camera and on-board usable battery), kg – 2,65;
- maximum load capacity of wing area, kg/m^2 – 12,4;
- minimum load capacity of wing area, kg/m^2 – 11;
- estimated position of the center of gravity (in fractions of MAC) – 0,3612 (36 %);
- position of the center of gravity (in millimeters MAC), mm – 69.

Main characteristics of PP UAV:

- type of engine – electric, three-phase with constant excitation, air cooling;
- type of propeller – two-bladed propeller of fixed pitch;
- PP weight, kg – 0,3;
- number of engines, un. – 1;
- engine power, h.p. – 1,0.

UAV main flight characteristics:

- maximum horizontal speed, km/h – 140;
- cruise speed, km/h – 62–75;

- lift-off speed, km/h – 49;
- reference speed, km/h – 58;
- stall speed, km/h – 44,5;
- operating ceiling, m – до 3500.

Main operational characteristics:

- flight duration, h – no less than 2,5;
- operating range (with a battery capacity of 28 A · h at cruising speed), km – up to 75;
- extreme rear position of the center of gravity (CG) – 36,8 % of MAC
- calculated CG position – in mm MAC / %MAC – 53,2 mm / 20%.

Aerodynamic surface profiles:

- wing – Wortmann FX63-137;
- tail fins – NACA 0010.

On-board target load:

- SONY FCB digital video camera – EV7500;
- «Microthermo» model MT-640 digital thermal imaging module.

On-board camera gyrostabilizer:

- type – biaxial (roll and pitch stabilization);
- installation method – integrated into the fuselage structure;
- method of target load replacement – mounting/dismounting cameras from the side of the battery compartment.

The main operational characteristics of the M106 UAV «OVOD»:

- weight of UAVC, kg – up to 55;
- transportation method – in two special crates;
- operating range with «on-line» connection, km – up to 22;
- the way to manage the target load – through the Web-interface of the IP camera and the Mission Planner program;
- deployment time, min – 15;
- weight of the KP-5 launcher, kg – 5.

The main aerodynamic characteristics of the UAV «OVOD» M106. The results of calculation of the values of aerodynamic quality, changes in stalling speed and required power for the maximum take-off weight of 4,95 kg of the «OVOD» M106 UAV are shown in Fig. 4.9.

Fig. 4.10 shows the dependence of the lift and drag coefficients on the angle of attack for the full configuration of the «OVOD» M106.

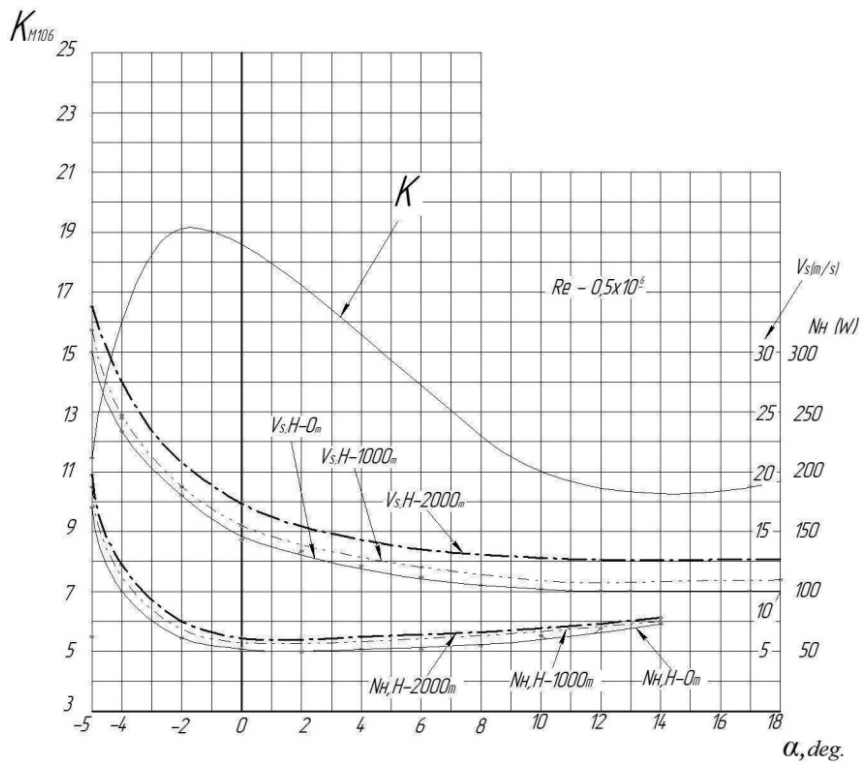


Fig. 4.9. Dependence of aerodynamic quality, stalling speed and required power of UAV «OVOD» M106 on the angle of attack

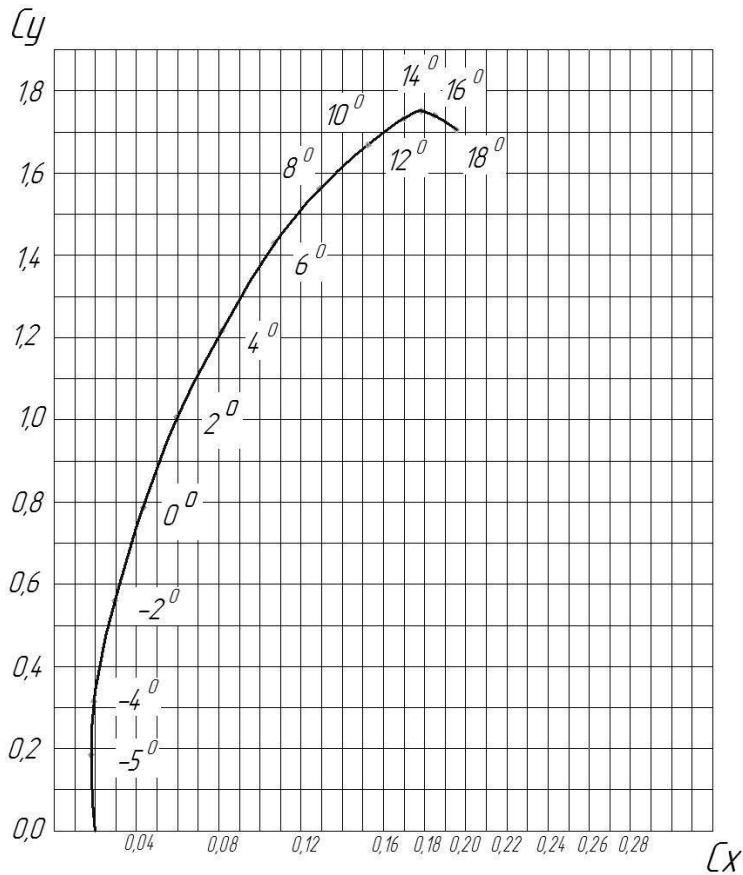


Fig. 4.10. Dependence of lift and drag coefficients on the angle of attack for the full «OVOD» configuration M106

Brief technical description of the control system UAV «OVOD» M106 and ground control station

1. Control system of UAV «OVOD» M106 is automatic and provides its flight according to preliminary specified flight plan with waypoints beyond optical visibility. Flight plan can be replanned or updated remotely. Control system allows operation of UAV according to instrument flight rules (IFR) and is restricted according to visual flight rules (VFR) in automatic, semi-automatic modes.

2. Flight plan is performed by aircraft autopilot in automatic mode. In semi-automatic mode waypoint (WP) target values are reached by manual control of remote pilot. In this case aircraft stabilizers maintain stabilize mode for UAV main functions and its velocity. Semi-automatic piloting of UAV or manual control (without stabilization) can be applied in the extreme cases with the help of method «see the plane from the side» within optical visibility.

3. UAV control system includes ground control station (GCS) and aircraft control system (ACS), necessary on-air control and communication lines. Radio command and telemetric radio line 0,915 GHz and a 2,4 GHz video line is used in this model of UAV.

4. Unmanned aerial vehicle ground control station (GCS) consists of the remote pilot (RP) and the target load operator workstation (W), remote controls, remote devices of displaying data on screens and transmission on the air. The image of combined piloting device (CPD) and telemetric data necessary for piloting UAV as well as virtual image of the location (map) from ground video archive or real image of location taken by UAV are displayed on remote pilot's screen.

5. The target load operator's monitor displays a real image of the terrain from aboard the UAV, a map of the area with objects tied to geographic coordinates, as well as the trajectory of the UAV with its flight plan.

6. Aircraft part of UAV control system provides receiving control signals, execution of commands by all its necessary parts, automatic stabilization of its position and support of flight navigational parameters, flight planning considering waypoints and flight plan adhering, replanning of flight plan, automatic/semi-automatic execution of flight plan, autopilot turning on/turning off as well as turning on the system of «self return to UAV base» and deployment of parachute.

7. Aircraft part of UAV control system consists of necessary sensors, blocks of data receiving and handling, receiving and transmitting unit of communication and control lines, antenna devices and servos for rudder/elevator, flaperons, servos of releasing and unhooking parachute, video camera/camera control servos, etc.

8. The navigation UAV is equipped with an inertial system, 3-D magnetic compass, GPS module, and an atmospheric pressure receiver. The barometric system and GPS module are used for altitude support.

9. Power supply of UAV aircraft control system is carried out from aircraft regular electrical batteries.

10. The ground control station (GCS) is powered from an external 12/24V battery or an electric generator via an uninterruptible power supply or from an external 380/220V electrical network.

The ground control station UAVC «OVOD» M106 is mobile and can be deployed in 10–15 minutes. The ground control station «OVOD» M106 consists of the following functional elements (Fig. 4.11 and 4.12):

- of a land-based secure computer in a case;
- GCS power supply battery;
- antenna for receiving-transmitting video signals together with a modem;
- telemetry reception-transmission antenna along with the modem;
- telescopic mast and device for automatic deployment of antennas in the direction of the UAV;
- KP-5 launcher.



Fig. 4.11. General view of the ground control station (ground secured computer in a case)



Fig. 4.12. Telescopic mast and automatic antenna deployment device in the direction of the UAV

Conformity UAVC «OVOD» M106. Signs and characteristics of compliance with DSTU V7371:2013 classification are given in Table 4.2.

Table 4.2

Conformity of the UAVC «OVOD» M106 to the classification

№	A sign of	Feature
Unmanned aerial vehicle complex (UAVC) «OVOD» M106		
1	Purpose	Reconnaissance
2	Scale of tasks	Tactical with a radius of action: with real-time video information transmission – at least 20 km; without transmitting video information in real time – at least 30 km
3	Location	Ground basing
4	The principle of lifting force	Aerodynamic
5	Frequency of use	Reusable with a lifetime of at least 100 applications
6	Number of engines	Single-engine
7	Type of engine in power plant	Power plant based on a three-phase electric motor
8	Maximum take-off weight	Maximum take-off weight up to 4,95 kg
9	Maximum flight altitude	Flight altitude up to 3500 m
10	Maximum operating limit speed	Up to 150 km/h
11	Maximum flight time	At least 2,5 hours at a temperature of at least minus 10°C
12	Type of take-off	Mechanical launcher
13	Type of landing	Parachute
14	Type of flight control system	Combination
15	Targeted gear	Reconnaissance tools

Characteristics of target equipment

The basis is an optical-electronic head with a SONY FCB-EV7500 video camera in an interchangeable housing, attached to the moving part of the gyrostabilizer. Brief technical specifications of the day camera are given in Table 4.3.

Table 4.3

Technical specifications of the SONY FCB-EV7500 day camera

Parameter	Values
Imager sensor	1 / 2,8 - type CMOS
Lens	30x
Picture quality	Full HD 1080p (1920 × 1080)
Minimum illumination	Colour: 0,35 lx; (F1.6, AGC on, 1/30 s)
Digital zoom	12× (360× with optical zoom)
Video output (HD)	Digital / analog
Video output (SD)	VBS
Mass	260 g
Dimensions	50 × 60 × 89,7 mm
Defog	Yes
High light compensation (HLC)	Yes
Wide dynamic range	Yes
Image stabilizer	Yes
Stable zoom	Yes
Auto IR-cut filter removal	Yes
Spherical privacy zone masking	Yes
Noise reduction	Yes
Slowing down the image	Yes

The infrared camera MT640 is housed in a similarly sized and mounted housing and can be replaced in the field. Its technical specifications are shown in Table 4.4.

Table 4.4

Technical specifications of the MT640 «Microtermo» camera

Parameter	Characteristics
Detector	Uncooled microbolometer matrix
FPA resolution / pixels	640 × 480 / 17µm
Temperature sensitivity	≤60mk at f/1,0 300K
Frame rate	50 Hz
Spectral range	8~14µm
Image process	Automatic correction + additional shutterless technology
Power on delay	< 3 s
Image enhancement	DDE
Image display resolution (pixels)	640 × 480
Image frequency	50Hz (PAL)
Lenses (optional)	12 mm, 19 mm, 35 mm, 40 mm, 50 mm
Adjusting the thermal image	Polarity (black, white /9 color channels)

Digital zoom	×2; ×4
Brightness / contrast	Automatic / manual
Flipping the image	Horizontal / vertical
Crossing	+
Electric power supply	Operating voltage range: direct current: +2,5V~+5,5V
Typical operating voltage	Direct current 3,7V
Power consumption	<1W
Reverse voltage protection	+
Overvoltage protection	+
Environmental parameters	Operating temperature range: -20 °C~ + 60 °C
Special use	-40 °C~+60 °C
Storage temperature range	-45 °C~+65 °C
Humidity	5 % ~ 95 % non-condensing
Vibration	GJB 150-16 2.3.1
axial:	GJB 150-18 test 7 100g/6ms
Temperature gradient	-5 °C/min (-40 °C~+60 °C)
Physical parameters	Mass - 33 g
Dimensions	24 × 24 mm (actual module)
Interface	External power output
Digital video output	14bit(50Hz))/BT.656 (option)
Control protocol	RS-232
Analog video output	BNC(75Ω); supports combined video from two outputs
Keyboard	Keypad with buttons

4.2. The unmanned aerial vehicle complex M-7-V5 «Nebesniy patrol»

The main purpose of the unmanned aerial vehicle M-7-V5 «Nebesniy patrol» is to perform aviation work related to obtaining a photo-, video- and IR images of planar and linear objects using special target equipment that located on the lower surface of the fuselage nacelle. General view of UAV M-7-V5 «Nebesniy patrol» are given in Fig. 4.13, *a*, *b*, and *c*.

The unmanned aerial vehicle M-7-V5 «Nebesniy patrol» is safely operated, does not require the use of complex piloting techniques, and performs all maneuvers inherent in the unmanned aircraft in the modes of take-off, altitude, horizontal flight, descent and landing with two engines, one engine and with idle engines. The unmanned aerial vehicle M-7-V5 «Nebesniy patrol» can operate a remote pilot of a medium qualification with the appropriate certificate for this type of UAV.



a



b



c

Fig. 4.13. General view of UAV M-7-V5 «Nebesniy patrol»

The unmanned aerial vehicle M-7-V5 «Nebesniy patrol» is made according to the scheme «monoplane-parasol» with two-piston engines and «H»-shaped tail. The main feature of UAV M-7-V5 is the use of the transverse arrangement of engines, which, together with other factors of additional lift, allows obtaining high take-off characteristics, which are 25% higher than traditional, different from the accepted layout. Fig. 4.14 shows the main growth factors, where 1 – is the lifting force of the «pure» wing; 2 – increase in the lift from flaps; 3 – increase in the lift from blowing the wing with propellers; 4 – vertical component of the thrust of the propellers.

At the same time, the accelerating of an UAV is sharply reduced, the requirements for the quality of runway coverage are reduced, and the height of the airfield increases. In order to better meet the needs of a wide range of customers in the construction of UAVs, in addition to the above, a number of technical solutions were applied, which are presented in Table 4.5.

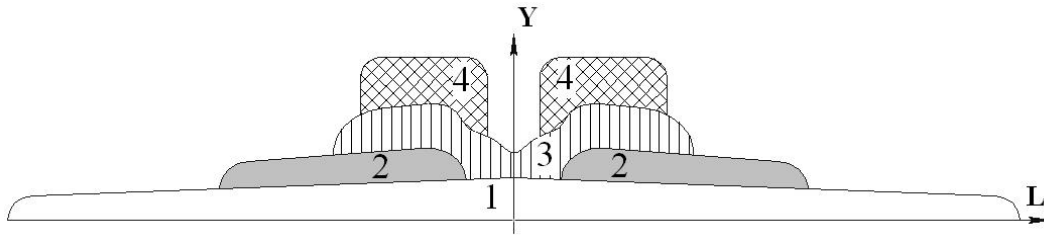


Fig. 4.14. Increase in the lift from the use of blowing the wing with propellers

Table 4.5

Main advantages of UAV M-7-V5 from the applied technical solutions

The adopted technical solution on the M-7-V5	The obtained advantage
The application of two engines	Permission to fly over populated areas. Reduced probability of flight interruption due to engine stop (flight will continue on one running engine)
Transverse location of the engines in front of the wing, on the centerplane with its blowing	Reducing the effects of electronic equipment vibration and the target payload located in the fuselage nacelle. Significant increase in lift can dramatically increase the take-off characteristics of the UAV; in particular, operation in high altitude conditions, high temperatures; roll for take-off reduction
The application of wing profiles with high aerodynamic quality indicators at the cruising value of the Re number	Allows you to significantly reduce fuel consumption in cruising mode and thus get an increased flight time without refueling – up to 8-10 hours
The use of a wing with a high/medium degree of mechanization	The use of slotted flaps and flaperons adds significant (up to 1,5 units) increase in coefficient to lifting force
The multi-section flaps and flaperons	Increasing the reliability of controls. The ability to get expanded range of UAV configurations
The application of single-slotted «inverted» horizontal empennage profile	Increasing the efficiency of UAV pitch control in modes with large angles of attack (especially on landing)
The use of the UAV modular design (detachable nacelle and the glider itself)	It allows you to quickly receive UAV modification increase the maintain ability of UAV
The tail beam, which «breaks» forward by turning 180°	The significant reduction of the UAV size in the transport position. Significant reduction in the time required to perform the operation of transfer from the working position to the transport position

The unmanned aircraft has a wing containing a center wing *1* (Fig. 4.15, *a*), on which the middle section of the Fowler flap *2* is fixed, and a wing console *3* with the wing section of the Fowler flap *4*. In turn, the heater *5* is equipped with the wing de-icing system (leading edge), middle flaperon section *7* with a weight compensator *6* and a lateral flaperon section *8* with a corresponding weight compensator *9*. Power plants with the closed profiled cowlings *10* are also fixed on the center wing *1*. A fixed part of a rectangular horizontal empennage *12* with a movable rudder *13* is fixed on the tail beam *11*. The movable steering wheel is equipped with a weight compensator *14* and the fixed part is equipped by the heater *15* (the leading edge de-icing system of the horizontal empennage).

Suspension arms of the flap sections and flaperons are closed by fairings *16* (Fig. 4.15, *b*). The intake of cooling air for the engines of power plants is organized through the inlet openings *17* made in the front of the profiled cowlings. The exhaust gas of the engines takes place through the exhaust pipes *18*. The main and front landing gear supports are equipped with wheels *19* with tires, which have increased resistance to lateral load (impact).

Power plants are equipped with three-bladed propellers *20* fixed-step (Fig. 4.15, *c*), and their hubs are closed with aerodynamic fairings *21*. The front part of the fuselage – the nacelle is closed by a fairing *22*. On the left side of the nacelle is a pitot tube (PT) – air pressure gauge *23*, which is required for measuring UAV airspeed. The front wheel is equipped with an aerodynamic switch *24* which reduces its aerodynamic drag. The swivel assembly of the front wheel is closed by the fairing *25*. On the fixed parts along the wingtips, navigation lights are installed *26*. On the left side of the tail beam there is a place for main switches, closed by a cover *27*. The tail beam *29* is moved from its working position to transport and vice versa using detachable and integral joints *28*. Beam cavity on the left side is closed by a cover *30*, which serves for mounting/dismounting and maintenance of communication facilities, which are located inside. The contour of the leading edge of the vertical empennage is equipped with deicing heaters *31*, *33* marks the contour of the aerodynamic compensator steering wheel *34*, *32* – load of the weight compensator of steering wheel. The fixed part of the vertical empennage is marked by *35*.

The tail part of the fuselage – nacelle is covered by a fairing *36*. On the fuselage – nacelle there is a shaft of the starter start buttons and input of airfield power, covered by a cover *37*. To reduce harmful aerodynamic resistance, the wheels of the main landing gear are also equipped with handles *38*. Camera (video- and IR) of the target payload cargo *39* is removed from the nacelle to provide a suitable field of view of the underfloor surface.

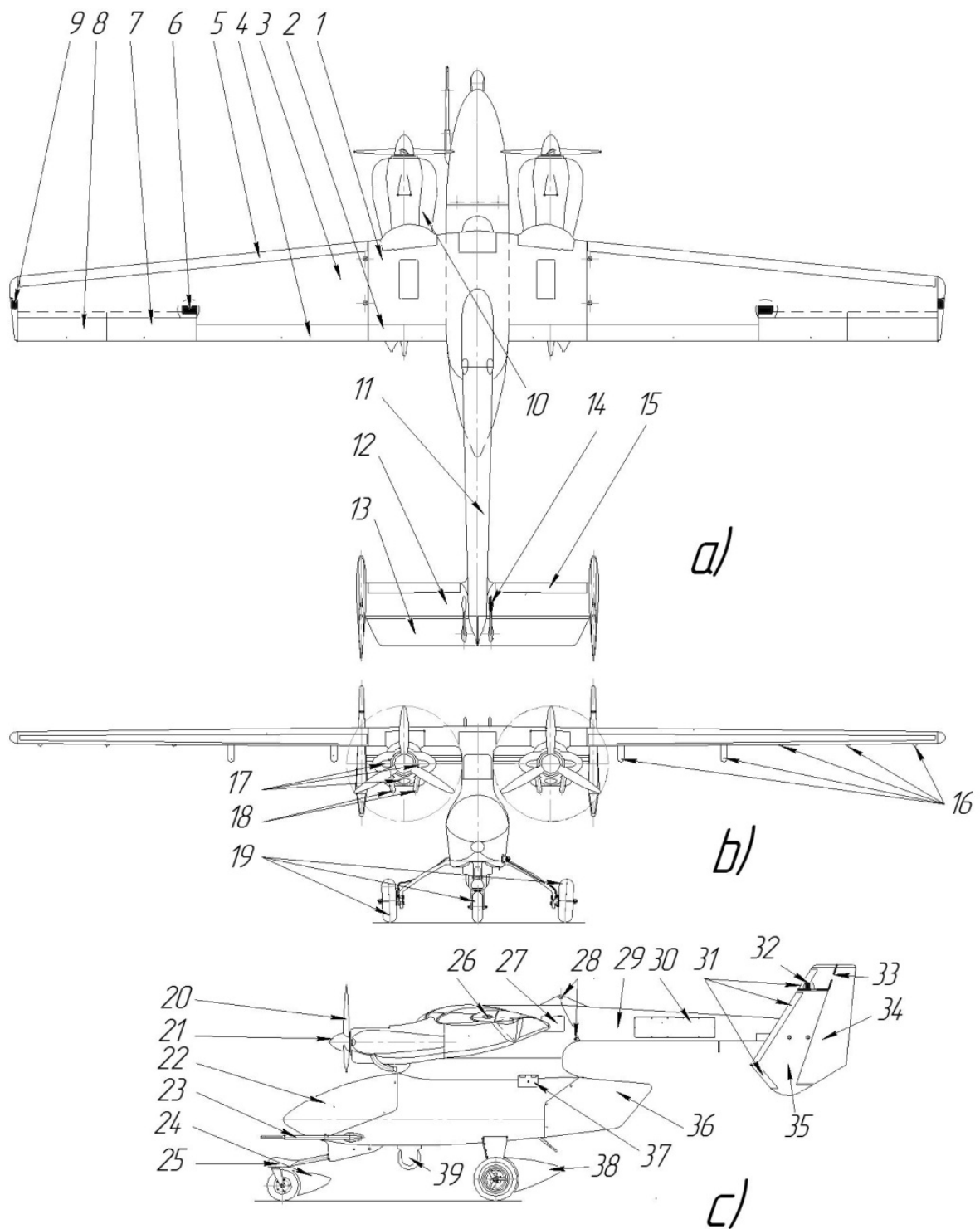


Fig. 4.15. General external design of UAV M-7-V5 «Nebesniy patrol»

The general internal design of the UAV M-7-V5 «Nebesniy patrol» is shown in Fig. 4.16.

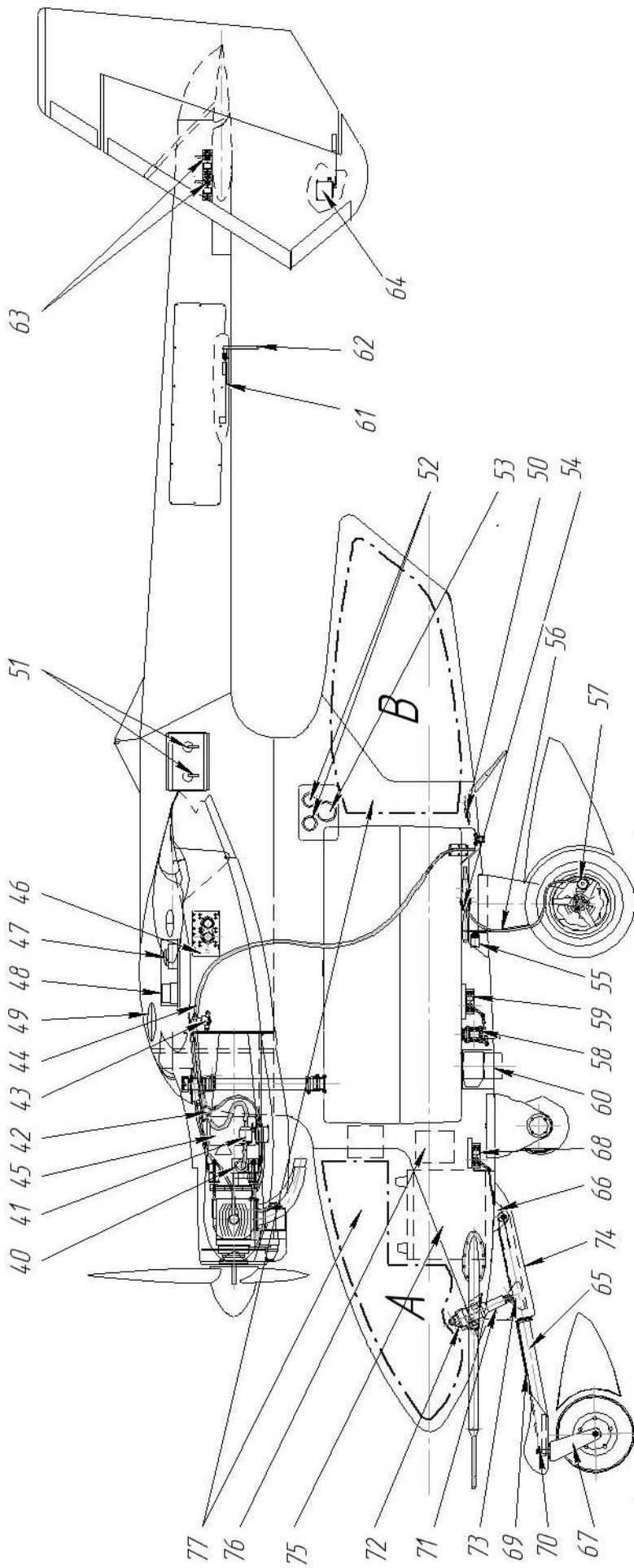


Fig. 4.16. General internal design of UAV M-7-V5 «Nebesny patrol»

The carburetor 40 of each of the two engines is supplied by a built-in pump with fuel passing through the filter 41, the spare fuel pump 42, and the fuel shut-off valve 43 from the individual fuel line 44. A fire extinguisher 45 is installed in each nacelle to provide fire extinguishing of the power plant. The triple-redundant autopilot 46 with its arbitrator calculates signals from the GPS navigation module 47, the short-range radio receiver 48, the satellite receiver 49, and the telemetry transceiver 50 shown with the antenna. Also, the autopilot processes signal from the pitot tube. The start of aircraft control systems of UAV occurs from the panel of the main switches 51. Starters of engines are started by buttons 52 of the starter's panel; the panel also has an electrical connector 53 for aerodrome power. The hydraulic brake system consists of separate main cylinders 54 for each wheel, separate servos 55 for these cylinders, the hydraulic line 56, and the wheel (working) cylinder 57.

The emergency fuel drainage system consists of a valve 58 with the assigned capacity and a servo 59 for opening the valve of the specified valve. As an option, in the fuselage – the nacelle can be located aerial camera 60; the transmission of data flow from all variants of the target payload, including airbrushing, is performed by the video modem 61 through the omnidirectional antenna 62.

The steering surfaces of the horizontal empennage are driven by servos 63 (one for each section of the rudder); each of the keels of the vertical empennage is equipped with a servo drive 64 to ensure the necessary deviation of the corresponding steering wheel keel.

The front support of the landing gear consists of a longitudinal, t-like lever 65, suspended on a rubber-metal hinge 66. At the opposite end of the t-like the lever is fixed to the node of rotation of the fork 67 of the front wheel. Its rotation is using a servo 68, the force of which is transmitted by a cable 69 type «bowden» to the lever-rocking chair 70 of the fork rotation. The oscillations of the suspension lever of the front support are perceived by a spring, pneumatic-hydraulic shock absorber 71 with adjustable damping force. In turn, the shock absorber is suspended on the upper and lower, respectively hinges 72 and 73. A fragment of the suspension lever with a rubber-metal hinge bracket and shock absorber is closed by a fairing 74. In the front part of the fuselage – nacelle mounted main 75 and emergency 76 on-board batteries. Item 77 indicates the free volumes in the nose (volume A) and tail (volume B) that can be loaded with additional payload while maintaining the established position of the UAV center of gravity within the limits required by the flight manual.

To increase the efficiency of horizontal empennage in the holding mode (large pre-landing angles of attack), which is associated with a decrease in flight speed to values close to the touchdown speed, horizontal empennage with the inverted profiled gap between fixed and

moving parts. The gap allows you to get an additional increase in the control force from the steering wheel height. This effect can be proved as follows.

Let UAV (Fig. 4.17) moves with a landing speed V_{land} and the fixed part of the empennage 79, fixed on the tail beam 78 is at the angle of attack α_{tail} .

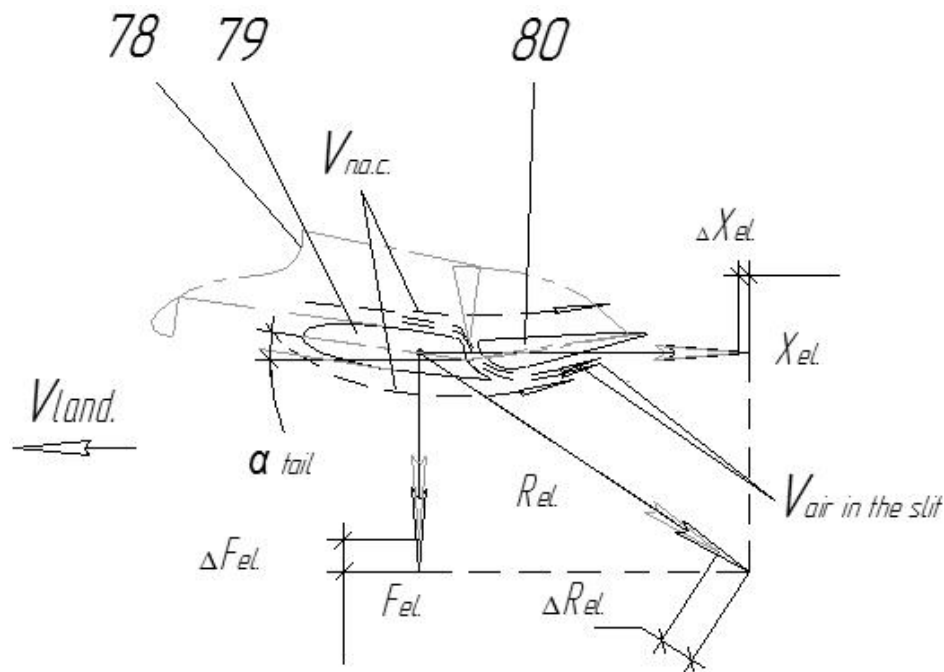


Fig. 4.17. The scheme of formation of an additional increase in the control force from the elevator of UAV M-7-V5 «Nebesniy patrol» elevator

The movable part of the empennage 80 (actually the elevator) is in a raised position, which is characteristic of the mode of «keeping» the UAV above the runway. When the empennage is slit-free, then on it, due to the well-known phenomenon of the formation of aerodynamic forces, the forces F_{el} and X_{el} are developed; respectively, the first is useful and control UAV on the pitch.

The second force is the force of harmful aerodynamic drag; as you know they can be replaced by an equivalent R_{el} . In this case, one of the factors of aerodynamic forces is the speed of flow, indicated in Fig. 4.17, as $V_{n.a.s}$. In the case of using an inverted slit, along with the speed $V_{n.a.s}$ an additional airflow is generated at a speed $V_{n.a.s}$, which is directed from the upper surface of the empennage under its bottom. Accordingly, the total flow velocity under the empennage will already be equal to the sum of the velocities $V_{n.a.s}$ and $V_{air\ in\ the\ slit}$ and it is well known fact that the increase in the speed of flow around the aerodynamic profile, along with other constant factors (empennage area, air density, and lift coefficient) leads to an increase in the

control force by ΔF_{el} , which makes it possible to increase the efficiency of the horizontal empennage of UAV at shutter speed mode.

Projections of UAV M-7-V5 «Nebesniy patrol» in the working (flight) position with the main dimensions is given in Fig. 4.18. In the transport position (with the wing consoles removed and the tail beam turned forward), the UAV is respectively shown in Fig. 4.19.

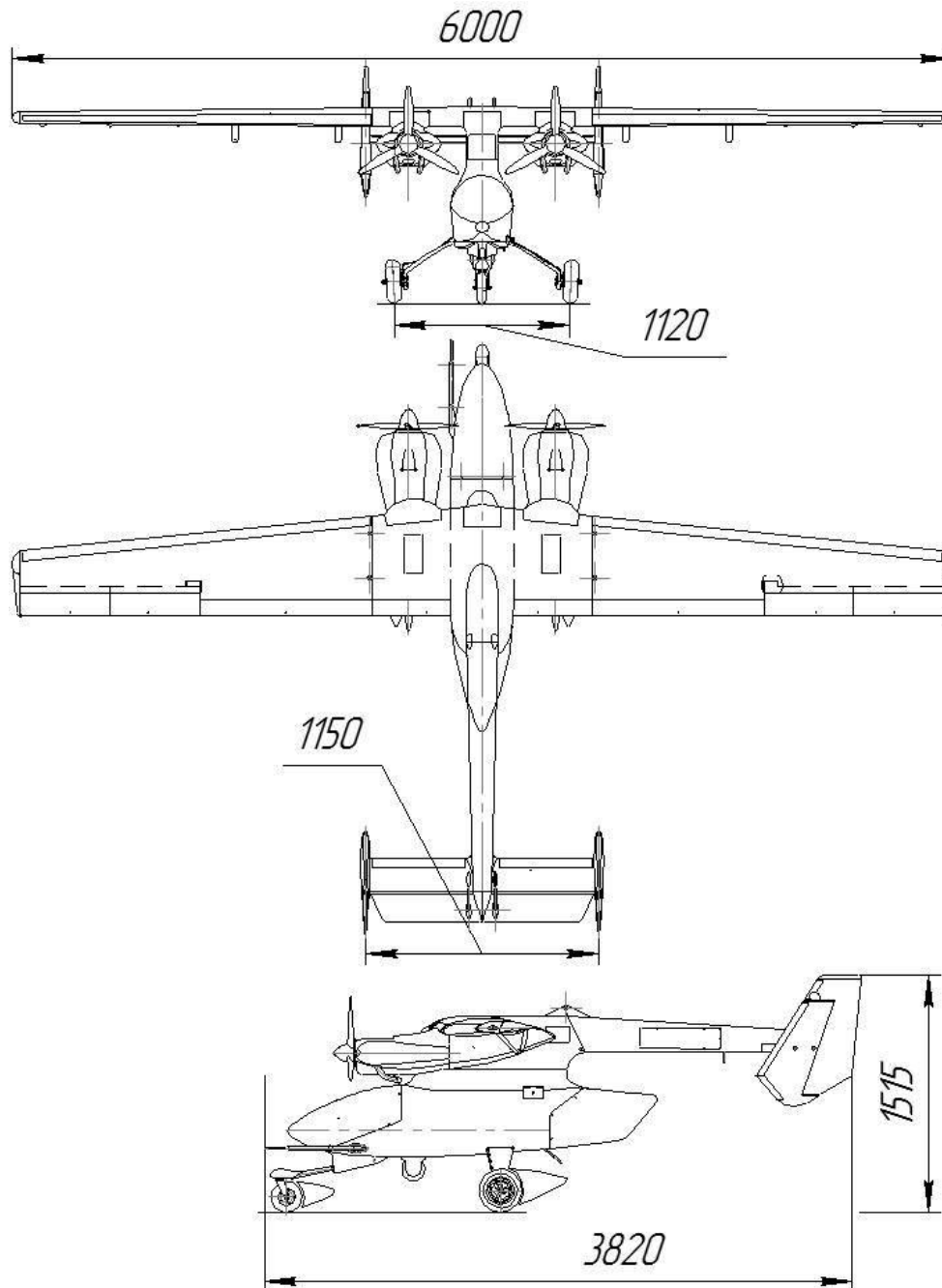


Fig. 4.18. Projections of UAV M-7-V5 «Nebesniy patrol» with overall dimensions in working (flight) position

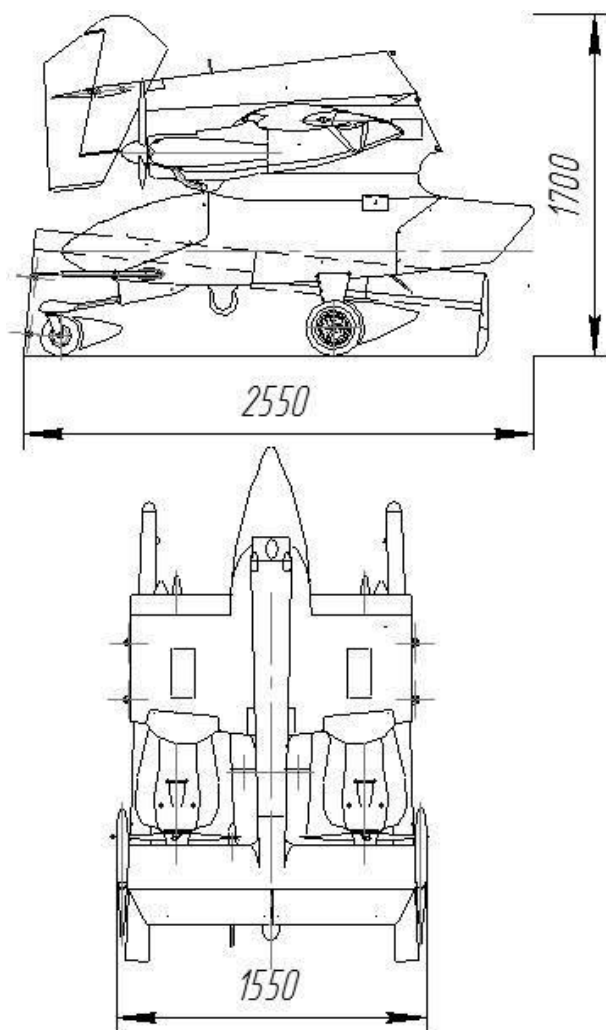


Fig. 4.19. Projections of UAV M-7-V5 «Nebesniy patrol» with overall dimensions in the transport position at the parking stand

To maintain the airworthiness of UAV M-7-V5 «Nebesniy patrol» in mobile use, the complex is equipped with a car trailer brand PGMF 8304-02, equipped for transportation and long-term storage of UAV.

Overall specifications of UAV in-flight position:

- length of UAV – 3,82 m;
- wingspan (projection) – 6,0 m;
- height at the parking stand (without fuel) – 1,52 m;
- landing gear track – 1,12 m.

Overall specifications of UAV in transport position (at the parking stand):

- length of UAV – 2,55 m;
- width – 1,55 m;
- height at the parking stand (without fuel) – 1,7 m.

Overall specifications of UAV in transport position (on the trailer):

- length – 4,18 m;
- width – 2,01 m;
- height at the parking stand (without fuel) – 2,5 m.

Minimum number of remote (ground) crew:

- unmanned aerial vehicle complex remote command pilot – 1;
- operator and remote co-pilot – 1;
- UAV aviation technician, car driver – 1.

Description of the standard performance of UAV. The design of the aircraft aerounatical, electronic and target equipment is given in Table 4.6:

Table 4.6

The design of the aircraft aerounatical, electronic and target equipment

Code	Name	Quantity
	On-board (section)	
VEAP007 kit	Kit 4x Autopilot Veronte (LOS 2,4 GHz + BLOS Radio)	
	4x Veronte Standby Autopilot for advanced UAV control. Includes 3 built-in Veronte autopilots and inputs / outputs for connection to external modules. 3x integrated two-way radio communication: LOS radio 2,4-2,48 GHz, FHSS, -109dBm sensitivity, 100 mW-1 W; BLOS HSPA + / 3,75G BLOS communication; BLOS data rate is not displayed. Includes sturdy aluminum housing and IP67 protection connectors	
CECN004	Autopilot harness with ring paired connector, including 50 cm wiring	1
CECN008	Harness to change the polarity of the autopilot. Circular paired connector with reverse polarity for auxiliary cans for 4x Veronte, including 50 cm wiring	1
CEAN006	2,4 GHz short antenna; 2,2DBi – SMA plug 6,2 cm	3
CEAN230	GPS – antenna expanded. Provides work with GPS/GLONASS/BeiDou/Galileo + L – Band – LNA: $\leq 2,5$ dB – 2,5 to 16 VDC – IP67; 32Dbi – 1m cable – 57 × 15 mm × SMA plug «dad»	3
CERF001	Coaxial cable 25 cm for the antenna; IP67 SSMA «dad» and IP67 SMA «mom»	3
CERF002	Coaxial cable 1m for the antenna; connectors IP67 SSMA «dad» and IP67 SMA «mom»	3

End of table 4.6

SESN001	Micro-radar altimeter; high accuracy up to 500m; 350 g; 4W; 7,32 V; CAN tyre	2
PITHE02	Heated air pressure receiver	3
The target board payload		
VEGI001	Day and IR cameras in one case, gyrostabilized	1

The target payload is located in the rotating body under the fuselage nacelle. The gyrostabilizer of the target payload provides stabilization of the camera optical axis in pitch, roll, and heading. Technical specifications of the VIDCA09 camera are given in the Table. 4.7. The standard target load VIDCA09 is located (marked target payload) under the bottom of the fuselage nacelle.

The video camera and IR camera are mounted in one housing on a 2-axis suspension with stabilization. Camera control allows you to get the following viewing angles (without shading objects with the image of the landing gear supports):

- solid angle from the vertical forward – 70°;
- solid angle from the vertical back – 60°;
- total solid angle of view – 130°.

Table 4.7

Technical specifications of the camera VIDCA09

Features	Description
Horizontal field of view, degrees	65° to 2,3° visible range / 18° – infrared range
Image stabilization	High-speed gyroscope
Image size	1920 × 1080 pixels (visible) / 640 × 512 (infrared)
Realtime video	1080 p 60 FPS (visible) / 480 p 60 FPS (infrared)
Infrared spectrum	7,5 – 13,5 μm
Thermal sensitivity	NEdT <50 mK
Zoom	30x optical (visible spectrum) / 10x image enhancing digital (infrared spectrum)
Weight	1,4 kg
Dimensions	210 mm × 179 mm × 153 mm
Power	12V, direct current
Image processing	Onboard picture processing with object segmentation and tracking of targets
Functions	Target tracking, geo-tagging, geo-location, fly-by-camera
Vehicle Detection Distance	18000 m (day) / 1950 m (night)
Vehicle Identification Distance	4000 m (day) / 250 m (night)
Human Detection Distance	6000 m (day) / 640 m (night)
Human Identification Distance	2000 m (day) / 80 m (night)

Target load option: SONY $\alpha 7$ camera with SONY SEL24F18Z lens which is located at an angle of $90^\circ (+/- 3^\circ)$ to the surface has the following angles:

- by frame width – 61° ;
- by Frame length – 61° .

Features and limitations of the M-7-V5 unmanned aerial vehicle «Nebesniy patrol» are presented in Table 4.8.

Table 4.8

M-7-V5 «Nebesniy patrol» UAV application limits

Operating conditions	Basic modification: 7B5.791100.101
Visual flight rules	+
Instrument flight rules	+
The time of day: in the night time in the day time	+ +
Weather conditions: good weather conditions adverse weather conditions at any time of the year	+ + +
Flight area: in the allocated airspace according to a previously filed application within a radius of 100 km and at an altitude of up to 6000 m	+
solving navigation and aircraft navigation tasks at all stages of flight from take-off to landing (any route) and (unequipped runways), as well as maneuvering in the area of the aerodrome according to SID and STAR schemes and performing APPROACH procedures	+
landing (the third category of ICAO)	+
vertical separation in 300 m	+
Physical and geographical conditions: above the plain, hilly and mountainous terrain above the water above the reference less terrain in the range of geographical latitudes from 70° north and 55° south, $+/-180^\circ$ in longitude	+ + + +

Fig. 4.20 shows the layout of the standard target load of the UAV and viewing angles for cameras and for the camera.

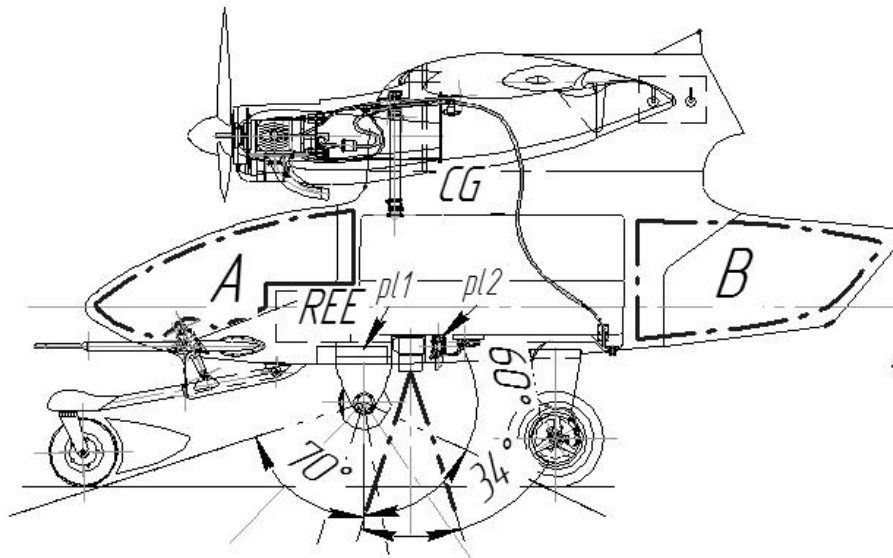


Fig. 4.20. Location of the standard target payload and permitted areas for the installation of additional target payload/useful payload/additional equipment of UAV M-7-V5 «Nebesniy patrol»

4.3. Unmanned aircraft M-6 «Zhayvir» for technology of biological protection of agricultural crops

Among the economically promising technologies for aviation chemical work (ACHW) should be noted the technology of using UAV for the introduction of biological plant protection products. The development of UAV M-6 «Zhayvir» is based on the scientific results of research on the effectiveness of the use of biological substances (trichograms) to control various pests of crops using UAV [1, 3].

The current ACHW technology provides for the use of An-2 aircraft, in which the specific fuel consumption is 2–3,5 l/ha. More modern aircraft models, such as NARP-1, have slightly better rates of 1,5–1,8 l/ha. However, the lowest fuel consumption is possessed by the UAV, because the equipment that protects and serves the pilot is excluded from them, so their take-off weight and overall dimensions are reduced accordingly. This is especially positive for the application of trichogramma (biological enemy of a number of pests of crops), the application rates of which range from 3 to 30 g/ha [4, 5, 6]. However, there is no data that would indicate the practical experience of operating such equipment in Ukraine. One of the reasons for this is the lack of practical development of specialized unmanned aerial systems (UAS) for ACHW [2, 7].

Developed in NAU UAV M-6 «Zhayvir» (Fig. 4.21) refers to civil aviation equipment that can be used in agricultural production as a carrier of hardware for protection of agricultural plants from pests, diseases and weeds by pollination [9].



Fig. 4.21. UAV M-6 «Zhayvir» on the launcher

It is common practice in the development of agricultural aircraft to install suspended replacement equipment (sprayer, sprayer, etc.), which expands the range of their applications. However, UAV class 10 kg, due to the narrow specialization and expansion of time limits for technological operations up to round the clock (e.g. work at night) can be developed on an integrated basis. This scheme provides for the combination in one design solution, the actual aircraft and hardware input, which was not implemented in the practice of developing the UAV.

Accordingly, the technical solutions adopted were aimed at making changes to the layout, which will ensure lower fuel consumption and increase the maneuverability and directional stability of the UAV while operating over the field.

The problem of improvement is solved by the fact that the wing is made arrow-shaped and rectangular in plan, the fuselage is made in a single structure, the power plant is installed directly in the bow of the fuselage, the tail is V-shaped and arrow-shaped, and the working bodies are located directly in the wing along its scope. The dispenser is located directly in the volume of the fuselage.

Potential consumers of the development are airlines that serve producers of crop agricultural products.

Brief description of UAV M-6 «Zhayvir». This UAV is a middle plan of a normal scheme with a rectangular arrow-shaped wing, significantly thickened in the middle part of the fuselage and straight V-shaped and arrow-shaped plumage.

The middle thickened part of the fuselage has a capacity of about 8 liters to accommodate the payload. In addition, a non-detachable wing is attached in this part, in which a profile with a relative thickness $\bar{c} = 14\%$ is used. It is equipped with single-section ailerons along the scope,

which can operate in aileron, flapeyron and air brake modes. Aileron servos are located on the lower surface of the wing in the mines. To transfer the UAV to the transport position, the wing is removed from the fuselage. The middle part of the fuselage together with the wing is closed by a hollow fairing, the internal volume of which is also useful. A fuel tank is located in the front part of the fuselage behind the nose frame. In addition, in the thickness of the wing are made channels of the working organs, which are designed to eject the dosed trichogram. The channel in the root part of the wing has an inlet. A trichogram injection tube is installed above the inlet of the canal, which connects to the dispenser outlet. The outlet is located at the end of the wing. Under the fairing there is a reducer of the drive of the dispenser of the trichogramma which are connected by a flat gear belt. The electronic regulator of the drive of the batcher is established on an end frame of a box of payload. If necessary, you can place a landing parachute in a free volume above the wing.

There are two modes of UAV control, namely automatic and semi-automatic. In the automatic mode the parameters of a course, a roll, a pitch, speed of flight and norms of entering of a trichogram on all declared area are supported by the program.

The design of the UAV glider (corpus) is combined. It widely presents composite materials. The engine is piston, single-cylinder, two-stroke, equipped with a two-bladed propeller. UAV is equipped with a promising two-flow dispenser (Fig. 4.22), consisting of a rotating hollow booker, dosing blades located on the periphery inside the hopper, and a receiving funnel connected at right angles to a fixed hollow axis [10]. The blades are made in each cavity separately and a separate receiving funnel is also installed for each cavity.



Fig. 4.22. UAV M-6 «Zhayvir» with open compartment of the dispenser

In order to reduce hydraulic losses during the reception of the metered trichogram from the blades, the funnels are separated from the fixed axis and separately removed through the side

holes made in the small bases of the dispenser, and the dispenser axis is integral and rotating. The schematic diagram of the developed batcher is presented in Fig. 4.23.

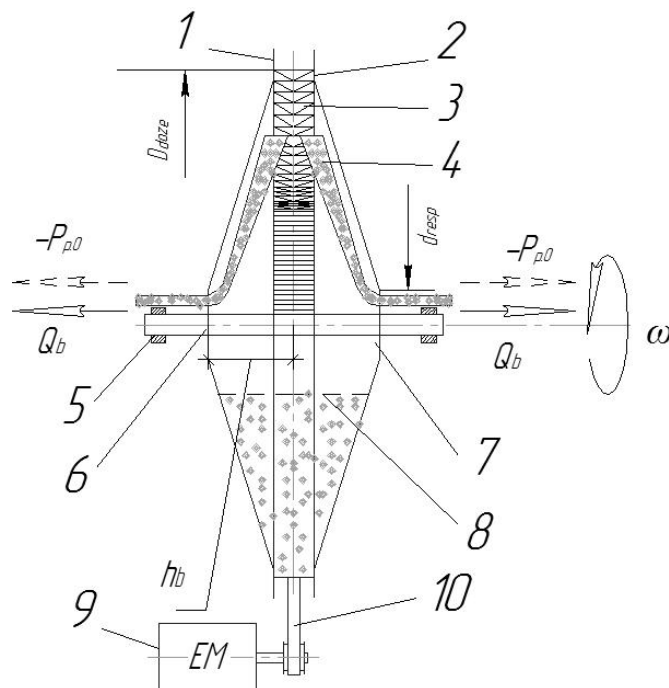


Fig. 4.23. Scheme of the UAV M-6 dispenser «Zhayvir»: 1 – the side of the drive pulley; 2 – bearing front wall; 3 – dosing blade; 4 – receiving funnel trichogram; 5 – dispenser support; 6 – the axis of the dispenser; 7 – side hole of the dispenser; 8 – the level of the trichogram in the dispenser; 9 – drive; 10 – apiary dispenser drive; $R_{r,b}$ – rarefaction from the working body; D_{dose} – diameter of the dispenser; d_{resp} – diameter of the side hole of the dispenser; h_b – is the height of one section of the dispenser; Q_b – consumption of trichogram

The total volume of the dispenser is determined by the formula:

$$V = 2 \cdot (0,26 \cdot 2h(D + d^2 + Dd)). \quad (4.1)$$

The scheme of operation of the dispenser is shown in Fig. 4.24. In the rotating hopper 1 through the side holes 2 fill the required amount of trichogram to level H . When you turn on the drive hopper begins to rotate at speed ω , blades 3 capture a certain amount of trichograms and rise to a level of angle β , where due to gravity, centrifugal and frictional forces specified amount flows from the blades into the receiving funnel 4 along the path 5. The dosed amount of trichogram enters the transport part 6 of the receiving funnel 4.

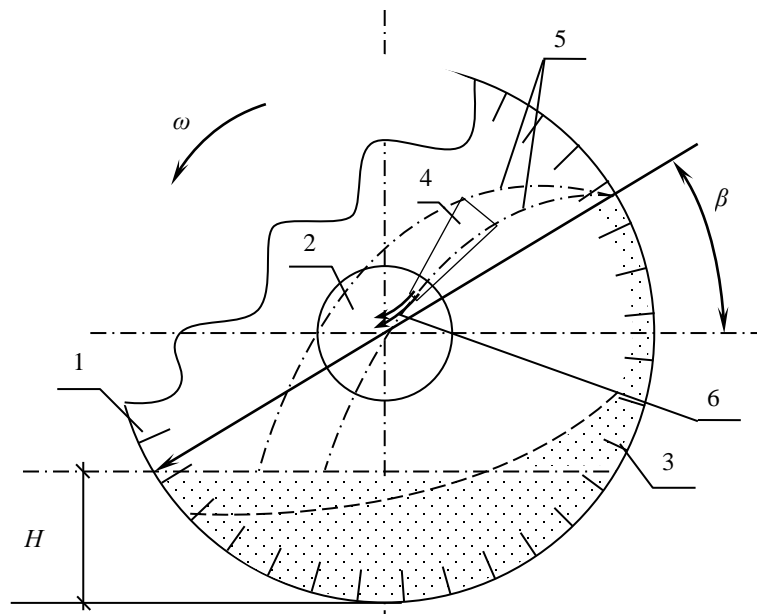


Fig. 4.24. The scheme of operation of the two-stream batcher UAV M-6 «Zhayvir»

The second consumption of trichogram for one stream of the specified dispenser can be calculated by the formula:

$$Q_c = \frac{m \omega \gamma V K_y}{2 \pi}, \quad (4.2)$$

where m – is the number of blades in one half of the dispenser, pcs.; ω – is the angular velocity of the dispenser; γ – trichogram density, g/cm^3 ; V – is the volume of the trichogram that captures one scapula, cm^3 ; K_y – is the coefficient of capture of the trichogram by the scapula, which is in the range of 0 – 1,0.

Accordingly, the change in Q_c is most convenient to adjust the speed of rotation of the dispenser. Therefore, the drive of the dispenser, consisting of a gearbox and an electric motor is made with an adjustable number of revolutions. Speed control is performed by an electronic regulator (Fig. 4.25).

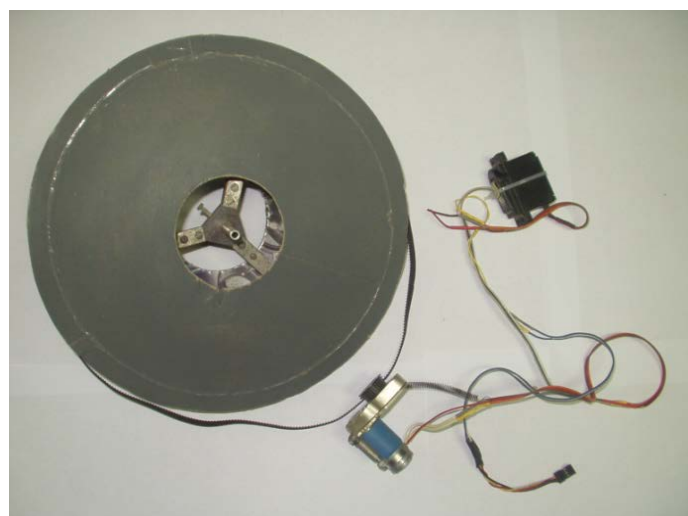


Fig. 4.25. General view of the sample of two-flow dispenser UAV M-6 «Zhayvir»

Technical characteristics of the M-6 «Zhayvir» UAV

Maximum take-off weight, kg – up to 5,5

Payload weight, kg – up to 2,3

Wingspan, m – 1,6

Maximum speed, km/h – 160

Engine power, kW – 1,5

Processing productivity, ha/h – up to 50

Maximum distance in automatic mode, km – 5

Minimum flight altitude, m – 1,5

The way to start – catapult or by hand

Method of landing – on a single-wheeled chassis or parachute

Estimated reduced fuel consumption, l/ha (excluding delivery by car) – 0,1 ... 0,15

Duration of one flight, h – 0,5

4.4. Unmanned aerial vehicle complex M-56 «Module»

Unmanned aerial vehicle complex (UAVC) M-56 «Module» is designed to perform aerial work in the interests of various customers. Typical aviation works for UAVC M-56 «Module» are considered to be aerial photography in different spectral ranges, as well as the transfer to the ground control station of video images in «on-line» mode. In power structures the complex is used as a carrier of high-precision weapons.

UAVC M-56 «Module» consists of an unmanned aircraft M-56 «Module», ground control station and launcher KP-6. Ground control station (GCS) is intended for control and monitoring of unmanned aircraft M-56 «Module» on the ground and when performing flights in assigned airspace. UAV and its GCS are operated by a remote crew of at least two people. The UAV M-56 «Module» and its ground control station are located in two or three containers/backpacks. UAVC M-56 «Module» is designed for non-airfield deployment.

Brief technical description of UAV M-56 «Module»

Unmanned aerial vehicle M-56 «Модуль» (Fig. 4.26) – is a single-engine, free-floating midplane made according to the «flying wing» scheme with a pusher propeller. M-56 «Module» is an aerodynamically perfect aircraft with an integrated, together with the fuselage, centroplane. The wing has profiles that ensure minimal movement of the focus from changes in the angle of attack. The wing has an elongation of 14,3 units, a sweep of the

focus line of 21° and strongly developed end winglets, significantly bent backwards, which allows to increase the track stabilizing moment. The glider is made mainly of fiberglass and carbon fiber; some structural elements are made of aluminum alloys.

The fuselage is a semi-monocoque structure with a composite multi-layer power skin and a removable upper fairing. The main UAV systems are located between the fuselage frames. Under the front fairing is a power battery with a tray. Under the front fairing there is a power battery with a housing. The flight controller panel is located in the middle part of the fuselage. A parachute with a release mechanism is located under the fairing gargrot.



Fig. 4.26. General view of UAV M-56 «Module» in the wheeled version

Opening of the fairing garrotte to release the parachute is servo-operated; during the parachute release the garrotte is dropped by the spring and the surging air stream and extracts the parachute. Communication modems are located in the middle part of the fuselage. The antennas of the modems are outside the fuselage. The electric engine of the power plant is fixed on the rear frame. Directly behind the motor is its regulator and power switch.

Under the bottom of the fuselage is a hatch that covers the assembled air cushion. The cushion is filled with an axial compressor with an electric motor. There is a suitable tray in the fuselage to install the cushion and compressor.

The single-spar wing consists of two removable planes. The wing spar flanges are made of glass roving. The skin is rigid, two-layer; the outer layer is made of fiberglass fabric. The elevons have axial aerodynamic compensation.

The power plant includes a three-phase electric motor of constant excitation with an electronic regulator and a two-blade pusher, folding propeller of constant pitch. The engine is mounted on the rear frame. The engine is cooled by air passing through the hood openings.

The UAV on-board electrical system is powered by a six-cell (6S) lithium polymer battery of conventional capacity. The wiring consists of signal and power lines connected in combined

cables. The individual consumers are supplied with the appropriate voltage from the on-board power supply.

The UAV is controlled in automatic and semi-automatic modes. The basic mode is automatic. Control signals are transmitted via digital shielded radio communication.

The standard target load is a gyrostabilized video camera/IR-camera controlled by the control system channels. Video camera – digital model DH-IPC-HDB4300F-PT. Thermal imager – digital model *Mobotix S15-6Mp*. Camera – model *Canon Power Shot SX100 IS* or similar. The target load is located in the forward part of the fuselage in a separate enclosure. The housings have a unified bayonet mount; each housing accommodates one type of target load.

KP-6 launcher is demountable and designed for organized aerodrome-free launch of the UAV at wind speeds up to 20 m/s. Launching of the UAV is automatic. KP-6 consists of a launching rail with a rubber accumulator and a movable carriage. The shock absorber is tensioned by a gear-driven electric motor. The mass of the launcher is up to 10 kg.

Fig. 4.27 shows a general view of the M-56 «Module» unmanned aerial vehicle complex with an UAV on the launcher.



Fig. 4.27. General view of the UAVC M-56 «Module» in unfolded form
(UAV M-56 «Module» on the launcher KP-6)

Unmanned aerial vehicle complex UAVC M-56 «Module» functionally consists of such systems, equipment and facilities.

Airframe and power plant UAV

Airframe:

- right half-wing;
- left half-wing;
- fuselage;

- pneumatic shock-absorbing inflatable cushion;
- compressor inflating the shock-absorbing cushion.

Power plant:

- electric engine;
- electronic engine regulator;
- propeller.

Parachute system

- landing parachute;
- parachute compartment opening servo;
- parachute release servo;
- servo actuator for opening the shock-absorber cushion shaft;
- shock absorber.

Aerial equipment for UAVs

Flight and navigation equipment:

- system of navigational equipment;
- aircraft telemetry system.

Control system:

- control system servos;
- mechanical control wiring;
- a flight controller that includes an on-board recorder of flight modes;
- UAV automatic parachute landing system.

Power supply system:

- on-board batteries;
- power supply units of on-board consumers;
- on-board electrical switch;
- on-board electrical wiring.

UAV radio-electronic equipment

Radio technical equipment:

- satellite communication and navigation system devices.

Equipment of radio lines:

- radio line control devices (telemetry);
- radio line video communication devices (target video signal).

UAV target load

- daytime video camera;

- IR-camera;
- aerial camera.

KP-6 launcher included

Ground control station of the UAV «Module» M-56

The ground control station functionally consists of the following systems, equipment and devices.

Remote pilot`s workstation (W1)

UAV control system:

- UAV control position №1;
- personal computer of the remote pilot (RP);
- devices of ground telemetry-radio-command system.

Devices of the ground flight and navigation system:

- ground telemetry.

Devices of control and management of the parachute descent system of the UAV.

Target load operator workstation (W2)

Data processing system of target information from the UAV:

- target information processing terminal.

UAV target load control facilities:

- facilities of the ground command radio line of the target load.

UAV flight support system:

GCS power supply system

Meteorological support system

Objective control system (flight data recorder)

The system of automatic turning of the ground receiving and transmitting antennas in the direction of the UAV

Verification equipment: a kit of control, measuring and special equipment for before- and after flight MT.

UAV Flight Simulator

UAV storage and transportation facilities.

UAV launcher included

Mounting kit

Spare parts, tools and accessories

A kit of tools

Set of operational documentation

Technical characteristics of the UAV M-56 «Module» and the UAVC based on it

Geometric characteristics of the UAV:

- wing span, m – 4,6;
- length, m – 1,71;
- height, m – 0,45;
- wing area, m² – 1,38;
- elevons area, m² – 0,098;
- mean aerodynamic chord of the wing, m – 0,32;
- parachute dimensions, m × m – square 3,9 × 3,9;
- dimensions of the pneumatic cushion, m – 1,16 × 0,6 × 0,15.

UAV main weight characteristics:

- maximum take-off weight, kg – 15;
- maximum weight of payload, kg – 4;
- weight of empty aircraft, kg – 5,5;
- maximum load capacity of wing area, kg/m² – 11;
- minimum load capacity of wing area, kg/m² – 9.

Main characteristics of PP UAV:

- type of engine – electric, three-phase with constant excitation, air cooling;
- type of propeller – two-blade, folding, constant pitch;
- PP weight, kg – 0,36;
- number of engines, un. – 1;
- engine power, h.p. – 2,6.

UAV main flight characteristics:

- maximum horizontal speed, km/h – 130;
- cruise speed, km/h – 75;
- lift-off speed, km/h – 41;
- reference speed, km/h – 48;
- stall speed, km/h – 32;
- operating ceiling, m – 3000.

Main operational characteristics:

- flight duration, h – no less 3;
- operating range with «on-line» communication, km – to 20;
- technical range at cruising speed (without «on-line»), km – to 35;
- deployment time, min – 30.

Aerodynamic surface profiles:

- wing – *BOEING* 106R.

The main weight characteristics of the UAVC M-56 «Module»:

- weight of UAVC, kg – to 65;
- transportation method – in three crates.

The results of calculation of the characteristic flight speeds for the take-off weight of 10,2 kg of the UAV M-56 «Module» are presented in Table 4.9.

Table 4.9

Calculated values of the characteristic speeds of the M-56 UAV (version with landing gear)

No	Parameter	Symbol	Values / units
1	Stalling speed (for a height of 0 m)	V_s	8,3 m/s
2	Rotation speed	V_R	9,2 m/s
3	Safe take-off speed	V_2	9,2 m/s
4	Reference landing approach speed	V_{REF}	≥ 11 m/s
5	Safe climb speed	V_{FTO}	≥ 11 m/s
6	Minimum steady flight speed in take-off	V_{s1}	11 m/s
7	Required lifting speed	V_{LOF}	12 m/s

Brief description of the M-56 «Module» UAV control system

1. UAV M-56 «Module» control system is automatic and provides its flight according to the plan drawn up in advance with waypoints (WP) beyond optical visibility. Flight plan can be replanned or updated remotely. Control system allows operation of UAV according to instrument flight rules (IFR) and is restricted according to visual flight rules (VFR) in automatic and semi-automatic mode.

2. Flight plan is performed by aircraft autopilot in automatic mode. In semi-automatic mode waypoint (W) is reached by remote pilot. In this case aircraft stabilizers maintain stabilize mode for UAV main functions and its velocity. Semi-automatic piloting of UAV can be applied in the extreme cases with help of method «see UAV from aside» within optical visibility.

3. UAV control system includes ground control station (GCS) and aircraft control system (ACS), necessary on-air control and communication lines. This UAV model uses a 0,915 GHz command and telemetry radio link and a 2,4 GHz video link.

4. Unmanned aerial vehicle ground control station (GCS) consists of remote pilot's workstation (W), remote control, remote devices of displaying data on screens and transmission on the air. The image of combined piloting device (CPD) and telemetric data necessary for piloting UAV as well as virtual image of the location (map) from ground video archive and/or a real image of the terrain from aboard the UAV are displayed on remote pilot's screen.

5. The target operator's monitor displays real images of the terrain from the UAV, a map of the area with geo-referenced objects, as well as the trajectory of the UAV with its flight plan.

6. Aircraft part of UAV control system provides receiving control signals, execution of commands by all its necessary parts, automatic stabilization of its position and support of flight navigational parameters, flight planning considering waypoints and flight plan adhering, replanning of flight plan, automatic/semi-automatic execution of flight plan, autopilot turning on/turning off as well as turning on the system of «self return to UAV base» and released of the parachute.

7. Board part of UAV control system consists of the necessary sensors, information acquisition and processing units, flight controller, communication and control line transceiver unit, antenna devices, as well as the elevon servos, the parachute release control servo, the parachute drop servo and the video camera/photocamera control servo.

8. UAV navigation is equipped with inertial system, 3-D magnetic compass, GPS module and air pressure receiver; altitude support – barometry and GPS module.

9. Power supply of UAV aircraft control system is carried out from aircraft electrical batteries.

10. Power supply of UAV ground control station (GCS) is powered from an external 12/24V battery or an electric generator via an uninterruptible power supply, or from an external 380/220V power grid.

11. The M-56 module's portable ground control station (GCS) is designed for pre-flight preparation of UAVs, pre-launch control, preparation of flight programs, control and management of UAVs in flight, as well as for training operators without actual UAV flights.

12. The portable GCS consists of: a control unit with a computer, two color monitors and a keyboard, and a rechargeable battery placed in a special PC compartment.

13. The remote signal from the UAV is received by the radio modem of the control station receiving unit and is transmitted to the GCS ground computer. Monitor № 1 displays information about current and target position of the UAV, its altitude, speed, course, angular position, as well as the voltage of the onboard battery of the UAV and other service telemetry information.

With the help of the control station computer it is possible to issue control commands manually. The video signal from the UAV is received by the receiving unit connected to the antenna and the control video monitor, which is received in real time on the GCS monitor № 2. The video information is recorded to the computer solid-state disk and can be viewed by the operator at a convenient pace – scrolling the image at a lower or higher speed, freeze frames, increasing the frame rate, etc.

The handheld computer has an auxiliary output from which the standard video signal can be fed to a remote monitor or any device with a standard video input.

The GCS is powered by a built-in battery. An external power supply is also possible. The GCS consists of:

- antenna feeders for receiving-transmitting telemetry and video signals;
- video reception-transmission antenna together with a modem;
- telemetry reception-transmission antenna;
- telemetry modem;
- telescopic mast for automatic deployment of antennas in the direction of the UAV;
- device for automatic deployment of antennas in the direction of the UAV.

The ground control station of the M-56 «Module» UAV can be deployed in 10–15 min.

Compliance with UAVC M-56 «Module» requirements. Unmanned aerial vehicle complex M-56 «Module» corresponds to the classification according to DSTU V7371:2013 (Table 4.10).

Table 4.10

Tactical and technical characteristics of the M-56 «Module» UAVC

№	A sign of	Feature	
1	Purpose	Reconnaissance	+
2	Scale of tasks	Tactical with a radius of action: with real-time video information transmission – at least 20 km; without transmitting video information in real time – at least 30 km	+
3	Location	Ground basing	+
4	The principle of lifting force	Aerodynamic	+
5	Frequency of use	Reusable with a lifetime of at least 100 applications	+
6	Number of engines	Single-engine	+
7	Type of engine in power plant	Power plant based on a three-phase electric motor	+
8	Maximum take-off weight	Maximum take-off weight up to 15 kg	+
9	Maximum flight altitude	Flight altitude up to 3000 m	+
10	Maximum operating limit speed	Up to 130 km/h	+
11	Maximum flight time	At least 3,0 hours at a temperature of at least minus 10 °C	+
12	Type of take-off	Mechanical launcher	+
13	Type of landing	Parachute	+
14	Type of flight control system	Combination	+
15	Targeted gear	Reconnaissance tools	+

4.5. Planning self-guided mini-munition PMB-03

Mini-ammunition PMB-03 refers to ammunition equipped with rigid aerodynamic surfaces for the formation of lifting force, navigation system and control system, and which are dropped from the aircraft carrier, reaching the target in planning mode. These mini-ammunition can be used during special operations and on the battlefield.

Guided cruise munitions began to be actively developed in the period before World War II. For example, the German «FX1400» or «Fritz-X, Ruhrstahl SD1400X» planning bomb was developed from 1938 on the basis of the typical SD1400X aircraft bomb [11].

Modern planning munitions are equipped with appropriate autonomous navigation guidance systems and secure telemetry channels, allowing them to be used in countermeasure electronic warfare (EW) environments and significantly increase their accuracy in hitting the target.

The «Dynamics GBU-69/B SGM» (U.S.) is a 27-kilo planning bomb designed to meet U.S. Special Operations Command (USSOCOM) requirements to cause minimal damage to objects surrounding the primary target [12].

The GBU-69 is equipped with a rotary wing and a grid type stabilizer: the flight distance is up to 50 miles.

The very small Hatchet planning bomb, which the American company Alliant Techsystems demonstrated in 2012, positions itself in a similar way [13].

The Hatchet, weighing 3,2 kg, has three wings, arranged radially at a 120° angle to each other, and three altitude control. This product can be used on «tactical» class UAV. The guidance system is available in options with satellite navigation only or a combination of GPS and laser guidance. The Hatchet planning bomb can be used in special missions for precision targeting of single objects.

The development of PMB-03 mini-ammunition is based on the objectives of improving their operational efficiency, reducing their take-off weight and reducing production costs through design simplification.

This goal is realized due to the unification of the body with the wing and tail, the absence of a power plant, the use of a wing with an increased angle of the transverse «V», the use of an inverted tail V-shaped tail and ensuring the inseparability of the steering servos, autopilot, navigation system, panel contacts of the autopilot and the connector of the on-board battery of the power supply from the housing of the planning mini-munition. Fig. 4.28 shows samples of planning mini-munitions PMB-03.

The planning self-guided mini-munition PMB-03 consists of the airframe 1, together with which the wing 2 and the fixed part 3 of the tail fins are made. The movable part of the tail 4

represents the controlling aerodynamic surfaces. The onboard battery 5 is set before activation in shaft 6 in the tail of the product and is electrically connected to the standard electrical system by a connector 7. The steering aerodynamic surfaces are driven by steering servos 8 by means of power pulls 9. The 40 mm underbarrel grenade 10 is inserted into the housing of the mini-munition from its nose bow by opening the nose fairing 11. The nose fairing contains a navigation system comprising a GPS receiver 12 and a magnetometer 13 integrated in one housing, and an autopilot 14; these devices are connected to the standard electrical system with appropriate connectors. Mounting of the planning self-guided mini-munition is carried out with the help of brackets 15 with holes entering into the corresponding recesses on the aircraft carrier.



Fig. 4.28. General view planning self-guided mini-munition PMB-03 (mockup)

The general structure of PMB-03 ammunition in the «side» projection is shown in Fig. 4.29.

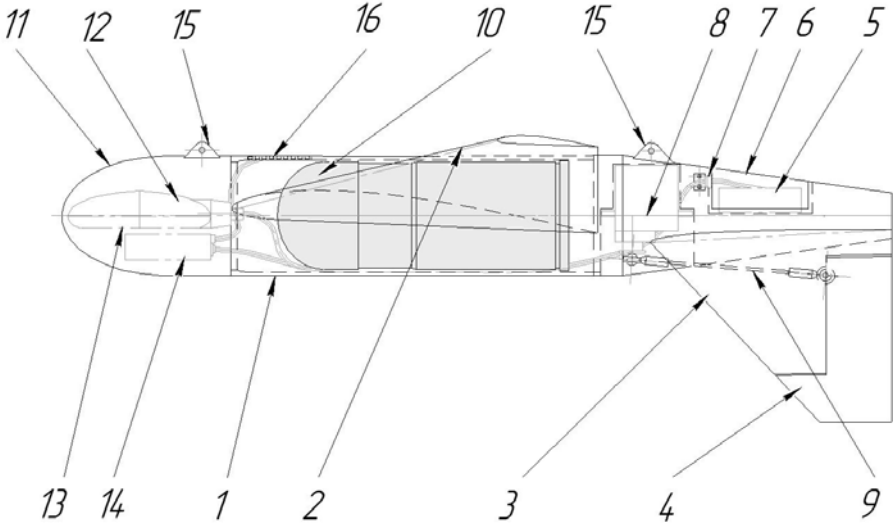


Fig. 4.29. General structure of a planning self-guided mini-munition in the «side» projection

The dumping of the mini-munition is controlled from the aircraft carrier. In order to send a specific task from the board of the latter to the autopilot of the mini-bomblet, a panel 16 clamping contacts, which are in a pressed state with the corresponding contacts on the carrier, is installed on its body. Electrical disconnection from the carrier takes place after the mini-bomblet is unhitched from the latter to perform an independent task [14].

Installation of a planning self-guided mini-munition onboard an unmanned aircraft carrier (Fig. 4.30) is shown on the example of a wing-mounted munition on the M-56 «Modul» carrier.



Fig. 4.30. Installation of a planning self-guided mini-munition onboard the aircraft unmanned carrier M-56 «Modul»

Main technical characteristics of the PMB-03 NAU planning self-guided mini-ammunition

Airframe

Maximum take-off weight (MTOW), kg – 0,55...0,6 (complete product with ammunition)

Aerodynamic quality K – 7...9

The average flight range from an altitude of 3000 m (wind 0 m/s), km – 20

Flight programming – just before launch from the carrier

Number of programmable targets – 1

Ammunition

The size of a grenade – 40 mm × 53 mm

Weight of grenade, kg – 0,3–0,35

Typical speeds PMB-03 NAU

Minimum operating speed, km/h – 130

Maximum diving speed at the corner of the trajectory 45 deg., km/h – 248

Maximum diving speed at the corner of the trajectory 90 deg., km/h – 295

List of references

1. Matiychyk M. P., Mikhailov G. M., Yun G. M. Economic efficiency of plant protection with unmanned aerial vehicles: Proceedings of Kyiv University of Economics and Transport Technologies. Ser. Economics and management. Vol. №9. 2007. P. 175–181.
2. Matiychyk M. P., Mikhailov G. M., Yun G. M. Justification of characteristics of unmanned aerial vehicles for agricultural purposes. *Visnyk of National Aviation University*. Kyiv, 2007, №1. P. 113–117.
3. Matiychyk M. P. Retrospects and modern problems of small-scale radio-controlled aircraft application for economic purposes: Proceedings of the National University «Kyiv-Mohyla Academy». Kyiv, 1999. Vol.9. P. 371–377.
4. Rules of organization and performance of aviation works in agriculture and forestry. Kyiv: Publishing house «VD» Manufaktura» Ltd, 2007. 112 p.
5. Matiychyk M. P. Justification of parameters of the device and technology of mechanized trichogramma settlement: PhD thesis abstract. Glevakha, 1994. 18 p.
6. Stutzer Z. I. Estimation of the costs of agricultural machinery. *Plant Protection*. 1989. №88. P. 60–62.
7. UAV systems: The Global perspective. Design and print bu Fotodirekt, Ltd, England 012773563111. 2005. P. 132–138.
8. Makeev V. E. Radio-controlled aeromodelling technique – a means of mechanisation of bioprotection of agricultural plants from pests. *Plant Protection*, 1992. №8. P. 55.
9. Matiychyk M. P., Rybalchenko O. S. Single-engine unmanned aerial vehicle for plant protection. Ukraine's patent for a useful model № 34952. Republished 26.08.2008. State Patent Bulletin of Ukraine № 16.
10. Matiychyk M. P., Kaminsky P. P., Yurashchuk O. A. Two-flow aerial dispenser of trichogram. Ukraine's patent for a useful model №38142. Republished 25.12.2008. State Patent Bulletin of Ukraine № 24.
11. Internet resource: «FX1400». Source access mode: <https://ru.wikipedia.org/wiki/FX-1400>.
12. Internet resource: USSOCOM, AFSOC test Block 1 GBU-69/B SGM datalink variant. Source access mode: <https://www.janes.com/article/87247/ussocom-afsoc-test-block-1-gbu-69-b-smg-datalink-variant>.
13. Internet resource: Ultra-small bombs: weapons for lightweight UAVs. Source access mode: <https://topwar.ru/46574-sverhmalnye-bomby-oruzhie-dlya-legkih-bpla.html>.
14. Matiychyk M. P., Kharchenko V. P., Matiychyk D. M. Unmanned bomber munition. Ukrainian Patent №132931. Published 25.03.2019. Bulletin №6.

Chapter 5

FEASIBILITY STUDY OF UNMANNED AERIAL VEHICLES AND UNMANNED AERIAL SYSTEMS

5.1. Analysis of the components of the unmanned aerial system efficiency

As defined, an unmanned aerial system (UAS) is a combination of an unmanned aircraft, a ground control station and communication lines. In general, the purpose of the UAS is to ensure the safe flight of an unmanned aircraft in a designated airspace while performing aviation works.

The question of the effectiveness of UAS has hardly been considered, since the term itself appeared recently and only conceptual approaches have been formed so far. Consequently, it is advisable to use the method of analogy of developments related to aviation and the efficiency of technical variety of systems.

Technical and economic evaluation of the effectiveness of aviation specialized systems (ASS) should be considered in terms of aircraft fleet optimization, where aircraft fleet optimization – finding and achieving the optimum ratio or ensuring the properties and type of some functions of the system that affect the quality and results of the system's functioning [1].

The optimization criteria for aircraft involved in aviation works can be formulated as follows:

- technical and economic assessment of aircraft should be considered in inseparable connection with the performed tasks;
- the assessment of the efficiency of a particular type of aircraft should be conducted based on the whole set of transport tasks and needs in aviation work.

At the same time the following characteristics or conditions of optimization problems should be defined and make sense:

- optimization criteria in the form of quality indicators, combined into a common criterion of economic efficiency;
- algorithms and calculation schemes (methods) for estimation of the general criterion indicator and check of optimality;
- determination of the general criterion indicator of economic efficiency at the change of arguments influencing the change of the value of an indicator of efficiency (calculation models).

Evaluation of the effectiveness of the use of aircraft in any variant or type of aviation work is mathematically determined only by numbers, the comparison of which allows you to choose the best option for their application.

It is emphasized that optimality is the best ratio of acceptable properties (parameters) of the aviation specialized system (ASS) following the accepted criterion of efficiency. Accordingly, the question of the efficiency of UAS is in the plane of optimality, i.e. the best ratio between its parameters.

Based on the analysis, the parameters and criteria for the effectiveness of UAS were developed, the relationship between which is shown in Fig. 5.1.

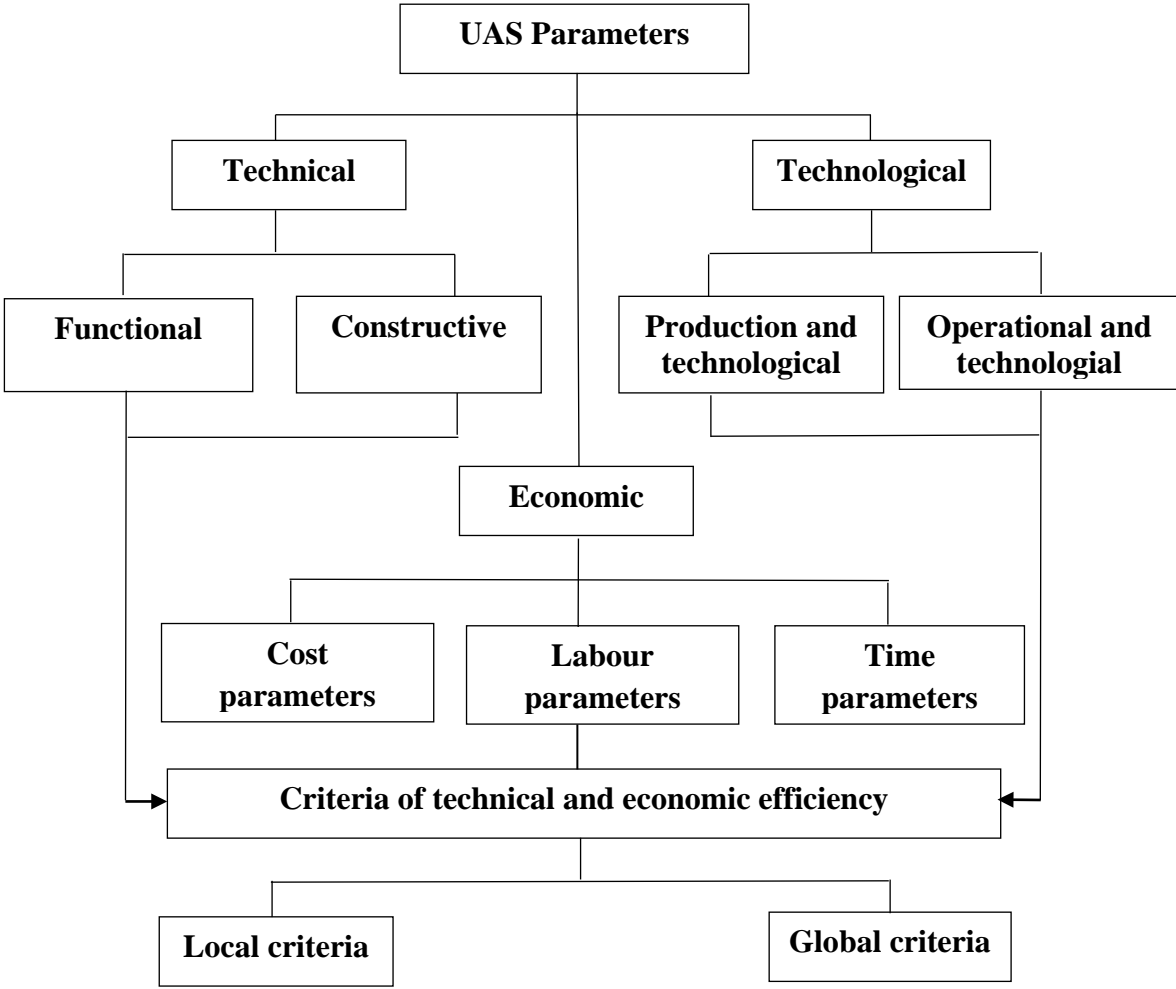


Fig. 5.1. Relationship between UAV parameters and criteria of its efficiency

UAS parameters are divided into three groups:

- 1) technical;
- 2) technological;
- 3) technical and economic.

The technical ones include functional (load capacity, flight range, the flight speed of UAV) and structural (geometric dimensions, the weight of structural parts of UAV, the weight of ground station, etc.).

Author Kulaev Y. F. in his work [2] showed that functional parameters determine the value of the criteria of target efficiency, and constructive – affect the functional, economic parameters and parameters of manufacturability. The latter includes the parameters of production and operational-repair manufacturability of elements of UAS.

The manufacturability of UAS elements in the production process is largely determined by their design continuity, which depends on the level of unification, standardization and normalization of structures. Of great importance for improving the manufacturability of UAS elements is the rational aggregation of their design and in particular the panel fuselage UAV and GCS. These factors determine the operational and repair manufacturability of UAS elements. However, the manufacturability of products in the process of their operation and repair is also influenced by several other specific indicators: the multiplicity of resources of systems (products), the degree of accessibility to their units and components, the complexity of their disassembly and assembly, and so on. The parameters of manufacturability significantly affect the economic parameters of the system elements. Their improvement can significantly increase productivity, reduce the size of the cycle and the cost of work during their production, repair and maintenance of system elements during operation.

Economic parameters are divided into cost, labour and time. They include the economic parameters of the UAS of its elements, respectively, as objects of creation, manufacture and operation. The specified parameters underlie the formation of the criterion for assessing the technical and economic efficiency of UAS and are elements of the triad of criteria «efficiency – cost – time» (W – K – T). These criteria form the general criterion of technical and economic assessment of UAS.

Among the economic criteria, one of the most important criteria is the criterion for assessing the effectiveness of UAS at the cost of a flight hours from its application. The cost of the flight hour of the aircraft is an integrated indicator that takes into account the direct material costs, labor costs, overhead costs and the cost of the aircraft at the airport. Evaluating the effectiveness of the «flight hour» is convenient and fast to find efficiency.

The cost of a flight hour should be considered as the sum of these components [3]:

$$S_{f,h} = S_{dmc} + S_{dlc} + S_{ods} + S_{oc} + S_{aerop}, \quad (5.1)$$

where S_{dmc} – direct material costs; S_{dlc} – direct labour costs; S_{ods} – other direct costs; S_{oc} – overhead costs; S_{aerop} – airport costs.

This calculation model is used in calculating the cost of flight hours in manned aircraft. However, to calculate the cost of a flight hours from the use of UAS, you need to consider the following.

First of all, the direct costs should include the costs incurred by the airline from the operation of the GCS – ground control station of the UAV, as well as from the movement of the UAV by road to the base.

On the second, as in UAS there is no flight and lifting structure the calculation of a salary has to consider it. Payment tariffs can be operator's tariffs and not pilots' tariffs.

Accordingly, the algorithms for calculating the cost of a flight hours can look like this:

- direct material costs for UAV and GCS;
- direct labour costs of the remote crew;
- contributions to the Pension Fund;
- contributions to the obligatory state social insurance in connection with a temporary disability;
- contributions to the obligatory state social insurance in case of unemployment;
- contributions to the obligatory state social insurance against accidents at work;
- depreciation deductions from the value of fixed assets;
- costs for all type of repair, technical inspection and maintenance of the UAV and GCS fleet;
- total expenditures;
- environmental tax;
- the fee to the State Innovation Fund;
- one-time tax on the right of ownership of UAS upon its acquisition.

On the case of for UAS based at a regular aerodrome, airport costs must be included in the calculation. The disadvantages of determining the efficiency of the «flight hour» include the lack of consideration of the costs of the new product development cycle, i.e research and developments work in full. There is also a method of determining the efficiency of the annual economic affect [4].

Regarding the determination of the efficiency of UAS, the algorithms for calculating the efficiency can be represented as follows: the main evaluation indicators are the annual economic effect of the consumer from the operation of UAS, annual savings of direct operating costs and annual labour savings in the operation of UAS.

The name of the indicators and their list are given in Table 5.1.

Table 5.1

Components of calculating the effectiveness of the use of UAS

Indicator name	Symbol
The cost of UAS	C
Service life of UAS, years	T
Renovation rate	P
Research and design works costs	C _r
Specific capital investments	S _i
Coefficient of economic efficiency	C _e
The costs are given	I _g
Duration of aviation works, days	D _w
Duration of change, hour	D _{ch}
Number of shifts	n _{ch}
Production rate, km ² area, <i>or other</i> : hourly; variable	N _h N _v
Number and category of service personnel: remote pilot; target load operator; UAS technician	P _n
Seasonal volume of work, km ² of area, <i>or other</i>	B _s
Daily salary of service personnel, UAH remote pilot; target load operator; UAS technician	DS _{rp} DS _{op} DS _{tech}
Coefficient of contributions to the special insurance fund and additional salary	K _c
Seasonal salary fund	S _{sf}
Depreciation rate, %	D _r
Depreciation deductions, UAH	D _{de}
Total fuel and lubricant costs (per 100 km ² or other)	q _m
Total fuel and lubricant costs, taking into account the total volume of aviation work	L _c
Direct operating costs	C _{op}

5.2. Calculation of productivity and comparison of full consumption on performance of route flights using unmanned aerial vehicle M-7-V5 and superlight plane NARP-1

To calculate the performance of aerial photography UAV M-7-V5 on linear objects (compared with NARP-1) used a known calculation schemes of planned aerial photography with one aircraft photocamera (APC). The layout of a planned aerial survey with one APC is shown in Fig. 5.2

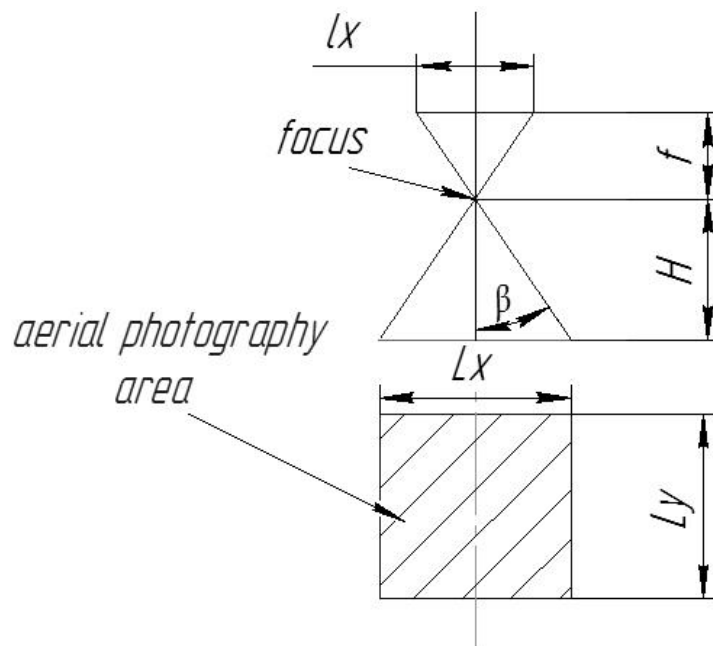


Fig. 5.2. Calculation scheme of the planned aerial survey with one APC:

l_x – is the size of the side of the aerial photography parallel to the direction of flight; L_x – capture on the ground by the longitudinal side of the aerial photography; L_y – capture on the ground by the transverse side of the aerial photography; F – is the focal length of the APC lens; β – half the angle of the APC image field; H – shooting height.

We assume that the cruising speed of NARP-1 – is 165 km/h (according to its number of flight operation (NFO) and the estimated cruising speed of UAV M-7-V5 – is 200 km/h.

Accordingly, the hourly distance for NARP-1 – is 165 km and for UAV M-7-V5, respectively – 200 km.

Incoming data. For aerial photography (Aph) we use UAV M-7-V5, onboard which is a Sony Cyber-Shot DSC-H70 camera on a gyro-stabilized platform.

The Sony Cyber-Shot DSC-H70 has a Sony G series lens with a focal length of $f_1 = 25$ $f_2 = 250$ mm. The image expansion at 16Mp is $l_x = 4608$ $l_y = 3456$ pixels per inch. Viewing

angle without approximation are: $\lambda_1 = 62^\circ$ horizontally and $\beta_1 = 48^\circ$ vertically, and at $\times 10$ magnification the angle are $\lambda_2 = 16^\circ$ horizontally and $\beta_2 = 12^\circ$ vertically.

Calculation of the processed area in one frame

We assume that the flight of UAV M-7-V5 takes place at an altitude of 3000 m (H). The size of the aerial photograph is found by the following formulas:

$$\frac{1}{2}L = H \operatorname{tg} \frac{1}{2} \lambda; \quad (5.2)$$

$$S_{\text{apa}} = L_x L_y. \quad (5.3)$$

Substituting specific values into formula (5.2), we get:

$$\frac{1}{2}L_{x1} = H \operatorname{tg} \frac{1}{2} \lambda = (3000 \operatorname{tg} 31^\circ) \cdot 2 = 3600 \text{ m};$$

$$\frac{1}{2}L_{y1} = H \operatorname{tg} \frac{1}{2} \beta = (3000 \operatorname{tg} 24^\circ) \cdot 2 = 2670 \text{ m}.$$

Calculation of the productivity of aerial photography of UAV M-7-V5

To calculate the productivity of aerial photography in one hours, we used the provision that APh performs the so-called continuous frame-by-frame shooting. With a longitudinal overlap of 20 % between image, the hourly flight of the UAV M-7-V5 can be regarded as its productivity, i.e the productivity of the survey (km^2/h or ha/h). The calculation formula is as follows:

$$P_{\text{APH}} = L_y V_c \text{ (km} \cdot \text{km/h)}. \quad (5.4)$$

After substituting the values we get:

$$P_{\text{APH}} = L_y V_c = 2,67 \cdot 200 = 534 \text{ km}^2(53\ 400 \text{ ha}).$$

Taking into account the overlap, we get:

$$P_{\text{APH.o}} = P_{\text{APH}} 0,8 = 428 \text{ km}^2(42\ 800 \text{ ha}).$$

Calculation of the productivity of aerial photography of UAV NARP-1

NARP-1 was compared on the same modes, except for its cruising speed, which is 165 km/h. The productivity of APh from aircraft NARP-1 is equal to:

$$P_{APH} = L_y V_c = 2,67 \cdot 165 = 440,55 \text{ km}^2(44\ 055 \text{ ha}).$$

Taking into account the overlap for the NARP-1 UAV, we get:

$$P_{APH.o} = P_{APH} \cdot 0,8 = 352,44 \text{ km}^2(35\ 244 \text{ ha}).$$

The difference in hourly productivity of UAV M-7-V5 and plane NARP-1 will be as follows:

$$P_p = P_{APH.p \text{ m-7-v5}} - P_{APH.p \text{ narp-1}} = 428 \text{ km}^2 - 352,44 \text{ km}^2 = 76,56 \text{ km}^2.$$

Comparison of fuel consumption for scheduled flights using UAV M-7-V5 and superlight plane NARP-1

To calculate fuel consumption in certain modes, the tactical and technical characteristics of the NARP-1 aircraft, which are specified in its flight manual, are used [5].

The combined indicators for the modes with the released flaps and without them are presented in Table 5.2.

Table 5.2

Calculation of fuel consumption for aerial photography with plane NARP-1

№	Flying-technical characteristics (estimated) plane NARP-1	Meaning
1	The maximum design speed of horizontal flight, km/h	185
2	Estimated cruising speed near the ground, km/h	165
3	Estimated dive speed, km/h	215
4	Stalling speed: – flaps are hidden, km/h – flaps released, km/h	90 75
5	Length of take-off for normal flight weight at the start from brakes, at the flaps released on 15°, m	120
6	Mileage for normal flight weight with brakes and flaps released at 15° m	150
7	Flight time at full refueling 50 l, h	3,5
8	Overload N_{max} N_{min}	+ 3,8 – 2,0
9	Fuel consumption per cruising mode, l/h (kg/h)	25/18,5
10	Fuel consumption on take-off mode, l/h (kg/h)	27/21
11	Maximum oil consumption, l/h (kg/h)	0,1/0,075

The calculation was carried out according to the method described in the source [6]. The initial data were as follows:

- annual air raid is accepted at 800 hours;
- type of flights for two aircraft: take-offs/landings in 3,5 hours.

For a flight of 800 hours a year NARP-1 will spend on the cruising mode about 15 000 kg / 20 000 l of fuel (gasoline A-98):

$$18,5 \cdot 800 = 2776 \text{ kg}/3608 \text{ l.}$$

Accordingly, for a flight of 800 hours per year UAV M-7-V5 will spend on cruising mode near: $3,47 \cdot 800 = 2776 \text{ kg}/3608 \text{ l.}$

For 1 year (800 l hours) the difference is formed: $20\ 000 \text{ l} - 3608 \text{ l} = 16\ 392 \text{ l.}$

In current fuel prices it will be equal to (as of 2021 in Ukraine):

$$16\ 392 \cdot 37,5 = 634\ 950 \text{ UAH.}$$

(USD 23 960; exchange rate – UAH 26,5 for USD 1: as of August 2021).

Then the hourly monetary gain on fuel consumption in M-7-V5 will be equal to:

$$22\ 539 \text{ USD}/800 = 28,17 \text{ USD.}$$

Incoming data:

- annual air raid is accepted at 800 hours;
- type of flights: take-offs/landings in 3,5 hours in NARP-1;
- UAV M-7-V5 lands/takes-off 1 time in 15 hours.

Let's determine the need for take-off/landing 800 hours.

For NARP-1 number of take-offs/landings is equal to:

$$800/3,5 = 229.$$

For M-7-V5 the number of take-offs/landings is equal to:

$$800/15 = 53,3 \text{ (let's take 54).}$$

The difference in the number of take-offs/landings is:

$$229 - 54 = 175.$$

It is known that in the take-off mode NARP-1 has a fuel consumption of 27 l/h / 21 kg/h.

Total time supplement at NARP-1 take-off (duration of take-off mode – up to 5 min):

$$5 \text{ min} \cdot 175 = 875 \text{ min (14,6 h).}$$

The total additive of gasoline at the take-off of NARP-1 (duration of take-off mode – up to 5 min):

$$14,6 \cdot 21 = 306 \text{ l.}$$

Accordingly, the additional costs in monetary form: $306 \cdot 37,5 = 11\ 475 \text{ UAH.}$ That means the plane NARP-1 additionally consumes 306 l of gasoline for UAH 11 475.

The reason for this is the increased fuel consumption of the NARP-1 aircraft in take-off mode and the need for a large number of take-offs/landings (229 in NARP-1 vs. 54 in UAV M-7-V5).

Total gasoline consumption per year (for 800 flight hours) in NARP-1:

$$20\,000 + 306 = 20\,306 \text{ l.}$$

Fuel will cost:

$$20\,306 \text{ l} \cdot 37,5 = 761\,475 \text{ UAH (28\,734,9 USD).}$$

The M-7-V5 unmanned aerial vehicle is (for a year) in take-off mode:

$$54 \cdot 5 = 270 \text{ min} = 4,5 \text{ h.}$$

Fuel consumption (for take-off mode) is 5,7 l/h. Then the total cost for all the time during which the UAV is on take-off mode is:

$$4,5 \cdot 5,7 = 26,7 \text{ l.}$$

Total gasoline consumption per year (per 800 flight hours) for the M-7-V5 is:

$$3608 + 26,7 = 3634,7 \text{ l.}$$

The total expenditure of money for the said gasoline is equal:

$$3634,7 \cdot 37,5 = 136\,301,25 \text{ UAH (5143,34 USD).}$$

From the calculations, it follows that the direct savings on gasoline from the use of UAV M-7-V5 on 800 flight hours (compared to the NARP-1) will be:

$$761\,475,00 \text{ UAH} - 136\,301,25 \text{ UAH} = 625\,173,75 \text{ UAH (23\,591,46 USD).}$$

5.3. Method of calculating the cost of flight hours when performing aviation works using UAV M-7-V5

It is known that the cost of a flight hour when performing aviation work is calculated according to the formula 5.5. [7]:

$$S_{f.h} = S_{dmc} + S_{dlc} + S_{ods} + S_{oc} + S_{aerop} , \quad (5.5)$$

where S_{dmc} – direct material costs; S_{dlc} – direct labour costs; S_{ods} – other direct costs; S_{oc} – overhead costs; S_{aerop} – airport costs.

The item «Direct material costs» (S_{dmc}) includes the cost of all types of fuel and other (including transport and procurement costs), used both directly for the performance of transportation (works, services) and technological operations during the preparation of rolling

stock, as well as the cost of fuel and lubricants for support and service, training and non-production raids.

The calculation of this cost item requires the determination of fuel costs per flight hour of the aircraft based on its technical characteristics, the ratio of non-production fuel consumption and fuel prices.

Accordingly, for UAV M-7-V5 hourly fuel consumption in cruising mode is 4,5 l/h (3,47 kg/h). To maintain the appropriate flight route of the UAV, it is also necessary to take into account the fuel consumption for the operation of the ground control station (GCS). GCS requires 2,5 l of fuel for one hour of operation.

Then the total fuel consumption is equal:

$$4,5 + 2,5 = 7 \text{ l/h (5,25 kg/h)}.$$

A95 automobile gasoline is used as fuel. According to fuel prices in 2021 (30,1 UAH/l or 40 UAH/kg of fuel) the cost of fuel per hour will be equal:

$$5,25 \text{ kg} \cdot 40 \text{ UAH/kg} = 210 \text{ UAH}.$$

The cost of fuel was determined by the formula:

$$S_{\text{fuel}} = (1 + K_{\text{npf}}) q C_{\text{fal}} \quad , \quad (5.6)$$

where S_{fal} – direct FAL costs, UAH/h; q – the fuel consumption per hour of aircraft production flight, kg/h; K_{npf} – coefficient of non-production fuel consumption at the time of production raid (5 %); C_{fal} – fuel cost, UAH/kg.

After substitution received:

$$S_{\text{fal}} = (1 + K_{\text{npf}}) q C_{\text{fal}} = (1 + 0,05) \cdot 5,25 \cdot 40 = 220,5 \text{ UAH}.$$

Direct labour costs (S_{dlc}) were calculated by determining the cost of basic and additional wages to employees who directly perform aviation work, according to salaries, piece rates, tariff rates following the existing payment systems at enterprises labour, taking into account any types of monetary and material surcharges.

Since there are currently no statutory rates for UAV ground crew members, the rates and other elements of calculation that are in force today in civil aviation for the aircraft commander and co-pilot were taken as a sample.

UAV ground crew itself consists of an remote pilot – CoUAV, and a target load operator (TLO). The following formula was used for calculation:

$$S_{\text{dlc}} = \frac{e_{i=1}^n H_{\text{dlc}i} t_{\text{pl}} + e_{i=1}^n D_i F_{\text{tf}}}{t_{\text{pl}}}, \quad (5.7)$$

where S_{dlc} – direct labour costs, UAH/h; i – the number of the employee of the remote crew ($i = 1; n$); $H_{dlc i}$ – the hourly rate of payment of the i -th employee of the remote crew per units of work performed, UAH/h; D_i – salary of the i -th employee of the remote crew (piecework for one flight hour), UAH/h; F_{tf} – working time fund, h/y; t_{pl} – planned production raid of the aircraft, h/y.

The planned production raid of UAV (h/y) should be 800 h/y. Then the salary will be equal to:

for CoUAV:

$$S_{dlc} = \frac{e_{i=1}^n H_{dlc i} t_{pl} + e_{i=1}^n D_i F_{tf}}{t_{pl}} = \frac{2,72 \cdot 110 \cdot 800 + 2,72 \cdot 13 \cdot 1600}{800} = 369,8 \text{ UAH/h;}$$

for TLO:

$$S_{dlc} = \frac{e_{i=1}^n H_{dlc i} t_{pl} + e_{i=1}^n D_i F_{tf}}{t_{pl}} = \frac{2,72 \cdot 90 \cdot 800 + 2,72 \cdot 10 \cdot 1600}{800} = 298,8 \text{ UAH/h;}$$

for two remote crew members:

$$369,8 \text{ UAH/h} + 298,8 \text{ UAH/h} = 668,6 \text{ UAH/h.}$$

Other direct costs (S_{dmc}) also include:

1) deductions for social measures from the salaries of employees directly involved in the performance of aviation work, namely:

– contributions to the Pension fund, which amount to 33,2 % of the amount of actual labor costs of employees, i.e:

$$534\,880 \text{ UAH} \cdot 0,332 = 171\,232,36/800 = 215,29 \text{ UAH/h;}$$

– contributions to mandatory state social insurance in connection with temporary disability, which amount to 1,5 % of the amount of labor costs of employees:

$$534\,880 \text{ UAH} \cdot 0,015 = 8023,2/800 = 10,1 \text{ UAH/h;}$$

– contributions to the obligatory state social insurance in case of unemployment in the amount of 1,3 % of the number of actual labour costs of employees:

$$534\,880 \text{ UAH} \cdot 0,013 = 6953,44/800 = 8,69 \text{ UAH/h;}$$

– contributions to the compulsory state social insurance against accidents at work and occupational diseases that have caused disability is 0,5 % of the actual labour costs of employees:

$$534\,880 \text{ UAH} \cdot 0,005 = 2674,4/800 = 3,43 \text{ UAH/h;}$$

2) amounts of depreciation deductions from the cost of fixed assets of the aircraft, calculated in accordance with the procedure, norms and conditions established by the current legislation of Ukraine and P(S)BO 7 «Fixed assets» and P(S)BO 8 «Intangible assets».

The rate of depreciation was calculated by the formula:

$$D_r = \frac{100}{T}; \quad (5.8)$$

$$D_r = \frac{100}{T} = 100/T = 100/15 = 6,66 \%,$$

where T – is the standard service life of fixed assets in years.

The annual amount of depreciation was determined by the formula:

$$A_d = (C_f D_{de})/100, \quad (5.9)$$

where C_f – the first time initial book value of a group of fixed assets (M-7-V5); D_{de} – annual depreciation rate.

Accordingly, after substitution we obtain:

$$A_d = (C_f D_{de})/100 = 2\,000\,000 \cdot 0,066/100 = 1320 \text{ UAH.}$$

Deductions for a flight hour are equal to:

$$1320/800 = 1,65 \text{ UAH/h;}$$

3) costs for all types of repairs, technical inspection and maintenance of the aircraft fleet.

Based on statistical data for scheduled calculations, when calculating maintenance costs, their value was chosen in the amount of 10 % of depreciation deductions. Maintenance costs:

$$1320 \cdot 0,1 = 132 \text{ UAH}/800 = 0,165 \text{ UAH/h.}$$

General production costs (S_{oc}) include costs associated with the management and maintenance of the production process, which are not taken into account in the previous articles. Using the expert data of airlines that perform aviation work, overhead costs for the maintenance of the production management staff, payment for business trips, and technical and information support of production management are 10 – 30 % of direct costs. Total direct costs are equal to:

$$668,6 + 140 = 808,6 \text{ UAH/h.}$$

Then the overhead costs are:

$$808,6 \cdot 0,2 = 161,72 \text{ UAH/h.}$$

The cost of aviation works also included environmental taxes – payments for environmental pollution:

$$51,18 \text{ UAH/ton} - \text{aviation gasoline (A95).}$$

So, gasoline will be consumed: $7 \cdot 800 = 5600$ l (4200 kg). Then the environmental tax for the year:

$$4,2 \cdot 51,18 = 214,96 \text{ UAH/y.}$$

According to the flight hour, respectively:

$$214,96/800 = 0,27 \text{ UAH/h.}$$

The fee to the State Innovation Fund – 1 % of the volume of sales (cost of services provided to the aircraft without VAT):

$$(800 \cdot 2000) \cdot 0,8 \cdot 0,01 = 1\,600\,000 \cdot 0,8 \cdot 0,01 = 12\,800/800 = 16 \text{ UAH.}$$

One-time tax on the ownership of the aircraft upon its purchase (1 UAH for each kg of the maximum take-off weight of the aircraft) and airport costs:

$$200 \text{ кг} \cdot 1 \text{ UAH} = 200 \text{ UAH}/800 = 0,25 \text{ UAH.}$$

Airport costs were determined based on the established rates of fees, which operate following the Order of the Ministry of transport and communications of Ukraine «On the establishment of airport fees for aircraft and passengers at airports of Ukraine» № 408/15099 of May 14, 2008, as amended in 2010, including:

– fee for take-off and landing of the aircraft 5,00 USD per tonne of maximum take-off weight (MTOW) of the aircraft:

$$5 \cdot 0,2 = 1 \text{ USD (for one flight hour);}$$

– aviation security fee – 1,00 USD for one ton of MTOW:

$$1 \cdot 0,2 = 0,2 \text{ USD (for one flight hour);}$$

– fee for excessive parking of the aircraft – 0,30 USD for each hour of overtime parking and each ton of MTOW aircraft:

$$0,3 \cdot 0,2 = 0,06 \text{ USD (for one flight hour).}$$

Airport costs (S_{aerop}) together are equal to:

$$1 + 0,2 + 0,06 = 1,26 \text{ USD (for one flight hour).}$$

Given the current exchange rate of the UAH to the USD, the costs of the airport will be:

$$1,26 \text{ USD} \cdot 26,6 \text{ UAH} = 33,52 \text{ UAH (for one flight hour).}$$

Cost per flight hour excluding VAT, taking into account the expected profitability ratio is determined by the formula:

$$C_{\text{fh}} = S_{\text{f.h}} k_r, \quad (5.10)$$

where $S_{\text{f.h}}$ – cost of one flight hour, UAH/h; k_r – profitability ratio (expected profit of the airline from the performance of a certain type of aviation works and services) was taken 1,3. The cost of one flight hour without VAT is equal to:

$$C_{\text{fh}} = S_{\text{f.h}} k_r = 661,276 \cdot 1,3 = 859,7 \text{ UAH.}$$

The results of the calculation of the cost of flight hours UAV M-7-V5 are summarized in Table 5.3.

Table 5.3

The results of the calculation of the cost of flight hours UAV M-7-V5

№	Indicator	Cost, UAH
1	Direct material costs	220,5
2	Direct labour costs	668,6
3	Contributions to the Pension fund	215,29
4	Contributions to the obligatory state social insurance in connection with a temporary disability	10,1
5	Contributions to the obligatory state social insurance in case of unemployment	8,69
6	Contributions to the obligatory state social insurance against accidents at work	3,43
7	Depreciation deductions from the value of fixed assets	1,65
8	Expenses for all types of repairs, technical inspection and maintenance of the fleet of aircraft	0,016
9	Overhead costs	161,72
10	Environmental tax	0,27
11	The fee to the State innovation fund	16
12	One-time tax on the ownership of the aircraft upon its acquisition	0,25
13	Airport costs	33,52
Total		1340,04
The cost of a flight hour without VAT, the profitability ratio is – 1,3		1742,05

A similar method was used to calculate the cost of a flight hour for a manned aircraft of the Civil aviation (CA) of Ukraine NARP-1 with a crew consisting of aircraft commander and co-pilot. The payment for their work is similar to the version with UAV. The results of the calculation are presented in Table 5.4.

From the calculations given in Table 5.3 and 5.4 it is clear that with the same profitability ratio of 1,3, the use of UAV M-7-V5 is cheaper for the airline by an amount equal to:

$$2501,25 - 1742,05 = 759,2 \text{ UAH.}$$

The annual gain from using the M-7-V5 UAV compared to the NARP-1 aircraft is:

$$759,2 \text{ UAH} \cdot 800 \text{ h} = 607\,363 \text{ UAH.}$$

Table 5.4

The results of the calculation of the cost of flight hours NARP-1

№	Indicator	Cost, UAH
1	Direct material costs	804,5
2	Direct labour costs	668,6
3	Contributions to the Pension fund	215,29
4	Contributions to the obligatory state social insurance in connection with a temporary disability	10,1
5	Contributions to the obligatory state social insurance in case of unemployment	8,69
6	Contributions to the obligatory state social insurance against accidents at work	3,43
7	Depreciation deductions from the value of fixed assets	1,65
8	Expenses for all types of repairs, technical inspection and maintenance of the fleet of aircraft	0,016
9	Overhead costs	161,72
10	Environmental tax	0,27
11	The fee to the State innovation fund	16
12	One-time tax on the ownership of the aircraft upon its acquisition	0,25
13	Airport costs	33,52
Total		1924,04
The cost of a flight hour without VAT, the profitability ratio is – 1,3		2501,25

5.4. Methodology for calculating the cost per flight hour for unmanned aerial vehicle of different classes at the National Aviation University

For the successful implementation of the technological process of aerial photography (APh) should be provided with the following composition of the complex:

- unmanned aerial vehicle;
- ground control station UAV;
- means of transporting UAV from the point of the base to the area of aerial photography (APh) execution (equipped car);

– a ground crew consisting of two people.

On the car are auxiliary technical means and spare parts for UAV and GCS, fuels and lubricants (FAL) and sets of rechargeable batteries from the car.

To determine the cost of performing aerial photography (APh) using UAV, the average costs associated with the operation of the base car will also be included.

The costs of the transport company can be grouped by the following articles and elements (Table 5.5) [8].

Table 5.5

Grouping of transport costs

№	Cost item	Elements of costs	
1	Direct material costs	1	Material costs
2	Direct labour costs	2	Labour costs
3	Other direct costs	3	Deductions for social activities
4	Overhead	4	Depreciation of fixed assets and intangible assets
5	Other operating expenses		

The item of calculation *Direct material costs* includes the cost of all types of fuel and other, including transport and procurement costs, used both directly for transportation (works, services) and for technological operations in the process of preparing rolling stock for operation (UAV battery charge), and also includes fuel costs for auxiliary service, training and non-production hours.

To calculate this item it is necessary to determine the fuel costs per hour of production flight time of the UAV according to the technical requirements and flight characteristics, the coefficient of non-production fuel consumption and fuel prices:

$$E_{fal} = (1 + K_{np})gC_{fal} , \tag{5.11}$$

where E_{fal} – direct material costs, money units /h; g – fuel consumption per hour of production flight B , kg/h; K_{np} – coefficient of non-production fuel consumption at the time of production raid; C_{fal} – the price of fuel.

For example, the estimated cost of one hour the work of the truck «Mercedes Sprinter», according to the data on the operation of trucks [9], is 2,8 USD, and in terms of one hour production flying time UAV we have about 30 USD/h.

An example of calculations is given in Table 5.6.

Table 5.6

Calculation of direct material costs

UAV type	M-10-2 «Oko»	M-6-3 «Zhayvir»	M-7-V5
Price, USD (as of 13.09.2017)	28 000	44 500	300 000
Fuel consumption for production raid according to the TTCH of the UAV engine (kg/h)	–	1,1	10
Additional non-production fuel costs at the time of production raid (percentage of the production raid)	–	10	10
Type of fuel	electro	A-95	A-95
The price of fuel, USD/kg	–	1,01	1,01
The total cost of fuel per flight hour, USD/h	–	1,21	20,2
The cost of car maintenance	30,0	30,0	30,0
Total costs	30,0	31,21	50,2

The calculation item *Direct labour costs* includes all costs for the payment of basic and additional salaries to employees directly engaged in the implementation of APh, calculated on salaries, piece rates, tariff rates following the university's existing payment systems, including any types of cash and material surcharges.

According to the above rules, it is proposed to calculate the labour costs of engineers for the use of aviation in industries (operators) per hour of production raid UAV according to the following formula:

$$S_{dlc} = \frac{\sum_{i=1}^n H_{dlc i} t_{pl} + \sum_{i=1}^n D_i F_{tf}}{t_{pl}}, \quad (5.12)$$

where S_{dlc} – direct labour costs, UAH/h; i – the number of the employee of the remote crew, $i = \overline{1, n}$; $H_{dlc i}$ – the hourly rate of payment of the i -th employee of the remote crew per unit of work performed, UAH/h; D_i – salary of the i -th employee of the remote crew, UAH/h; F_{tf} – working time fund, h/y; t_{pl} – planned production raid of the UAV, h/y.

The calculations were performed according to the following input data:

$$n = 2, H_{dlc i} = 2,0 \text{ USD/h}, D_i = 0,8 \text{ USD/h}, F_{tf} = 1958 \text{ h/y}, t_{pl} = 100 \text{ h/y}.$$

The results of the calculations showed that the direct labor costs for the types of UAV shown in Table 5.6, amounted to 55,33 USD/h.

The calculation of the item *Other direct costs* includes:

1. Deductions from the labour costs of employees directly involved in the implementation of APh, namely:

– contributions to the Pension fund, which amount to 22,0 % of the number of actual labour costs of employees. Accordingly, for the example under consideration, the number of deductions from employee labour costs will be 12,17 USD/h for each type of UAV.

2. Amounts of depreciation deductions from the cost of fixed assets of UAVC accrued in accordance with the procedure, norms and conditions established by the current legislation of Ukraine.

For use in the calculation, straightforward and tax methods of depreciation were considered.

According to the straight-line method, the annual amount of depreciation is determined by dividing the depreciable amount by the useful life of the item of property, plant and equipment:

$$A = \frac{C_a}{T}, \quad (5.13)$$

where A – is the annual amount of depreciation deductions, monetary units; C_a – depreciable value, monetary units; T – is the expected useful life of the object, years.

The depreciable value is calculated by the formula:

$$C_a = C_n - L, \quad (5.14)$$

where C_n – the initial cost of fixed assets, monetary units; L – liquidation value of the object, monetary unit.

The university applies the norms and methods of depreciation of fixed assets stipulated by tax legislation.

For depreciation following the Law Ukraine «On Corporate Income Tax», it was determined to which group the fixed assets (namely UAV) of the university belong. According to this law and the State classification of Ukraine «Classification of fixed assets DK 013-97» dated 19.08.97, № 507, UAV and other aircraft belong to the third group of fixed assets [10].

According to the amendments to the Law of Ukraine «On corporate income tax» dated 01.07.04 № 1957-IV (section «Transitional provisions»), the Law of Ukraine «On corporate income tax» dated 28.12.94 № 334/94-VR *quarterly depreciation rates of fixed assets* of the third group are 6 % of the book value of fixed assets.

However, in accounting, in contrast to the tax principle, depreciation is calculated not as a whole for a group of fixed assets, but separately for each object. The results of the calculations are set out in Table 5.7.

Table 5.7

**Depreciation calculations for the first year of operation of UAVC
(At the estimated volume – 100 hours of flight for each UAV)**

Type of UAV, approximate cost	T, years	According to the straight-line method		According to the norms of tax legislation	
		Annual depreciation rate	A/100 flight hours, USD/h	Depreciation rate (for the quarter)	A/100 flight hours, USD/h
Airborne, M-10-2 «Oko» (28 000 USD)	2	50,00 %	125,0	6,00 %	67,2
Airborne, M-6-3 «Zhayvir» (44 500 USD)	3	33,33 %	120,0	6,00 %	106,8
Airborne, M-7-V5 (300 000 USD) (as of 13.09.17)	6	16,66 %	483,33	6,00 %	–

3. Expenses for all types of repairs, technical inspection and maintenance of the UAVC fleet.

According to statistics, it is recommended to take into account the costs of repairs and maintenance of UAV in the amount of about 10 % of depreciation deductions for planned calculations. UAV «Oko» maintenance also includes replacement of batteries (8500 UAH per year).

The article also includes preparations for the production of maps, namely the grid of horizontals for the terrain, which is obtained using Shuttle Radar Topography Mission (SRTM) – data on the height of the Earth's surface obtained from the satellite. Based on the complexity of the process of cartographic reference to the area, one such operation costs in the range of 150 – 250 UAH and is executed once for each field and then stored in the database.

The calculation item *Overhead costs* includes: costs associated with the management and maintenance of the production process, which are not provided in the previous articles. At the university, the general production costs for the maintenance of the production management staff,

payment for business trips, technical and information support of production management are 15 % of direct costs; costs for compensation of utilities, energy and amount to 5,3 % of the total cost.

Compulsory costs associated with payments provided by law:

- risk insurance fee;
- CASCO aviation insurance – 40 % of the cost;
- aviation liability insurance to third parties – 2000,0 UAH for each UAV.

VAT is also charged separately, namely 20 % of the total cost.

Table 5.8 shows the results of calculations of the planned cost of the flight hour for the implementation of aerial photography (APh) with the use of UAVC for NAU.

Table 5.8

**Results of calculations of the cost of performing APh, USD/h
(100 flight hours for each UAV)**

Type of UAV in UAVC	Direct material costs	Direct labour costs	Other direct costs	General production costs	VAT	Total for UAVC
Airborne, M-10-2 «Oko»	30,0	55,33	90,1	204,57	76,0	456,0
Airborne, M-6-3 «Zhayvir»	31,21	55,33	130,3	305,16	104,4	626,4
Airborne, M-7-V5	50,2	55,33	150	330	585,5/ VAT-117,1	702,6

Example of calculating the cost of performing APh per 1 km² of area.

For an altitude of 300 m (UAV M-10-2 «Oko»):

«Canon» IXUS 220 HS viewing angles:

- across – 50°;
- along – 38°.

The size of the image on the ground:

- along – 200 m;
- across – 260 m.

Cruising speed of UAV M-10-2 «Oko» – 21 m/s (75 km/h).

Hourly productivity (strip width – 210 m: overlap across 20 %):

$$P_h = 75 \text{ km/h} \cdot 0,21 \text{ km} = 15,75 \text{ km}^2/\text{h}.$$

Taking into account the reversals: $15,75 \text{ km}^2/\text{h} \cdot 0,7 = 11 \text{ km}^2/\text{h}$.

Longitudinal overlap of images: 20 %.

The need for the number of pictures:

$$N_p = 75 \text{ km} / (0,2 \text{ km} \cdot 0,8) = 469 \text{ pictures.}$$

At the cost of one flight hour M-10-2 «Oko»:

$$456 \text{ USD} / 11 \text{ km}^2 = 41,5 \text{ USD} / \text{km}^2.$$

For an altitude of 500 m (M-6-3 «Zhayvir»):

«Canon» IXUS 220 HS viewing angles:

- across – 50° ;
- along – 38° .

The size of the image on the ground:

- along – 340 m;
- across – 466 m.

Cruising speed of UAV M-6-3 «Zhayvir» – 33,3 m/s (120 km/h).

Hourly productivity (strip width – 466 m: overlap across 20 %):

$$P_h = 120 \text{ km/h} \cdot 0,372 \text{ km} = 44,64 \text{ km}^2/\text{h}.$$

Taking into account the reversals: $44,64 \text{ km}^2/\text{h} \cdot 0,7 = 31,25 \text{ km}^2/\text{h}$.

Longitudinal overlap of images: 20 %.

The need for the number of pictures:

$$N_p = 120 \text{ km} / (0,34 \text{ km} \cdot 0,8) = 441 \text{ pictures.}$$

At the cost of one flight hour M-6-3 «Zhayvir»:

$$626,4 \text{ USD} / 31,25 \text{ km}^2 = 20,04 \text{ USD} / \text{km}^2.$$

List of references

1. Portnikov B. A. Criteria of technical and economic efficiency of aviation specialised system. *Vestnik of the Orenburg State University*. № 5. May, 2007. [Electron resource]. Mode of access to the source: www.osu.ru.
2. Kulaev Y. F., Shchelkunov V. I. Economics of civil aviation of Ukraine. K.: Feniks, 2010. 736 p.
3. Kostromina E. V. The economy of the airline in market conditions. M.: NOU VKSH «Aviabiznes» 1999. 209 p.
4. Yun G. M., Mikhailov G. M., Matiychyk M. P. Economic efficiency of plant protection with unmanned aerial vehicles: Proceedings of Kyiv University of Economics and Transport Technologies. Ser. Economics and management. Issue №9. 2007. P. 175–181.
5. NARP-1 aircraft flight operation manual. Internet resource: emaasterix.weebly.com. Source access mode: www.eymaasterix.weebly.com > rukovodstvo-po-letnoj-ekspluatacii-narp-1.
6. Derevyanko V. S. Application of aviation in sectors of the economy. Krasnodar: Sov. Kuban, 2002. P 13–28.
7. Management of special-purpose aviation projects: guidelines for coursework / co-writer O. E. Sokolova. K.: Publishing house of National Aviation University «NAU-Druk», 2011. 36 p.
8. Methodological recommendations on the formation of the cost of transportation (works, services) on transport, approved by Order of the Ministry of Transport of Ukraine № 65 of 05.02.2001.
9. The car in the enterprise: from acquisition to disposal. J. Semenchenko, V. Kuznetsov, M. Boitsova, O. Andrus. 10th edition, revised and supplemented. X.: Factor, 2008. 447 p.
10. DK 009:2005. National classifier of Ukraine. Classification of types of economic activity. Order of the State Consumer Standard of Ukraine of 26.12.2005 № 375. Valid from 01.04.2006.

Chapter 6

PROSPECTIVE PROJECTS OF UNMANNED AERIAL VEHICLE NATIONAL AVIATION UNIVERSITY

6.1. Rationale and design parameters of an optionally piloted cargo-passenger aircraft (project)

Due to significant changes in the means of automatic flight control, namely ensuring reliable tracking of all known modes of flight of civil aircraft, their maximum approximation to the approval in civil aviation, to date, the prerequisites for the solution of «external» and «internal» task of the next «re-equipment» of the aircraft fleet with more advanced [1].

Promising and attractive, in terms of the cost of transportation and, in particular, the cost of the flight hour, is the market of domestic airlines (DAL) aviation; the weight category of aircraft – normal to 5,7 tons. These planes provide transportation of up to 9 passengers + 2 pilots.

The following will contribute to the successful solution of the task of «re-equipment» of the DAL aircraft fleet:

- significant advances in the widespread use of unidirectional and multidirectional polymer composites in aircraft construction;
- availability in Ukraine of a certified AI-450C aviation engine (*cert. TD0070*) suitable for use on aircraft of this category;
- availability and preliminary agreements with European manufacturers of a 3-redundant onboard controller and associated servos; these manufacturers are ready to participate in certification and proper support of the optionally piloted cargo-passenger aircraft (*Optionally Piloted Vehicle – OPV*);
- availability in Ukraine of experience and relevant production facilities with a closed cycle of developments, testing, production and support of aircraft of domestic civil aviation (CA) airlines.

Grounds for activating the project of the optionally piloted cargo-passenger aircraft

It is known that the modern market of «pure» UAVs (exclusively unmanned aerial vehicles) is unstable and is activated mainly in case of military operations. Therefore fast and regular sales of a UAV by Ukraine, even better than the RQ-9, are unlikely due to the «closed» military theme in the world, the complexity of its practical implementation by the operator

(unknown personnel, ground control station, complicated maintenance, etc.). It takes a significant amount of time (about 4-6 years) to bring the project of «clean» UAVs to the state of sales, which is associated with significant expenditures of funds and the struggle with the corporations of the leading countries of «clean» UAVs that have long been known on the market.

In case the project costs are determined and approved, it is currently advisable to create an optionally piloted aircraft (transformed, converted), when the airframe and power plant will be the same for the whole family of aircraft, both manned and unmanned. The manufacturer in this case can significantly reduce the risks of lack of product sales: in case of demand for piloted conventional modification control posts for pilots are installed. Conversion into an unmanned modification takes place as follows: the airframe, together with power plant, is fitted with equipment for «unmanned» flights. Unification of airframe and power plant during «conversion» can reach 90–95 %.

The first step in this project is the development and testing of a manned twin-engine cargo aircraft of the normal category. This will allow to really promote the project and demonstrate to potential customers its main advantage – availability of unmanned mode. As the «credibility» of this aircraft increases and the aviation authorities are ready to certify the unmanned aircraft, the sales market will gradually expand [2]. Therefore, an opportunity arises for the «pioneer» manufacturer to set the tone in the new market and, accordingly, receive additional commercial benefits.

Considering the prospects in the global market for the development of domestic airline aircraft, an analysis of the state of this segment was carried out in terms of types of DAL aircraft, their years of manufacture and countries of operation. The results of the analysis are summarized in Table 6.1.

Table 6.1

Distribution of some types of aircraft of domestic airlines on the world market

№	Type aircraft DAL	Years of production	Units released	Operators (selective)	Modifications	Unit cost (mln USD)	Cost, f. h
1	L 410	1969-2016	1200	Russia, Libya, Czech Republic	Civilian	n/d	n/d
2	An 28	1983-1998	198	Ukraine, Russia, Guinea, Madagascar	Civilian/military	n/d	n/d
3	Dornier Do 228	1981-1998	270	Bangladesh	Civilian/military	n/d	n/d

End of table 6.1

4	Viking Twin 400 DH-6	1965-2008	800	Benin	Civilian/ military	6,5	n/d
5	AP.68TP-600 A-Viator	2011 to the present	431	USA, Germany, Australia and other	Civilian/ military	2,6	800 – 900 EUR
6	Evector	2010 to the present	29	Czech Republic, Russia	Civilian	2	n/d
7	P2012 Traveller	2011 to the present	Currently 277; the plan is 1150 by 2028 year	USA, Germany, Australia and other	Civilian/ military	2,3	n/d
8	PA-31-350 Chieftain	1973– 1983	3500	USA, Canada, Brazil	Civilian/ military	n/d	n/d
9	Embraer EMB-820	1975– 1983	156	USA, Canada, Brazil	Civilian/ military	n/d	n/d
10	Piper PA-31T Cheyenne	1969	823	USA, Canada, Brazil	Civilian/ military	n/d	n/d
11	Beechcraft B65 Queen Air	1960– 1978	930	USA, Canada, Brazil, Colombia, Algeria and other	Civilian/ military	0,6	n/d

The technical and economic aspect of future applications of unmanned cargo aircraft

The additional value that can be obtained from the use of unmanned aircraft depending on the distance of transportation and the amount of cargo carried per week (tons) is presented in the model of Fig. 6.1.

According to this model, the peak (6 %) of efficiency gain from cargo transportation by unmanned aircraft (as applied to manned aircraft) is at distances of 6700 – 7750 miles and quantity of cargo transported in a week about 100 tons. At a distance of about 1250 miles and 500 tons of cargo, the efficiency of the application will increase by only 4 % [3].

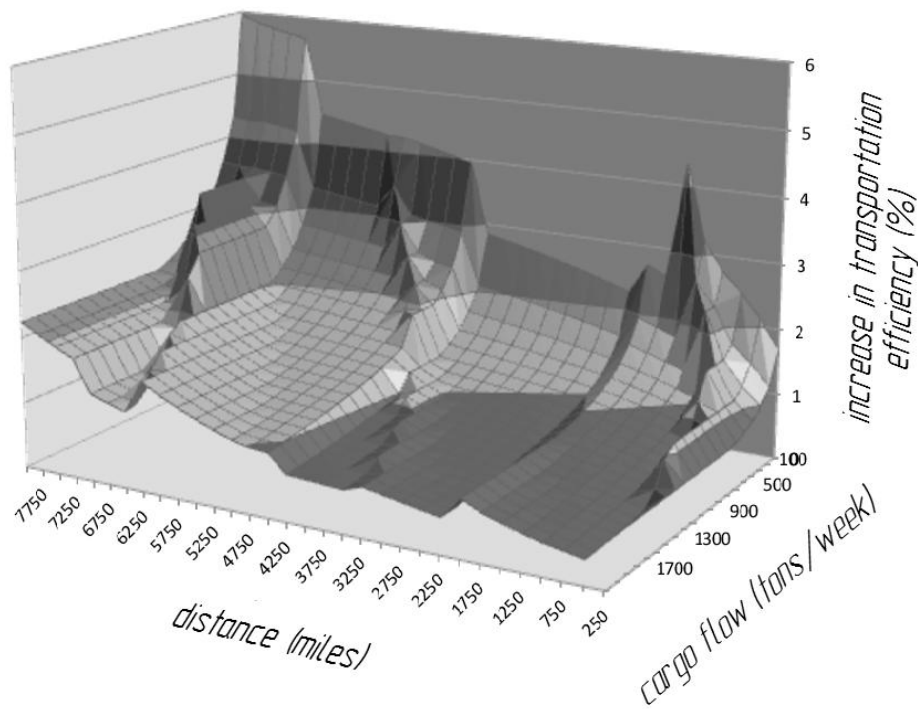


Fig. 6.1. A model of surplus value generation from the use of unmanned aircraft for cargo transportation

Practical implementation of OPV aircraft in the world. The development and practical implementation of OPV aircraft gained intensity in the late 1980s in connection with the development and miniaturization of computers and other automation components to ensure aircraft control. Examples of some aircraft that can be converted from manned to unmanned and vice versa are given in Table 6.2.

Table 6.2

Practical implementation of OPV aircraft in the world for the period 1993–2013

Manned aircraft	Unmanned aircraft	Year of manufacture of the aircraft
Raptor D-1	Raptor D-2	1993
J-5 Marco	BAE Systems Herti	2004
Stemme ASP S15	SAGEM Patroller	2009
DA42 Twin Star	Dominator XP	2010
AHRLAC	N G, Firebird	2011
Stemme SK 202 A	Stemme SK 202 B	2013

Also to date, projects Surveyor 2500, Viper 1000C, TARGUS and others have been implemented. As an example, we can cite the modern transformation (conversion) of the Tecnam P2006T Twin aircraft into of UAV TARGUS (Fig. 6.2 and 6.3).



Fig. 6.2. Tecnam P2006T Twin manned aircraft (Italy)



Fig. 6.3. TARGUS unmanned aerial vehicle (Spain)

Critical components of an optionally piloted aircraft. The critical components of an optionally piloted aircraft include the flight controller, engines, and servos.

An example of modern airborne avionics (airborne controller), providing the application of any aircraft piloting mode, is considered in [4].

The appearance of the modern «X-KIT» flight controller is shown in Fig. 6.4.



Fig. 6.4. Image of the «X-KIT» controller for transforming a manned aircraft into an optionally piloted (manned into unmanned and vice versa)

General characteristics of the modern flight controller «X-KIT» of OPV aircraft (optionally piloted vehicle/helicopters)

Functionality:

- fully automated take-off and landing (ATOL);
- line of sight (LOS) and beyond line of sight (BLOS) communications control;
- flight with extraordinary duration;
- control of electrical systems (landing gear, flaps, variable pitch propeller, etc.).

Critical to the safety of the controller:

- complex redundancy on the scale of the entire system;
- airspace integration systems (transponders, air traffic control radio, etc.);
- programmed actions in case of emergencies.

Flexible software architecture:

- supports fixed wing and rotary wing aircraft;
- applies to almost any type of aircrafts;
- contains a wide range of extraneous (peripheral) systems.

The use of the controller for existing manned aircrafts:

- a cost-effective alternative to civil aviation development;
- a way of developing risk reduction aviation;
- preserving the status of the aircraft during certification.

Easy controller installation:

- rapid conversion to manned/unmanned depending on market conditions;
- use of available maintenance resources (as for a conventional aircraft);

- easy return to the original aircraft.

As the power plant of the optionally piloted cargo-passenger aircraft, it is proposed to install two AI-450C engines manufactured by «Motor Sich» (the developer of the «Progress» design bureau) [5].

Aviation engine AI-450C (Fig. 6.5) has the certificate of airworthiness TD0070. It is designed for installation on aircraft and is currently already in operation on aircraft An-148, DART-450 and UTL-450.



Fig. 6.5. Turboprop aircraft engine AI-450C (general view)

Technical characteristics of the AI-450C engine

Weight and dimensions

Dry mass, kg – 103

Length, mm – 1085

Width, mm – 536

Height, mm – 515

Operating characteristics

Takeoff power, hp – 465

Cruising power, hp – 300

Extraordinary mode, hp – 495

Resource, h – 12 000

Compressor – single-stage, centrifugal

Turbine – supersonic single-stage

Control – electronic FADEC, two-channel with additional hydro-mechanical backup channel

Air flow rate, kg/c – 1,72

Specific fuel consumption, kg/kGf (hp) h – 0,297

**A brief description of optionally piloted modifications
cargo-passenger aircraft weighing 4000 kg**

The unified airframe and power plant are common for different modifications of the 4000 kg optionally piloted cargo-passenger aircraft. In such conditions the manufacturer gets significant advantages in the aviation market by increasing sales of produced aircraft through diversification by modifications: in case sales of the manned version decrease, the required flight controller is installed on the unified airframe with power plant and the aircraft is sold as an unmanned aircraft. In this context, the reverse operation can also be discerned. Table 6.3 shows the comparison of functional capabilities of the manned and unmanned versions of the optionally piloted cargo-passenger aircraft of 4000 kg.

Table 6.3

**Comparison of functional capabilities of manned and unmanned modifications of an
optionally piloted 4000 kg cargo-passenger aircraft**

Manned aircraft	Unmanned aircraft
Passenger; 9 passengers, 2 pilots	–
Transport – maximum payload up to 1200 kg; the aircraft is equipped with a removable transporter and telpher	Transport – maximum payload up to 1600 kg; the aircraft is equipped with a removable transporter and telpher
Aeromedical – 6 stretchers with patients, 8 seats and one place for a medical worker	–
Landing – for training paratroopers and dropping up to 10 people	–
Patrol – a crew of 4 people	Patrol without a crew and with the appropriate target load
Headquarters, civilian and military purposes	–
Passenger aircraft with VIP-cabin	–
Reconnaissance, military purpose	Reconnaissance, military purpose
Training	Training for practicing relevant procedures regarding UAVs

Fig. 6.6 shows the projections of an optionally piloted cargo-passenger aircraft with a take-off weight of 4000 kg, and in Fig. 6.7 – «side view» projections of its main modifications.

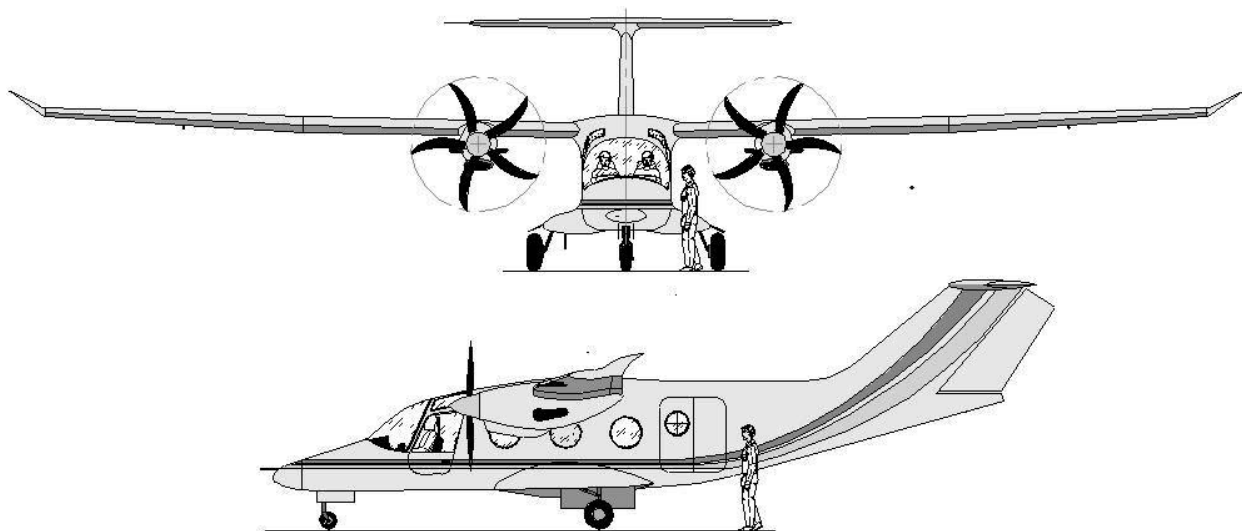


Fig. 6.6. Projections of an optionally piloted cargo-passenger aircraft with a take-off weight of 4000 kg

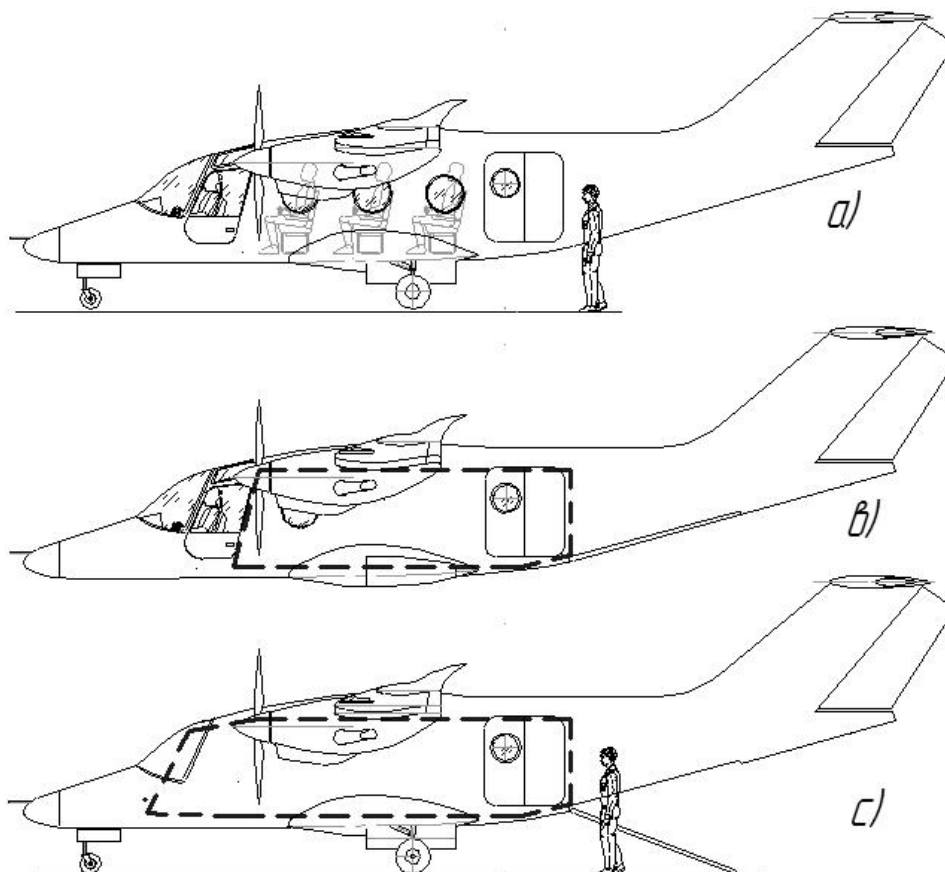


Fig. 6.7. Modifications of the optionally piloted cargo-passenger aircraft with a take-off weight of 4000 kg; the dashed line shows the contour of the cargo hold: *a* – passenger, manned modification M4000P; *b* – cargo, manned modification M4000T; *c* – unmanned cargo modification M4000T-UAV

The design tactical and technical characteristics and flight performance in the first approximation for an optionally piloted cargo-passenger aircraft with a take-off weight of 4000 kg are shown in Table 6.4.

Table 6.4

General design tactical and technical characteristics and flight performance of an optionally piloted cargo-passenger aircraft with a take-off weight of 4000 kg

Parameter	Values
Geometrical characteristics	
Wing span, m	20,87
Wing area, m ²	27,5
Length, m	13,4
Parking height, m	4,3
Take-off weight, kg	4000...4200
Weight characteristics	
Payload of manned cargo modification, kg	1200
Payload of unmanned cargo modification, kg	1600
Engine type/model	Turboprop engine/AI-450C
Cargo hold	
Length, m	4,7
Maximum width, m	1,2
Minimum width, m	0,98
Maximum height, m	1,37
Minimum height, m	1,2
Full scope, m ³	8,7 in a manned one, when there is a cockpit
Full scope, m ³	10,0 in unmanned, when there is no cockpit room
Flight performance	
Flight duration, h	6...8
Cruise speed, km/h	320
Maximum horizontal speed, km/h	420-450
Distance of non-stop flight, km	1800
Operating ceiling, m	5500-6500

Technical and economic evaluation of the implementation of the project of an optionally piloted cargo-passenger aircraft with a take-off weight of 4000 kg

The implementation of the project is calculated for three years. According to Part-21 (p. 2.A.17.2b), during this period the aircraft must pass the appropriate certification procedures and obtain a certificate of aircraft type [6]. The total cost over this period is about 20 million USD (Table 6.5).

Table 6.5

Approximate distribution of funds (by item) for the project of an optionally piloted cargo-passenger aircraft with a take-off weight of 4000 kg

№	Cost items	Percentage of amount	
		Aircraft modification	
		Aircraft	UAV
1	Aircraft development	44	38
2	Administrative costs	0,5	0,5
3	Testing and certification	14,5	14,5 (+6)
4	Development of production design and workshop planning	1	1 + 1
5	Aircraft assembly shop equipment	4,5	4,5-1
6	Equipping the composite parts shop	3	3
7	Assembly shop equipment	4	4
8	Stands and special (technological) equipment of the assembly shop	12	12
9	Composite assembly shop equipment	4	4
10	Stands and special (technological) equipment of the composite assembly shop	12	12
11	Office and computer equipment	0,5	0,5
12	The total amount of funds for the project, million USD	~ 20	
13	Time consumption for the development and certification of transport modification of the aircraft, years	3	

As can be seen from the table, the largest costs are planned for the actual creation of the aircraft project and for its testing. Rather significant costs are planned for the technological equipment, especially with regard to composite materials.

6.2. Double-engine multi-purpose convertible aircraft KM-3 «Kubok» (project)

The goal of the project is to create and certify a multi-purpose convertible («convertiplane») with a take-off weight of 3500...4500 kg. This weight category is considered promising, since the market niches of 7500...27000 kg convertibles are already occupied by V-22 and AW-609 products. The KM-3 «Kubok» convertible can be used in areas with an underdeveloped network of airfields to ensure speeds comparable to those of domestic airlines and provide takeoffs/landings without the presence of an airfield runway. Operators of the utility model can be both civil airlines and government agencies.

At the same time, it is known that there is no civilian component in the convertibles market today. Consequently, early demonstration of a new proposal in this technologically complex aircraft market gives developers and manufacturers an advantage and allows them to take advantage of previous customers' funds even before the production of marketable products.

According to DSTU.3974-2000, to date, the project is at the stage of «Technical proposal».

The main technical solutions for the layout, power plants, design and power scheme and other technical solutions have been adopted. Patents № 86553, № 94184, № 105751 (2016) and № 139703 (2019) were received as a results of the work.

A seven-year business plan has also been developed, similar to the convertible. At present the markets, component suppliers, periodicity of funds receipt, terms of beginning/end of activities for development, manufacturing, flight tests and certification of the sample are determined. The estimated cost of development is in the range of 40-45 million USD. The probable cost of the production prototype is in the range of 6-8 million USD.

In terms of practical implementation, the only convertiplane implemented to date in the U.S. Marine Corps and Special Operations Forces is the Bell V-22 «Osprey» [7]. Its various modifications have a take-off weight of 23 to 27,5 tons and payload weight – of 4,54 to 6,14 tons. Bell V-22 «Osprey» is not used in civil aviation and, accordingly, did not pass type certification. Its sphere of application – is the power structures of state aviation, where commercial performance is in the background.

Regarding technical solutions, the V-22 «Osprey» has a major disadvantage – the power plants – gas turbine engines, which turn the exhaust pipes downward during landing. This creates a danger for personnel and passengers on the parking lot, since the hot exhaust gases are in the immediate vicinity of cargo loading/unloading routes and passenger traffic routes.

This disadvantage is deprived by a new development of Bell company – Bell V-280 «Valor» convertible [8]. Rotating propellers and fixed power plants ensure that hot gases are vented outside the cargo and passenger routes. However, it is known that the V-tail it is equipped with develops more destructive moments on the tail beam than traditional tail, which will negatively affect the service life of the convertible. In addition, the usable volume contained in the cavities of this type of fins is technically quite difficult to integrate into the usable volume of the fuselage, as is usually the case with traditional fins.

The anglo-italian «Aqusta Westland» convertible, called the «Bell-Aqusta 609», is a civil aircraft of transverse layout with power plants located at the ends of the wings and propellers rotating with them [9]. This is a significant drawback, since the «Bell-Aqusta 609» is intended for the commercial, civilian market; accordingly, hot gases from the engines during parking would pose a hazard to staff and passengers. At the same time, the fuselage of this convertible has a round cross-section, which does not allow optimal use of its internal volume.

The multi-purpose twin-engine KM-3 «Kubok» convertible aircraft consists of a fuselage *1* (Fig. 6.8, *a*) with a cockpit *2* and an air pressure receiver *3* in the nose [10]. The extended tail boom *4* is integrated with the vertical tail *5*, on which the rudder *6* is mounted. On top of the vertical tails, horizontal tails *7*, which have a slight V-shape, are attached. The double-engine convertible aircraft, when parked, is supported by the front landing gear support *8*, which is equipped with a pair of wheels. The main landing gear *9* is equipped with supports with one wheel each. On the sides of the fuselage, in its lower part, there are side sponsons *10* in which the main landing gear supports are concealed. In the «parked» position of convertible aircraft the propeller *11* are turned horizontally, turning gearbox output shafts *12* are vertical, and the power plants *13* together with the gearboxes (input shaft, gearbox housing and a set of cogwheels) remain stationary. The position «A» denotes the direction of hot gas flow from the exhaust device of the gas turbine engine.

In level flight (Fig. 6.8, *b*), the rotary gearbox output shafts are set in a level attitude (item 14), and the planes of the propellers are rotated vertically. Power plants together with gear-reduction box's (input shaft, housing and set of gears) remain stationary in level flight, as well as in parking position. In level flight, the front and main landing gear mounts are hidden in the fuselage recess and in the side sponsons respectively (item 15).

The convertible aircraft is equipped with a wing *16* with a reverse sweep (Fig. 6.9). This solution, in particular, provides reduction of risk from probable collision of propeller blades with the wing.

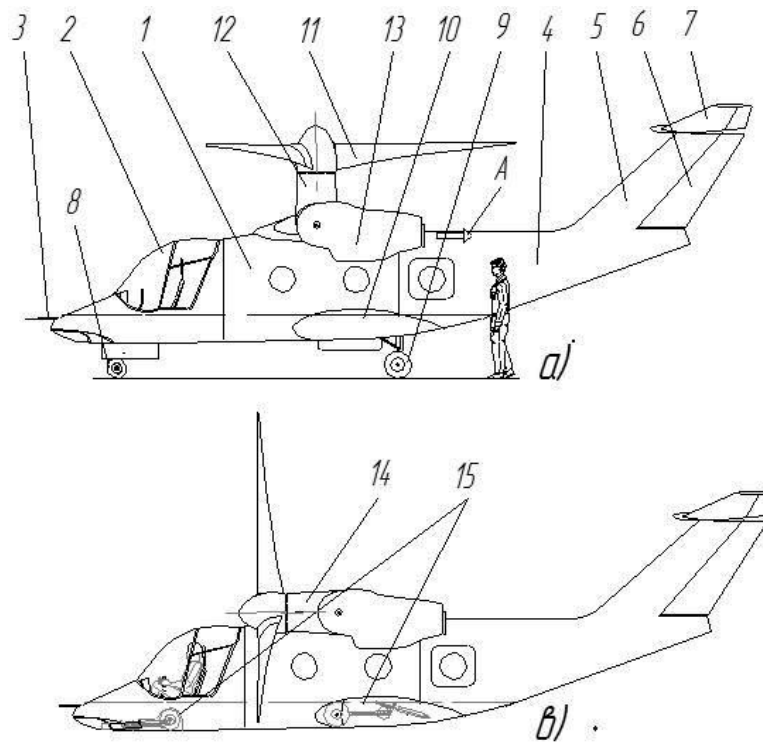


Fig. 6.8. Side projections of the multi-purpose double-engine convertible aircraft on parking and in flight

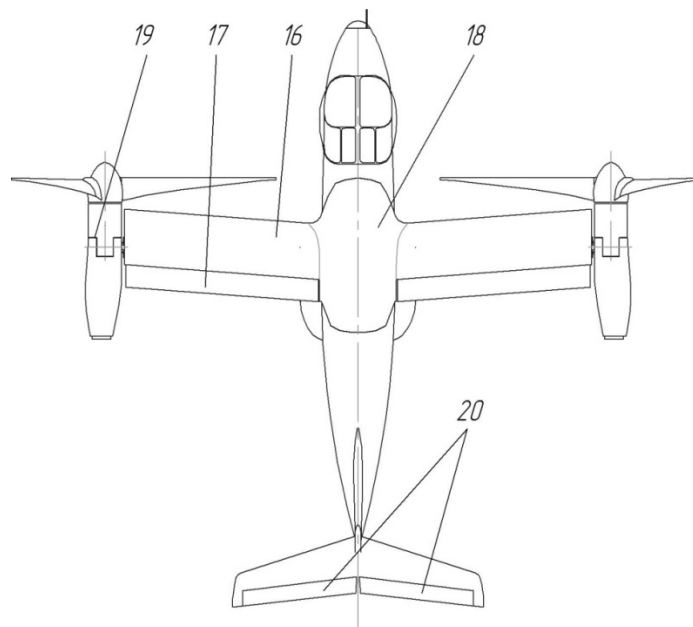


Fig. 6.9. Projection «top» of the multi-purpose double-engine convertible aircraft (propellers in level flight position)

The wing is equipped with ailerons 17, which are the aileron control in level flight in the «airplane» mode. The wing and the fuselage are aerodynamically united by the fairing 18, which serves to reduce harmful drag arising at the junction of the fuselage and the wing mounted on top of it. The position 19 marks the contour of the output shaft pivot from the «helicopter mode» position to the «airplane mode» position. On the horizontal tail, there are divided elevation rudders 20, which are synchronously deflected. The engine air intake 21 is located at the bottom of the nacelle (Fig. 6.10) and turned towards the oncoming air stream.

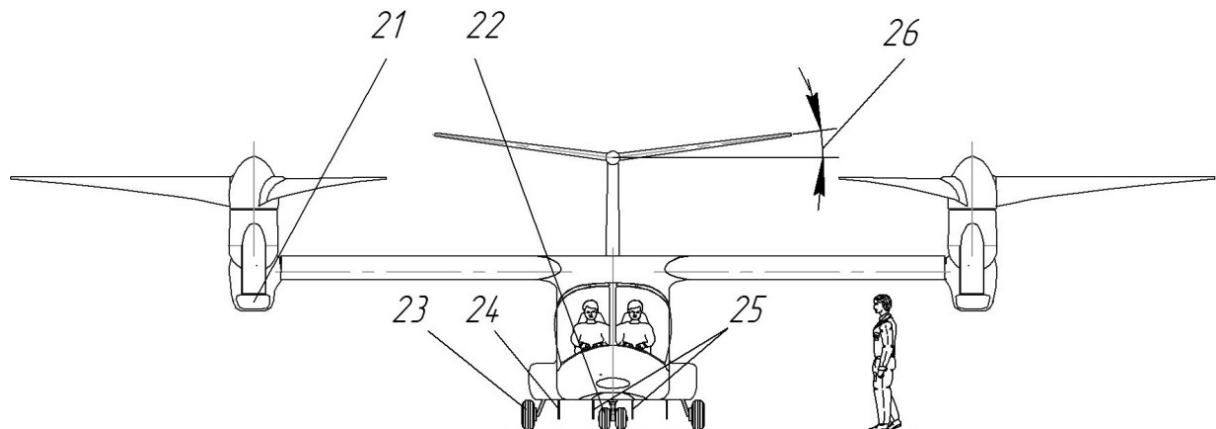


Fig. 6.10. Projection «in front» of the multi-purpose double-engine convertible aircraft at the parking lot

Position 22 indicates the twin wheels of the front landing gear support, which are closed by flaps 25 when concealed in the fuselage recess. The main landing gear wheel 23 is hidden in the side sponson and closed by flap 24. Horizontal tail when viewed from the front has a small transverse «V» angle (item 26).

Fig. 6.11 shows characteristic positions of the convertible aircraft when its landing gear is compressed. In particular, Fig. 6.11, *a* shows the position of the landing gear compressed to 100 %; this case occurs as a result of touching the pad with an overload characteristic of the «helicopter» mode.

Crimping by 50 % is typical for a fully loaded convertiplane at parking (Fig. 6.11, *b*). Crimping with shock absorbers output «up to the limiter» (0 %) is characteristic for the moment of the convertiplane detachment from the surface of the pad in the «helicopter» mode (Fig. 6.11, *c*).

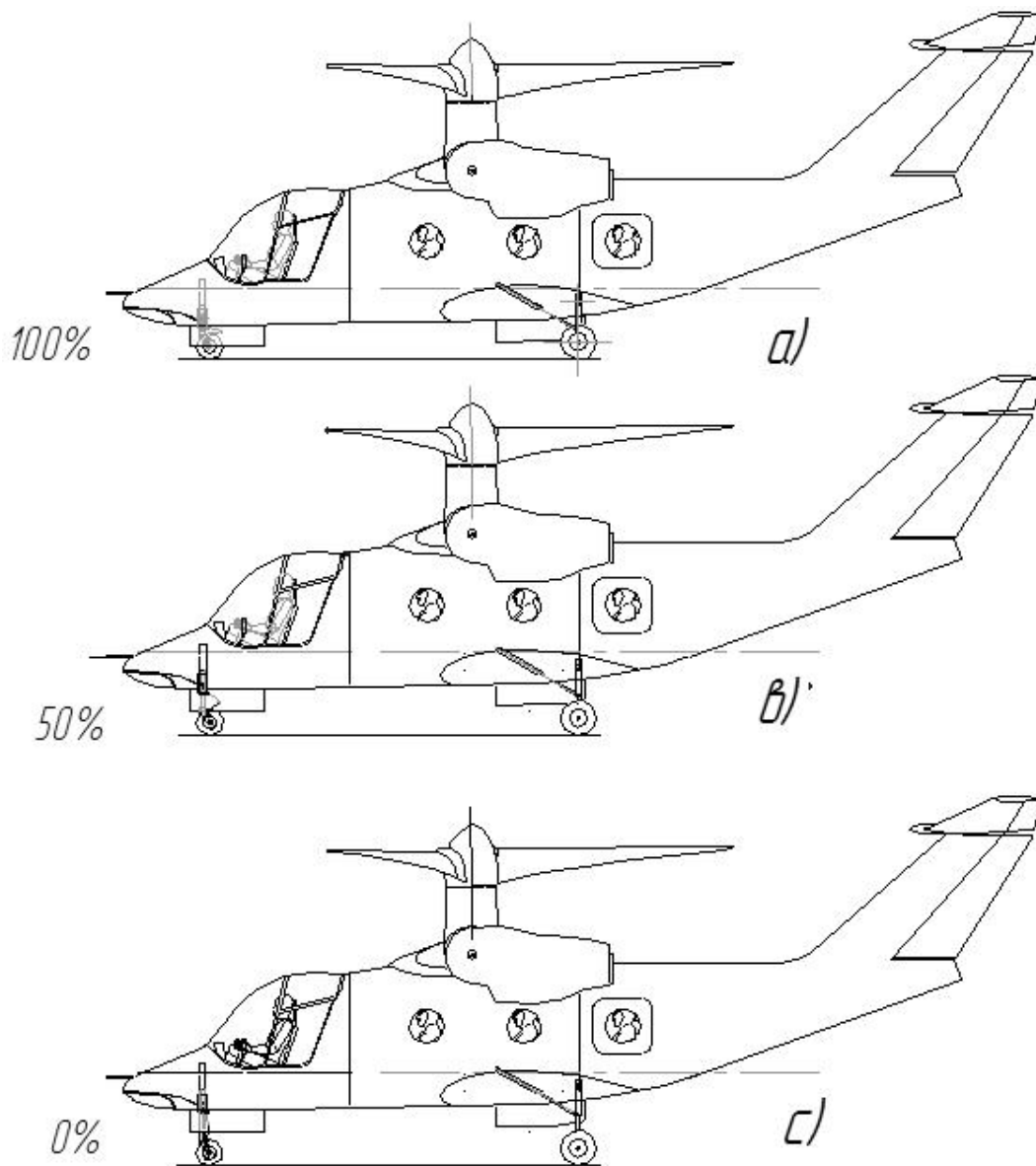


Fig. 6.11. Degrees of crimping the landing gear of a multi-purpose double-engine convertible aircraft

Fig. 6.12 shows modifications of the convertible. Multi-purpose convertible can be offered in a fully passenger version, for this purpose it (Fig. 6.12, a) is equipped with passenger seats 27 for passenger accommodation according to the formula $2 + 2 + 1$, that is the first two rows of seats are doubled and the third one is single. For passengers entry/exit the door 28 is located on the starboard side of the convertible, and for emergency exit the door 29 is additionally located on the port side. The contour (item 30) indicates the volume, which can be occupied by additional cargo.

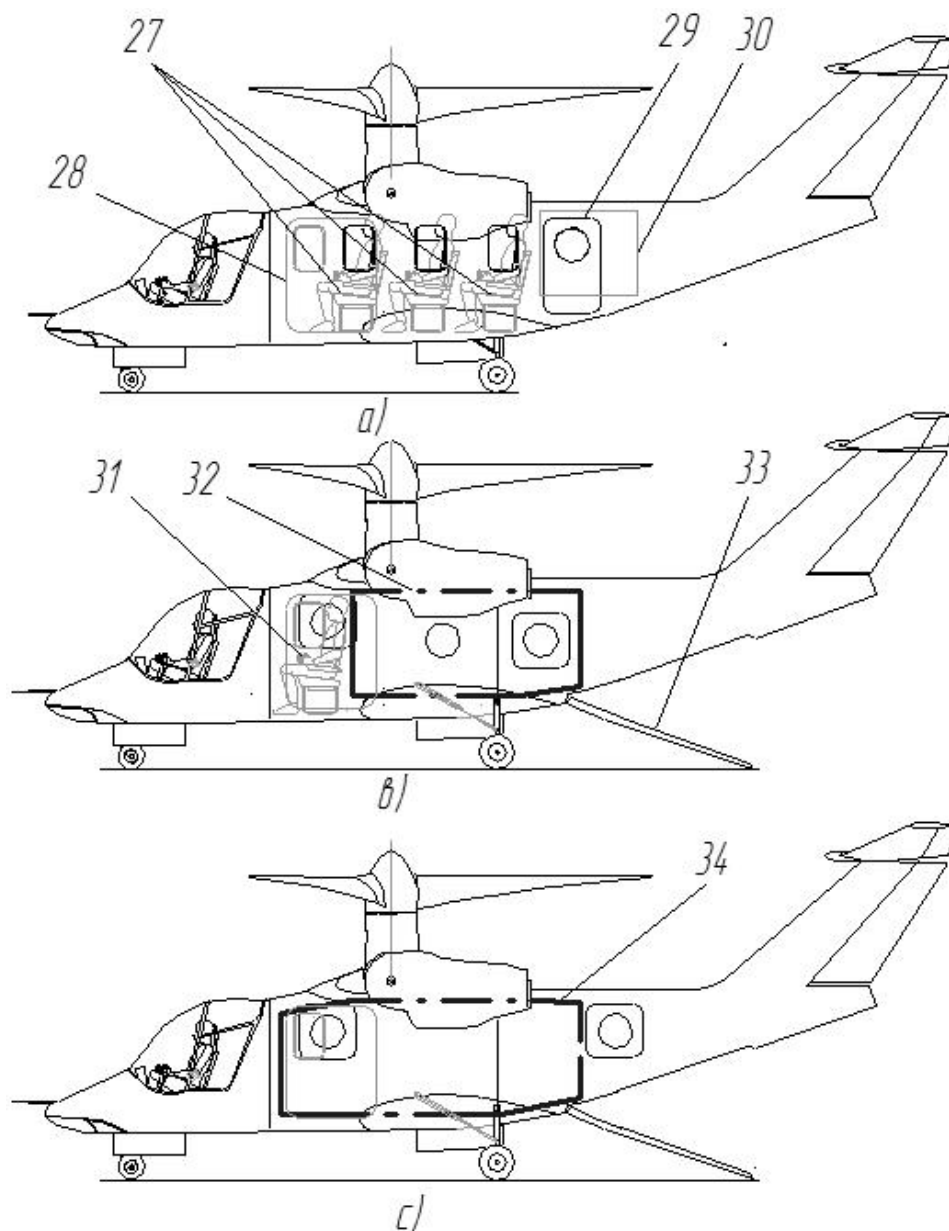


Fig. 6.12. Projections of the «side» modifications of the multi-purpose double-engine convertible

The cargo-passenger modifications (Fig. 6.12, *b*) has two passenger seats *31*. The contour (item *32*) shows the volume that can be occupied by cargo loaded on board through the rear ramp *33*, formed by the bottom of the tail beam part; also the hinged bottom can serve for dropping cargo and paratroopers.

The cargo modification of the convertiplane does not provide for passenger seats in the cargo compartment. Accordingly, it is the largest of the modifications considered; its outline (Fig. 6.12, *c*) is marked with position *34*. A co-pilot's seat may be used for cargo escort, if a flight task provides for it. Loading/unloading of cargo is performed through the rear ramp. Design specifications of multi-purpose double-engine convertible KM-3 «Kubok» are given in Table 6.6.

Table 6.6

Technical specifications of the KM-3 «Kubok» double-engine convertible project

Parameter	Values
Length, m	10,7
Height (landing gear pressed by 50 %), m	4,1
Maximum take-off weight (in «propeller under 45°» mode), kg	4300
Payload weight, not more, kg	1100
Speed capability, km/h	530
Flight duration, h	5
Number of passengers, people	1 pilot + 5 passengers or 2 pilots + 4 passengers
Flight altitude, m	6000
Equivalent take-off power of engines, hp	2×1000

Fig. 6.13 shows an exterior view of a multi-purpose double-engine convertible aircraft (V-fin version).



Fig. 6.13. Exterior view of the multi-purpose double-engine convertible aircraft KM-3 «Kubok»

6.3. Stratospheric pseudosatellite PS-11 «Krokus»

The concept of an «atmospheric satellite» was first introduced in 2001 by Ray Morgan, president of AeroVironment, who described the concept as follows: «We are trying to create what is called an atmospheric satellite, performing many of the functions of a satellite in space, but this is very close, atmospheric». At the time, AeroVironment was developing a Pathfinder

aircraft, which had a solar cell power plant. Conceptually, the term has now been refined and specified; an aircraft of this class is defined as a «stratospheric pseudosatellite» (*HAPS – high-altitude pseudo-satellite*).

The main feature of «stratospheric pseudosatellites» is the onboard power installation on solar cells of film type. This guarantees almost absolute independence of its flight from the onboard hydrocarbon fuel supply, because solar radiation is continuous due to the absence of clouds at a given altitude.

From an applied point of view, pseudosatellites (PS) can take over the functions of a satellite constellation to perform them in real time within an entire region. Thus, at an altitude of 20–30 km a pseudosatellite can successfully compete with by spacecraft. From the commercial point of view it is proved that one square kilometer of captured images from a pseudosatellite is seven times cheaper than its counterpart – the image provided by space means. The peculiarities of the atmosphere at these altitudes and the improved quality of the images obtained from the pseudosatellite contribute to this. As for the speed of data transfer, it is beyond competition.

The main problems of pseudosatellites are in providing them with the necessary amount of energy at the stage of cruising flight at night; also little known are the techniques and methods of its delivery to a high altitude in conditions of abrupt changes in wind strength and direction at echelons, a large gradient in atmospheric temperature (from +25 to –56,5 C°), reduction of air density by more than 13 times and changes in light due to changes in position relative to the Sun and cloudiness.

The purpose of the pseudosatellite PS-11 «Krokus». Pseudosatellite PS-11 «Krokus» is designed to test the critical elements of technology for long-term flights in the stratosphere. Taking into account the processing of technical characteristics of the existing modern samples of manned aircraft and pseudosatellites (PS) powered by solarcells, it was found that the aircraft includes:

- the fuselage with the kit of avionics systems, the electrical battery (EB) and vertical empennage with the solar film on the tail beam surface;
- the right and left center wing consoles with a set of solar films on the surface (top);
- the right and left side wing consoles with a set of solar films on the surface (top);
- the two power plants in the kit;
- the horizontal plumage with a set of solar films on the surface (top);
- the transport and launch equipment and transport packaging for storage and transportation of a prototype pseudosatellite.

The on-board power plant of the pseudosatellite shall consist of solar films of the «C-60 Sunpower 125x125 Monocrystalline Silicon Maxeon GEN II Solar Cells» model in the amount of 306 films over the entire surface of the pseudosatellite, in particular:

- solar films on the surface of the tail beam - 22;

- solar films on the right and left center consoles of the wing - 72×2;
- solar films on the right and left side consoles of the wing - 48×2;
- solar films on horizontal plumage - 48.

Voltage of the onboard power supply of the pseudosatellite, B – 24.

Additionally, a lithium-polymer battery for 9 A·h (24V) must be located on board of the pseudosatellite to provide power to on-board consumers at night (during the descent of the pseudosatellite) and at critical moments of taking off, when the sun is blocked by clouds at an altitude of 0–6000 m. The main design characteristics of the pseudosatellite are given in Table 6.7.

Table 6.7

Main characteristics of the pseudosatellite

№	Parameter	Values
1	Wing span, m	11
2	Length, m	4,8
3	Height, m	1,1
4	Wing area, m ²	5,4 – 6,0
5	Maximum take-off weight, kg	16 – 22
6	Payload mass, kg	up to 1
7	Power-to-weight ratio (specific power), W/kg	28,5 – 30,0
8	Specific weight, kg/W	approximately 0,033–0,035
9	Load per unit area, kg/m ²	approximately 2,5–3,5
10	Maximum speed, m/s (at the altitude 0 m)	15
11	Maximum speed, m/s (at the altitude 20 000 m)	35
12	Cruising speed, m/s (at the altitude 0 m)	11
13	Cruising speed, m/s (at the altitude 20 000 m)	27
14	Stall speed, m/s (at the altitude 0 m)	6
15	Stall speed, m/s (at the altitude 20 000 m)	23
16	Engine power, kW (maximum)	2×1,5 = 3
17	Battery type	Li-ion
18	Altitudes, m	0–19 000
19	Ceiling, m	20 000
20	Maximum flight duration, h	18–20
21	Maximum range, km (within the range of the one ground control station)	60

Power flows (and their distribution) from a kit of solar films and a lithium-polymer battery are automatically controlled by the appropriate controller and additional power supplies. The lithium-polymer battery is located in a special thermal box to maintain its performance at low pressures and temperatures. Solar films on the surfaces of the pseudosatellite should be covered with a protective transparent film to protect against moisture and external damage.

As the result of the statistical processing of primary data on known designs, the choice was made towards the normal layout (aerodynamic) scheme of the pseudosatellite.

The question of one-, two- or multi-beam design is solved as follows. It is known that the torques that the horizontal and vertical empennage develop in a normal circuit are aimed at controlling (or stabilizing) the aircraft. Their value is quite certain, the given flight restrictions are included in the airworthiness standards. The regulation of the stiffness and strength parameters of one tail beam is also a well-defined process and can be calculated by methods acceptable for aviation, while two-, three- or multi-beam constructions require the development of acceptable methods of calculation and testing, and can constitute a completely separate research topic. Moreover, multi-beam constructions are much more complex and more material-intensive; the result of their use can lead to a significant increase in the weight of the tail, which must be compensated somehow in the nose part.

Regarding the cross-section of one tail beam, the decision was made in favor of a triangular, truss, the upper edge of which is turned up, to place additional solar cells on it. The beam should consist of three rods and the corresponding braces connected inseparably; the entire beam must be covered with a high-strength mylar to make the aerodynamic surface.

The wing is selected with a constant chord along the span to simplify its manufacture. The wingspan of about 11 m is organized by dividing it into four parts, i.e. to the two central and two side consoles. Side consoles should be installed at a certain angle.

Structurally, the wing should be equal to the side member with a rigid one, $\frac{3}{4}$ profile brackets, trim, and $\frac{1}{4}$ soft. The connection of the wing parts through extensions, located in the cavities of the spar. The fuselage nacelle should be stacked, composed of longitudinal and transverse elements and diagonal struts and rods. In the conditions of the prototype, this makes it possible to maneuver for the probable rearrangement of aircraft equipment. A significant part of the aircraft devices, radioelectronic equipment (REE), electrical battery, etc. are concentrated in the nacelle. The aerodynamic shape of the nacelle is provided by a removable fairing, which is attached to the inner set (frame) of the nacelle.

The empennage is chosen crosswise with an all-turning stabilizer and compensated rudder. A bicycle-type landing gear with the main support, which has twin wheels; the landing

gear is retracted in flight to reduce harmful resistance. The power plant should be with two engines located on pylons under the wing.

In the take-off configuration, the aircraft is located on the transport launch to reduce the risks of structural damage and organize an automatic launch.

Solar cells are located on all accessible surfaces of the wing, horizontal empennage, and tail beam. The surfaces of all cells are protected by a thin film with low light transmission losses.

Fig. 6.14 show the main approximations for making technical decisions on the final layout of the pseudosatellite.

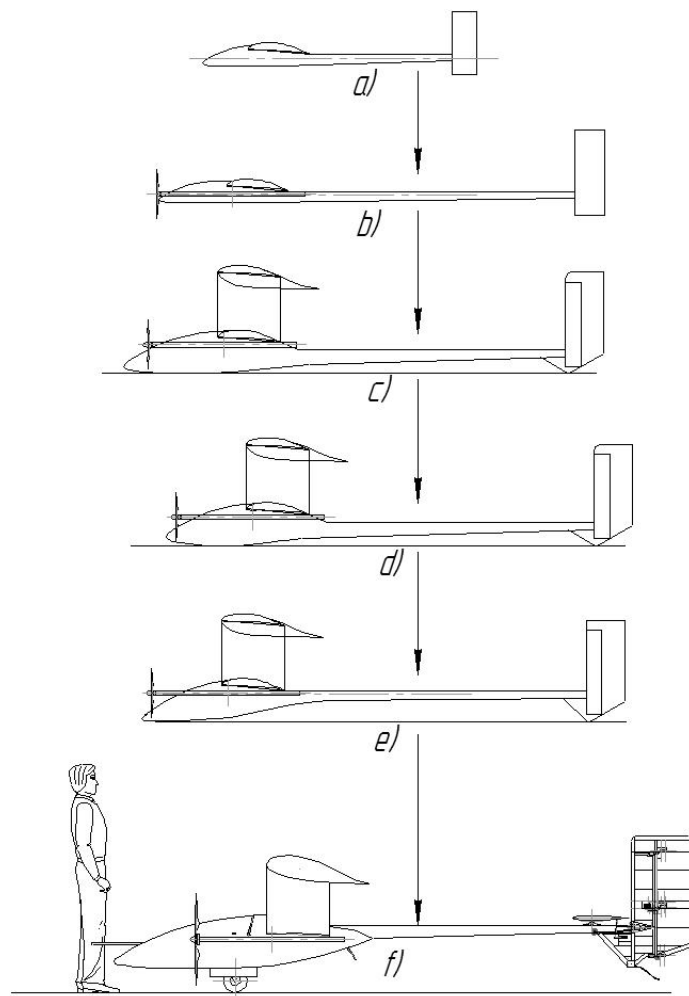


Fig. 6.14. The main stages of obtaining the final conceptual solution for the layout of the pseudosatellite

In particular, the position of Fig. 6.14, *a* corresponds to the initial idea of the location of the wing, vertical empennage, and fuselage nacelle; there are no solutions for the use of the U-shaped wing. The decision to use the U-shaped wing and power plants on the pylons appears at the positions marked in Fig. 6.14, *c*. The location of the horizontal empennage in front of the vertical one and the retractable landing gear are reflected in the final concept (Fig. 6.14, *f*).

Fig. 6.15 show the appearance of the stratospheric pseudosatellite PS-11 «Krokus».



Fig. 6.15. External view (3/4 right) of stratospheric pseudosatellite PS-11 «Krokus»

For the convenience of assembly operations during the usage of the pseudosatellite sample, it is necessary to pay attention to the certain components division scheme, taking into account the following:

- additional components for the connector should not significantly increase take-off weight;
- additional nodes should not reduce the accepted values of safety factors;
- their design should be as simple as possible.

Aircraft wing connectors. Since the wing has one spar, which is a closed-loop, this circumstance provides the technical possibility of placing an extension cord in the cavity of the spar, which is an acceptable way of organizing the transmission of the flows of bending forces that occur when loading the wing.

Wings and fuselage connectors. The wings and fuselage connectors are arranged correspondingly with the difference that the extension insert connects the two central parts of the wing (right and left) and the power frames of the fuselage.

The torques through the connectors is transmitted as follows:

- the wing/fuselage; through threaded rods that are fixed along the edges of the end profile; ribs enter the corresponding sockets of the side fuselage ribs;
- the center/sidewall consoles of the half-wing via the threadless positioners that fit into the corresponding sockets and are located on the edges of the end nerves of the center/sidewall consoles of the half-wing.

The electrical equipment of the consoles and the fuselage is disconnected/connected via the corresponding electrical connectors.

The horizontal empennage connectors are made by mounting/dismantling the empennage rotary axis, the thrust tip by the servomechanism, and the corresponding electrical connector. The directions and installation diagram of the main components of the pseudosatellite are shown in Fig. 6.16.

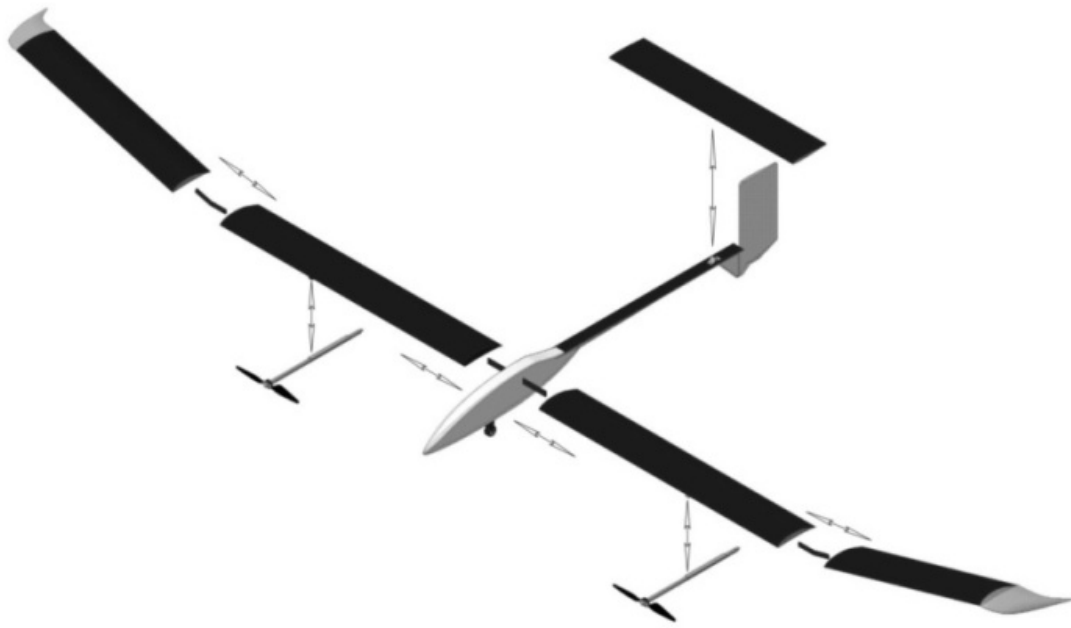


Fig. 6.16. Spatial explosion-connector diagram of the pseudosatellite main components

According to the chosen layout scheme and taking into account the size of individual solar cells, as well as the need for on-board voltage of 24V, it was decided to place solar cells and their batteries (sections) on the outer surfaces of the pseudosatellite in suitable areas.

The selected layout scheme made it possible to arrange the sections of solar cells, at the rate of 1 section = 48 cells, on almost the entire surface of the wing, horizontal empennage, and fuselage (Fig. 6.17). In this figure, positions 1, 2, 3, 4, 5, and 6 indicate sections of 48 cells.

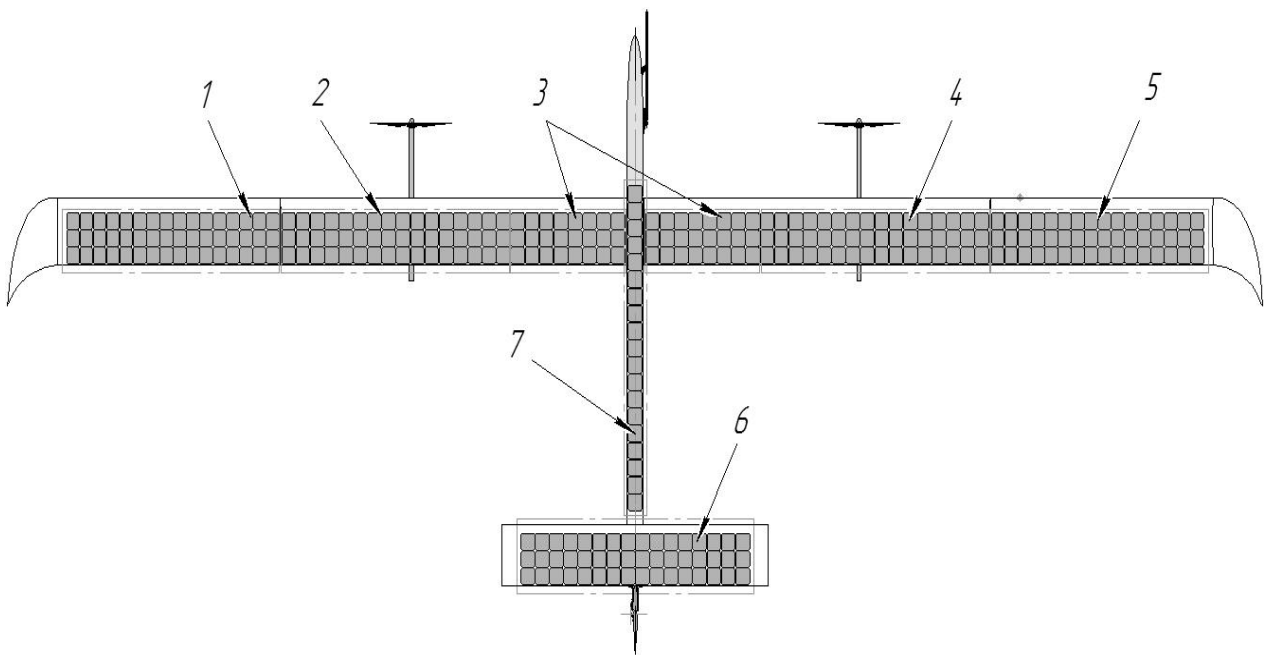


Fig. 6.17. The layout of solar cells on the outer surfaces of the pseudosatellite

This number of cells in the section is motivated by the fact that one cell develops a voltage of about 0,5V, and to obtain 24V on-board voltage, a serial connection of 48 cells is necessary. To obtain the appropriate voltage force, all 6 sections are connected to the on-board power supply network in parallel. Section 7 (14 cells) is auxiliary and provides power to the automation of the control system, other systems, and aeronautical lights. The values of the geometric indicators of the energy supply system of the pseudosatellite with solar cells are presented in Table 6.8.

Table 6.8

**Geometric characteristics of solar cells and their sections
on the outer surfaces of the pseudosatellite**

№	Feature	Values
1	Area of one solar cell type S60, m ²	0,014
2	Section area of 48 solar cells, m ²	0,672
3	Area of the five main wing sections, m ²	3,36
4	Area of the six main sections, m ²	4,04
5	Area of additional fuselage solar cells, m ²	0,266
6	Total area covered by solar cells, m ²	4,306
7	Fill factor of the wing area, $K_{f,w}$	0,79
8	Fill factor of the horizontal empennage area, $K_{h,p}$	0,61

Fig. 6.18 shows the location of a section of 48 solar cells on the surface of the pseudosatellite horizontal plumage.



Fig. 6.18. Arrangement of the section of 48 solar cells on the horizontal plumage PS-11 «Krokus»

General technical description of the pseudosatellite. According to the scheme, the pseudosatellite is an high-wing aircraft of the normal scheme with two, transversely located power plants, U-form wing with side consoles raised by 15° and cross-shaped tail. The pseudosatellite is equipped with a hidden bicycle-type landing-gear with a main wheel support and a spring-type tail support. The wing of the pseudosatellite is rectangular on the plan (Fig. 6.19, *a*), it is equipped with a profile FX 76–MP120 (MAC 500 mm) and consists (for an example the left one) of the inner console 1, outer console 2 and winglet of the console 3.

On the power ribs of the center console tubular nacelle 4 is mounted where the motor 5 is mounted to which the engine is attached 6. To the output shaft of the engine through the hub is hinged to the blades 7 of the propeller with the mechanism of their rotation. The hub of the propeller is closed by an aerodynamic fairing 8. The design of the right wing is similar to the design of the left wing. S60 solar cells are located on the entire surface of the wing. In order to provide the onboard supply voltage of 24V solar cells (SC) are electrically combined in a module of 48 elements; the total number of SC on the wing – 240 and the total number of modules on the wing – 5.

However, because of the design, 120 elements of the left wing physically are divided into groups 9 and 10; the left wing, respectively, contains groups 11 and 12. The number of elements in these groups is as follows: groups 9 and 12 contain 48 elements and groups 10 and 11 – at 72. On the flat surface of the top of the fuselage and tail beam there are 18 additional SC, collected in modules 13 and 14. These SC are designed for power supply of separate, vital pseudosatellite systems. On the horizontal plumage there is a module 15, consisting of 48 SC and is the sixth, onboard battery of 24V.

The total number of SCs on board – is 306. The total area covered by SCs on the surfaces of the pseudosatellite is – 4,78 m². The nose part of the fuselage is equipped with a fairing 16 (Fig. 6.19, *b*); during landing, the pseudosatellite rests on the main support of the landing gear, which has paired wheels 17. In flight, the landing gear is hidden. Vertical plumage (VP) 18 is equipped with a symmetrical profile NASA0009 (MAC 450 mm) and is completely rotatable; the axis of rotation is at the focus point, which allows to balance the hinge moments from its return. To bring the axis of rotation to the line of focus in the VP a special cut is made.

Horizontal plumage (HP) 19 is equipped with a symmetrical profile NASA0009 (MAC 450 mm) and is completely rotatable; the axis of rotation is at the point of focus, which allows you to balance the hinge moments of its rotation. To bring the axis of rotation to the line of focus, the HP is equipped with a bow with fixed and moving parts. The fixed part is fixed to the rods of the tail beam truss and the movable part to the power ribs of the HP.

The propeller blades rotate on the hinges *20* and can be in the working position when they produce thrust. The non-operating position (to reduce drag the blades are folded along the flow) corresponds to the mode of gliding and direct approach to landing.

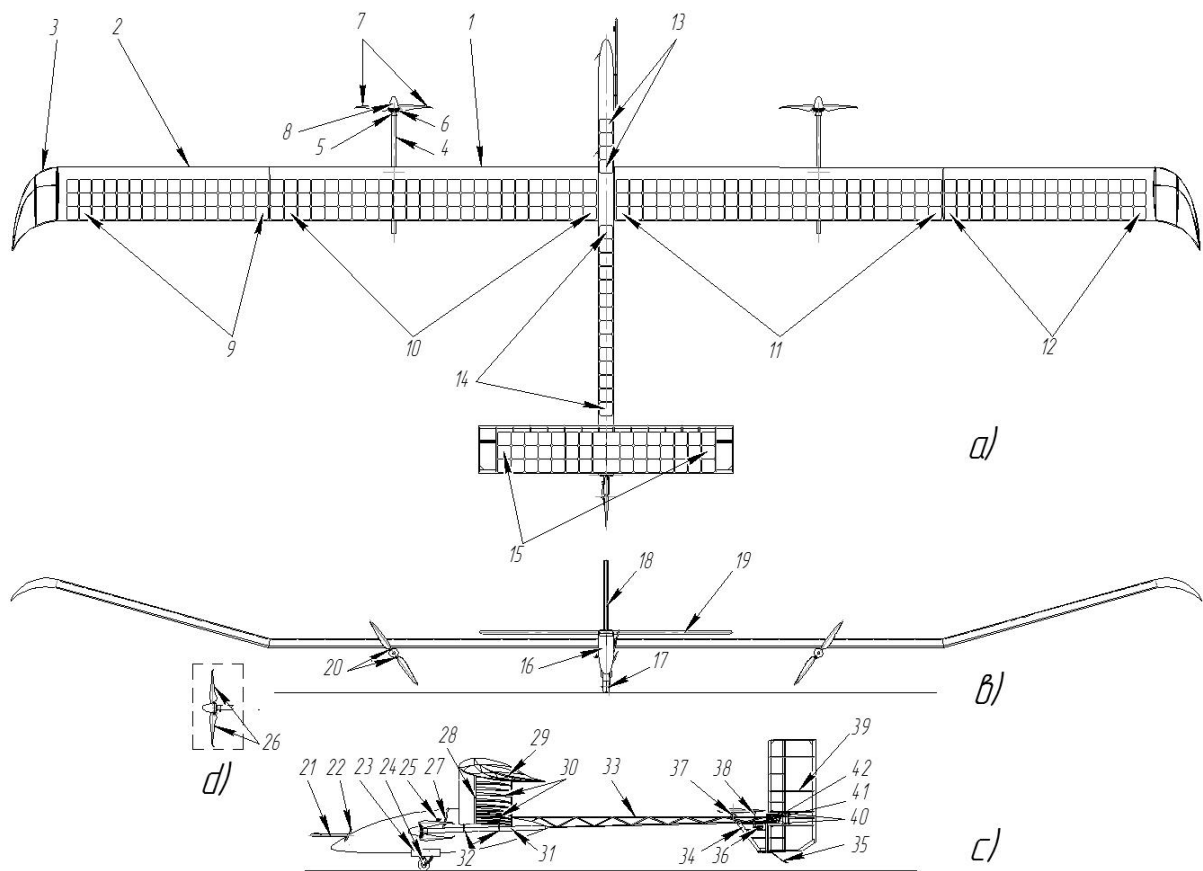


Fig. 6.19. Projections of the general appearance of the pseudo-satellite

On the nose part (Fig. 6.19, *c*) of the fuselage nacelle, on its starboard side, a full air pressure receiver *21* is mounted. On the left side antenna *22* of the telemetry modems is installed. At the bottom of the nacelle there are the sash *23* of the landing gear shaft, in which it is hidden by a mechanism *24*. Power supply for power plants and pseudosatellite systems is turned on/off by an electric key *25*. To ensure the transmission of useful video and photo information from the board, an antenna for the video modem *27* is installed on the left side.

The wing has two shelf spars *28*. The end of the wing is a complex profiled winglet *29*, the frame of which is covered with soft cladding. The upper casing of the wing and the cladding of its bottom to the spar – are rigid. The bottom trim from the spar to the trailing edge – is soft, supported by a set of typical ribs *30*.

The power plant is mounted on a tubular pylon *31*, which is connected to the wing through the bows *32*.

The gondola is rigidly connected to the tail beam 33 of the truss structure, which forms a longitudinal power element – the fuselage. At the edge of the tail beam a lower keel 34 is installed, which in addition to the aerodynamic function serves to secure the rear support of the landing gear 35. Along with this, in the thickness of the lower keel is a servo 36 for rotating HP.

On top of the tail beam is a fixed bow 37 for securing the HP. The drive of the HP is by means of a rigid rod 38, which connects by means of ball joints the lever of the HP and the lever of the servo 36.

The vertical plumage 39 is fixed and rotates in the supports 40, which cover its tubular spar. The return of the vertical plumage occurs from the servo 41 by means of a rigid rod 42 with ball tips.

Position 26 (Fig. 6.19, *d*) shows the working position of the blades of the propeller of the pseudosatellite.

Fastening of solar cells is provided by their dense pressing to the main covering by means of an additional mylar, transparent and strong film. An example of fastening to the wing skin surface is shown in Fig. 6.20, where the wing profile contour is organized by typical ribs 18. A three-layer composite panel 19 is attached to the rib and spar contour, which maintains the appropriate profile configuration and prevents flight torques. The solar cells 20, which are pre-electrically connected in the battery, are suitably located on the surface of the wing casing and pressed by an additional transparent strong film 21, which is tightly stretched to the solar cells, which are flexible, completely repeat the contour of the profile. The electrical conductors to which the film elements are connected are combined into suitable harnesses 22 and are led inside the wing (tail beam and stabilizer) through holes 23. All conductors from the solar film elements are electrically connected to each other and connected to the general mains pseudosatellite.

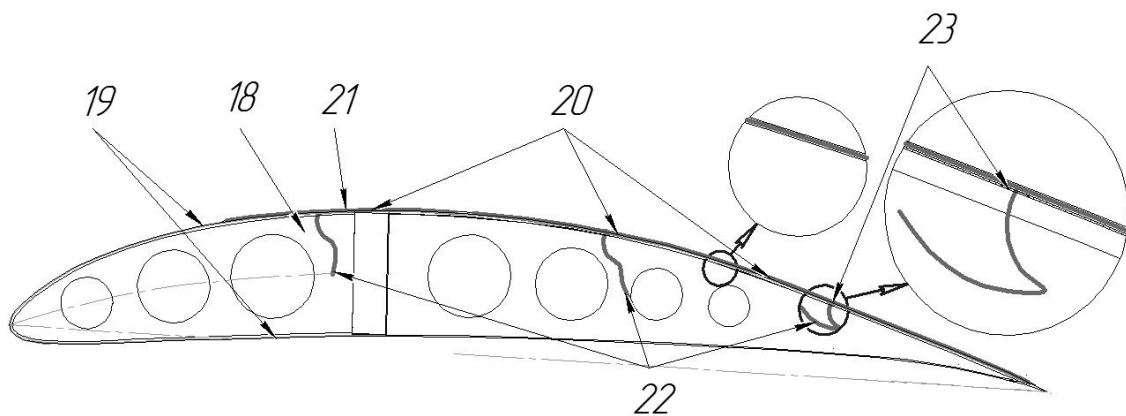


Fig. 6.20. View of a typical cross-section of a pseudosatellite wing with a diagram of the solar cells

Technical solutions of elements of power set of wings and empennage. In a typical cross-section, the wing is a single-spar structure with a mostly rigid skin. Spar 1 (Fig. 6.21, *a*) receives bending loads. It is connected to a typical rib 2, which together with the spar is covered by a combined casing 3, designed to form an aerodynamic profile and the perception of torque from the wing.

Two-shelves spar (Fig. 6.21, *b*), consists of lower and upper shelves 4, made of carbon fiber (roving) in a mixture with epoxy resins. Between the shelves walls 5 are installed and this set is «dressed» in a «stocking» of carbon fabric. The cavity of the spar is filled with expanded polystyrene. A typical rib consists of a spout 6 and a shank 7 made of expanded polystyrene. To reinforce the lower bow of the shank glued strip 8 of carbon panel with a cross section of 10×0,5 mm.

The upper bow of the profile is covered with a rigid casing 9, which is a carbon fiber «sandwich panel». The front part of the lower bow of the profile to the spar is closed by a similar «sandwich panel» 10. Thus, the torques are mainly compensated by the contour «spar – top skin – bottom skin to the spar». The lower part of the bow of the profile is closed by a covering from a high-strength mylar film; this solution allows relatively easy access to the wing cavity without making additional holes in the main, rigid casing.

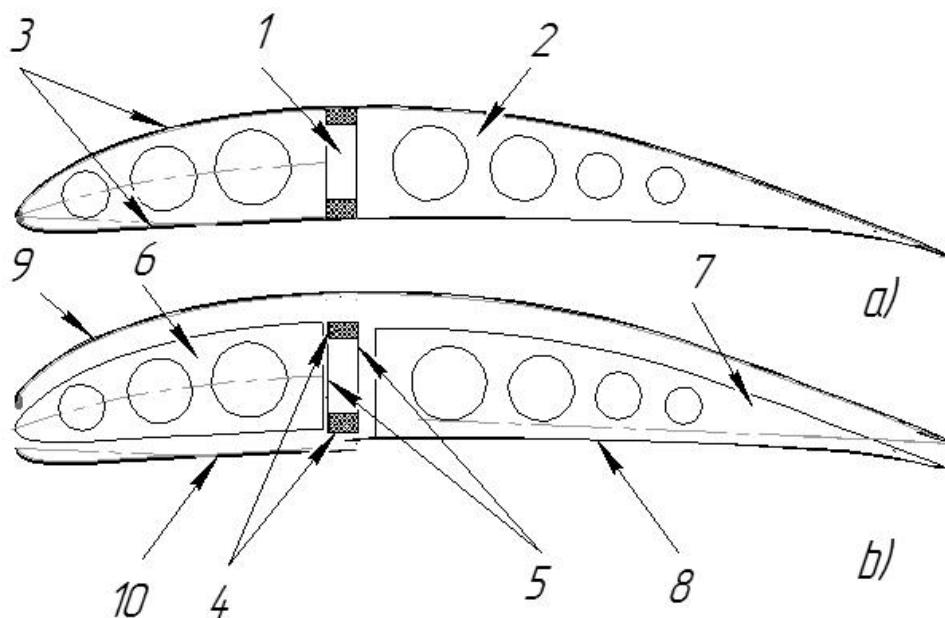


Fig. 6.21. The structure of a typical cross section of a pseudosatellite wing

Horizontal plumage is made of discrete elements and covered with high-strength mylar film (Fig. 6.22, *a*).

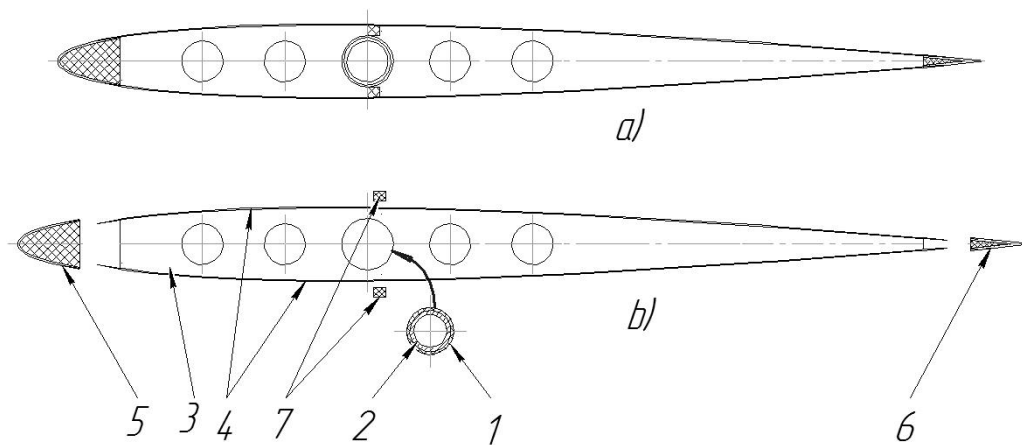


Fig. 6.22. Typical section of horizontal plumage and its components

The basis of the HP is a tubular spar *1* (Fig. 6.22, *b*), which is reinforced in the necessary places with tubular inserts *2*. On the spar «strung» typical ribs *3*, which are made of polystyrene and branded to strengthen the contour plates *4* of carbon fabric. The nose of the HP is closed by the front U-shaped edge *5*, glued from carbon fiber and filled with polystyrene foam. The shank of the rib is closed with a V-shaped edge *6*. To prevent excessive deflection of the soft skin along the spar glued ridge *7* to support the skin. The design of a typical section of vertical plumage is similar to the design of HP. Table 6.9 shows the main geometric characteristics of the stratospheric pseudosatellite PS-11 «Krokus».

Table 6.9

**Summary of basic geometric characteristics of stratospheric pseudosatellite PS-11
«Krokus»**

Parameter	Value
Wing	
Wingspan, m (projection on the horizontal)	11,20
Wing area, m ² (projection on the horizontal along with the fuselage overlap)	5,522
MAC wings, m	0,5
Narrowing of the wings, η	1,0
Elongation of the wing, λ	22,40
Center console	
Central console span, m (horizontal)	3,10
Central console area, m ² (horizontal)	1,55
Side console	
Scope of the side console, m (in projection)	2,415

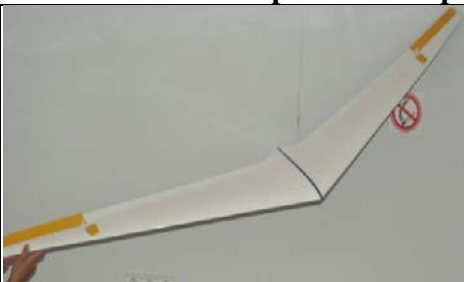
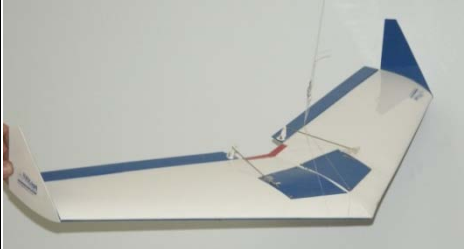



End of table 6.9

Scope of the side console, m (horizontal)	2,46
Area of the side console, m ² (in projection)	1,173
Side console area, m ² (horizontal)	1,232
Fuselage	
Length, m (+ pitot tube)	4,80
Height, m (chassis hidden; + VP)	1,135
Height, m (chassis released, uncompressed; + VP)	1,215
Height, m (chassis released, compressed; + VP)	1,190
Side area, m ² (chassis hidden; + pitot // – VP)	1,261
Horizontal plumage	
Span of horizontal plumage, m	2,390
Area of horizontal plumage, m ²	1,10
MAC of horizontal plumage, m	0,45
Narrowing of horizontal plumage, η	1,0
Elongation of horizontal plumage, λ	5,31
Vertical plumage	
Height vertical plumage, m	1,040
Area of vertical plumage together, m ²	0,51
Area of the fixed part of the vertical plumage, m ²	0,202
Area of the moving part of the vertical plumage (steering wheel), m ²	0,308
MAC vertical plumage (without the lower keel), m	0,5
Profiles of aerodynamic planes	
Wing	
Wortmann, FX 76-MP-120; relative thickness, %	12
Horizontal plumage	
NASA 0009, relative thickness, %	9
Vertical plumage	
Symmetrical, relative thickness, %	8






List of references

1. Sarymsakov H. G. Agricultural aircraft. M.: Mashinostroenie, 1979. 138 p.
2. STANAG 4671. Unmanned aircraft systems airworthiness requirements (USAR). [Electronic resource]. Source access mode: <https://standards.globalspec.com/std/13430067/STANAG%204671>.
3. J. S. F. Hoeben. A value analysis of unmanned aircraft operations for the transport of high time-value cargo//Faculty of Aerospace Engineering, Delft University of Technology, the Netherlands. 2015.
4. X-KIT for Manned/UAS/OPS. Manned/Unmanned/Optionally Piloted System Conversion Kit. [Electronic resource]. Source access mode: <https://s-plane.com/products/opv-kit/>.
5. AI-450C family engines. [Electronic resource]. Source access mode: <http://www.motorsich.com/ukr/products/aircraft/tr/ai-450s/>.
6. The State Aviation Service has adopted the certification requirements for the procedures of the ARU 21 (Part-21). [Electronic resource]. Source access mode: <https://avia.gov.ua/derzhaviasluzhba-prijnyala-dlya-zastosuvannya-vimogi-dlya-sertifikatsiyi-zaprosedurami-apu-21-part-21-certification-specifications-ss-diyuchi-v-yevropejskomu-agentstvi-z-bezpeki-polotiv-european-uni/>.
7. Bell Boeing V-22 Osprey. [Electronic resource]. Source access mode: https://en.wikipedia.org/wiki/Bell_Boeing_V-22_Osprey.
8. M. Greenwood. Bell V-280 Valor Tilt-Rotor Aircraft Aces Speed Test. [Electronic resource]. Source access mode: https://www.engineering.com/Advanced_Manufacturing.
9. AW609. Faster. Further. Higher. [Electronic resource]. Source access mode: <https://www.leonardocompany.com/en/products/aw609>.
10. Matiychyk M. P., Kharchenko V. P. Double-engine convertible with rotary shafts of airscrew propellers. Ukraine's patent for a useful model №105751. Published 11.04.2016. Bulletin № 7.

**Developments of unmanned aerial vehicles of the Scientific and Production Center of
Unmanned Aviation «Virage» of the National Aviation University in chronological order**

№	UAV name	Image of the UAV	Year of creation	Purpose of development	Wing span, m; mass, kg (m//kg) kg*
Completed UAV projects					
1	Concept № 1		2002	Investigation out the geometry of the wing of great elongation	2,1//1,7
2	Concept № 2		2002	Investigation out the geometry of the low-elongation wing	1,1//0,9
3	Concept № 3		2002	Investigation of the effects of slat (of the leading edge) and suspended ailerons on flight performance	1,4//2,2
4	Concept № 4		2002	Investigation of high levels of manageability	1,1//3,8
5	Concept № 5		2003	Investigation of high levels of manageability	1,1//3,6

Continuation of the appendix

№	UAV name	Image of the UAV	Year of creation	Purpose of development	Wing span, m; mass, kg (m//kg) kg*
6	Concept № 6		2003	Investigation of the split V-tail	1,3//2,5
7	Concept № 7		2004	Investigation of the inverted V-tail	1,4//3,1
8	Concept № 8		2004	Investigation of the V-tail and electric power plant	2,2//2,1
9	M6 «Zhayvir»		2004	Mechanised trichogram application (ACHW)	(1,8//7)2,5*
10	Concept «Vector»		2005	Testing elements of the automatic flight control system	(1,7//4,1)1,5*

Continuation of the appendix

№	UAV name	Image of the UAV	Year of creation	Purpose of development	Wing span, m; mass, kg (m//kg) kg*
11	M4 «Agro»		2005	Providing ACHW in automatic mode, flying laboratory	(3,5//45)20*
12	«Mai-jor»		2006	Investigation out the stability and controllability of the airplane of the normal scheme	1,97//4,9
13	M-7 «Nebesniy patrol»		2009	Investigation of asymmetric tandem arrangement of power plants	(4,0//50)25*
14	M-10 «Oko»		2010	Practising automatic piloting	1,99//2,2
15	M-10-1 «Oko»		2010	Testing the autopilot of the NAU design	(2,02//3,8)1,0*


Continuation of the appendix








№	UAV name	Image of the UAV	Year of creation	Purpose of development	Wing span, m; mass, kg (m/kg) kg*
16	M-7-V5 «Nebesniy patrol»		2011	Typical Civil aviation unmanned aerial vehicle (for obtaining a type certificate)	(6,0//200)30*
17	M-7-D «Nebesniy patrol»		2011	Flight mode training for M-7-V5 «Nebesniy patrol»	(5,16//150)25*
18	M-22 «Aerotester» (1)		2012	Testing the autopilot of the NAU design	(2,5//18)4,0*
19	M-22D «Aerotester» (2)		2013	Modification of M-22 to provide flight training on twin-engine UAVs	(3//25)6,0*
20	PC-08		2014	An electric six-engine unmanned helicopter for monitoring and reconnaissance	Diameter at screw edges (0,8//3,8)1,1*



Continuation of the appendix

№	UAV name	Image of the UAV	Year of creation	Purpose of development	Wing span, m; mass, kg (m/kg) kg*
21	M-49 «Haydamaka»		2015	Battlefield scout	(0,81//≤4,0)1,5*
22	M-6-3 «Zhayvir»		2015	Tactical-class force UAVs; reconnaissance	(3,0//20)4,2*
23	NAU PC-11		2016	An electric six-engine unmanned helicopter for monitoring and reconnaissance	Diameter at screw edges (1,1//5)1,5*
24	M-57 «Svitanok»		2016	Electric unmanned aircraft for monitoring and reconnaissance	(3,8//10)2,0*
25	M-10-2 «Oko»		2016	Electric unmanned aircraft for monitoring and reconnaissance	(2.15//4,95)1,0*
26	M-10-2 «Oko» (UAVC)		2016	The M-10-2 «Oko» unmanned aerial vehicle complex (adopted by the Ukrainian Armed Forces in 2017 for trial operation)	—

Continuation of the appendix

№	UAV name	Image of the UAV	Year of creation	Purpose of development	Wing span, m; mass, kg (m//kg) kg*
27	M-56 «Module»		2017	Multi-functional UAV	(4,95//20)4,0*
28	M-6-3T «Zhayvir»		2017	Transportation of valuable cargo in automatic mode at a distance of up to 800 km	(3,0//22)4,0*
29	ПКМ-14 «Saturnia»		2018	Cargo transportation in retail chains (developed for a foreign customer)	Diameter at screw edges (2,15//10)2,0*
30	M-10-2U «Oko»		2018-2019	Training modification of the M-10-2 «Oko»	2,15//4,95
31	PS-11 «Krokus»		2020	Demonstrator of solar cells aircraft flights at altitudes up to 20 000 m (commissioned by the Cabinet of Ministers of Ukraine)	(11,0//20)1,0*
32	«Ovod» M106		2020	Electric unmanned aircraft for monitoring and reconnaissance (flight time – 3 hours)	(2,3//4,95)1,1*

№	UAV name	Image of the UAV	Year of creation	Purpose of development	Wing span, m; mass, kg (m//kg) kg*
33	PMB-03 NAU		2020	Planning self-guided mini-munition	(0,275//0,6)0,3*
34	«Sokil» 300		2020	Full-size mock-up of a striking UAV (on behalf of «Luch» Design Bureau, Kyiv, Ukraine)	(14,5//400)300,0*
Prospective UAV and aircraft projects					
35	KM-3 «Kubok»		2016	The project of a multipurpose convertible aircraft for local airlines (for a European customer)	(9,6//3500)≤1100*
36	M1200		2017	The project of a single-engine optional-piloted CA aircraft	(14,7//1200)300*
37	SP-80		2017	Project for an promising solar cells stratospheric platform	(150//80)35,0*
38	NAU PK-14		2018	A project for a high-tech unmanned helicopter for monitoring and reconnaissance	(1,05//4,5)1,5*
39	M4000		2019	The project of a double-engine optional-piloted aircraft of the CA of local airlines	(20,9//4100)1600*

№	UAV name	Image of the UAV	Year of creation	Purpose of development	Wing span, m; mass, kg (m//kg) kg*
40	BVM-16		2020	The project of an unmanned helicopter for monitoring	(6//16)1,4*
41	BVVV-20		2021	Unmanned high-altitude cargo helicopter project	(3,64//80)20,0*

* payload weight

Наукове видання

**ТЕОРІЯ І ПРАКТИКА
БЕЗПЛОТНИХ АВІАЦІЙНИХ
СИСТЕМ
НАЦІОНАЛЬНОГО
АВІАЦІЙНОГО УНІВЕРСИТЕТУ**

*За загальною редакцією
доктора технічних наук, професора М. Г. Луцького*

Монографія

(англійською мовою)

Керівник видавничого проєкту *В.І. Зарицький*
Дизайн обкладинки *О.Б. Тараненко*
Авторська редакція

Підписано до друку 28.10.2022. Формат 70x100^{1/16}.
Папір офсетний. Друк офсетний. Гарнітура Times New Roman.
Умовн. друк. аркушів – 20,8. Обл.-вид. аркушів – 18,56.
Тираж 300

Видавець і виготовлювач: ТОВ «Видавництво Ліра-К»
Свідоцтво № 3981, серія ДК.
03142, м. Київ, вул. В. Стуса, 22/1
тел./факс (044) 247-93-37; (050) 462-95-48
Сайт: lira-k.com.ua, редакція: zv_lira@ukr.net